CATEGORY 1

REGULATORY INFORMATION DISTRIBUTION SYSTEM (RIDS)

ACCESSION NBR:9603010125 DOC.DATE: 95/12/31 NOTARIZED: NO DOCKET #
FACIL:
AUTH.NAME AUTHOR AFFILIATION
* Interior, Dept. of, Geological Survey
RECIP.NAME RECIPIENT AFFILIATION

SUBJECT: "USGS - Yucca Mountain Project Branch,1995 Milestone Rept 3GCH510M."

DISTRIBUTION CODE: NH03D COPIES RECEIVED:LTR 0 ENCL 1 SIZE: 190
TITLE: High Level Waste Tech Info re NNWSI Sites - General

NOTES:

	RECIPIENT ID CODE/NAME	COPIES LTTR	COPIES ENCL	RECIPIENT ID CODE/NAME	COPIES LTTR	COPIES ENCL
	RECIP..........	1	1			
INTERNAL:	ACNW	6	6	FILE CENTER 01	1	1
	HLUR/BC	1	1	NMSS/DWM/DEPY2	1	0
	NMSS/ENGB 7J9	1	1	NMSS/HLUR 7J9	1	1
	NMSS/PAHB 7J9	1	1	OGC/NWMS	1	1
EXTERNAL:	CNWRA	1	1	NRC PDR	1	1
	NUDOCS FULL TXT	1	1			

C A T E G O R Y 1 D O C U M E N T

see enclosure on shelf

NOTE TO ALL "RIDS" RECIPIENTS:
PLEASE HELP US TO REDUCE WASTE! CONTACT THE DOCUMENT CONTROL DESK, ROOM OWFN 5D-5(EXT. 415-2083) TO ELIMINATE YOUR NAME FROM DISTRIBUTION LISTS FOR DOCUMENTS YOU DON'T NEED!

TOTAL NUMBER OF COPIES REQUIRED: LTTR 9 ENCL 16

102.8

Ficha ... From: Chad Glenn

U.S. GEOLOGICAL SURVEY - YUCCA MOUNTAIN PROJECT BRANCH

1995 MILESTONE REPORT 3GCH510M

PROGRESS REPORT ON DATING QUATERNARY SURFICIAL DEPOSITS

by

J.B. Paces, S.A. Mahan, K.R. Ludwig, L.M. Kwak, L.A. Neymark, K.R. Simmons, L.D. Nealey, B.D. Marshall, A. Walker

---

CHARACTERISTICS AND DEVELOPMENT OF ALLUVIAL SOILS OF THE YUCCA MOUNTAIN AREA, SOUTHERN NEVADA

by

Lundstrom, S.C., McDaniel, S.M., Guertal, W., Nash, M.H., Wesling, J.R., Cidziel, J., Cox, S., and Coe, J.

PROGRESS REPORT ON DATING QUATERNARY SURFICIAL DEPOSITS

by

J.B. Paces, S.A. Mahan, K.R. Ludwig, L.M. Kwak, L.A. Neymark, K.R. Simmons, L.D. Nealey, B.D. Marshall, A. Walker

ABSTRACT

Quaternary geological records provide a means of assessing the paleoseismic and paleoenvironmental history at Yucca Mountain. Information from these records can then be used to predict future geological conditions over time scales appropriate to isolation of radioactive waste. Reliable geochronological control is central to defensible estimation of the rates of seismic activity, erosion/deposition, and climate-controlled episodes of surface-water activity. This report presents unpublished geochronological data obtained from surface deposits exposed in trenches, pits and natural outcrops associated with concurrent studies in the tectonics and surface-mapping programs. It also compiles some of the previously-published geochronological data from the same sites and re-interprets age estimates in a manner consistent with knowledge gained in the last several years. A parallel study of the physical morphology and bulk properties of some of the same surface deposits by Lundstrom and others is included with this report. The longer-term goal of this type of combined investigation is to understand the kinetic process of soil development at Yucca Mountain and to construct a chronostratigraphic framework for Quaternary surface deposits at the site.

The importance of geochronological control in placing rate limits on geological processes demands a high degree of confidence. The lack of accepted standard materials for Quaternary dating techniques requires objective criteria for assessing the accuracy of age estimates including reproducibility and internal consistency checks, agreement with stratigraphic control, concordant results using independent chronometers, and theoretical viabilityfor dating methods. Given the nature of the surface deposits at Yucca Mountain, two dating techniques have been used extensively: uranium-series disequilibrium dating of carbonate- and silica-rich materials in soils, and thermoluminescence dating of the fine-grained, eolian components present in most of the surficial deposits. Both techniques give consistent and generally concordant results for materials ranging from several thousands to several hundreds of thousands of years and older. Technical advances in uranium-series disequilibrium dating introduced through micro-sampling and mass spectrometric analysis have dramatically improved the quality of geochronological data compared to much of the alpha spectrometric data collected in the past. A discussion of the theoretical and geological problems inherent with previously-published uranium-trend data is presented with the conclusion that all subsequent reference to and consideration of uranium-trend "ages" from soil profiles at Yucca Mountain and elsewhere be abandoned with regards to numerical age significance. Tephrochronological investigation of several of the felsic and basaltic ash occurrences is also discussed with regards to the potential for providing chronostratigraphic control in the future.

All geochronological data currently available are systematically presented in a series of tables and illustrations organized on a trench-by-trench basis.

TABLE OF CONTENTS

ABSTRACT 1

1. INTRODUCTION 2

2. GEOCHRONOLOGICAL APPROACH 3

   2.1 Dating Strategy 3

   2.2 Purpose of Report 3

3. CRITERIA FOR DEFENSIBLE DATING 3

4. ANALYTICAL TECHNIQUES 4

   4.1 Uranium-series disequilibrium 4

      4.1.1 Mass spectrometric technique: .. 4

      4.1.2 Data treatment 4

      4.1.3 Materials sampled 5

      4.1.4 General results 6

4.1.5 Comparison to previous alpha-decay approaches.....7
4.2 Comments on U-trend method.....7
4.2.1 Historical background.....7
4.2.2 Methodological Problems.....8
4.2.3 Geological Problems.....9
4.2.4 Conclusions on uranium-trend data.....9
4.3 Thermoluminescence.....10
4.3.1 Methodology.....10
4.3.2 TL Sample Status and Progress Report.....11
4.4 Tephrochronology.....13
4.4.1 Introduction.....13
4.4.2 Potential uses in YMP.....13
4.4.3 Identification.....13
4.4.4 Affinity of two unknown felsic ash samples.....14
4.4.5 Basaltic ashes.....14
5. DATA PRESENTATION.....15
5.1 Format of Presentation.....15
5.1.1 Uranium-series disequilibrium data.....15
5.1.2 Thermoluminescence data.....16
5.1.3 Logs/diagrams showing geochronologic data.....16
5.2 Systematic Data Presentation.....17
5.2.1 Rock Valley Fault system.....18
5.2.2 Paintbrush Canyon Fault.....18
5.2.2.1 Alice Ridge.....19
5.2.2.2 Midway Valley T4.....20
5.2.2.3 Busted Butte.....21
5.2.3 Bow Ridge Fault.....22
5.2.4 Ghost Dance Fault.....23
5.2.5 Stagecoach Road Fault.....24
5.2.6 Solitario Canyon Fault.....25
5.2.6.1 Trench 8.....25
5.2.6.2 Trench 3.....26
5.2.7 Fatigue Wash Fault.....27
5.2.8 Windy Wash Fault.....28
5.2.9 Bare Mountain Fault.....29
5.2.10 Lathrop Wells Cone.....30
5.2.11 Fortymile Wash.....31
5.2.12 Midway Valley Soil Pits/ Trenches.....32
5.2.13 Coyote Wash Trenches.....33
REFERENCES.....34

1. INTRODUCTION

Safe isolation of radioactive waste in a geologic repository demands knowledge of the geologic, hydrologic and climatic processes which may impact the potential repository block over the time scales of the radioactive isotopes present. In many cases, some level of quantification of the rates at which these processes occur is also important, so that probabilities can be assigned to performance assessment scenarios. Because waste must be isolated for up to hundreds of thousands of years, models of future physical conditions affecting the potential repository must take into account the geologic record of natural processes that have occurred over the past several hundred thousand years. If these records can be accurately dated, reasonable estimates of probabilities can be extracted permitting constraints to be placed on models of the hydrologic and geologic conditions that are likely to be experienced during the critical periods of waste isolation.

Determination of accurate ages for these geologic records is particularly crucial for models of future seismic hazards and hydrologic fluxes on and within Yucca Mountain. Tectonic, sedimentologic and pedogenic processes commonly leave records as Quaternary deposits that can be used to establish relative histories of events. This report specifically addresses the establishment of a reliable chronological record within these deposits.

Surface deposits at Yucca Mountain comprise a variety of subaerial clastic deposits including alluvium, colluvium and eolian materials. Nearly all deposits formed under oxidizing conditions resulting in the destruction of organic materials originally present. Dating of these clastic materials, where organic carbon for radiocarbon dating is conspicuously absent, has proven difficult owing to the nature of the materials and the limited number of Quaternary dating techniques applicable to these materials. A body of geochronologic information on surficial deposits at Yucca Mountain was developed in the 1980's and early 1990's; however, many of the data was based on empirical or controversial techniques that were not rigorously tested. The vulnerability of the geochronological database is of particular concern given a regulatory environment that demands high degrees of confidence in order to assure public safety.

With this recognition, an accelerated geochronology effort was initiated in FY1995. The main goals of this effort are to provide a credible and defensible geochronology for surficial deposits at Yucca Mountain. In addition to ages of deposition, soil development modifies the original morphology of the sediments and is dependent, in part, on the amount of time the deposits have been exposed at the surface. A parallel study that examines the field morphology and laboratory data from surface deposits is being conducted. The goal of these two studies is to combine detailed morphological data with geochronological control to establish a chronostratigraphic framework for surface deposits at Yucca Mountain. Current results of this morphological study are presented in a companion paper (Lundstrom et al.) included at the end of this (geochronology) report.

2. GEOCHRONOLOGICAL APPROACH

2.1 Dating Strategy

Because no single dating method applied to Quaternary of surfaces and soils can guarantee accurate results, and because appropriate materials are not universally available, an accurate geochronological database must be constructed utilizing multiple dating techniques. Given the nature of the arid to semi-arid, oxidizing surface conditions in southern Nevada, we have chosen to aggressively pursue two dating techniques that have been applied widely throughout the world in recent years: uranium-series disequilibrium dating of carbonate- and silica-rich materials in soils, and thermoluminescence dating of the fine-grained, eolian components present in most of the surface deposits. Although the two methods generally date different geological events, we have attempted to collect samples amenable to both techniques at the same sites where possible, in order to compare results between the two independent techniques. Other techniques appropriate for site-specific situations may be utilized in greater detail in the future. In particular, tephrochronology, although of limited use due to the paucity of airfall ash deposits, may provide important time horizons where present. Radiocarbon dating on young (less than about 40 ka*) soil carbonate may provide consequential checks for consistency of the younger uranium-series disequilibrium ages.

Many sites have been chosen to supply specific age control to paleoseismic problems, with samples coming from trenches excavated across Quaternary faults. The data set is therefore biased towards materials developed on less-stable surfaces with different rates of sediment accumulation, erosion, hillslope and water saturation/infiltration characteristics than the flatter, more-stable surfaces representing most of the surface area at Yucca Mountain underlain by Quaternary deposits. Because soil formation is a complex process influenced by a wide spectrum of physical factors, additional sites in Midway Valley and Fortymile Wash were sampled to help assess the possible variations in relationships between ages and physical morphologies in a variety of different local environments.

Data: descri

2.2 Purpose of Report

This report documents the progress made in the first year of a multiple-year investigation. It is intended to provide a means of disseminating numerical age estimates to project activities requiring geochronologic control. It is also intended to document some of the advances made in refining dating techniques so that input from the community of Quaternary geologists can provide feedback on how to design experiments to best address the geological uncertainties surrounding the interpretation of these ages estimates.

3. CRITERIA FOR DEFENSIBLE DATING

The lack of accepted age standards for Quaternary dating methodologies requires a more critical evaluation of data than may be necessary for other

* ka = kilo-annum (10^3 years before present)

technical issues. Fortunately, objective criteria can be established for evaluating geochronological data. These criteria include:

1) Multiple age determinations for materials representing a single geological event must be self-consistent and internally reproducible. This includes comparisons of ages to stratigraphic controls where appropriate.

2) Age estimates for the same event using independent chronometers must be concordant.

3) Dating techniques must be theoretically robust and widely accepted by the scientific community overall, and specifically by the geochronologic community.

4) The physical character of the dated materials and their relationships and significance to the age estimates must be well documented.

These criteria should be applied in all cases, but in particular in instances required to withstand the regulatory environment and the licensing process. This includes data that are currently being acquired as well as previously-published data.

4. ANALYTICAL TECHNIQUES

4.1 Uranium-series disequilibrium

4.1.1 Mass spectrometric technique: All uranium-series data collected in FY1995 utilized direct measurement of atomic ratios by thermal ionization mass spectrometry rather than by decay-counting by alpha spectrometry as was the general practice in the past. Both of these techniques take advantage of the systematic decay of natural daughter-isotopes of ^{238}U at constant rates under closed-system conditions (no loss or gain of parent or daughter isotopes other than by radioactive decay). Two clocks in the ^{238}U decay chain, $^{230}Th/U$ dating and $^{234}U/^{238}U$ dating, are commonly used to date minerals precipitated from aqueous solutions. The $^{230}Th/U$ clock uses the in-growth of ^{230}Th from an initially negligible abundance to radioactive secular equilibrium in the following decay scheme:

$$^{238}U \xrightarrow{4.5Ga} {}^{234}U \xrightarrow{245ka} {}^{230}Th \xrightarrow{75ka} \ldots {}^{206}Pb(stable)$$

The main factor determining the dating limits for this chronometer is the half life of ^{230}Th which, in practice, places an upper limit of 300 to 500 ka on most natural materials. Alternatively, if the initial $^{234}U/^{238}U$ values are well characterized, the decay of an initial excess of ^{234}U to secular equilibrium can provide an additional clock. An advantage of this chronometer is that it is capable of extending the dating range up to about 1500 ka due to the longer half life of ^{234}U. The theoretical and mathematical relations defining the isotopic evolution of the system are well understood (Rosholt and Antal, 1962; Broecker, 1963; Broecker et al., 1968; Ku 1976; Faure 1986; Edwards et al., 1987; Ivanovich and Harmon 1992)

The practical difference between mass-spectrometric and alpha-spectrometric techniques is the approximately 500 times greater measurement efficiency of the former, resulting in substantial differences in sample size requirements and analytical precision. Alpha-decay counting is limited by the number of atoms placed in the detector, detector efficiency and the decay constants (probability of disintegration within a given time period) that are inherent to each isotope. In practice, carbonate samples with 1 to 3 ppm uranium concentrations analyzed by alpha-decay counting range in size from one to five grams (5 to 10 micrograms of uranium) and are counted for two to four weeks with a resulting precision of from one to five percent. In contrast, atom counting in thermal-ionization mass spectrometers is not dependent on natural decay rates and even with low ionization efficiency, large numbers of atoms are counted in short periods of time. In practice, 0.1 to 0.3 grams of carbonate can supply 0.1 to 0.3 micrograms of uranium, resulting in $^{234}U/^{238}U$ and $^{230}Th/^{238}U$ precisions better than 1% in one to two hours of analysis time. Sample size can be reduced still further (less than 0.03 grams) using materials containing higher uranium contents, such as opaline silica.

4.1.2 Data treatment: In near-surface environments at Yucca Mountain, uranium is oxidized to the hexavalent state and is readily transported in solution by natural waters as a complexed species. In contrast, thorium remains in the tetravalent state resulting in a negligible solubility.

Therefore, essentially all ^{230}Th present in a mineral precipitated purely from aqueous solution arises from decay of ^{238}U and ^{234}U incorporated at the time of formation. However, many samples of authigenic materials in the surface deposits at Yucca Mountain contain substantial amounts of ^{232}Th indicating the presence of a non-hydrogenic component (usually detrital silicates that cannot be physically separated from the hydrogenic component prior to analysis). The uranium and thorium isotopic contribution from this non-hydrogenic component must be subtracted from the measured analysis before an age for the hydrogenic component can be calculated.

Several techniques are available to correct for thorium and uranium isotopes inherited at the time of mineral precipitation. Leach-residue and total-digestion isochron techniques have been utilized on Yucca Mountain samples in the past (Szabo et al., 1981; Szabo and O'Malley, 1985; Muhs et al., 1990, unpublished manuscript; Lou and Ku, 1991; Paces et al, 1994; Peterson et al, 1995). These techniques presume that samples consist of a binary mixture of a hydrogenic component free from ^{232}Th (and thus initial ^{230}Th) and a thorium-bearing detrital component. Several mathematical techniques have been used to extrapolate the $^{234}U/^{238}U$ and $^{230}Th/^{238}U$ composition of the ^{232}Th-free component for which an age can then be calculated (Osmond et al., 1970; Rosholt, 1976; Ludwig and Titterington, 1994). A number of assumptions are inherent to these detritus-correction techniques. The first is that there is only one ^{232}Th-bearing component (single phase or a homogeneous mixing end member) so that the assumption of simple binary mixing is satisfied. The second is that the samples comprising any mixing line indeed represent a cogenetic suite of materials. The third is that no laboratory fractionation of uranium and thorium occurs during any leaching process so that all chemically-produced mixtures retain their original $^{230}Th/^{238}U$. Observed scatter in excess of analytical uncertainty is often present on these isochrons (e.g., Paces et al., 1994) attesting to the failure of one or more of the above assumptions. In addition, an obvious requirement of the isochron technique is that multiple analyses are needed to determine a single age. Ages calculated on single leach-residue pairs (two points defining the regression) represent the least statistically-robust results, whereas the greater the number of samples that define the isochron, the greater the statistical reliability. An advantage of the isochron technique is that it does not require knowledge of the isotopic composition of the detrital component. Some disadvantages are the multiple analyses required, the difficulty in obtaining a truly cogenetic sample suite and the likelihood of complex, multiple-component mixtures.

A different approach for obtaining ages is to estimate the isotopic composition of the ^{232}Th-bearing component and use the abundance of ^{232}Th observed in the analysis to correct the observed $^{234}U/^{238}U$ and $^{230}Th/^{238}U$ to a ^{232}Th-free state. The degree of correction is greatest for samples with high ^{232}Th abundances (i.e., low $^{230}Th/^{232}Th$ activity ratios) and negligible in samples with low ^{232}Th abundances (i.e., high $^{230}Th/^{232}Th$ activity ratios). Therefore, in samples with reasonably high $^{230}Th/^{232}Th$, only small corrections (and propagated uncertainties) on the final age estimates are introduced. A great advantage of this approach is that a maximum amount of geochronological information is obtained from the available analytical information. The larger number of age estimates form a population distribution that may contain additional information concerning the nature of the complexities of the soil components that are not available when only a single age estimate is obtained by the isochron technique. A disadvantage of this method is that the isotopic composition of the detrital phase must be assumed rather than measured. Because of this, samples with high amounts of detrital components cannot be analyzed.

4.1.3 Materials sampled: The latter approach, combined with the smaller sample-size capability inherent to the mass spectrometric technique, was utilized in the present study. Macroscopic samples consisted of a variety of calcite- and opal-rich materials introduced into the sediments during pedogenesis. These include volcanic clasts with adhering rinds (Fig. 1), individual rhizoliths (petrified roots or root casts), segregations of relatively pure carbonate layers which generally contain plant microfossils (Fig. 2), and detrital matrix that is flooded with secondary cement (Fig. 3).

In addition, the suitability of pedogenic opaline silica for uranium-series disequilibrium dating was investigated much more thoroughly than in the past. Typically, the higher uranium contents in silica-rich samples (5 to 20 ppm U or higher compared to 2 to 5 ppm U for carbonate-rich materials; data presented tables later in this report) result in lower

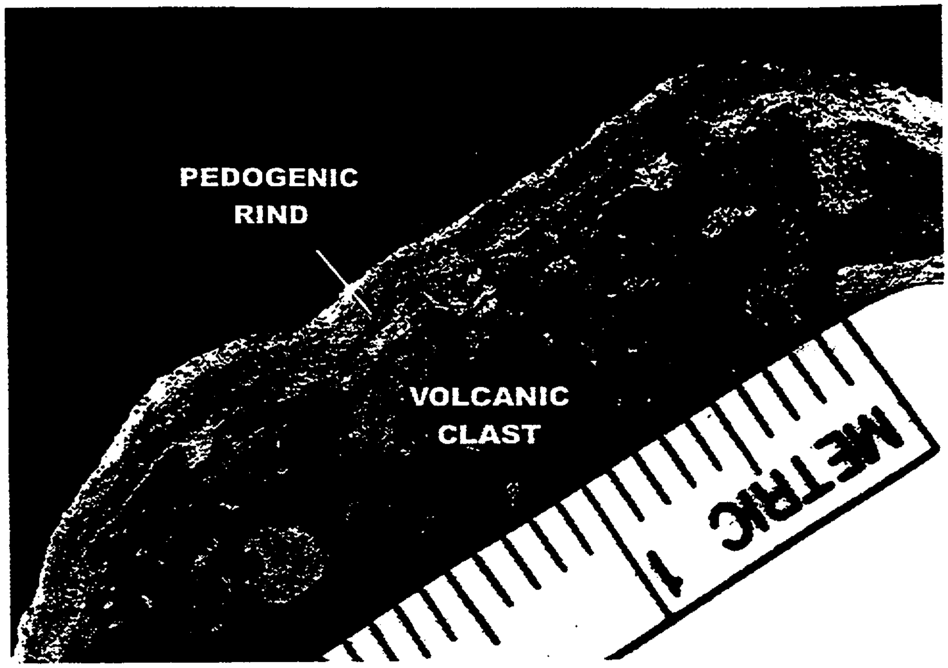

Figure 1: Photograph of a banded pedogenic rind coating a rounded clast of tuff (sample HD1626). Scale is in centimeters.

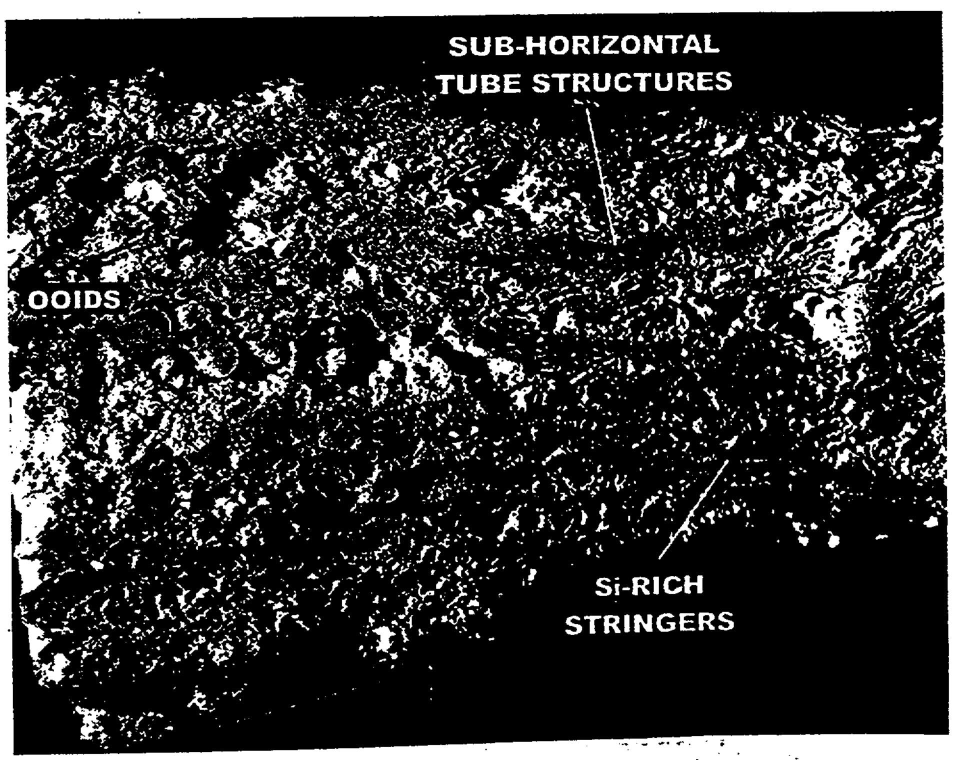

Figure 2: Photograph of a detritus-poor, carbonate-rich layer (sample HD1643) showing micro-textures attributed to fossil roolet structures. Note thin, darker stringers enriched in silica. Scale is in centimeters.

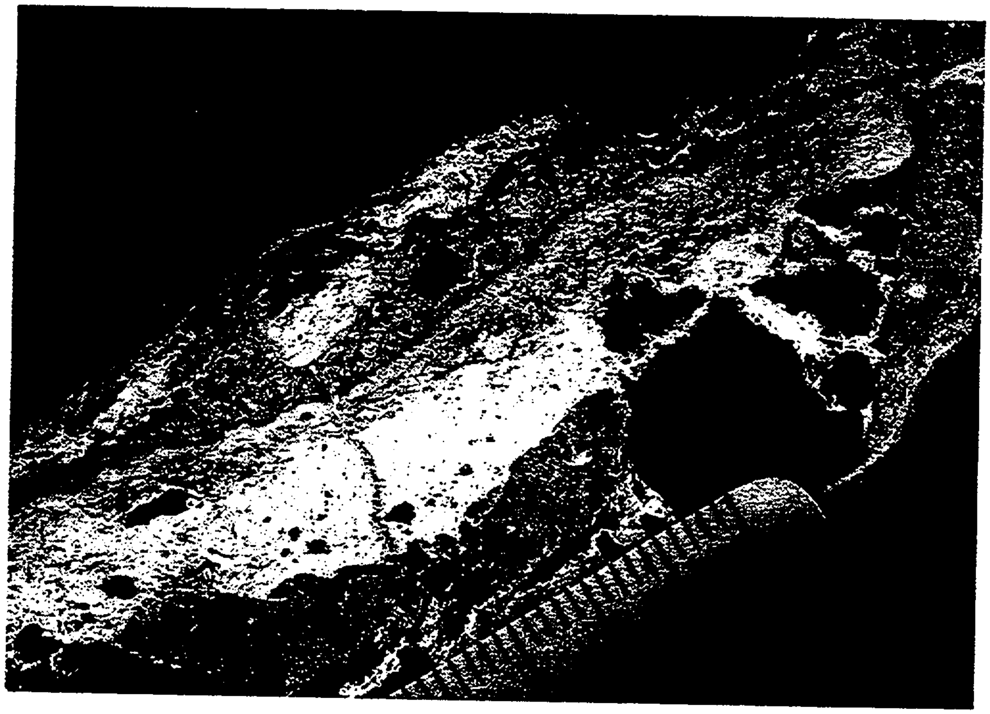

Figure 3: Photograph of a calcrete slab (sample HD1723) showing complex textural relationships within the detrital matrix that has been highly cemented with carbonate and silica cement. Scale is in centimeters.

Th/U and higher $^{230}Th/^{232}Th$. This translates to a smaller detrital correction and a greater precision of the resulting age estimate. Data presented later in this report also attest to the generally closed-system behavior of opaline silica at Yucca Mountain. Isotopic relationships show that very few samples appear to have lost uranium preferentially to thorium, as measured by the near-absence of points plotting to the right of the closed-system evolution curves. Samples older than about 300 ka are extremely sensitive to this constraint, yet most of the analyses presented in this report yield isotopic compositions that lie along the theoretical decay paths for materials of reasonably uniform initial $^{234}U/^{238}U$. In addition, closed-system evolution of samples showing relatively constant initial uranium activity ratios ($^{234}U/^{238}U_{initial}=1.6 \pm 0.2$) precludes substantial effects of mixing very old material in secular equilibrium with recent input from modern soil-forming processes. Therefore, the uranium-series disequilibrium results obtained from the silica-rich materials presented below objectively verify the general analytical and geochemical success of the techniques.

Textural relations between coexisting carbonate and silica in Yucca Mountain soils are highly complex and require more-detailed investigation. Macroscopic observations suggest that silica can replace pre-existing carbonate. However, microscopic examination of many silica-rich materials indicates a very intimate coexistence of the two phases. Backscatter electron imagery and semi-quantitative energy-dispersive x-ray fluorescence analysis indicates the presence of mixed Si-Ca material as well as relatively pure interlaminated Si-rich (opal) and Ca-rich (calcite) phases. Textures in some samples also indicate processes involving "unmixing" of an originally homogeneous Si-Ca material resulting in calcite micro-spherulites within a pure silica matrix. These observations suggest that no all-inclusive genetic or time distinctions can be made when attempting to generalize carbonate-silica relationships in this environment. In addition to these complex relationships within well-developed carbonate-rich soils, thin (less than 0.5 mm) silica-rich rinds are present on the undersides of cobbles in deposits as young as 3 to 5 ka (dated by thermoluminescence of the eolian silt within the sediment matrix). These rinds are currently being analyzed to determine uranium-series disequilibrium age estimates. Preliminary results suggest that they have comparable ages to the eolian silt deposits and were developed *in situ* (unreviewed data not included at the time of this report). The results of this type of work will be important not only for dramatically extending the usefulness of uranium-series disequilibrium dating applications, but also for the implications that the innermost rinds on clasts can form within several thousand years after deposition, and retain their closed-system behavior for periods of time greater than the limits of the disequilibrium systematics.

Multiple aliquots of samples were obtained during the FY1995 collection period by slabbing and polishing sections of volcanic clasts with rinds, rhizoliths or cemented matrix materials, followed by use of carbide micro drills to obtain small amounts (~0.1 g) of the most detritus-free materials. This was accomplished either by excavating a trench within the desired layer and obtaining a powdered sample, or by removing the undesired layers adjacent to the aliquot (either tuff clast or softer, matrix material) to form a thin septum which was then broken off and gently crushed. In some cases fragments were then hand-picked under magnification to remove as much detrital-bearing material as possible. Ultimately, the type of material that was analyzed in any given sample was dictated by the availability and purity of secondary precipitates. Analyses of sub-samples presented below are biased towards the hardest, least-porous materials available in any given sample in order to maximize the uranium-rich silica component.

Aliquots were then weighed, spiked with known amounts of tracer isotopes (typically ^{236}U, ^{233}U, and ^{229}Th) and totally digested in concentrated acids (HF, HNO_3, HCl, and $HClO_4$) in Teflon containers. After complete digestion, uranium and thorium were purified by ion chromatography, loaded on rhenium ribbons, and run as metal ions on either a VG ISOMASS 54E single collection or a Finnigan MAT 262 multi-collection thermal ionization mass spectrometer.

4.1.4 General results: A variety of materials were analyzed for uranium-series ages; both to investigate the usefulness and reproducibility of ages on a range of materials, and because of the limited availability of well-developed clast rinds or rhizoliths in some deposits. Silica-rich rinds adjacent to volcanic clast substrates provided the oldest ages when multiple materials were sampled from the same horizon.

Intermediate and outer layers from the same thick rinds typically yield ages that are commonly in depositional order (Fig 4). Isolated silica-rich seams and stringers within the weakly- to densely-cemented matrix typically yielded the youngest ages. Rhizoliths can show a variety of age distributions within a single unit from tightly-clustered distribution of ages to ages spanning several hundred thousand years.

4.1.5 Comparison to previous alpha-decay approaches: In the past, approaches used to sample soil carbonate for uranium-series disequilibrium analysis differed substantially from that described above. The cause for this lies in the larger sample sizes required by alpha-decay counting, and in the use of isochron techniques to determine age estimates. In general, fist-sized bulk samples containing the greatest amounts of carbonate cement were selected for analysis. Calcrete blocks were cleaned of as much non-cemented detritus as possible, gently crushed, and physically separated on the basis of particle size into three or four size fractions; typically coarser than 0.15 mm (100 mesh), 0.15 to 0.075 mm (100-200 mesh), 0.075 to 0.044 mm (200-325 mesh) and finer than 0.044 mm (325 mesh). The conceptual justification for this practice was based on the need to obtain a spread in $^{232}Th/^{238}U$ (that is, different mixtures of the authigenic and detrital components) for regression purposes. The secondary carbonate, being generally softer than the silicate detritus, was expected to be concentrated in the finer fractions. Although this strategy is generally demonstrated to be valid on the basis of the proportions of dilute acid-soluble and -insoluble constituents, high $^{230}Th/^{232}Th$ (i.e., low detrital component) was not always observed in the fine fractions — probably because of the presence of a finely-dispersed clay-sized materials. In a further attempt to separate authigenic carbonate and detrital silicate constituents, dilute acid leaches (typically 0.25 N HNO_3) were often employed.

The effects of these practices may bias the resulting age estimates. The fact that bulk samples were used, as well as the process of homogenizing materials by crushing and sieving prior to analysis, necessitates thorough mixing of multiple secondary components present within the bulk sample that have natural age variations. As a result, these composite samples will have an average age somewhere between the oldest and youngest soil components. The final age estimate will possess a value dependent on the mass balances among the relative amounts of the various constituents and their ages. The average age for these larger, composite samples will reflect the oldest soil age only when subsequent, climate-controlled influxes of carbonate are negligible. Age estimates determined from composite samples still represent valid minimum ages for the sedimentary deposit, but, considering the complexities of soil-forming processes, they may not represent close minimum ages. The only way to assess this effect is to return to the same samples and specifically search for the oldest components using micro-sampling techniques.

The effects of dilute acid leaching in the laboratory are less clear. For the $^{230}Th/U$ dating technique to provide accurate information, it is critical that uranium and thorium present in the spiked analyte have the same proportions as the sample prior to chemical processing. This can be assured only when all of the sample is taken into complete solution (total digestion). In contrast, leach solutions, designed to extract only the dilute-acid soluble portions, may preferentially incorporate uranium as dissolved ions while leaving the more-insoluble ^{230}Th derived from that uranium behind along with the residue. Although leach techniques have been widely applied (Ku et al., 1979; Ku and Liang 1984; Szabo and Sterr 1978; Ku and Joshi, 1980; Kaufman, 1971; Schwarcz and Latham 1989; Szabo et al., 1981; Szabo and O'Malley, 1985; Paces et al., 1994), independent checks that evaluate the possibility of laboratory fractionation are typically unavailable. Indeed, there is a general recognition of this problem, resulting in a movement towards total digestion techniques (Bischoff and Fitzpatrick, 1991; Luo and Ku, 1991; Paces et al., 1994). In an attempt to eliminate the potential for laboratory fractionation during chemical processing, some of the previously-published leach-residue data are mathematically recombined in this report and treated as single whole-rock analyses for age estimation.

4.2 Comments on U-trend method

4.2.1 Historical background: Some of the problems inherent to uranium-series disequilibrium dating of the pedogenic carbonates discussed above became apparent during the early stages of geochronological investigation at the Nevada Test Site in the late 1970's. Age estimates were also required for clastic deposits lacking well-developed calcrete horizons at a time when other Quaternary

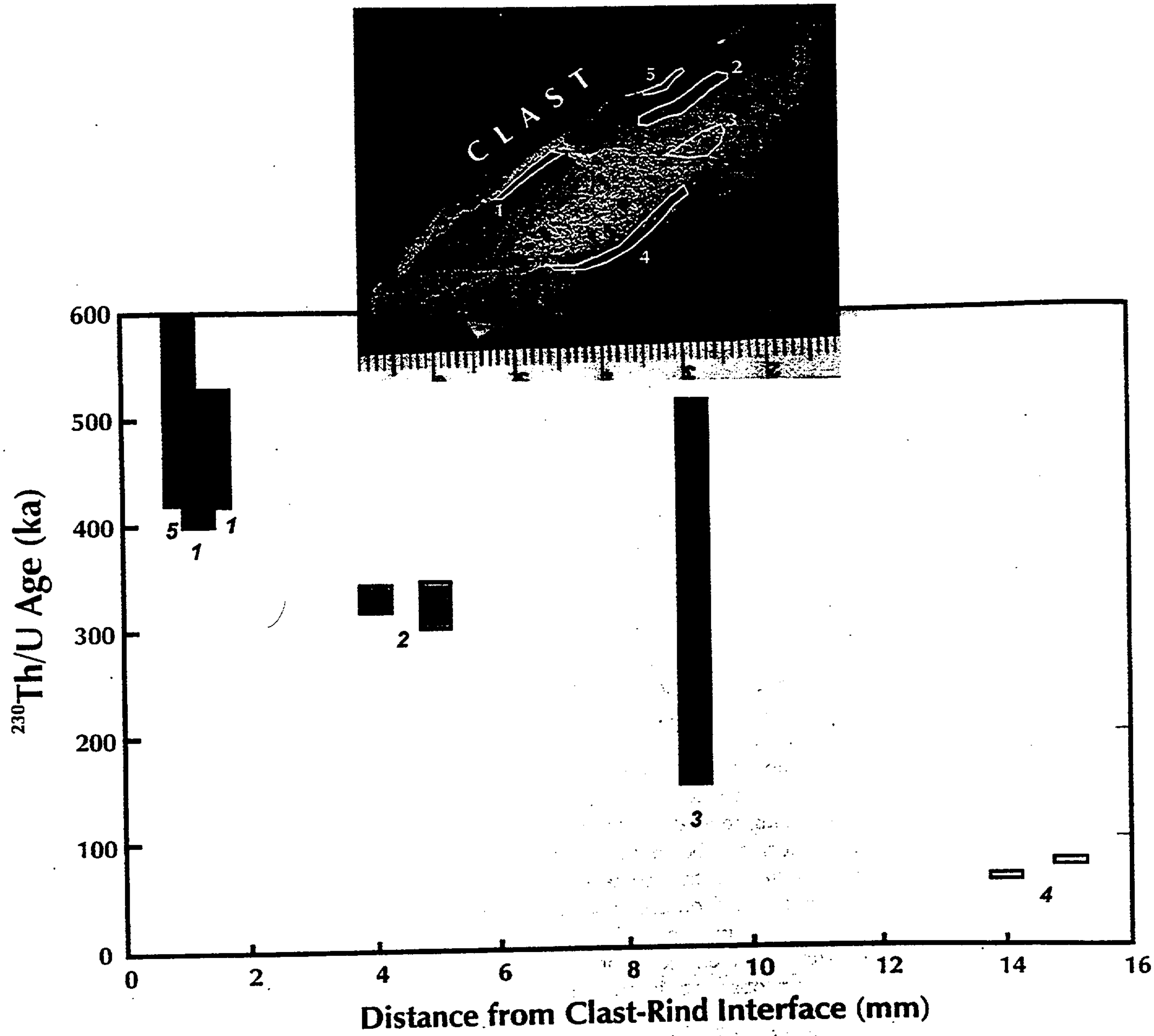

Figure 4: Distribution of ages (vertical bars represent range of 95% confidence level uncertainties) of micro-samples of opal-rich lenses within a thick, complex clast rind plotted against distance from clast-rind interface. Numbers correspond to sample areas shown in inset photograph (scale in centimeters).

geochronological techniques were unavailable or inapplicable. As a means, in part, of satisfying this need, a new technique utilizing disequilibrium between ^{238}U daughter products was developed that was not based on closed-system behavior. Instead, this innovative technique, named the uranium-trend method, technique is based on the assumption of open-system water fluxes through a column of sediments. The method was developed and implemented by J.N. Rosholt and co-workers at the U.S. Geological Survey and has been described and applied in a series of U.S.G.S. Open-File Reports (Rosholt, 1980; 1985; Szabo and Rosholt, 1982; Rosholt et al., 1985a, b, 1986, 1988). Muhs and others (1989) further discussed the method and identified some of the geologic factors affecting its potential reliability. The method has never received wide-spread use by the Quaternary geochronologic community and has since been abandoned by the U.S. Geological Survey geochronologists.

The technique assumes that ^{238}U is transported in solution through a column of sediments leaving a trail of daughter products adsorbed onto grain surfaces in a systematic fashion. The technique attempts to quantify ages in systems open to uranium fluxes even though the large number of geochemical variables "precludes the definition of a rigorous mathematical model for uranium migration*." Therefore, an empirical approach was adopted based on comparison of uranium-trend characteristics in known-age deposits. The uranium-trend clock starts at the initiation of water flow through the sediment. Although the flux is greatest shortly after deposition, there is no allowance for episodic fluxes related to varying climate pulses. Ages are estimated by comparing isotope ratios of an unknown sample to those obtained from independently-dated deposits through the use of an empirical calibration curve. By dividing a surface deposit into vertical sub-samples, the differences in $^{230}Th/^{238}U$ and $^{234}U/^{238}U$ activity ratios between sub-samples will ideally define trends that can be related to a U-flux parameter whose "actual physical significance is not well understood." The flux is assumed to vary exponentially with time, however the half-period of the flux is represented as a constant in a series of algorithms written in the form of Bateman equations. The flux parameter calibration curve is based on four primary calibration points collected from Late Wisconsin age loess deposits from Minnesota (12 ka radiocarbon date), glacial till from northwest Wyoming (150 ka obsidian hydration date), a zeolitized ash in Tuff A in Lake Tecopa, CA (600 ka K-Ar date), and altered Tuff B at Lake Tecopa, CA correlated to Bishop Ash (730 ka K-Ar age).

In the only attempt to use the uranium-trend technique by any laboratory other than that of Rosholt and co-workers, Atkins (1986) failed to yield results that were consistently compatible with the established chronostratigraphy. Although the method never received appropriate tests by any other independent laboratories, more than 30 estimates of uranium-trend ages were produced from trenches in the vicinity of the Nevada Test Site and, since then, have strongly influenced Yucca Mountain soil chronostratigraphy.

4.2.2 Methodological Problems: More-recently, Latham (unpublished manuscript) has critically evaluated the original uranium-trend model as well as additional models for open-system behavior. He concludes that there are fundamental flaws in the underlying methodology in addition to the potential geological problems identified previously (Muhs et al., 1989). First, the method does not attempt to clarify the meaning of open-system uranium mobility in terms of differentiating between contrasting models of continuous or multiple-episode fluxing. Calibration points as well as unknowns are all treated identically although the range in climate history between sample sites and physical characteristics controlling water migration between samples is extreme.

Second, the flux-attenuation parameter is treated like a decay constant in the empirical equations. In contrast to the fixed constants that control radioactive decay, this variable is "theoretically, if not practically, unique to each sediment." This results in the situation were sediments of the same age may have different uranium-trend curves because of variations in the flux-attenuation parameter, variations in the initial uranium isotopic conditions or both. Indeed, there is no clear unidirectional relationship been the age of the calibration points and their position on the calibration curve used to estimate the uranium-flux factor.

Third, isotopic compositions of the introduced uranium and its daughter products are central to the

* All quotations in this paragraph from Rosholt et al., 1985a.

age of the sediment, yet no critical assessment of the contribution from these isotopes from the sediment source has been made, either via *in situ* exchange or through laboratory procedures. Rosholt and co-workers recognized the need to ensure that sub-samples used to construct uranium-trend regressions represent a single, coeval sedimentary package. This was accomplished by examining the ^{232}Th characteristics from the same laboratory analyses used to produce uranium-trend ratios. Since ^{232}Th is neither a recoil decay-product of ^{238}U nor a component of the fluxed solutions, it must necessarily be derived from the clastic substrate during laboratory leaching. Ions other than ^{232}Th are introduced into solution at the same time, and no corrections for the ^{238}U decay-chain isotopes introduced from the same substrate source have been applied to the ratios used to estimate uranium-trend ages. Hence, isotopic ratios used to calculate uranium-trend ages are, at least in part, artifacts of the laboratory treatment.

Fourth, although the concepts of uranium fluxing are central to the uranium-trend argument, no attempt was made to demonstrate that this is actually observed in sedimentary sections. Mobile uranium should be concentrated in the upper portions of a given sediment package and show systematic attenuation with depth. Published studies (Muhs and others, 1989) have shown this to be, in general, untrue. The lack of these systematic observations distracts significantly from the concept of quantifying the uranium flux process in terms of age predictions.

Fifth, the statistical treatment of the uranium-trend age errors, large as they are, virtually guarantees that quoted age uncertainties will be significant underestimates. Error correlations in the isotope ratios were ignored, first-derivative error-expansion mathematics were used even though the isochron-slope errors are grossly non-Gaussian, and one-sigma errors without the appropriate student's-t multiplier were used instead of 95% conffidence errors.

4.2.3 Geological Problems: Muhs and others (1989) discuss a variety of geological complexities which may cause the failure of uranium-trend results to provide extractable information. These conditions include 1) mechanical mixing of sediments of different ages, 2) sediments where fixed-phase uranium concentrations are significantly greater than that introduced by solution fluxes, 3) variations in dissolved uranium concentrations during multiple-stage fluxing histories, 4) deep burial of sediments by low-permeability, younger deposits that effectively isolate the buried sediments from fluxing solutions, 5) deposits containing substantial uranium-bearing components behaving as closed isotopic systems (i.e., secondary calcium carbonate) 6) sediments exhibiting low or variable sorptive capacitance for mobile uranium, 7) sediments with homogeneous mineralogy resulting in monotonic U-Th abundances, and 8) sediments out of the age range of resolvability of the technique (<5 or >700 ka). Complex depositional and erosional history of a sediment pile also may strongly effect the cumulative effects of solution fluxing and resulting uranium-trend accumulations.

Another important consideration stems from our current work with small components in complex soils. Results summarized above and shown below verify the complex, multiple-generations of soil components preserved on very small scales (sub-centimeter scale). Once formed, these components apparently behave as closed systems and demonstrate the complex nature of episodic water fluxes through these soils. These data indicate that the kilogram-sized channel samples obtained for uranium-trend analyses clearly have the potential to incorporate multiple generations of mobile uranium fluxes.

4.2.4 Conclusions on uranium-trend data: Although no Quaternary dating technique is without potential uncertainties in how well the inherent assumptions are met, uranium-trend dating methods are considered fundamentally flawed from a technical viewpoint. Although the general philosophy of uranium migration through surficial deposits over time remains unchallenged, quantification of these open-system processes cannot be demonstrated. By definition, open-system processes are intractable because the historical record is incomplete. A more tractable problem is to prove that the uranium-decay systematics within a given component of soil has evolved as a closed system without showing the effects of subsequent uranium migration. Given the lack of methodological verification and the inherent uncertainties of open-system processes, we recommend in the strongest terms that all subsequent reference to and consideration of previously-published uranium-trend "ages" from soil profiles at Yucca Mountain and elsewhere be abandoned with regards to numerical age significance. No other uranium-series geochronologists have ever came to the defense of the technique or the published results resulting from its application.

4.3 Thermoluminescence

4.3.1 Methodology: The thermoluminescence (TL) dating method relies on metastable traps within the crystal lattices of certain minerals (primarily quartz and feldspar) that can be filled with electrons excited by interactions with alpha, beta, gamma and cosmic radiation sources. Trapped electrons are released by additional heat or electromagnetic energy sources (ultraviolet radiation) and are effectively reset by sunlight during eolian transport of fine-grained sediments. Following deposition and burial, the traps systematically refill with electrons as a result of the ambient radiation environment thereby acting as a natural radiation dosimeter. This natural radiation dose arises primarily from the decay of ^{40}K, ^{235}U and it's daughters (the ^{235}U decay chain), ^{238}U and its daughters, and ^{232}Th and it's daughters. Cosmic Rays and the decay of ^{87}Rb make lesser contributions. For TL dating, 4-11 μm silt is often used because all three types of radiation can penetrate grains of this size and the subsequent luminescence can easily escape to be detected upon laboratory heating (Wintle and Huntley, 1982).

When applied to dating sedimentary materials (sand, loess, or silt) thermoluminescence dating relies on the following assumptions: 1) during eolian or fluvial transport, mineral grains are exposed to sunlight of sufficient duration and intensity to clear the defect sites of electrons (reset the clock), and 2) following burial, exposure to natural ionizing radiation gradually repopulates the defect sites with electrons. A thermally-stimulated light emission (referred to as thermoluminescence signal), proportional to the concentration of trapped electrons, can be measured quantitatively in the laboratory. Light emission occurs during the transition of the metastable electrons from their trapped configurations to normal lattice positions occupying lower energy states and can be triggered by heating (Zeller, 1955). If the cumulative thermoluminescence signal can be related to the total radiation dose and dose history, then an age estimate can be directly obtained. In order to estimate the total cumulative dose, increments of known artificial radiation are added from a calibrated irradiator and the resulting luminescence signal measured. The response of the a suite of sub-samples artificially irradiated at different levels (curves with greater TL intensity than the one marked "Natural" on Fig. 5a) is compared to the response of the natural sample (no artificial irradiation; curve marked "Natural" on Fig. 5a) and a sunlight-bleached sub-sample (electron traps reset by exposure to sunlight; curve with lowest TL intensity on Fig. 5a) in order to obtain the total equivalent dose (ED). Ages are then calculated using the following equation

$$\text{Age} = \frac{\text{ED}}{\text{DR}}$$

where ED = radiation dose acquired by the sample [= signal/(signal/unit dose)] and DR = natural radiation dose rate (dose/ka). Techniques used in this study closely follow methods outlined in detail by Millard and Maat (1994).

A flow chart of the laboratory procedures for separating the silt from the bulk sample is shown in Figure 6. This separation pre-treatment typically takes one week for completion and four to six samples are processed through pre-treatment in parallel. After separation, the fine-silt-sized fraction (4-11 μm, polymineralic) is washed in 4N HCl (to remove carbonate) followed by a 30% H_2O_2 solution (to destroy organic carbonate) and dispersed in a sodium pyrophosphate solution. Fine-silt particles are plated onto 10 mm diameter aluminum disks (slurry taken to dryness by evaporation) and their luminescence measured by a brief pulse of infrared light to compensate for the effects of unequal sample amounts and distributions between disks resulting from variations inherent during plating (IRSL-normalization; see discussion below). Ideally, four experiments are conducted in order to obtain the final age estimate of a sample including sunlight sensitivity tests, anomalous fading tests (Wintle, 1973), a total bleach experiment (Singhvi and others, 1982) and a partial bleach experiment (Wintle and Huntley, 1980).

Before thermoluminescence measurements are made, disks are preheated at 124°C for 64 hours to remove the low-temperature, unstable electrons that are loosely held in traps (Wintle 1977; Berger 1985). Thermoluminescence measurements were made using a Daybreak Model 1100 Instrument with blue transmitting filters Schott UG-11 and Kopp 7-59. Blue wavelengths include quartz emissions and an apparently stable component of potassium feldspar emissions (Balescu and Lamothe, 1992). A heating

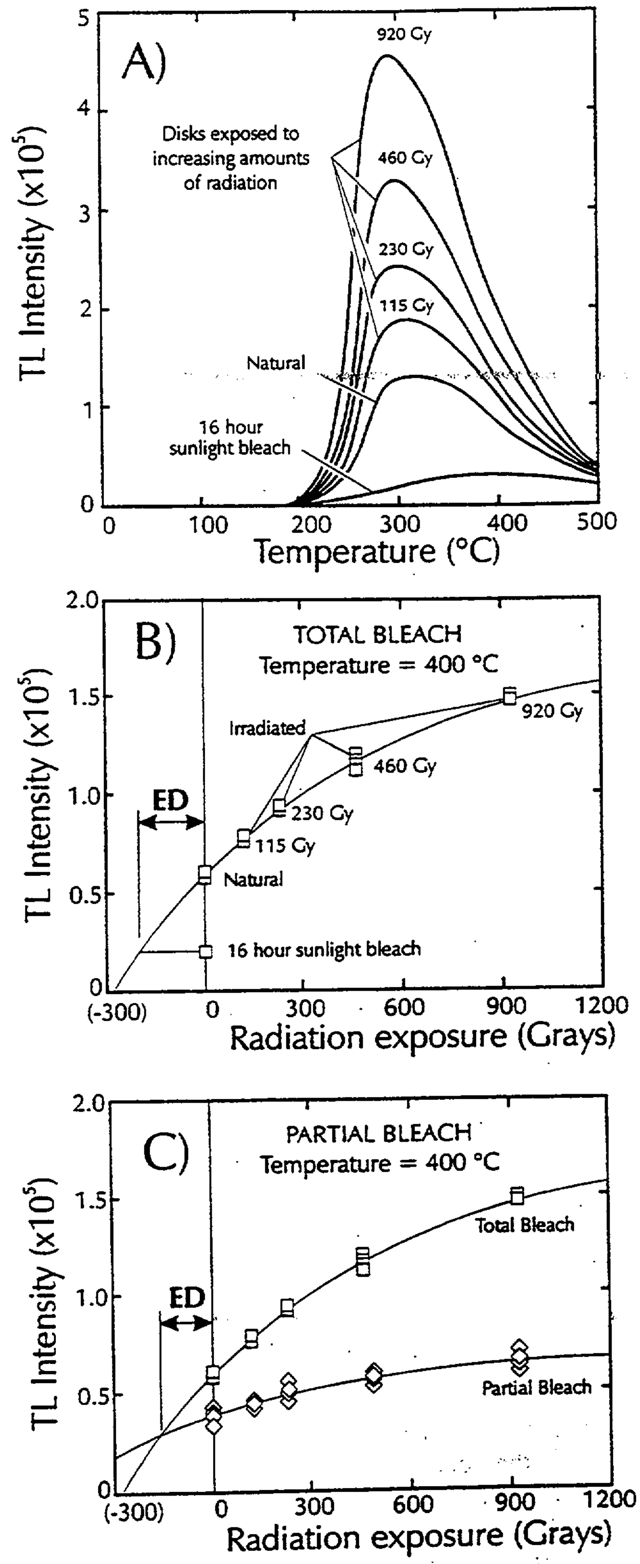

Figure 5: Example of TL data and techniques used to determine equivalent dose (ED). See text for further explanation. A) TL glow curves for irradiated, bleached, and natural disks from a single sample. B) TL growth curve at a single temperature showing determination of total bleach ED. C) Same sample showing partial bleach ED.

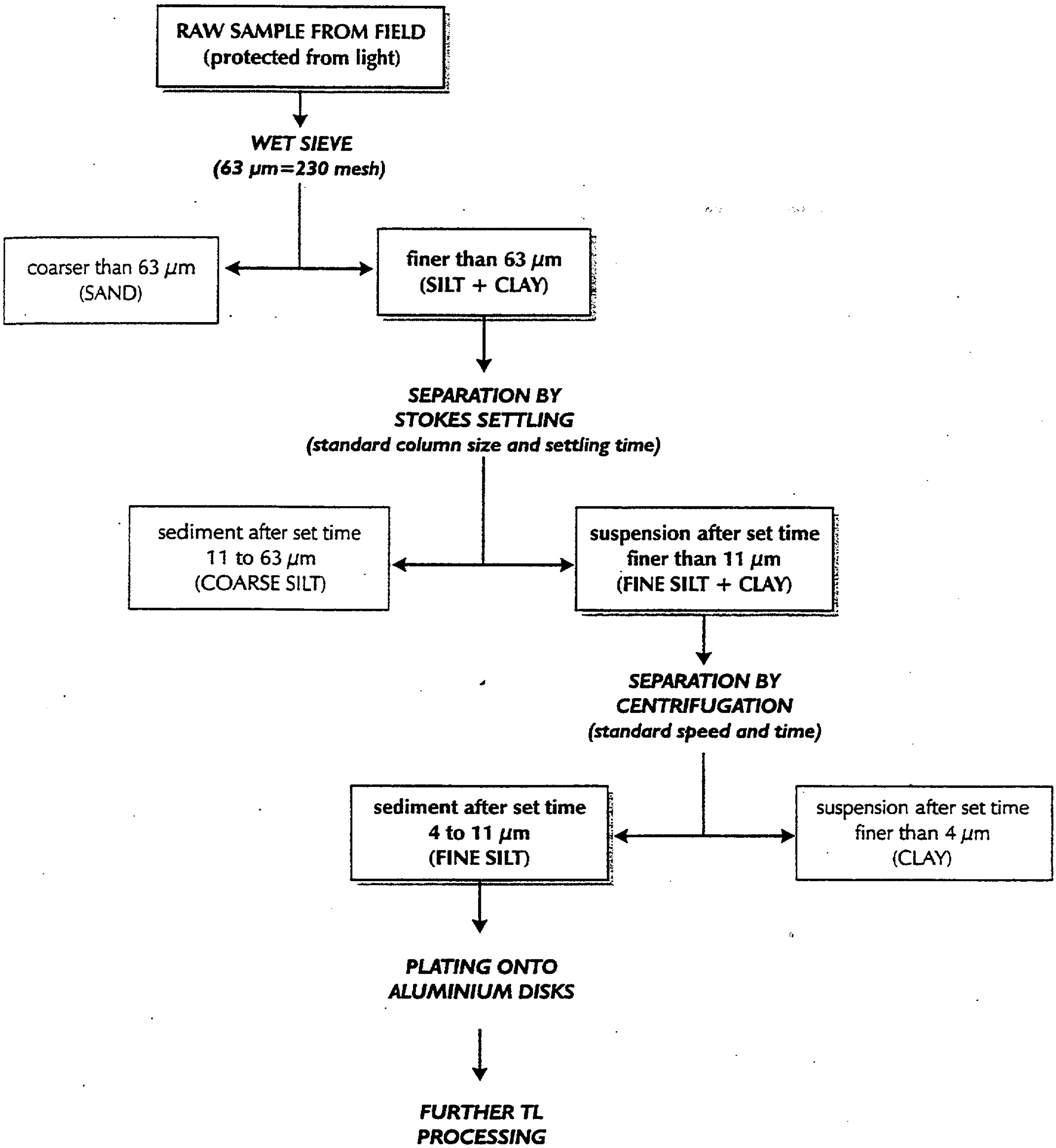

Figure 6: Flow diagram for sample pre-treatment processing of thermoluminescence samples. All processing done in laboratory under safe light conditions (after Millard and Maat, 1994).

rate of 5°C/s was employed and samples were heated in a nitrogen environment after initial evacuation of the glow oven.

The determination of sunlight sensitivity establishes the efficiency of natural sunlight for bleaching a given sample. The fraction of the thermoluminescence signal remaining at the various laboratory temperatures is plotted against the sunlight bleach time. The resulting family of curves is used to determine the best sunlight bleach times for the total bleach and partial bleach methods. Using natural sunlight (at 1800 m elevation), samples are taken through a series of approximately 10 bleach exposures ranging in duration from 5 to 1920 minutes.

The thermoluminescence technique requires that samples receive large doses of laboratory irradiation over a short period of time in contrast to the natural dose rates accumulated *in situ* over geologic time. As a means of assessing the response of each sample to calibrated beta sources and the effectiveness of the preheat treatment, tests for anomalous fading are conducted prior to final age estimation. Anomalous fading experiments allow both the stable and unstable components generated by the beta radiation source ($^{90}Sr \rightarrow ^{90}Y$) to be assessed, as well as an evaluation of how well the less-stable component is removed by preheating (Berger, 1992; Forman et al., 1987; Berger, 1987; Templer, 1985). Results from this experiment can be used to eliminate those samples which exhibit an extremely unstable thermoluminescence response which cannot be easily corrected with preheating, rendering the sample unsuitable for dating. Four sets of disks are exposed to radiation, and subsequently subjected to various combinations of preheat and storage prior to glowing. If ratios from the glow curve integrals between various combinations of these experimental conditions yield values of unity (within 10%), the sample is considered to be amenable to thermoluminescence dating. Samples with ratios outside of this range are either reconsidered separately or deemed unreliable for age interpretations. This experiment typically takes one month to complete.

The total bleach experiment generates growth curves by irradiating natural disks for various lengths of time on calibrated 100 mCi and 200 mCi $^{90}Sr \rightarrow ^{90}Y$ radiation sources (Fig. 5b). We chose the longest of these times to produce about eight times the assumed ED (based largely on the postulated age) for a particular sample. The resulting thermoluminescence signals are plotted against the artificial radiation dose and a growth curve is mathematically fit to the measured data. The growth curve defines the response of the sample to a range of radiation environments. This curve is then extended from the natural sample (no irradiation, no bleaching) to the intersection with a residual-level baseline defined by the thermoluminescence signal from a natural disk exposed to sunlight for 16 hours (zeroed TL state). The amount of radiation corresponding to the difference between the extended growth curve intersection point and zero (natural sample with no artificial irradiation) is used to estimate the cumulative dose acquired in the sample subsequent to last re-zeroing (amount of radiation equivalent to the line-segment labeled ED in Fig 5b). This procedure takes approximately two weeks to complete.

For the partial bleach experiment, the growth curve derived from the total bleach experiment is combined with a second growth curve generated by irradiating another set of plated disks and exposing them to sunlight for a period of time chosen (from the sunlight sensitivity test) to remove the rapidly-bleached component. The intersection of these two growth curves again defines an equivalent dose on the radiation axis (line-segment labeled ED in Fig. 5c). As with the total bleach method, uncertainty in the shapes of the growth curves introduces error into the determination of the equivalent dose. However, the error is greater than the total bleach method because two curves must be extrapolated instead of one. This procedure typically takes two weeks to complete and is only initiated after the total bleach experiment for a given sample is complete.

4.3.2 TL Sample Status and Progress Report: Initial thermoluminescence work in the Yucca Mountain area was conducted from 1984 through 1988, largely in support of paleoseismic studies (Forman, 1988). Work was reinitiated in 1992 using the USGS TL laboratory and has continued through the present. Results from samples collected during the more recent 1992-1995 period of study are shown in various tables presented below. Many of the these samples were collected for the purposes of evaluating fault movement from trenches exposing prominent Quaternary fault traces, as well as from more-stable alluvial surfaces. All samples were collected to avoid extensive bioturbation, contamination of silt material from above or below, and intense pedogenesis involving downward translocation of silt particles or changes in oxidation state leading to migration of radionuclides or their daughters in the decay chain. Samples are collected under a dark cloth or after sunset to avoid exposure to sunlight. *In situ* gamma spectrometry is performed at each sample site using a portable gamma spectrometer with a 3"x3" sodium iodide detector inserted 20" into the sample hole.

Two modern sediments were collected to test the assumption that materials in the Yucca Mountain area are sufficiently re-zeroed by sunlight during transport and sedimentation prior to burial. Samples consist of fine-grained eolian material collected beneath a living bush and fluvial material collected from the active channel of Sever Wash at the gap between Midway Valley and Fortymile Wash. Sunlight sensitivity tests were then performed on these samples. The eolian sample shows the same level of natural thermoluminescence intensity as those observed from sunlight-bleached disks. The fluvial sample shows minor amounts of thermoluminescence signal retention. The low level of thermoluminescence in this sample may be explained by incomplete resetting during fluvial transport or by the in situ accumulation of thermoluminescence response, or a combination of either. Both samples exhibit only one to two percent of the TL signal typically observed in young surface deposits. These results suggest that inherited thermoluminescence signals in Yucca Mountain samples are negligible. This assertion is supported by observations for silt-size material analyzed in this study that typically shows complete resetting to residual levels after as little as 15 minutes exposure to sunlight.

Luminescence intensity is a function of the number of trapped electrons and is dependent on both trapped-electron density (i.e., age), as well as the amount of silt being glowed. In order to correct for the variations of luminescence due to differences in mass arising from non-uniform silt coverage on aluminum disks, all plated disks from a given sample must be normalized to a common value (typically to the glow intensity of a plated disk closest to the average value of all disks treated under the same glow conditions). Two different normalization procedures are currently being evaluated: IRSL-normalization (Infra-Red Stimulated Luminescence) immediately after plating, and TL-normalization (re-irradiation of plated disks after laboratory heating for age determinations). In particular, samples collected from Lathrop Wells vicinity are being dated using both normalization techniques. Since at least one of these samples relies on being reset from the heat of the overlying basalt flow (Fig 52), rather than from sunlight, tests of the methods were thought to be relevant. Initial testing of the IRSL and TL-normalizations resulted in good agreement between the two normalization techniques. Additional experiments from other samples associated with basaltic ashfalls in the vicinity of the cone gave mixed results.

Sample TL-38 represents a re-sampling of a site previously analyzed by Steve Forman (1988) and resulted in ages that showed acceptable interlaboratory agreement using the TL-normalization procedures, but gave an age that was twice as old using IRSL-normalizations. Sample TL-40 also showed a large difference in ages calculated by the different normalization techniques. However, for two other duplicate samples of the same horizon (TL-39A and TL-39B) the difference in equivalent dose determinations resulted in age differences within the overall analytical uncertainty. All four samples, intended to date the same geologic datum (eolian activity prior to eruptive-event #2 airfall), give reasonable agreement using IRSL-normalizations. Comparisons of resulting ages obtained using both normalization techniques have previously been performed on loess samples from elsewhere in the middle and eastern parts of the U.S. (Millard and Maat, 1994). Results for these experiments show an equivalency between the two normalization techniques. Although most other thermoluminescence laboratories apply TL-normalization, polymineralic samples from the Yucca Mountain area are more mineralogically-complex (in particular, an abundance of devitrified tuff), and may not respond well with artificial irradiations after glowing to 500° C. Additional experiments are currently underway to evaluate these effects. All thermoluminescence dates quoted in this report use the IRSL-normalization unless specifically noted.

Grain mounts from various samples are in the initial stages of investigation and quantification. Preliminary data suggests there is a larger component of devitrified tuff (up to 40%) in the 4 to 11 μm silt portion than previously assumed. These grains consist of micron to sub-micron domains of unmixed quartz, and feldspar. In a few samples, biotite is present in this fraction, as well as small amounts of pyroxene. Zircon has been observed as an acid-resistant detrital phase in Yucca Mountain soils, however it has not yet been identified in the 4 to 11 μm silt fraction. Correlations between quality of the thermoluminescence behavior and mineral contents within a given sample remains to be determined.

Reproducibility and internal consistency of thermoluminescence age estimates are required to establish confidence in the dating technique. In general, where multiple thermoluminescence samples are present at a single site, resulting age estimates almost invariably show stratigraphic consistency although several exceptions have been observed. Several of these exceptions have been resampled (TL-02 resampled as TL-26; TL-15 resampled as TL-25; TL-17 resampled as TL-28) and in all cases, the second attempt resulted in age estimates with reduced uncertainties that were consistent with stratigraphy (Fig. 34 and 35). In the case of TL-17, geometric complexity in the third dimension is a likely causes for the discrepancy.

Interlaboratory comparisons also remains an important issue to resolve. Thermoluminescence standard materials do not exist. Acquisition of thermoluminescence ages on duplicates of the same Yucca Mountain sample by an independent laboratory would provide a test of our beta irradiator calibration, laboratory procedure, preheat and photomultiplier operations. In only case, noted above, where we collected a sample from the same site previously analyzed by Forman (1988), we obtained an identical age using TL-normalization (25 ka for TL-38, Table 31, compared to Forman's 24 ka and 29 ka results). Although the older ages obtained by using IRSL-normalization is preferred, the rest of the procedure appears to yield results that are reproducible in at least one other laboratory. This is an encouraging comparison, but additional tests need to be conducted.

4.4 Tephrochronology

4.4.1 Introduction: Tephrochronology is one of many dating methods used to determine ages of geologic materials (Rosholt et al., 1991). Its use depends on the identification of volcanic ash based on a unique set of chemical or petrographic parameters. In general, only widespread ashes are characterized completely enough for use as identifiable time horizons. Tephrochronology encompasses two sub-disciplines: tephrostratigraphy and tephrochronometry (Sarna-Wojcicki and Davis, 1991). Only tephrostratigraphy, the use of ash correlation to yield an age, has been used within the Yucca Mountain Project.

4.4.2 Potential uses in YMP: The loci of Quaternary volcanism in the western United States are fairly well known (Luedke and Smith, 1991). However, the distributions of major ash beds are not as well known due to their ephemeral nature and accompanying lack of preservation. While many ash beds could be preserved in the vicinity of Yucca Mountain, only the Bishop ash bed (0.74 Ma) and the Glass Mountain-D ash bed (1.0 Ma) have been recognized (Sarna-Wojcicki and others, 1991; Izett and others, 1988). There are other ash beds that could be present in soils around Yucca Mountain. These include the Lava Creek-B ash bed (0.62 Ma; Sarna-Wojcicki and others, 1991) and an ash bed exposed at Lake Tecopa (0.16 Ma; Morrison, 1991). These are ashes in the age range of surficial deposits exposed near Yucca Mountain with known exposures in southern Nevada.

Although large ash eruptions provide excellent time markers, there are some assumptions inherent to their use in chronostratigraphy. With the exception of areas of low-energy deposition (e.g. lakes), ash layers are rarely preserved without some reworking. Also, ash beds may be thickened in areas of eolian deposition. Therefore, the age of a correlated or dated ash bed is a maximum age for that portion of the sedimentary sequence. However, in cases where dilution of the ash by other detrital material is minimal, a resulting tephrostratigraphic age estimate is likely to be a close maximum.

4.4.3 Identification: Felsic ash beds are difficult to distinguish from one another because of their similar chemical compositions (Sarna-Wojcicki and Davis, 1991). This problem is compounded by the fact that multiple ash beds preserved in stratigraphic sections at distal sites often originate from different eruptions from the same volcanic center (i.e., Long Valley for Bishop and Glass Mountain ash beds). Furthermore, simple whole-rock chemical analyses must be avoided because of winnowing of phenocryst phases and inevitable contamination of the ash by other detritus in the environment of deposition. Therefore, the chemical analyses are performed on separated glass shards. The problem of contamination is exacerbated around Yucca Mountain because the background sedimentary component contains substantial amounts of pre-Quaternary felsic volcanic detritus.

4.4.4 Affinity of two unknown felsic ash samples: As part of the effort to map surficial deposits in the Yucca Mountain vicinity, S. Lundstrom collected two samples of slightly reworked volcanic ash from lenses in alluvium underlying younger surficial deposits. Figure 7 shows this locality in Yucca Wash as well as localities of previously identified ash beds from Izett and others (1988). Glass was separated from these samples by flotation in a sodium polytungstate solution followed by a quick, cold HF leach and analyzed for trace elements by energy dispersive x-ray fluorescence. The data from these two samples, as well as published data on previously identified ash beds from southern Nye County, are given in Table 1.

A sample of an ash bed identified by Izett and others (1988) as Glass Mountain-D is included for comparison. These data are plotted relative to the Bishop Tuff air-fall average (Izett et al., 1988) in Figure 8. These data show that there are potential problems in correlating the Yucca Wash ash bed with Bishop ash beds identified at nearby localities. Also evident is the significant differences between the two samples from Yucca Wash. The samples do not correlate well with the Glass Mountain-D ash bed either. Possible explanations for these differences include the use of different procedures for separating the glass from phenocrysts and alteration products, and the use of different analytical methods (Izett and others (1988) used neutron activation). Therefore, although these samples may be correlative with the Bishop ash, these chemical parameters are, at best, weak evidence for this identification.

Strontium isotope ratios were also measured on the glass separates from the Yucca Wash ash bed. These data are presented in Table 2 along with data from the literature on Bishop Tuff air-fall. Sample HD-1017 has a similar strontium composition to Bishop ash, but HD-1016 is substantially more radiogenic. Earliest Bishop Tuff tends to be more radiogenic (Halliday et al., 1984) as do the Glass Mountain eruptions from the same caldera (Halliday et al., 1989).

It seems possible that the two Yucca Wash samples are indeed Bishop ash, but more careful separations, chemical procedures and sample collection need to be carried out to positively confirm or deny this correlation. New localities have been identified during mapping of surficial deposits and these, as well as the known localities (Izett et al., 1988), will be sampled by the end of this fiscal year. These samples will be treated identically for more comparable analytical results.

4.4.5 Basaltic ashes: In addition to widely dispersed felsic ashes, a number of localities at Yucca Mountain contain fissuring fillings and stratabound sandy horizons containing significant components of fine basaltic ash. Since ash clouds associated with basaltic eruptions do not attain the great heights possible in more volatile-rich and energetic felsic eruptions, the sources for basaltic ash must have a more local source. The Yucca Mountain Project volcanism program addresses the issues of basaltic volcanism in the local vicinity through the efforts of research being done through Los Alamos National Laboratories (LANL). It was hoped that the presence of these basaltic ash occurrences could be chemically correlated with dated eruptive events from the small number of local Quaternary eruptive sources. These sources include Lathrop Wells, Sleeping Buttes and Crater Flat cones.

To date, no unequivocal primary airfall tephra deposits have been identified in any of the trenches or exposures at Yucca Mountain. Typically, basaltic ash constitutes only a dilute, though recognizable, constituent in some of the eolian strata; generally at concentrations less than 10%. This fact significantly reduces the amount of geochronologic information that can be interpreted from these occurrences. The time required between eruption and mixing with other non-basaltic detrital constituents is unknown, although it is generally perceived that the presence of the ash represents at least a maximum age for that strata (the eolian deposit can be no older than the eruptive age of the ash). Ash is found in greater concentrations only in several fissure filling occurrences on the west side of Yucca Mountain. The most striking example is at the base of the ~0.3 m wide fissure in Solitario Canyon Fault Trench 8 (see Fig. 38), although ash is also present in fault fissures in other Solitario Canyon Fault trenches and Crater Flat Trench CF1 (Fatigue Wash Fault). These occurrences may be important not only for tephrochronological purposes, but also for the implications regarding coupled tectonic and volcanic processes.

Geochemical characterization of the basalts in the Yucca Mountain region allows discrimination

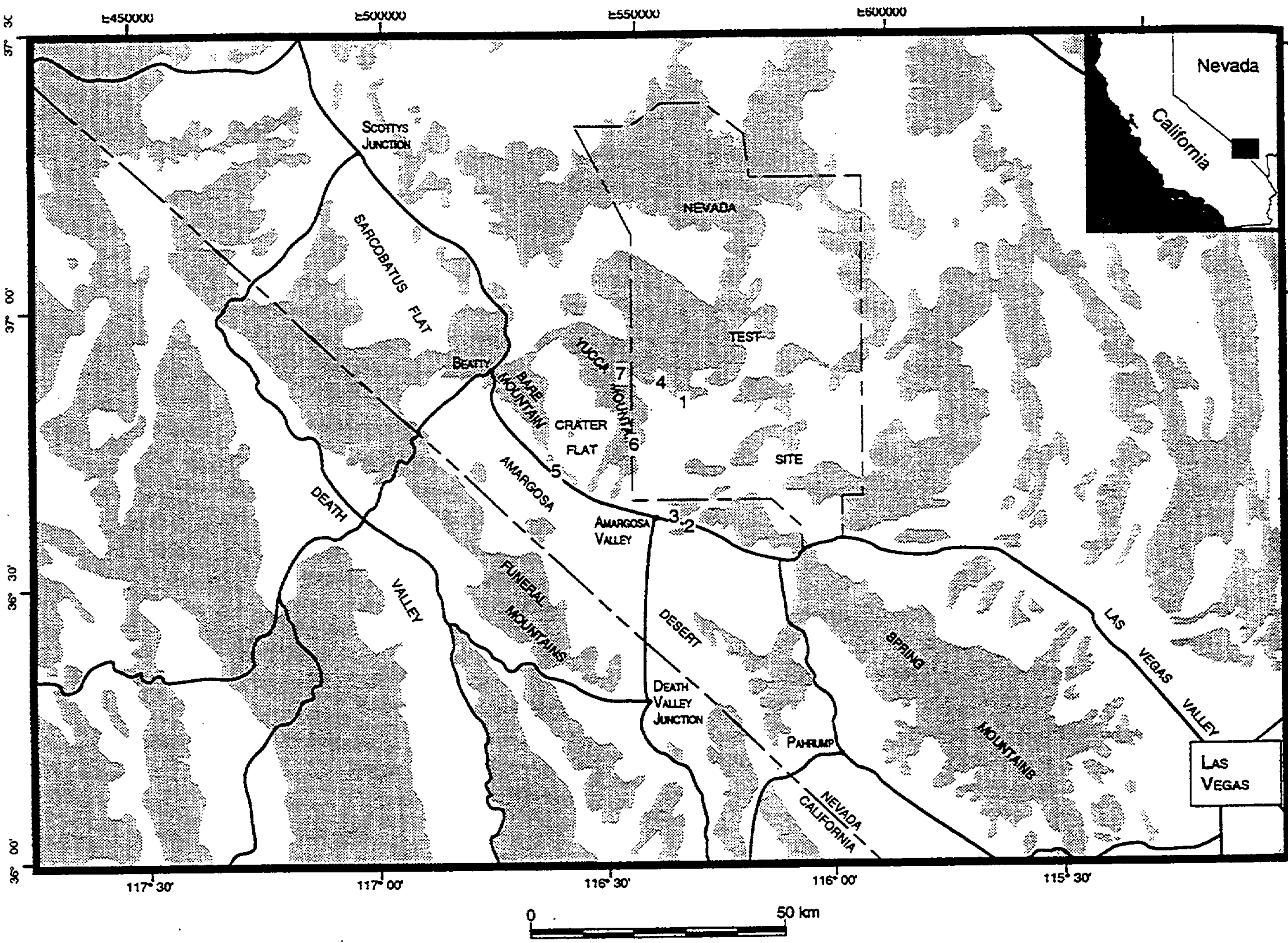

Figure 7. Map showing ash bed localities numbered 1-7.

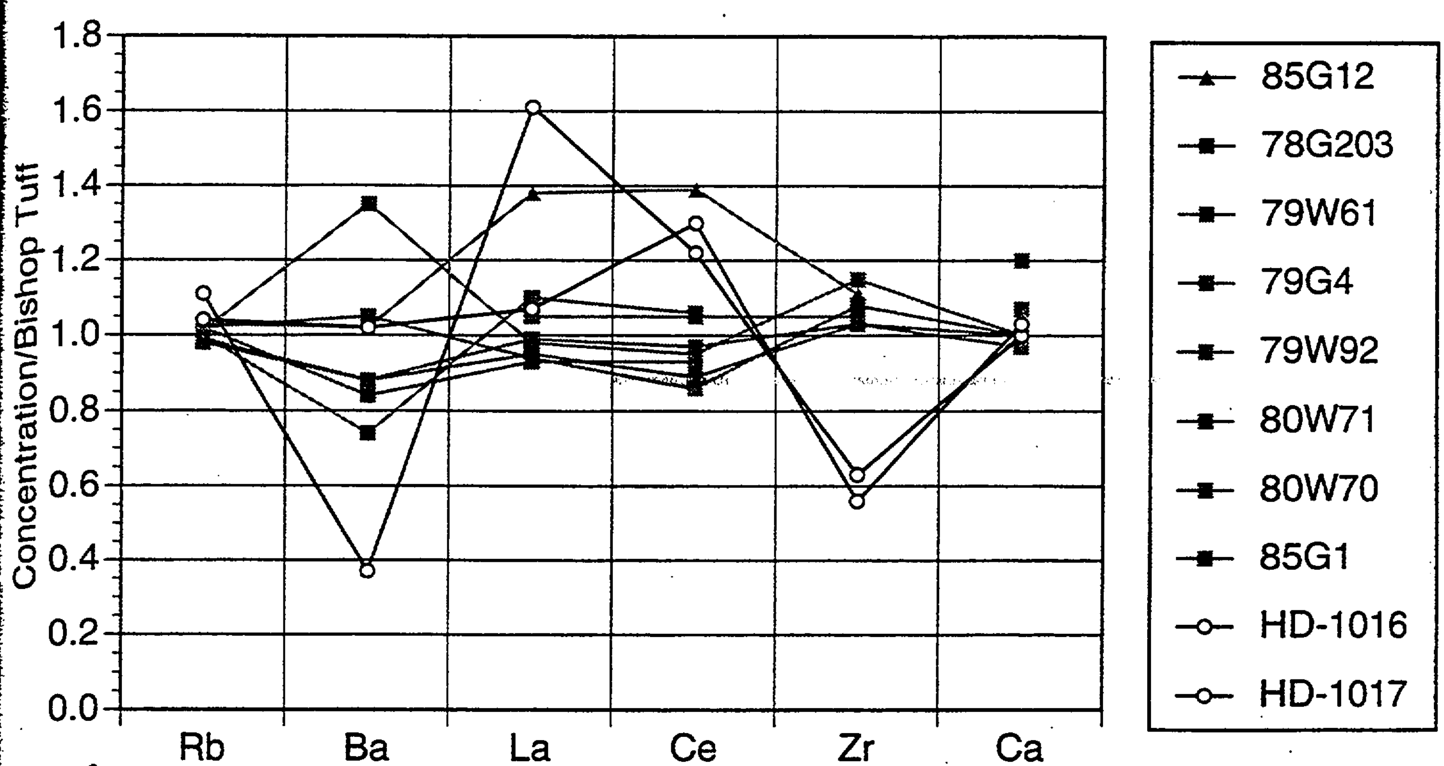

Figure 8. Concentrations of selected elements in two unknown ash samples as compared to Bishop ash bed and Glass Mountain-D ash bed (Izett and others, 1988); concentrations are normalized to average Bishop Tuff air-fall (Izett and others, 1988).

Table 1. Selected elemental concentrations in ash beds from southern Nye County, Nevada

Loc #	Sample ID	Locality	Rb[1]	Ba[1]	La[1]	Ce[1]	Zr[1]	Ca[2]
Bishop ash (Nye County, Nevada)[3]								
1	78G203	Jackass Flats	159	38	16.0	32.2	124	0.30
2	79W61	Skeleton Hills	162	58	16.5	34.3	138	0.30
3	79G4	Striped Hills	163	45	15.8	31.3	129	0.30
4	79W92	Calico Hills	157	38	16.7	35.1	124	0.29
5	80W71	Big Dune quad	163	36	15.7	33.8		0.36
5	80W70	Big Dune quad	160	32	18.4	38.4		0.32
6	85G1	Busted Butte	161		17.7	37.9	126	
Bishop Tuff air-fall mean composition[3]			160	43	16.8	36.2	120	0.30
Glass Mountain-D (Nye County, Nevada)[3]								
6	85G12	Busted Butte	165	44	23.1	50.2	133	
Unknown ash lens[4]								
7	HD-1016	Yucca Wash	177	16	27	44	76	0.30
7	HD-1017	Yucca Wash	167	44	18	47	67	0.31

1 In ppm by weight.
2 In percent by weight.
3 From Izett and others (1988).
4 Collected by S. Lundstrom (SPC00009744 and SPC00009745, respectively).

Table 2. Strontium isotopic compositions of Yucca Wash ash bed and Bishop Tuff air-fall.

Sample (reference)	$^{87}Sr/^{86}Sr$
HD-1016 (this report)	.71098
HD-1017 (this report)	.70974
BT-6 (Christensen and DePaolo, 1993)	.70969[1]
B104 (Halliday and others, 1984)[2]	.70939[1]

1 Corrected to our measured NBS-987 value of .71025.
2 Whole rock sample; glass would have a higher ratio.

between most of the various eruptive centers. Discrimination is based largely on incompatible trace element concentrations and ratios. Thorium exhibits some of the widest variations in concentrations between the centers and is particularly diagnostic when coupled against other constituents such as the rare earth element contents (Frank Perry, written communication, 1995). Thorium contents in the Quaternary centers exhibit variations from 6 to 7.5 ppm for Lathrop Wells, 8.3 to 8.7 ppm for Little Black Peak and 11 to 12 ppm for Hidden Cone (both from the Sleeping Butte center), and typically >9 ppm for the 1200 ka cycle of eruptions in Crater Flat (Frank Perry, written communication, 1995).

Basaltic ashes from four Yucca Mountain localities were concentrated, cleaned, and submitted to LANL for geochemical analysis by instrumental neutron activation analysis and X-ray fluorescence. Results for a suite of major and trace-elements are not available at the present time, however thorium concentrations have been measured by isotope dilution at the U.S. Geological Survey. These results are listed in Table 3. Samples of ash concentrate from Solitario Canyon Trench 8 (HD1070-BA, Fig. 38), Crater Flat Trench CF1 (HD1728-BA, Fig. 44) and Stagecoach Road Trench 1 (HD1826-BA, Fig. 34) have thorium contents ranging from 7.2 to 7.4. These concentrations are within the range of values observed for the three major cycles of activity at Lathrop Wells. In particular, thorium concentration from the ash sampled at the base of the Solitario Canyon Fault Trench 8 fissure is inconsistent with the bulk of materials erupted from the million year old cycle from Crater Flat centers (Northern Cone, Black Cone, and Red Cone), although the results may overlap products from the Little Cone center.

In contrast, sample HD1628-ID from Alice Ridge Trench A1 (Fig. 12) has a significantly higher thorium content of 8.5 ppm. This is clearly outside the range of Lathrop Wells eruptive products but is identical to the compositions of basalt from Little Black Peak at Sleeping Butte. This interpretation is consistent with geochronological data from both Trench A1 (ash occurs at the base of an eolian unit containing rhizoliths with ages between 220 and 270 ka) and from Little Black Peak (~300 ka, REF).

Final interpretation of basaltic ash data is not possible at the current time pending final geochemical results, geochemical correlation models (including elemental ratio discrimination), and final age estimates for Lathrop Wells eruptive cycles. If final data treatment, based on a more convincing set of geochemical criteria than the preliminary thorium concentrations provided here, permit interpretation of consistent results, several other strata containing dilute basaltic ash, as well as trenches with fissures exhibiting cross-cutting relationships that include both an older and a younger ash, can be investigated further.

5. DATA PRESENTATION

5.1 Format of Presentation

All geochronological data currently available are presented in the following series of tables and illustrations organized on a trench-by-trench basis.

5.1.1 Uranium-series disequilibrium data: Uranium-series disequilibrium data are presented in tables giving a minimum of sample weights, uranium and thorium concentrations, $^{230}Th/^{232}Th$ activity ratios, detritus-corrected $^{230}Th/U$ ages and initial $^{234}U/^{238}U$ ratios, and a brief description of the sample and aliquot type. Correction for a detrital component involves subtraction of an appropriate amount of ^{234}U, ^{238}U, and ^{230}Th, based on the observed $^{232}Th/^{238}U$ ratio and the assumption that the detrital component has isotopic compositions appropriate to a secular equilibrium material with an atomic Th/U ratio of 4. Data from mass spectrometric and alpha spectrometric analytical techniques have been kept separate on different tables. In addition, minimum $^{230}Th/U$ ages are given for some samples and represent the calculated finite ages using $^{234}U/^{238}U$ and $^{230}Th/^{238}U$ at the upper and lower limits, respectively, of their analytical uncertainty. $^{234}U/^{238}U$ ages are also given for some samples with $^{230}Th/U$ ages greater than 500 ka, but with present-day $^{234}U/^{238}U$ greater than unity. These ages assume an initial $^{234}U/^{238}U$ of about 1.65 ± 0.20 plus analytical uncertainties. Alpha-spectrometry tables also include data for leaches and residues and the mathematical recombinations to obtain whole-rock sums. Ages are given only for total digestions (sub-samples designated by the suffix *-W*) and for leach-residue recombinations (sub-samples designated by the suffix *sum*).

In addition to data present in tabular form, detritus-corrected $^{230}Th/^{238}U$-$^{234}U/^{238}U$ data are shown on uranium-series disequilibrium evolution plots. These are useful for several reasons. First, they provide a means by which to critically evaluate

Table 3: Uranium and thorium concentrations in basaltic ash samples from Yucca Mountain localities determined by isotope dilution analysis. All uncertainties are given at the 95% confidence level.

Sample Name	Location	Sample type	Elemental Concentration	
			U ppm	Th ppm
Basaltic ash concentrates from statabound or fissure occurrences in Yucca Mountain Trenches				
HD1628-ID	Alice Ridge Trench A1	Stratabound eolian unit	2.123 ± 0.006	8.479 ± 0.050
HD1070-BA	Solitario Canyon Trench #8	Fissure filling	2.118 ± 0.007	7.386 ± 0.032
HD1728-BA	Crater Flat Trench CF1	Fissure filling	2.213 ± 0.007	7.203 ± 0.034
HD1826-BA	Stagecoach Road Trench #1	Stratabound eolian unit	1.965 ± 0.006	7.365 ± 0.032
Basaltic ash concentrates from airfall sheet #2 proximal to Lathrop Wells cinder cone				
HD1632-C	Lathrop Wells cone	Primary airfall deposit	1.858 ± 0.010	6.670 ± 0.043
LW122-FVP BA	Lathrop Wells cone	Primary airfall deposit	1.967 ± 0.007	7.826 ± 0.034
Lathrop Wells basalt used as a LANL in-house geochemical standard.				
LW27-FVP-P7A	Lathrop Wells cone	Basalt lava flow	2.015 ± 0.009	7.008 ± 0.044
LW27-FVP-P7B	Lathrop Wells cone	Basalt lava flow	2.019 ± 0.007	6.992 ± 0.045

the closed-system evolution required of the $^{230}Th/U$ age estimation. The curved evolution lines (concordia) represent the loci of $^{230}Th/^{238}U$ and $^{234}U/^{238}U$ compositions for two hypothetical systems evolving with time assuming no initial $^{230}Th/^{238}U$ (all ^{230}Th derived through ^{238}U decay, i.e., no detrital thorium) and starting $^{234}U/^{238}U$ compositions of 1.4 and 1.8. Straight lines connecting the two concordia represent $^{230}Th/U$ isochrons that become more closely-spaced as the upper limit of the $^{230}Th/U$ clock is approached. The $^{230}Th/^{238}U$ of samples experiencing open-system uranium loss will be modified to increased, and will yield either apparent ages that are older than the true ages, or excess ^{230}Th, in which case, the points will be moved to the right of the evolution curve limit. Closed-system evolution of materials with uniform $^{234}U/^{238}U$ will also follow curved paths similar to the ones shown for starting compositions of 1.4 and 1.8. The vast majority of data shown in these plots (size of the error ellipses corresponds to propagated analytical uncertainties and detrital-correction uncertainties) fall within the finite-age field (to the left of the infinite-age isochron) or along the concordia down to secular equilibrium values of unity. Samples older than about 300 ka are extremely susceptible to disruption by uranium loss, yet very few plot to the right of the limiting concordia. These older samples show no evidence for more-recent uranium mobility. Although younger samples do not incorporate a similar geochemical check, they are not expected to behave in a significanlty different fashion. In addition, the vast majority of the data fall with the bounds defined by initial $^{234}U/^{238}U$ of 1.4 and 1.8 evolution curves. This observation suggests a restricted range of initial $^{234}U/^{238}U$ in the pedogenic environment at Yucca Mountain. The uniformity of this value is used to help identify analytically-questionable results. Data which yield finite $^{230}Th/U$ ages with calculated initial $^{234}U/^{238}U$ of greater than 2 or less than 1.2 are generally considered suspect until additional data can confirm these anomalies.

The distributions of detritally-corrected uranium-series disequilibrium ages (symbols) and uncertainties (shaded horizontal bars) are also shown on cluster plots with age given on the abscissa in log units. All dates are $^{230}Th/U$ ages unless otherwise noted. Different symbols denote the different types of samples analyzed. The purpose of these plots is to allow a rapid visualization of the size of the sample population (i.e., the number of analyses), the distribution of ages within the sample population and an assessment of the types of materials that were analyzed. In general, a greater degree of confidence can be placed in the age of a sample that exhibits a clustering of age determinations, and a smaller degree where only a few ages that show a large degree of dispersion are available for a given sample.

5.1.2 Thermoluminescence data: Thermoluminescence data are presented in tables summarizing all available data up to as recently as the middle of August 1995. Field and saturation moisture contents are determined by differences in weight between low-temperature oven-dried sediment and the unmodified sediment, and sediment that has been centrifuged at speeds approximating the sample's overburden, respectively (Millard and Maat, 1994, Appendix C). Radiation doses are measured *in situ* and are converted to dose rates, given in grays per thousand years, using both the field and saturation moisture levels. Saturation moisture dose rates are always lower than field moisture dose rates due to the greater absorptive capacity of water filling pore space relative to air. Equivalent doses are given, in grays, for both total bleach and partial bleach experiments. Unless otherwise noted, equivalent doses have been determined using IRSL normalization. Doses, as well as ages, are given for both IRSL and TL normalizations where the additional information is available. Total bleach ages and partial bleach ages are presented using dose rates calculated for both the field and saturation moisture levels. Considering the anomalously arid conditions at present, ages somewhat greater than those calculated for field moisture contents for sediments greater than about 5 ka are likely. The total range in ages is given for both total and partial bleach experiments and is simply the analytical uncertainty subtracted from the field moisture age and added to the saturation moisture age.

TL a moisture

5.1.3 Logs/diagrams showing geochronologic data: Schematic diagrams showing the relationships between samples and generalized stratigraphy are presented for most sites. These graphics are included to aid in evaluation of age information within stratigraphic contexts and to provide a ready means of comparison between uranium-series disequilibrium and thermoluminescence data. Age estimates for each analyzed sample are compiled from the appropriate tables are listed along with a brief description of the material in the case of uranium-series disequilibrium results. All age estimates are given in ka. Thermoluminescence results are given as the age estimate calculated using the field moisture dose rate in boldface, followed by the whole age range in parentheses.

5.2 Systematic Data Presentation

5.2.1 Rock Valley Fault system

Trenches RV3/3a and RV4/4TP2

Table 4: Mass spectrometric U-series results from Rock Valley

Figure 9: U-series concordia plot for samples from Rock Valley

Table 5: Thermoluminescence results for Rock Valley samples

Table 4: Uranium-series disequilibrium results from Rock Valley Trenches 4 and 3a. Data determined by mass spectrometry. All errors are given at the 95% confidence level.

Sample Name	Sample wt. (g)	Concentration U ppm	Concentration Th ppm	$^{230}Th/^{232}Th$ activity	Detritus-corrected Age (ka)	Detritus-corrected $^{234}U/^{238}U_{initial}$	Sample Type
Trench 4, south wall, east end (sta.8 to 22)): Rhizoliths in a gravelly-alluvial unit underlying main carbonate soil.							
HD1803-B1	0.467	12.5	0.0113	1160	26.5 ± 0.2	1.617 ± 0.009	Individual rhizolith
Trench 4, south wall, east end (sta.7.6: Calcrete containing thin lenses of carbonate/opal, ~20 cm below Bt-K boundary.							
HD1805-E1	0.260	14.6	0.367	25.6	16.4 ± 0.3	1.489 ± 0.008	Si-rich stringer in coarse sand matrix
Trench 3a, west wall: Weak soil in pebble conglomerate containing a discontinuous opal stringer below sandy lens.							
HD1813-A	0.325	19.1	4.82	0.96	1.2 ± 3.1	1.372 ± 0.017	Very thin Si-rich stringer in sandy matrix
HD1813-B	0.388	19.6	4.76	1.11	2.2 ± 2.9	1.402 ± 0.017	Very thin Si-rich stringer in sandy matrix

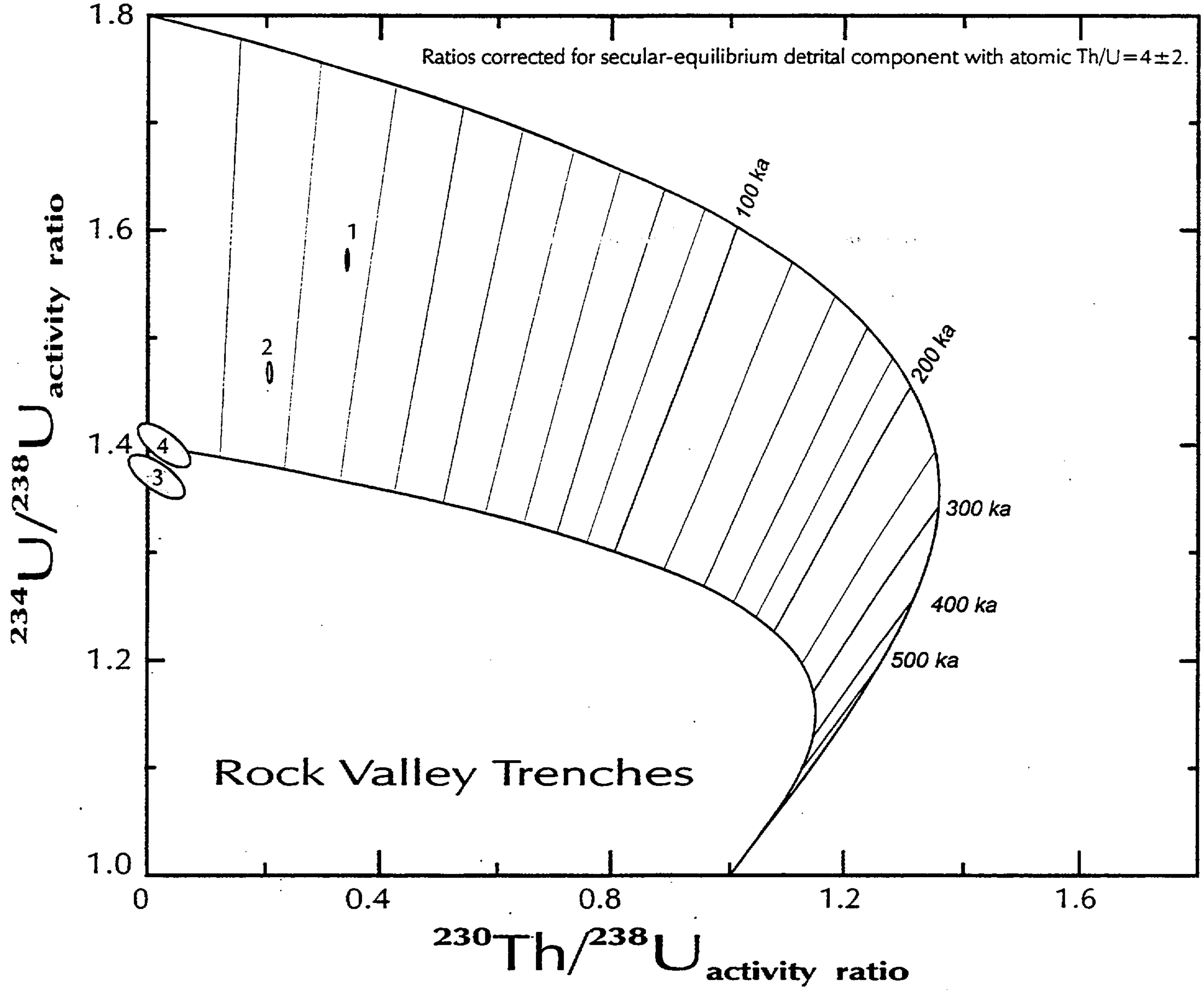

Figure 9: Uranium series disequilibrium evolution diagram showing analyses of samples from Rock Valley Trenches 4a and 3. Error ellipses from the same sample are shaded in the same pattern. Data are given in Table 4 and correspond to the following sample names: 1=HD1803-B1; 2=HD1805-E1; 3=HD1813-A; and 4=HD1813-B.

d:\ym\data\tecton\rv\rv-ccrd.cdr
date updated: 8/23/95

Table 5: Thermoluminescence results from Rock Valley Trenches 3, 3a, 4 and 4TP2. All errors given at the 95% confidence limit.

Sample Name	Field Moist. (%)	Saturation Moist. (%)	Dose Rate (Gy/ka)		Total Bleach Eqivalent Dose (Gy)	Total Bleach Age (ka)			Partial Bleach Eqivalent Dose (Gy)	Partial Bleach Age (ka)		
			Field H_2O	Saturation H_2O		for field moisture H_2O	for saturation moisture H_2O	Total Range		for field moisture H_2O	for saturation moisture H_2O	Total Range
TL-57	*[Trench RV-3, west wall, approx. 160 cm above level line at sta. 16.8 and about 28 cm below surface: brown silty horizon overlying reddened Bt horizon]*											
	DATA NOT AVAILABLE AT PRESENT											
TL-58	*[Trench RV-3a, east wall, ~11 m north of the south end of the trench, 120 cm below surface: Sandy lens within alluvial channel. Oldest unfaulted unit.]*											
	DATA NOT AVAILABLE AT PRESENT											
TL-53	*[Trench RV-4, east wall, upper bench within zone representing main fault trace: Buried Av plus underlying brown sandy material.]*											
	7.3	18	5.4±0.4	4.7±0.4	13 ± 3	2.5 ± 0.5	2.8 ± 0.6	2.0-3.4				
TL-54	*[Trench RV-4, south wall near east end of trench, ~25 cm below level line @ sta. 12.8: Silty-sand lens in a fine-grained alluvial gravel]*											
	0.1	23	5.7±0.4	4.5±0.3	506 ± 415	88 ± 72	113 ± 93	16-206				
TL-55	*[Trench RV-4TP2, east wall, sampled within fissure: Reddened, clay-rich fissure-fill.]*											
	13	23	5.6±0.4	5.0±0.4	53 ± 2	10 ± 1	11 ± 1	9-12				
TL-56	*[Trench RV-4TP2, west wall in center of main fissure: Fissure fill across trench from TL-55, but material is browner and less clay-rich]*											
	DATA NOT AVAILABLE AT PRESENT											

5.2.2 Paintbrush Canyon Fault

5.2.2.1 Alice Ridge

Table 6: Mass spectrometric U-series results from Alice Ridge Trench A1

Figure 10: U-series concordia plot for samples from Alice Ridge Trench A1

Figure 11: Distributions of U-series ages for Alice Ridge Trench A1 samples

Table 7: Thermoluminescence results for Alice Ridge Trench A1 samples

Figure 12: Schematic log of Alice Ridge Trench A1 showing dating results

Table 6: Uranium-series disequilibrium results from Alice Ridge Trench A1. Data determined by mass spectrometry
All errors are given at the 95% confidence limit.

Sample Name	Sample wt. (g)	Concentration U ppm	Concentration Th ppm	$^{230}Th/^{232}Th$ activity	Detritus-corrected Age (ka)	Detritus-corrected $^{234}U/^{238}U_{initial}$	Sample Type
North wall, Unit 3b of Ponti (1995): Laminar soil carbonate near top of the Unit 3/4 carbonate soil.							
HD1622-U1	0.083	4.94	1.69	2.7	16 ± 4	1.67 ± 0.04	Carbonate-rich rootlet mass
HD1622-U2	0.074	6.09	1.18	3.8	14 ± 2	1.67 ± 0.02	Carbonate-rich rootlet mass
South wall, Unit 2b of Ponti (1995): Well-preserved rhizoliths in clast-poor sandy horizon just above the Unit 2 carbonate soil.							
HD1623-U1	0.059	9.33	0.392	88.5	224 ± 21	1.61 ± 0.07	Individual Rhizolith
HD1623-U2	0.107	21.5	0.258	265.1	126 ± 7	1.64 ± 0.05	Individual Rhizolith
HD1624-U1	0.041	4.58	0.403	25.2	71 ± 2	1.579 ± 0.012	Individual Rhizolith
HD1624-U2	0.099	4.77	1.00	17.2	195 ± 18	1.62 ± 0.07	Individual Rhizolith
HD1624-U4	0.141	8.92	0.607	55.5	266 ± 9	1.61 ± 0.02	Individual Rhizolith
HD1624-U5 opal	0.092	7.83	0.330	85.1	218 ± 6	1.55 ± 0.02	Individual Rhizolith
South wall of slot, Unit 1b of Ponti (1995): Layer of carbonate about 30 cm below the top K horizon associated with the Unit 1carbonate soil.							
HD1625-A1a	0.349	9.49	2.26	15.1	700 +inf/-200	2.0 ± 0.2	Si-rich clast rind
HD1625-C1a	0.226	4.23	3.67	3.8	900 +inf/-420	2.0 ± 0.2	Si-rich clast rind
HD1625-C1b	0.151	21.2	1.28	64.7	Excess Th	undefined	Cc-Si rootlet mass
HD1625-U1	0.133	8.31	2.70	11.2	640 +inf/-180	2.0 ± 0.2	Cc-Si rootlet mass
North wall of slot, Unit 1b of Ponti (1995): Clasts with thin Si-Cc rinds in sandy matrix ~100 cm below the top of the Unit 1 carbonate soil							
HD1626-B1a	0.136	2.81	4.56	1.9	~secular equilibrium	undefined	Si-rich clast rind
HD1626-C1a	0.073	3.02	3.25	2.9	Excess Th	Depleted 234U	Si-rich clast rind
HD1626-D1	0.082	3.15	3.90	2.5	Excess Th	Depleted 234U	Si-rich clast rind
HD1626-U2a	0.088	2.43	5.58	1.3	Excess Th	Depleted 234U	Si-rich clast rind
South wall of slot, Unit 1b/c of Ponti (1995): Large (8 cm diameter) rhizolith oriented sub-horizontally adjacent to fault							
HD1627-U1	0.014	10.1	0.362	92.4	129 ± 3	1.72 ± 0.012	Si-rich rhizolith domain
HD1627-U2	0.051	2.84	0.283	46.7	403 +64/-47	2.4 ± 0.2	Cc-rich rhizolith domain
South wall of slot, Unit 2a/b of Ponti (1995): Irregular pod of loose sand with ~10% coarse, basaltic ash. Apparently strata-bound.							
HD1628-ID	0.057	2.12	8.48				Basalt ash concentrate
North wall, Unit 3a of Ponti (1995): Distinct thin (2-5 cm) layer of carbonate dipping easterly at low angle. Apparently fault controlled.							
HD1640-A2	0.049	9.57	2.10	14.0	134 ± 5	1.53 ± 0.02	Si-rich clast rind
HD1640-B1	0.026	9.54	1.04	28.2	127 ± 4	1.58 ± 0.02	Si-rich clast rind

Table 6: continued.

Sample Name	Sample wt. (g)	Concentration		$^{230}Th/^{232}Th$	Detritus-corrected		Sample Type
		U ppm	Th ppm	activity	Age (ka)	$^{234}U/^{238}U_{initial}$	
North wall, Unit 3a/b of Ponti (1995): Carbonate-coated clasts and cemented sandy matrix within the Unit 3/4 carbonate soil.							
HD1641-A1	0.013	9.36	1.41	18.2	101 ± 4	1.57 ± 0.02	Si-rich clast rind
HD1641-A2	0.285	9.69	2.62	9.0	85 ± 4	1.53 ± 0.03	Si-rich clast rind
HD1641-B1	0.018	10.5	1.67	16.8	102 ± 4	1.52 ± 0.02	Si-rich clast rind
HD1641-C1	0.124	9.22	1.40	7.1	26.1 ± 1.7	1.56 ± 0.02	Si-rich seam in sandy matrix
North wall, Unit 2c of Ponti (1995): Thin layer of carbonate below the bulk of the upper-most soil, and above the Unit 2 carbonate soil							
HD1643-A1	0.198	6.12	0.371	61.0	193 ± 6	1.66 ± 0.02	Si-rich seam in rootlet mass
HD1643-A2	0.175	3.17	0.626	21.7	351 ± +79/-51	2.00 ± 0.19	Si-rich seam in rootlet mass

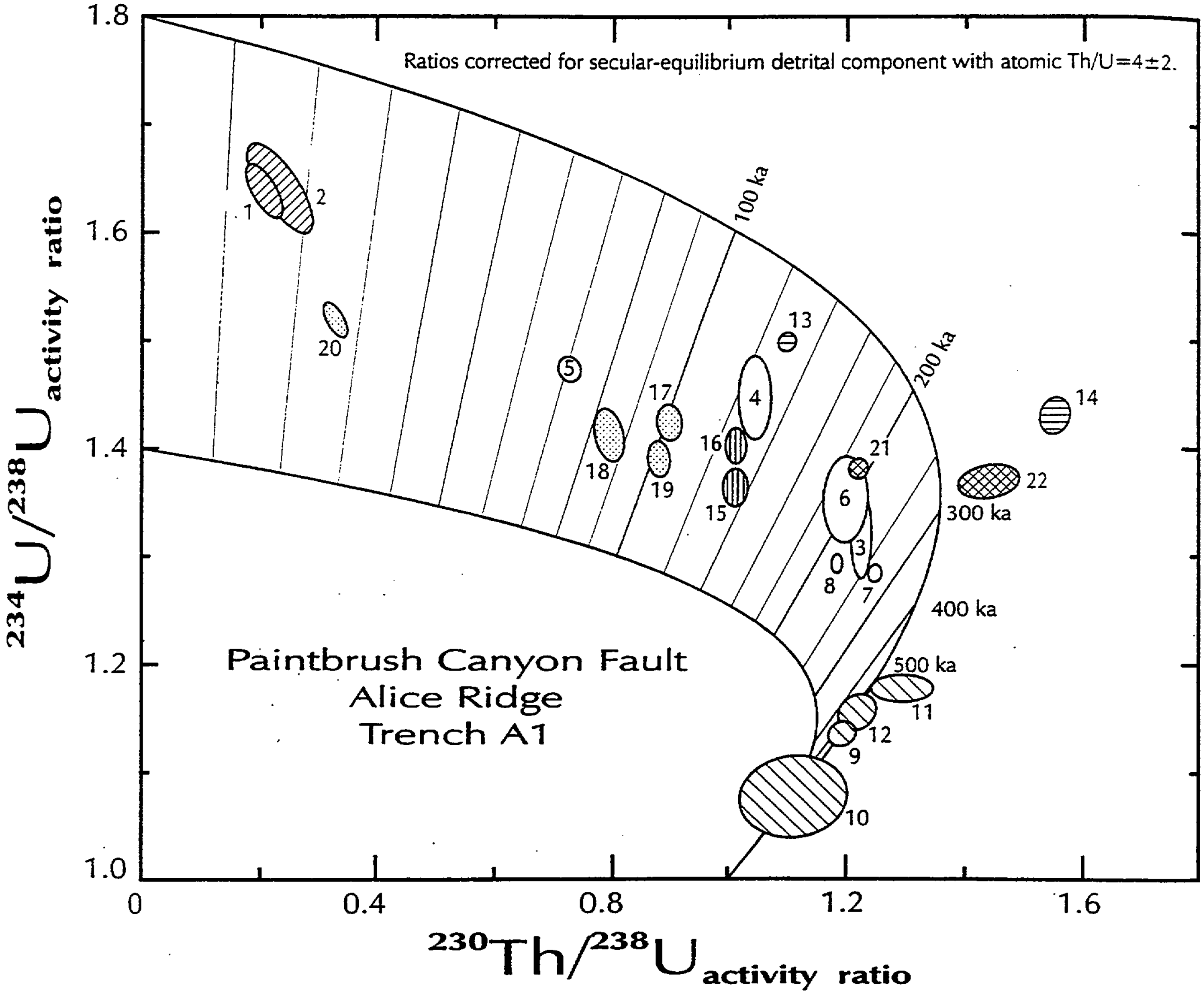

Figure 10: Uranium-series disequilibrium evolution diagram showing analyses from Alice Ridge Trench A1. Error ellipses from the same sample or horizon are shaded in the same pattern. Data are from Table 6 and coresopnd to the following sample names: 1=HD1622-U1; 2=HD1622-U2; 3=HD1623-U1; 4=HD1623-U2; 5=HD1624-U1; 6=HD1624-U2; 7=HD1624-U4; 8=HD1624-U5; 9=HD1625-A1a; 10=HD1625-C1a; 11=HD1625-C1b; 12=HD1625-U1; 13=HD1627-U1; 14=HD1627-U2; 15=HD1640-A2; 16=HD1640-B1; 17=HD1641-A1; 18=HD1641-A2; 19=HD1641-B1; 20=HD1641-C1; 21=HD1643-A1; and 22=HD1643-A2.

d:\ym\data\tecton\alice\a1-ccrd.cdr
date updated: 8/10/95

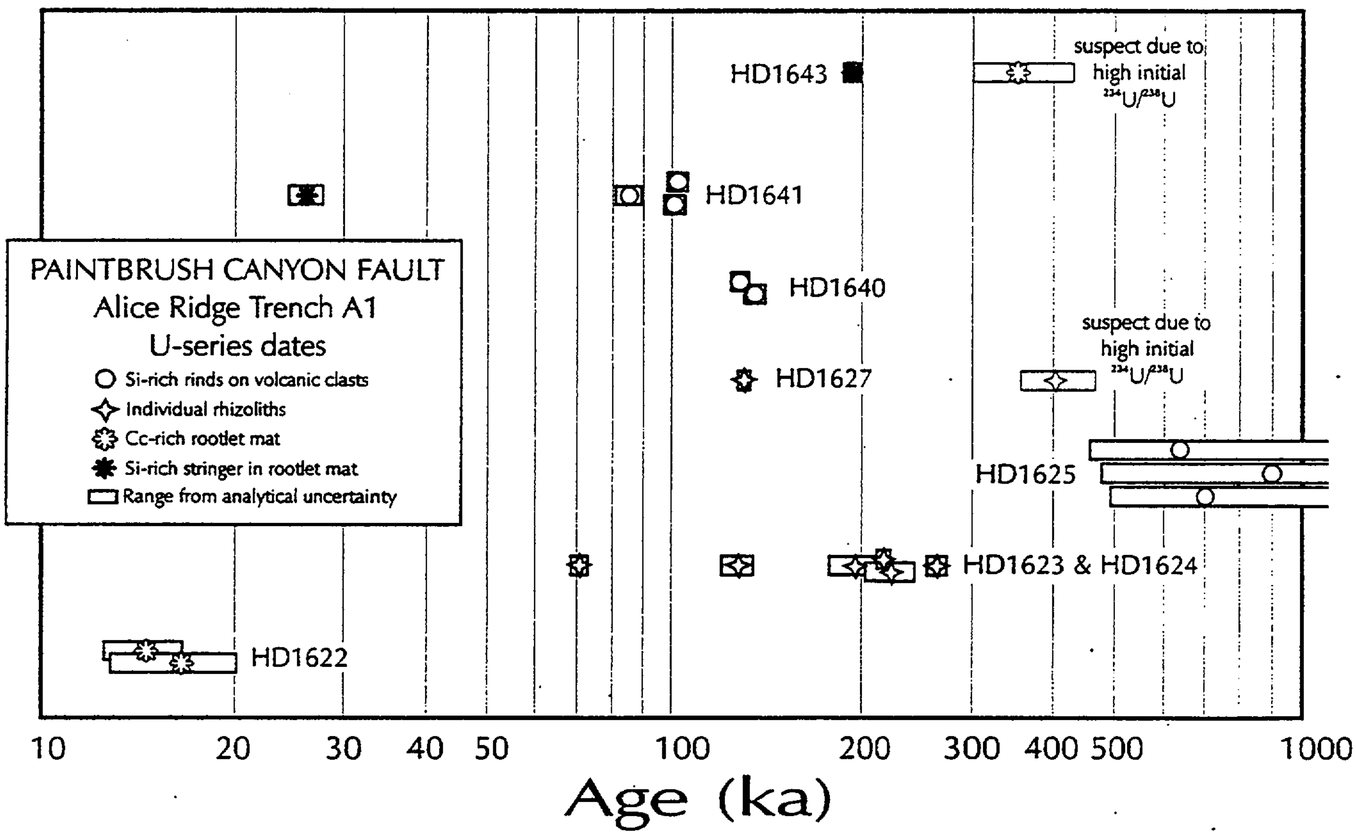

Figure 11: Distribution of uranium-series disequilibrium ages for samples from Alice Ridge Trench A1. Data are from Table 6.

d:\ym\data\tecton\alice\a1-age.cdı
updated 9/20/95

Table 7: Thermoluminescence results from Alice Ridge Trench A1. All errors given at the 95% confidence limit.

Sample Name	Field Moist. (%)	Saturation Moist. (%)	Dose Rate (Gy/ka) Field H_2O	Dose Rate (Gy/ka) Saturation H_2O	Total Bleach Eqivalent Dose (Gy)	Total Bleach Age (ka) for field moisture H_2O	Total Bleach Age (ka) for saturation moisture H_2O	Total Bleach Age (ka) Total Range	Partial Bleach Eqivalent Dose (Gy)	Partial Bleach Age (ka) for field moisture H_2O	Partial Bleach Age (ka) for saturation moisture H_2O	Partial Bleach Age (ka) Total Range
TL-34	*[north wall, up-thrown block, Unit 5 of Ponti (1995)]: Modern Av horizon*											
	0.1	28	8.3±1.1	6.1±0.9	75.8 ± 6.2	9.2 ± 1.5	12.4 ± 2.1	8-15	76 ± 34	9 ± 4	13 ± 6	5-18
TL-35	*[north wall, up-thrown block, Unit 4c of Ponti (1995)]:. Buried A horizon immediately below modern Av horizon*											
	5.3	31	8.2±1.1	6.3±0.9	137 ± 4	17 ± 2	22 ± 3	14-25	141 ± 10	17 ± 3	22 ± 4	14-26
TL-36	*[south wall, up-thrown block, Unit 3c of Ponti (1995)]: Well-developed, reddened Bt horizon.*											
	8	44	7.7±1.1	5.5±0.8	190 ± 120	25 ± 16	35 ± 22	9-57	190 ± 150	25 ± 20	35 ± 28	5-63
TL-37	*[south wall, down-thrown block, Unit 2b of Ponti (1995)]: Loose sand-rich, gravel-poor unit containing abundant rhizoliths*											
	0.5	27	7.5±1.0	5.6±0.8	1219 ± 91	163 ± 26	216 ± 35	137-251	1240 ± 190	166 ± 34	220 ± 46	131-266

Note: Only oldest U-series disequilibrium dates for each sample are shown.

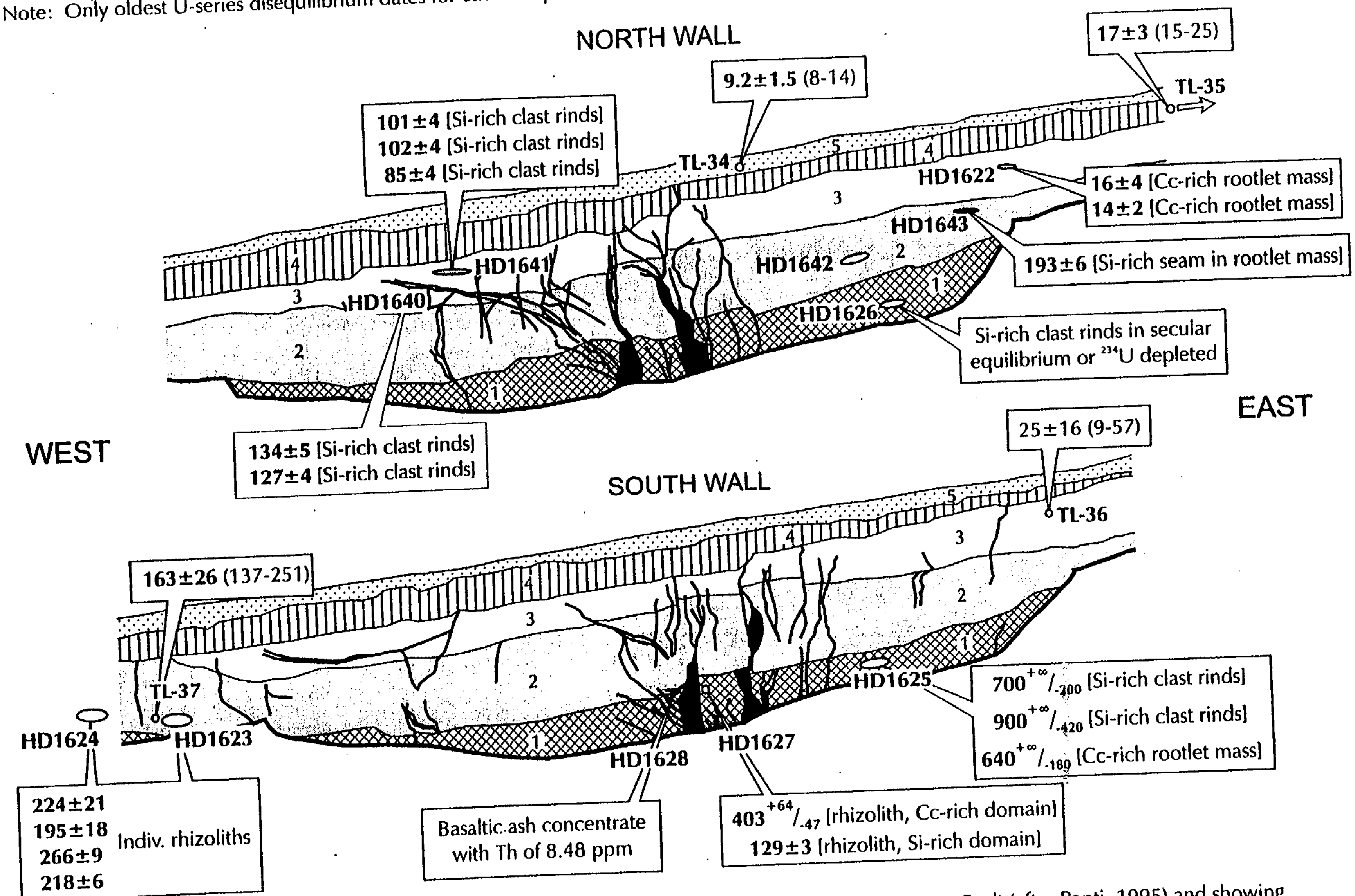

Figure 12: Generalized geologic log of Alice Ridge Trench A1 exposing the Paintbrush Canyon Fault (after Ponti, 1995) and showing geochronological data (in ka). Uranium-series disequilibrium data (HD sample names) are from Table 6 and thermoluminescence data (TL sample names) are from Table 7. See section 5.1 in text for explanations.

5.2.2.2 Midway Valley Trench 4

Table 8: Mass spectrometric U-series results from Midway Valley Trench 4

Figure 13: U-series concordia plot for samples from Midway Valley Trench 4

Figure 14: Distributions of U-series ages for Midway Valley Trench 4 samples

Table 9: Thermoluminescence results for Midway Valley Trench 4 samples

Figure 15: Schematic log of Midway Valley Trench 4 showing dating results

Table 8: Uranium-series disequilibrium results from Midway Valley Trench 4. Data are determined by mass spectrometry. The detrital component is assumed to be in secular equilibrium with an atomic TH/U of 4±2. All errors given at the 95% confidence level.

Sample Name	Sample wt. (g)	Concentration		$^{230}Th/^{232}Th$ activity	Detritus-corrected		Sample Type
		U ppm	Th ppm		Age (ka)	$^{234}U/^{238}U_{initial}$	
South wall, up-thrown block, near base of laminar K horizon (unit 2 of Wesling et al., 1994): Carbonate-rich soil directly overlying bedrock.							
HD1368-A	0.201	9.30	1.67	16.0	232 ± 15	1.11 ± 0.02	Carbonate-rich fine-rootlet mass
HD1368-B	0.213	6.49	0.983	20.9	344 ± 35	1.18 ± 0.03	Carbonate-rich fine-rootlet mass
South wall, down-thrown block near top of Unit 4 (Wesling et al., 1994); Thin, sub-horizontal, carbonate-rich lens within coarse colluvium							
HD1370-A1	0.234	44.7	0.259	599	423 +50/-38	1.39 ± 0.05	Si-rich stringer in carbonate matrix
HD1370-B	0.168	53.6	0.431	414	383 ± 24	1.29 ± 0.02	Si-rich stringer in carbonate matrix
South wall, down-thrown block, Unit 4c of Wesling et al. (1994): Unconsolidated sandy unit containing abundant large rhizoliths.							
HD1371-A1	0.183	6.43	0.090	120	44.0 ± 0.5	1.704 ± 0.009	Individual Rhizolith
HD1371-B1	0.172	7.36	0.156	91.8	55.0 ± 0.5	1.663 ± 0.008	Individual Rhizolith
HD1371-B2	0.094	10.7	0.806	28.6	63.0 ± 1.6	1.665 ± 0.011	Individual Rhizolith
South wall, down-thrown block, Unit 4c of Wesling et al. (1994): Unconsolidated sandy unit containing abundant large rhizoliths.							
HD1372-A1	0.106	14.5	0.344	129	118.8 ± 1.6	1.632 ± 0.010	Individual Rhizolith
HD1372-A2	0.089	12.2	0.856	46.4	131 ± 3	1.664 ± 0.013	Individual Rhizolith
South wall, down-thrown block, Unit 4c of Wesling et al. (1994): Unconsolidated sandy unit containing abundant large rhizoliths.							
HD1373-A1	0.254	4.77	0.736	19.4	133 ± 5	1.50 ± 0.02	Individual Rhizolith
HD1373-A2	0.300	4.21	0.815	15.8	140 ± 5	1.50 ± 0.02	Individual Rhizolith
South wall, down-thrown block adjacent to fault scarp, Unit 1 of Wesling et al. (1994): Densely-cemented calcrete in lower portion of rotated block.							
HD1589-A1	0.290	4.40	2.46	5.2	Undefined	234U depleted	Composite Soil Carbonate
HD1589-A3	0.322	5.09	1.559	9.8	Undefined	234U depleted	Si-rich lens in carbonate matrix
HD1589-A4	0.374	4.54	1.10	12.9	Undefined	234U depleted	Composite Soil Carbonate
HD1589-A5	0.506	11.2	0.049	741	600 +inf/-170	1.3 ± 0.2	Si-rich lens in carbonate matrix
HD1589-D1	0.369	12.3	0.102	462	Excess Th; 600 ka min.	Undefined	Si-rich lens in carbonate matrix

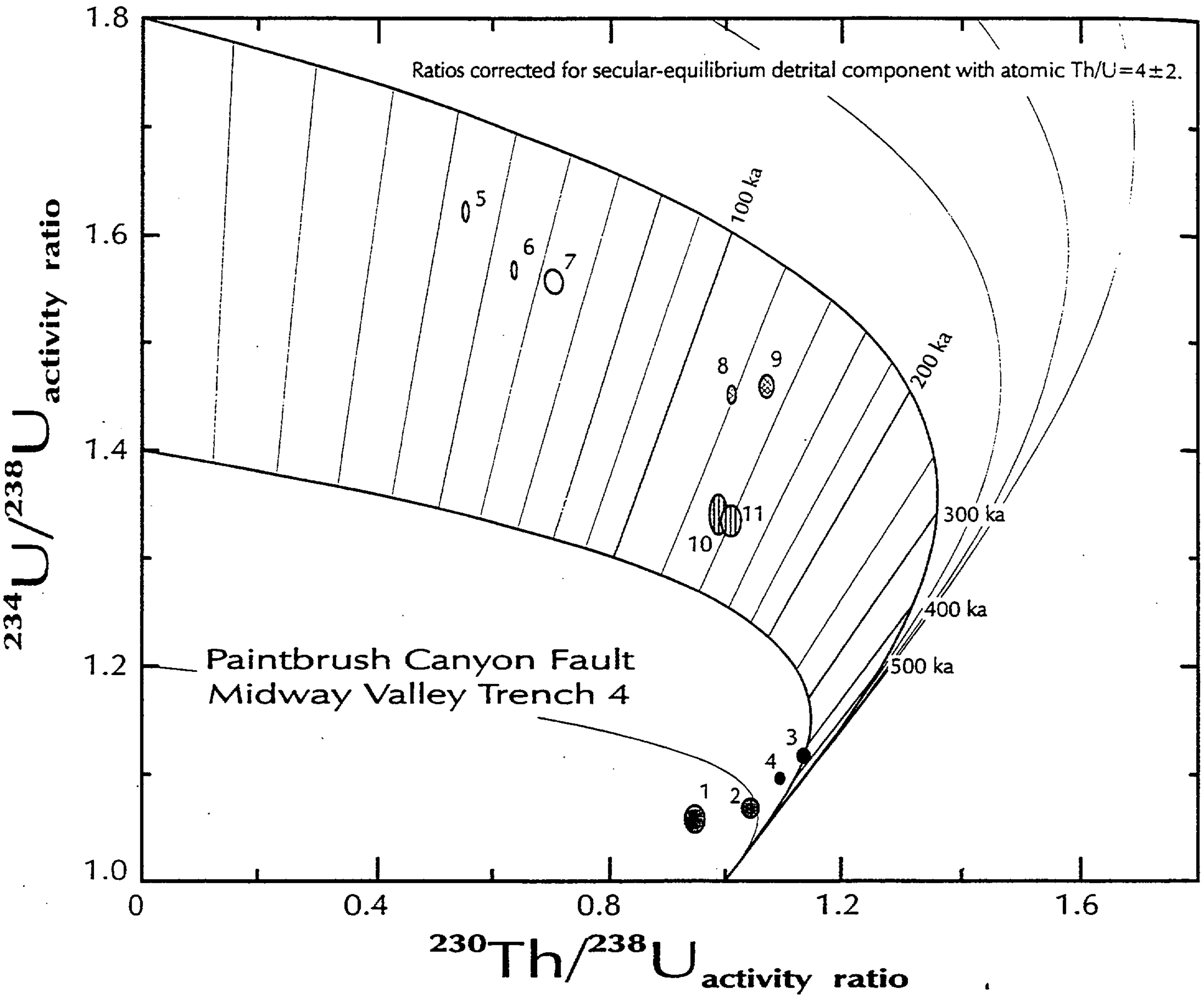

Figure 13: Uranium-series disequilibrium evolution diagram showing analyses of samples from Midway Valley Trench 4. Error ellipses from the same sample are shaded in the same pattern. Data are given in Table 8 and correspond to the following sample names: 1=HD1368-A; 2=HD1368-B; 3=HD1370-A1; 4=HD1370-B; 5=HD1371-A1; 6=HD1371-B1; 7=HD1371-B2; 8=HD1372-A1; 9=HD1372-A2; 10=HD1373-A1; 11=HD1373-A2.

d:\ym\data\tecton\mwv\t4-ccrd.cdr
date updated: 9/20/95

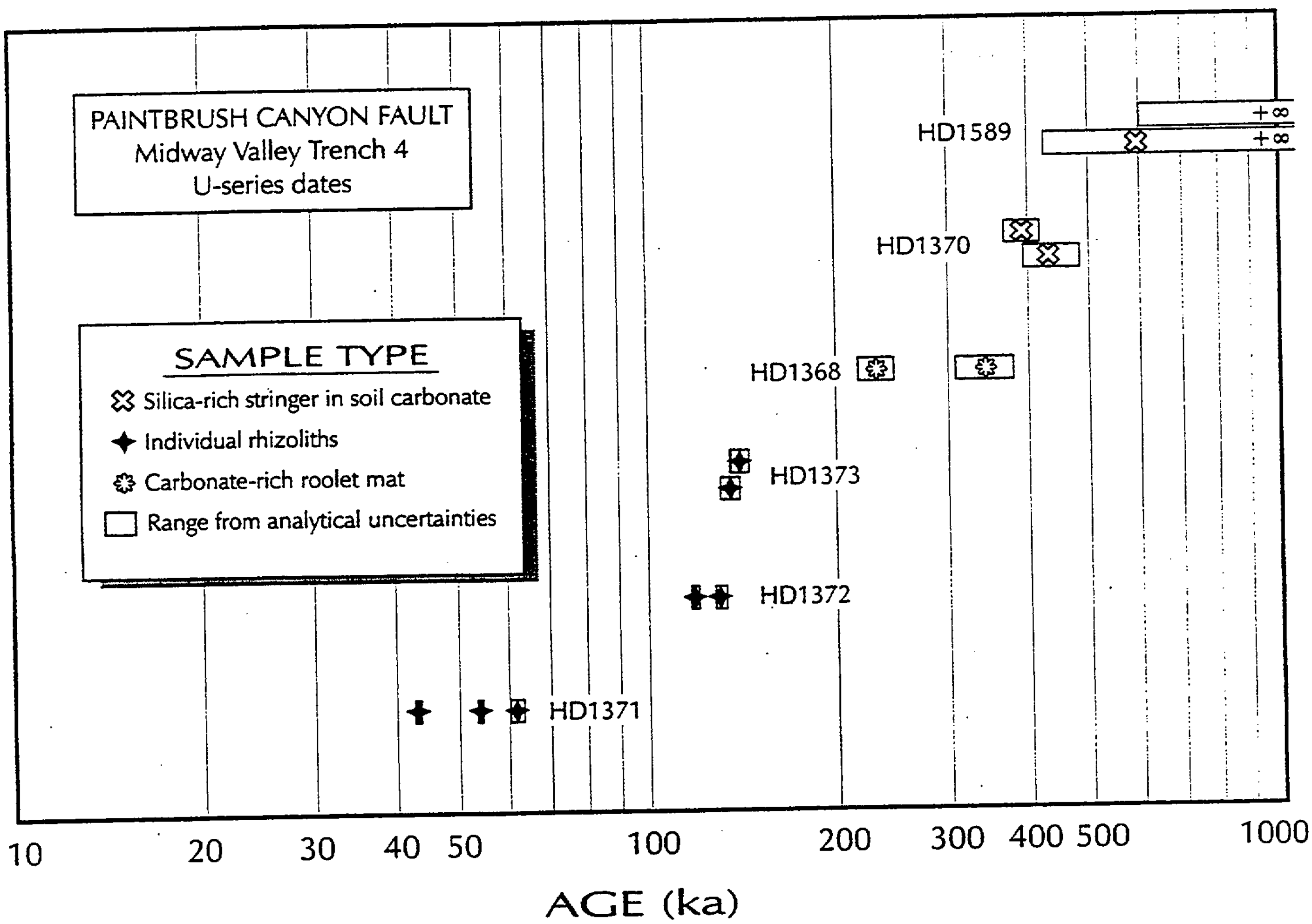

Figure 14: Distribution of uranium-series disequilibrium ages for samples from Midway Valley Trench 4. Data are given in Table 8.

d:\ym\data\tecton\mwv\t4-ages.cdr
updated 8/11/95

Table 9: Thermoluminescence results from Midway Valley Trench 4. All errors given at the 95% confidence limit.

Sample Name	Field Moist. (%)	Saturation Moist. (%)	Dose Rate (Gy/ka) Field H_2O	Dose Rate (Gy/ka) Saturation H_2O	Total Bleach Eqivalent Dose (Gy)	Total Bleach Age (ka) for field moisture H_2O	Total Bleach Age (ka) for saturation moisture H_2O	Total Bleach Age (ka) Total Range	Partial Bleach Eqivalent Dose (Gy)	Partial Bleach Age (ka) for field moisture H_2O	Partial Bleach Age (ka) for saturation moisture H_2O	Partial Bleach Age (ka) Total Range
TL-03	*North wall, unit 4h of Wesling, et al., 1994: Gravely sand within colluvial wedge.*											
	0.5	20	7.7±1.0	6.1±0.9	558 ± 118	73 ± 9	91 ± 23	64-114	749 ± 111	98 ± 19	122 ± 25	79-147
TL-04	*North wall, unit 5b of Wesling, et al., 1994: Gravely sand within colluvial wedge.*											
	0.5 (est.)	20 (est.)	7.4±0.9	5.9±0.8	280 ± 20	38 ± 6	47 ± 7	32-54	253 ± 195	34 ± 27	43 ± 33	7-76
TL-05	*North wall, unit 6 of Wesling, et al., 1994: Modern Av horizon.*											
	0.5 (est.)	20 (est.)	7.7±1.0	6.1±0.9	48 ± 8	6.2 ± 1.3	7.8 ± 1.7	4.9-9.5	71 ± 93	9.2 ± 12	12 ± 15	0-27

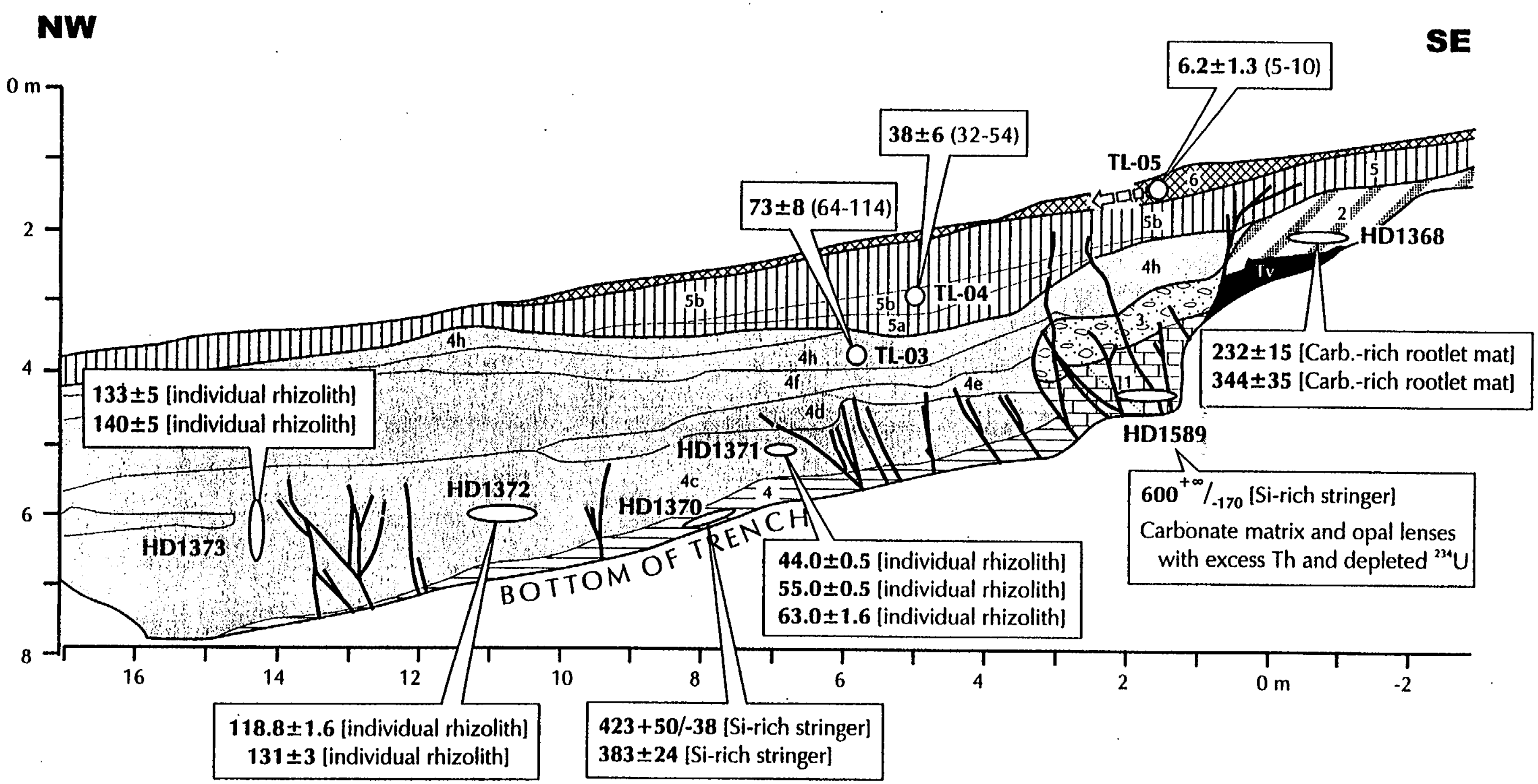

Figure 15: Generalized geologic log of the north wall, Midway Valley Trench 4 exposing the Paintbrush Canyon Fault (after Wesling et al., 1994) showing geochronological data (in ka). Uranium-series disequilibrium data (HD sample names) are from Table 8 and thermoluminescence data (TL sample names) are from Table 9. See section 5.1 in text for explanations

5.2.2.3 Busted Butte

Table 10: Mass spectrometric U-series results from Busted Butte

Table 11: Alpha spectrometric U-series results from Busted Butte

Figure 16: U-series concordia plot for samples from Busted Butte Wall 1

Figure 17: U-series concordia plot for samples from Busted Butte Wall 4

Figure 18: Distributions of ages for samples from Busted Butte

Table 12: Thermoluminescence results for samples from Busted Butte

Figure 19: Schematic log of Busted Butte Wall 4 showing dating results

Table 10: Uranium-series disequilibrium results from Busted Butte natural exposures. Data determined by mass spectrometry. The detrital component is assumed to be in secular equilibrium with an atomic Th/U of 4±2. All uncertainties given at the 95% confidence level.

Sample Name	Sample wt. (g)	Concentration		$^{230}Th/^{232}Th$ activity ratio	Detritus-corrected		Sample Type
		U (ppm)	Th (ppm)		Age (ka)	$^{234}U/^{238}U_{Initial}$	
Down-thrown block, prominent soil developed near top of Unit 8 (Menges et al., 1994); Layer of carbonate with large lenses of opal replacement.							
HD1449-F1	0.153	3.53	0.227	50	224 ± 9	1.31 ± 0.02	Carbonate-rich rootlet layer
HD1449-F2	0.106	40.89	0.027	6090	270 ± 11	1.63 ± 0.03	Si-rich lens in carbonate matrix
Up-thrown block, prominent sand unit with well developed rhizoliths (Unit ?? of Menges et al., 1994): Individual rhizoliths from newly excavated exposure.							
HD1453-1A	0.190	3.34	0.309	40	Excess Th	Undefined	Individual Rhizolith
HD1453-2A	0.245	4.70	0.237	63	212 ± 25	1.31 ± 0.04	Individual Rhizolith
HD1453-3A	0.180	5.19	0.245	75	342 ± 50	1.43 ± 0.07	Individual Rhizolith
HD1453-4A	0.201	5.96	0.128	172	210 ± 9	1.62 ± 0.03	Individual Rhizolith
HD1453-5A	0.152	3.65	0.109	124	235 ± 27	1.58 ± 0.08	Individual Rhizolith
HD1453-A	0.495	3.91	0.199	71	454 +76/-51	1.55 ± 0.10	Individual Rhizolith
HD1453-A dup#1	0.083	3.66	0.237	57	590 +inf/-130	1.9 ± 0.2	Individual Rhizolith
HD1453-B	0.337	4.13	0.222	42	63.7 ± 1.2	1.75 ± 0.02	Individual Rhizolith
Thin platy K (Bk) soil overlying main fault trace (Unit ?? of Menges et al., 1994): Sandy matrix with distinct clots of carbonate/silica associated with plant rootlets.							
HD1455-95B1	0.093	6.17	1.70	12	173 ± 9	1.54 ± 0.03	Carb/Si-rich rootlet clot
HD1455-95B2	0.086	23.58	1.23	8.1	9.7 ± 0.8	1.50 ± 0.07	Si-rich stringer in small rootlet clot
HD1455-C	0.073	4.62	2.60	2.9	43 ± 8	1.47 ± 0.05	Composite platy soil carbonate

Table 11: Uranium-series disequlibrium results from Busted Butte natural exposures. Data collected previously by alpha spectrometry (Paces et al., 1994). Criteria for calculating age estimates includes: 1) Whole rock analyses (either total digestion or leach/residue recombination; 2) Suffiently small detrital component correction (i.e., 230Th/232Th >~2); 3) Reasonable initial 234U/238U composition (i.e., 1.6±2). Analyses given in boldface below meet these critera. The detrital comonent is assumed to be in secular equilibrium with an atomic Th/U of 4±2. All uncertainties are given at the 95% confidence level.

Sample Name	Sample wt. (g)	Concentrations U (ppm)	Concentrations Th (ppm)	Measured ^{230}Th/^{232}Th activity ratio	Detritus-Corrected Activity Ratios ^{234}U/^{238}U	Detritus-Corrected Activity Ratios ^{230}Th/^{238}U	Corr.Coef. ρ(08-48)	AGE (ka)	Initial ^{234}U/^{238}U activity ratio	Aliquot Type
Wall 1: Platy K soil overlying laminar surface; Composite sample gently crushed & seived.										
HD954-AL	3.44	2.48	1.81	3.15	1.357 ± 0.053	0.701 ± 0.076	-0.306			<325 mesh; 0.3N HNO3 leach
HD954-AR	0.51	9.94	13.78	1.81	1.32 ± 0.14	0.73 ± 0.18	-0.130			<325 mesh; 0.3N HNO3 residue
HD954-AL/R sum	**3.96**	**3.45**	**3.36**	**2.44**	**1.346 ± 0.094**	**0.711 ± 0.103**	**-0.219**	**79 ± 20**	**1.43 ± 0.12**	**<325 mesh; math. recombination**
HD954-AW	**2.32**	**3.48**	**3.47**	**2.40**	**1.370 ± 0.078**	**0.717 ± 0.104**	**-0.353**	**77 ± 19**	**1.46 ± 0.10**	**<325 mesh; total digestion**
HD954-BW	**3.31**	**3.49**	**4.82**	**1.77**	**1.43 ± 0.14**	**0.70 ± 0.17**	**-0.426**	**70 ± 28**	**1.53 ± 0.17**	**200-325 mesh; total digestion**
HD954-CW	1.46	3.65	15.01	0.58	-2.5 ± 30	4.5 ± 30				100-200 mesh; total digestion
Wall 1: Rhizoliths from footwall; Composite sample gently crushed & sieved.										
HD955A-AW1	4.23	4.19	10.96	1.08	1.40 ± 0.47	0.79 ± 0.57	-0.331			100-200 mesh; total digestion
HD955A-BW1	**2.91**	**5.31**	**4.67**	**3.28**	**1.262 ± 0.057**	**0.935 ± 0.085**	**0.014**	**137 ± 27**	**1.39 ± 0.09**	**200-325 mesh; total digestion**
HD955A-CL	2.42	3.98	2.15	5.12	1.254 ± 0.044	0.895 ± 0.064	0.138			<325 mesh; 0.3N HNO3 leach
HD955A-CR	0.78	10.12	7.87	3.66	1.221 ± 0.061	0.922 ± 0.100	0.149			<325 mesh; 0.3N HNO3 residue
HD955A-CL/R sum	**3.20**	**5.47**	**3.54**	**4.33**	**1.240 ± 0.071**	**0.907 ± 0.067**	**0.124**	**134 ± 23**	**1.35 ± 0.11**	**<325 mesh; math. recombination**
HD955A-CW1	**3.00**	**5.42**	**3.61**	**4.36**	**1.255 ± 0.038**	**0.948 ± 0.061**	**0.008**	**142 ± 20**	**1.38 ± 0.06**	**<325 mesh; total digestion**
Wall 1: Carbonate-cemented sand at top of hanging-wall; Composite sample gently crushed & sieved.										
HD959-AL	2.17	4.19	1.41	2.50	1.282 ± 0.027	0.207 ± 0.046	-0.366			<325 mesh; 0.3N HNO3 leach
HD959-AR	0.46	11.35	6.69	1.81	1.285 ± 0.037	0.235 ± 0.083	-0.553			<325 mesh; 0.3N HNO3 residue
HD959-AL/R sum	**2.63**	**5.44**	**2.33**	**2.15**	**1.283 ± 0.036**	**0.217 ± 0.058**	**-0.387**	**20.02 ± 6.1**	**1.30 ± 0.04**	**<325 mesh; math. recombination**
Wall 4: Lower buried carbonate soil, downthrown block, containing abundant plant microfossils. Composite sample gently crushed & seived.										
HD961-AL	2.60	3.56	1.47	6.99	1.268 ± 0.027	0.946 ± 0.045	0.088			<325 mesh; 0.3N HNO3 leach
HD961-AR	0.69	7.09	6.37	4.14	1.091 ± 0.041	1.292 ± 0.107	0.228			<325 mesh; 0.3N HNO3 residue
HD961-AL/R sum	**3.29**	**4.30**	**2.50**	**5.46**	**1.213 ± 0.037**	**1.055 ± 0.053**	**0.146**	**196.3 +36/-28**	**1.37 ± 0.07**	**<325 mesh; math. recombination**
HD961-AW	**2.07**	**3.86**	**2.43**	**5.58**	**1.134 ± 0.034**	**1.191 ± 0.067**	**0.266**	**750 +inf/-430**	**2.1 ± 0.3**	**<325 mesh; total digestion**
HD961-BW	2.19	**4.33**	**2.98**	**4.91**	**1.124 ± 0.037**	**1.138 ± 0.073**	**0.221**	**400 +inf/-130**	**1.4 ± 0.3**	**200-325 mesh; total digestion**
HD961-CW	2.10	**4.54**	**6.20**	**2.48**	**1.149 ± 0.076**	**1.18 ± 0.16**	**0.228**	**410 +inf/150**	**1.5 ± 0.3**	**100-200 mesh; total digestion**
Wall 4: Upper buried carbonate soil, downthrown block, containing abundant plant microfossils and opal lenses. Composite sample gently crushed & seived.										
HD962-AL	2.29	3.69	1.08	11.8	1.237 ± 0.026	1.149 ± 0.048	0.276			<325 mesh; 0.3N HNO3 leach
HD962-AW	**1.80**	**4.81**	**1.57**	**11.7**	**1.251 ± 0.030**	**1.277 ± 0.050**	**0.369**	**340 +140/74**	**1.66 ± 0.21**	**<325 mesh; total digestion**
HD962-BW	**2.23**	**5.44**	**1.33**	**14.6**	**1.210 ± 0.024**	**1.196 ± 0.046**	**0.289**	**300 +82/-53**	**1.49 ± 0.11**	**200-325 mesh; total digestion**
HD962-CW	2.07	5.48	4.02	5.05	1.188 ± 0.041	1.272 ± 0.085	0.323	Excess Th	Undefined	100-200 mesh; total digestion

Table 11: continued.

Sample Name	Sample wt. (g)	Concentrations U (ppm)	Concentrations Th (ppm)	Measured $^{230}Th/^{232}Th$ activity ratio	Detritus-Corrected Activity Ratios $^{234}U/^{238}U$	Detritus-Corrected Activity Ratios $^{230}Th/^{238}U$	Corr.Coef. ρ(08-48)	AGE (ka)	Initial $^{234}U/^{238}U$ activity ratio	Aliquot Type
Wall 4: Upper buried carbonate soil, downthrown block, containing abundant plant microfossils and opal lenses. Composite sample gently crushed & seived.										
HD1449-AL2	2.34	1.28	0.06	119	1.610 ± 0.030	1.844 ± 0.051	0.431			<325 mesh; 7.6N HNO3 leach
HD1449-AR2	0.63	16.30	0.06	763	1.023 ± 0.014	0.888 ± 0.021	0.282			<325 mesh; 7.6N HNO3 residue
HD1449-AL/R2	***2.97***	***4.45***	***0.06***	***250***	***1.156 ± 0.020***	***1.103 ± 0.020***	***0.351***	***272 ± +35/-28***	***1.34 ± 0.05***	***<325 mesh; math. recombination***
HD1449-BL	1.76	1.57	0.15	53.1	1.561 ± 0.032	1.740 ± 0.050	0.455			200-325 mesh; 0.3N HNO3 leach
Wall 4: Platy K soil overlying main fault trace. Composite sample gently crushed & seived.										
HD1455-AL2	1.84	1.65	5.23	1.42	3.0 ± 4.7	3.7 ± 6.4	0.978			<325 mesh; 7.6N HNO3 leach
HD1455-AR2	1.21	10.17	1.69	15.3	1.260 ± 0.020	0.831 ± 0.025	0.221			<325 mesh; 7.6N HNO3 residue
HD1455-AL/R2	***3.06***	***5.03***	***3.83***	***3.85***	***1.336 ± 0.058***	***0.959 ± 0.066***	***0.021***	***127 ± 19***	***1.48 ± 0.09***	***<325 mesh; math. recombination***
HD1455-BL	1.42	1.91	6.11	1.28	2.9 ± 4.6	3.0 ± 4.9	0.964			200-325 mesh; 0.3N HNO3 leach
Wall 4: Lower buried carbontae soil, downthrown block, containing abundant plant microfossils. Composite sample gently crushed & seived.										
HD1456-AL2	2.23	1.19	1.47	6.28	2.00 ± 0.25	3.29 ± 0.56	0.943			<325 mesh; 7.6N HNO3 leach
HD1456-AR2	0.69	15.18	1.17	41.5	1.026 ± 0.015	1.054 ± 0.027	0.288			<325 mesh; 7.6N HNO3 residue
HD1456-AL/R2	2.92	4.50	1.40	13.3	1.171 ± 0.026	1.387 ± 0.040	0.363	Excess Th	Undefined	<325 mesh; math. recombination
HD1456-BL	2.28	1.29	1.83	5.07	2.06 ± 0.31	3.15 ± 0.65	0.945			200-325 mesh; 0.3N HNO3 leach

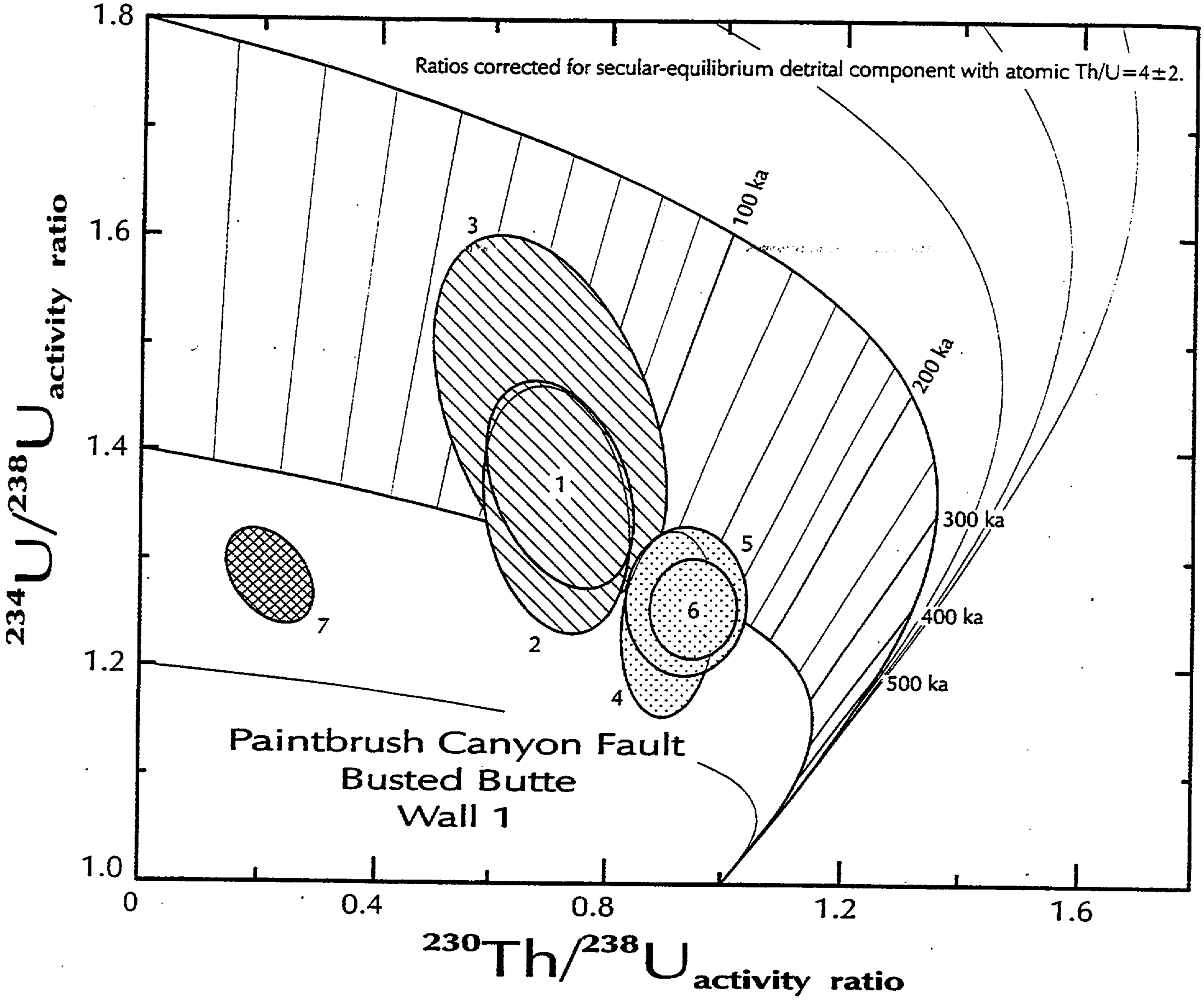

Figure 16: Uranium-series disequilibrium evolution diagram showing analyses of samples from Busted Butte Wall 1. Error ellipses for aliquots of the same sample are shaded in the same pattern. Data are given in Table 11 and correspond to the following numbers: 1=HD954-AL/R sum; 2=HDHD954-AW; 3=HD954-BW; 4=HD955A-BW1; 5=HD955A-CL/R sum; 6=HD955A-CW1; 7=HD959-AL/R sum.

d:\ym\data\tecton\bb\bb-ccrd.cdr
date updated: 8/10/95

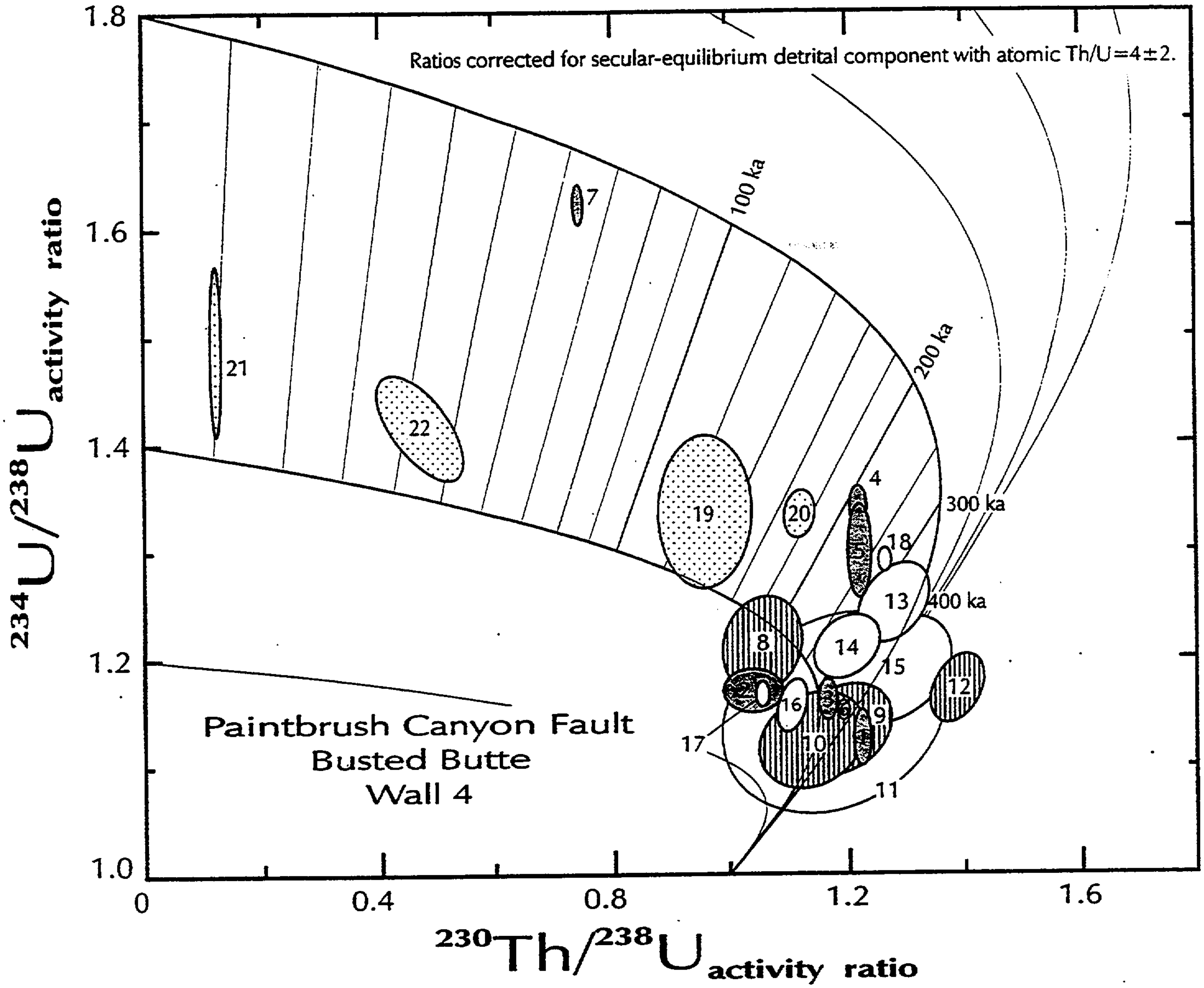

Figure 17: Uranium-series disequilibrium evolution diagram showing analyses of samples from Busted Butte Wall 4. Error ellipses for aliquots of the same sample are shaded in the same pattern. Data are given in Tables 10 and 11 and correspond to the following numbers: 1=HD1453-1A; 2=HD1453-2A; 3=HD1453-3A; 4=HD1453-4A; 5=HD1453-5A; 6=HD1453-A; 7=HD1453-B; 8=HD961-AL/R sum; 9=HD961-AW; 10=HD961-BW; 11=HD961-CW; 12=HD1456-AL/R sum; 13=HD962-AW; 14=HD962-BW; 15=HD962-CW; 16=HD1449-AL/R2 sum; 17=HD1449-F1; 18=HD1449-F2; 19=HD1455-AL/R sum; 20=HD1455-95B1; 21=HD1455-95B2; 22=HD1455-C.

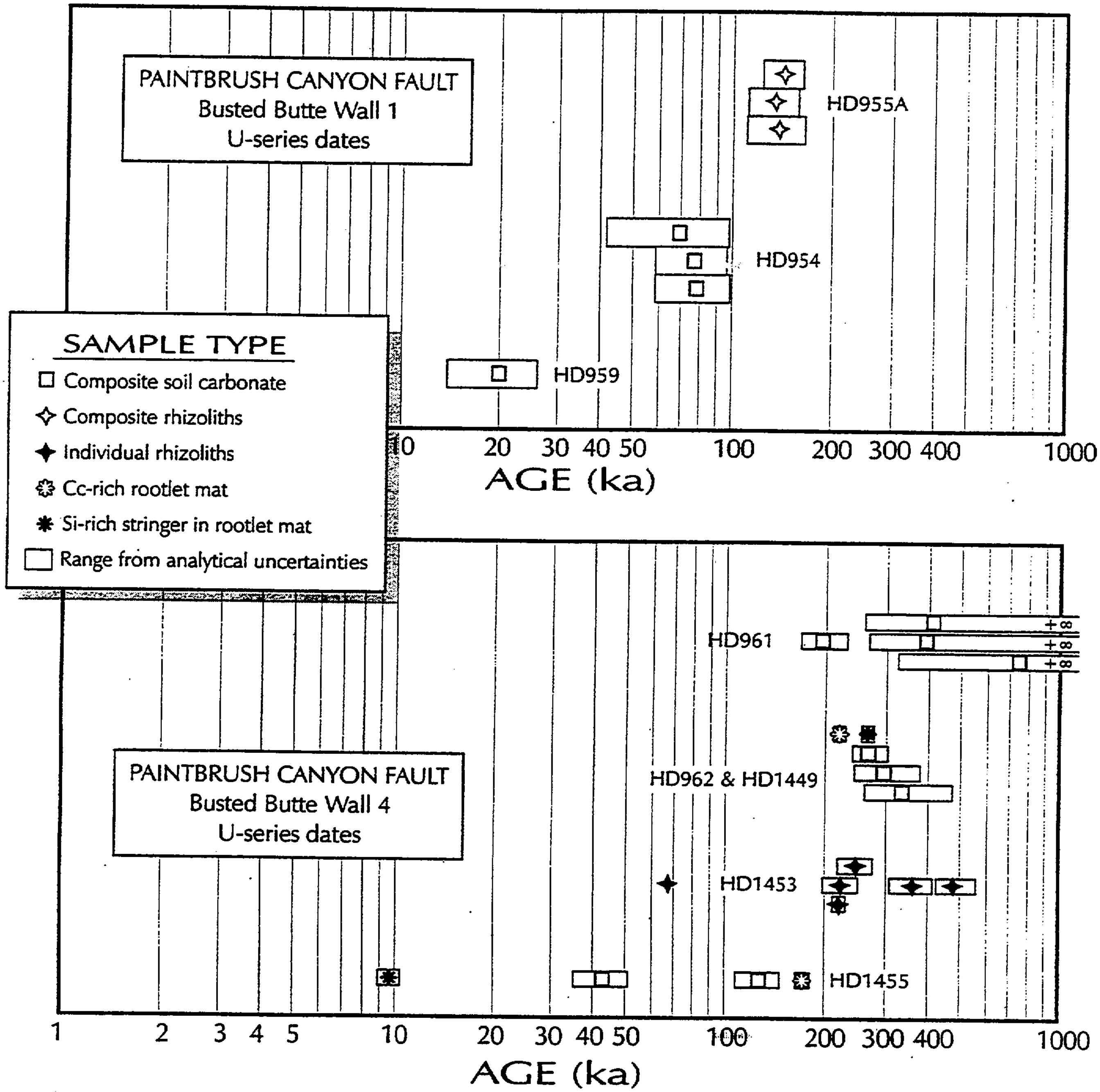

Figure 18: Distribution of uranium-series disequilibrium ages for samples from Busted Butte sand ramps. Data are given in Tables 10 and 11.

d:\ym\data\tecton\bb\bb-age.cdr
updated 8/11/95

Table 12: Thermoluminescence results from Busted Butte natural exposure. All errors given at the 95% confidence limit.

Sample Name	Field Moist. (%)	Saturation Moist. (%)	Dose Rate (Gy/ka)		Total Bleach Eqivalent Dose (Gy)	Total Bleach Age (ka)			Partial Bleach Eqivalent Dose (Gy)	Partial Bleach Age (ka)		
			Field H_2O	Saturation H_2O		for field moisture H_2O	for saturation moisture H_2O	Total Range		for field moisture H_2O	for saturation moisture H_2O	Total Range
TL-07	*[Wall 4, Unit 9 of Menges: Sandy unit just below modern soil]*											
	0.5	25	7.9±1.1	6.0±0.9	282 ± 70	36 ± 10	47 ± 13	26-60	310 ± 143	39 ± 19	51 ± 25	20-76

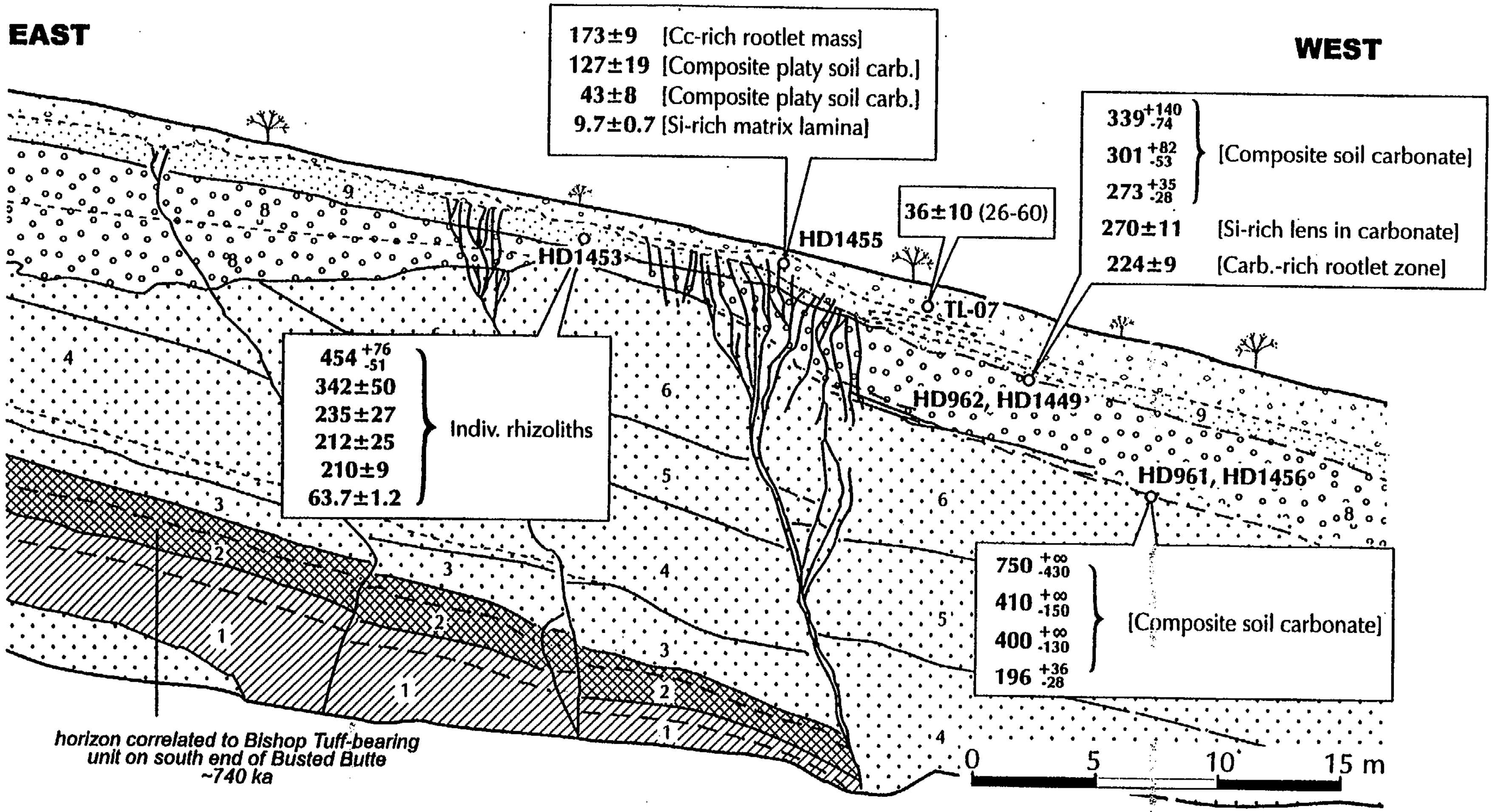

Figure 19: Generalized geological of Wall 4, west side Busted Butte sand ramps exposing the Paintbrush Canyon fault (after Menges et al., 1994) showing geochronological data (in ka). Uranium-series data (HD sample names) are from Tables 10 and 11, and thermoluminescence data (TL sample names) are from Table 12. See section 5.1 in text for explanations.

5.2.3 Bow Ridge Fault

Trench 14C/14D

Table 13: Alpha spectrometric U-series results from Trench 14C & 14D

Figure 20: U-series concordia plot for samples from Trench14C

Figure 21: U-series concordia plot for samples from Trench 14D

Figure 22: Distributions of U-series ages for samples from Trench 14C & 14D

Table 14: Thermoluminescence results for samples from Trench 14D

Figure 23: Schematic log of Trench 14c showing dating results

Figure 24: Schematic log of Trench 14d showing dating results

Table 13: Uranium-series disequlibrium results from Midway Valley Trenches 14c and 14d. Data collected previously by alpha spectrometry (Paces et al., 1994). Criteria for calculating age estimates includes: 1) Whole rock analyses (either total digestion or leach/residue recombination; 2) Suffiently small detrital component correction (i.e., 230Th/232Th >~2); 3) Reasonable initial 234U/238U composition (i.e., 1.6±2). Analyses given in boldface below meet these critera. The detrital comonent is assumed to be in secular equilibrium with an atomic Th/U of 4±2. All uncertainties are given at the 95% confidence level.

Sample Name	Sample wt. (g)	Concentrations U (ppm)	Concentrations Th (ppm)	Measured $^{230}Th/^{232}Th$ activity ratio	Detritus-Corrected Activity Ratios $^{234}U/^{238}U$	Detritus-Corrected Activity Ratios $^{230}Th/^{238}U$	Corr.Coef. ρ(08-48)	AGE (ka)	Initial $^{234}U/^{238}U$ activity ratio	Aliquot Type
Trench 14c: Soil carbonate from lower-most K horizon. Composite sample gently crushed and seived.										
HD965-AL	2.825	2.58	2.00	4.90	1.251 ± 0.057	1.32 ± 0.14	0.317			<325 mesh; 0.3N HNO3 leach
HD965-AR	0.354	4.66	5.86	2.65	1.161 ± 0.069	1.14 ± 0.15	0.192			<325 mesh; 0.3N HNO3 residue
HD965-AL/R sum	***3.179***	***2.81***	***2.43***	***4.29***	***1.237 ± 0.068***	***1.29 ± 0.13***	***0.301***	***400 ± +inf/-230***	***1.7 ± 0.3***	***<325 mesh; math. recombination***
HD965-AR2	0.481	4.08	5.58	2.73	1.170 ± 0.082	1.36 ± 0.21	0.337			<325 mesh; 0.3N HNO3 residue
HD965-BL	1.857	3.18	1.76	4.73	1.249 ± 0.038	0.838 ± 0.054	-0.002			200-325 mesh; 0.3N HNO3 leach
HD965-BR	1.132	2.43	4.45	2.95	1.35 ± 0.23	2.48 ± 0.79	0.724			200-325 mesh; 0.3N HNO3 residue
HD965-BL/R sum	***2.989***	***2.90***	***2.78***	***3.65***	***1.272 ± 0.073***	***1.20 ± 0.11***	***0.340***	***240 ± +140/-71***	***1.5 ± 0.2***	***200-325 mesh; math. recombination***
Trench 14c: Soil carbonate from boundary between massive & platy K horizons. Abundant plant microfossils. Composite sample gently crushed and seived.										
HD966-AL	2.501	4.11	2.77	4.74	1.292 ± 0.044	1.068 ± 0.070	0.171			<325 mesh; 0.3N HNO3 leach
HD966-AR	0.640	9.40	8.77	4.35	1.285 ± 0.059	1.44 ± 0.13	0.479			<325 mesh; 0.3N HNO3 residue
HD966-AL/R sum	***3.141***	***5.18***	***4.00***	***4.56***	***1.290 ± 0.053***	***1.199 ± 0.077***	***0.287***	***229 ± +70/-47***	***1.55 ± 0.14***	***<325 mesh; math. recombination***
HD966-AR2	0.783	9.11	7.60	4.92	1.306 ± 0.059	1.45 ± 0.15	0.412			<325 mesh; 0.3N HNO3 residue
HD966-BL	2.264	4.13	2.24	6.46	1.291 ± 0.036	1.181 ± 0.059	0.290			200-325 mesh; 0.3N HNO3 leach
HD966-BR	1.424	7.88	6.39	4.28	1.272 ± 0.060	1.18 ± 0.13	0.265			200-325 mesh; 0.3N HNO3 residue
HD966-BL/R sum	***3.688***	***5.58***	***3.84***	***5.06***	***1.281 ± 0.053***	***1.181 ± 0.082***	***0.278***	***224 ± +70/-47***	***1.53 ± 0.13***	***200-325 mesh; math. recombination***
Trench 14d: Carbonate-cemented gravel from oldest soil unit (Unit I of Menges). Composite sample gently crushed and seived.										
HD968-AL	2.254	3.55	5.18	1.98	0.904 ± 0.077	0.93 ± 0.16	0.100			<325 mesh; 0.3N HNO3 leach
HD968-AR	0.804	8.60	15.08	1.72	0.974 ± 0.090	0.99 ± 0.21	0.032			<325 mesh; 0.3N HNO3 residue
HD968-AL/R sum	3.058	4.88	7.78	1.85	0.934 ± 0.087	0.95 ± 0.18	0.060	Excess Th	^{234}U depleted	<325 mesh; math. recombination
HD968-CL	1.469	4.58	5.37	2.47	0.916 ± 0.053	0.93 ± 0.12	0.084			100-200 mesh; 0.3N HNO3 leach
HD968-AW	2.315	4.84	8.35	1.82	0.952 ± 0.087	1.06 ± 0.21	-0.006	Excess Th	^{234}U depleted	<325 mesh; total digestion
HD968-BW	3.020	5.05	8.72	1.78	0.944 ± 0.087	1.03 ± 0.21	0.003	Excess Th	^{234}U depleted	200-325 mesh; total digestion
Trench 14d: Sub-horizontal layer of soil carbonate w/ abundant plant microfossils within Unit II of Menges. Composite sample gently crushed and seived.										
HD969-AW	2.218	5.31	5.39	3.57	1.147 ± 0.052	1.26 ± 0.11	0.288	Excess Th		<325 mesh; total digestion
HD969-BW	***3.148***	***5.05***	***3.96***	***4.33***	***1.150 ± 0.038***	***1.15 ± 0.08***	***0.203***	***340 ± +inf/-120***	***1.40 ± 0.12***	200-325 mesh; total digestion
HD969-BL	1.808	3.43	3.12	4.24	1.173 ± 0.049	1.36 ± 0.11	0.378			200-325 mesh; 0.3N HNO3 leach
HD969-BR	1.357	7.51	6.98	3.79	1.147 ± 0.065	1.21 ± 0.14	0.282			200-325 mesh; 0.3N HNO3 residue
HD969-BL/R sum	3.164	5.18	4.78	3.96	1.157 ± 0.064	1.27 ± 0.11	0.305	Excess Th		200-325 mesh; math. recombination
Trench 14d: Sub-horizontal layer of soil carbonate w/ abundant plant microfossils at base of Unit III of Menges. Composite sample gently crushed and seived.										
HD970-AW	***3.082***	***7.12***	***2.30***	***9.47***	***1.110 ± 0.018***	***1.007 ± 0.053***	***0.133***	***234 ± +47/-35***	***1.21 ± 0.04***	***<325 mesh; total digestion***
HD970-BW	3.273	6.80	2.86	8.40	1.119 ± 0.021	1.183 ± 0.053	0.196	Excess Th; 360 ka min.		200-325 mesh; total digestion
HD970-BL	1.964	5.68	2.63	8.37	1.166 ± 0.026	1.314 ± 0.051	0.317			200-325 mesh; 0.3N HNO3 leach
HD970-BR	1.707	8.82	3.55	10.00	1.066 ± 0.035	1.364 ± 0.072	0.250			200-325 mesh; 0.3N HNO3 residue
HD970-BL/R sum	3.671	7.14	3.06	9.25	1.108 ± 0.038	1.343 ± 0.053	0.265	Excess Th	Undefined	200-325 mesh; math. recombination

Table 13: continued.

Sample Name	Sample wt. (g)	Concentrations U (ppm)	Th (ppm)	Measured $^{230}Th/^{232}Th$ activity ratio	Detritus-Corrected: Activity Ratios $^{234}U/^{238}U$	$^{230}Th/^{238}U$	Corr.Coef. ρ(08-48)	AGE (ka)	Initial $^{234}U/^{238}U$ activity ratio	Aliquot Type
Trench 14d: Platy K bulk sample in lower portion of Unit V of Menges. Composite sample gently crushed and seived.										
HD971-AL	3.907	3.39	2.44	3.98	1.442 ± 0.060	0.929 ± 0.068	-0.031			<325 mesh; 0.3N HNO3 leach
HD971-AR	0.361	10.50	21.39	2.32	1.54 ± 0.33	2.17 ± 0.72	0.852			<325 mesh; 0.3N HNO3 residue
HD971-AL/R sum	***4.268***	***4.00***	***4.04***	***3.24***	***1.456 ± 0.097***	***1.107 ± 0.098***	***0.216***	***139 ± +34/-27***	***1.68 ± 0.16***	***<325 mesh; math. recombination***
HD971-CL	3.419	3.94	3.03	4.03	1.431 ± 0.064	1.029 ± 0.074	0.106			100-200 mesh; 0.3N HNO3 leach
HD971-CR	1.468	6.92	10.27	2.27	1.458 ± 0.162	1.18 ± 0.18	0.326			100-200 mesh; 0.3N HNO3 residue
HD971-CL/R sum	***4.888***	***4.83***	***5.21***	***2.99***	***1.441 ± 0.101***	***1.085 ± 0.104***	***0.177***	***137 ± +36/-28***	***1.65 ± 0.16***	***100-200 mesh; math. recombination***
HD971-AW	***2.527***	***4.05***	***4.14***	***3.25***	***1.454 ± 0.094***	***1.127 ± 0.104***	***0.243***	***144 ± +37/-28***	***1.68 ± 0.15***	***<325 mesh; total digestion***
HD971-BW	***3.389***	***4.70***	***3.68***	***3.47***	***1.411 ± 0.062***	***0.870 ± 0.072***	***-0.149***	***98 ± 15***	***1.54 ± 0.09***	***200-325 mesh; total digestion***

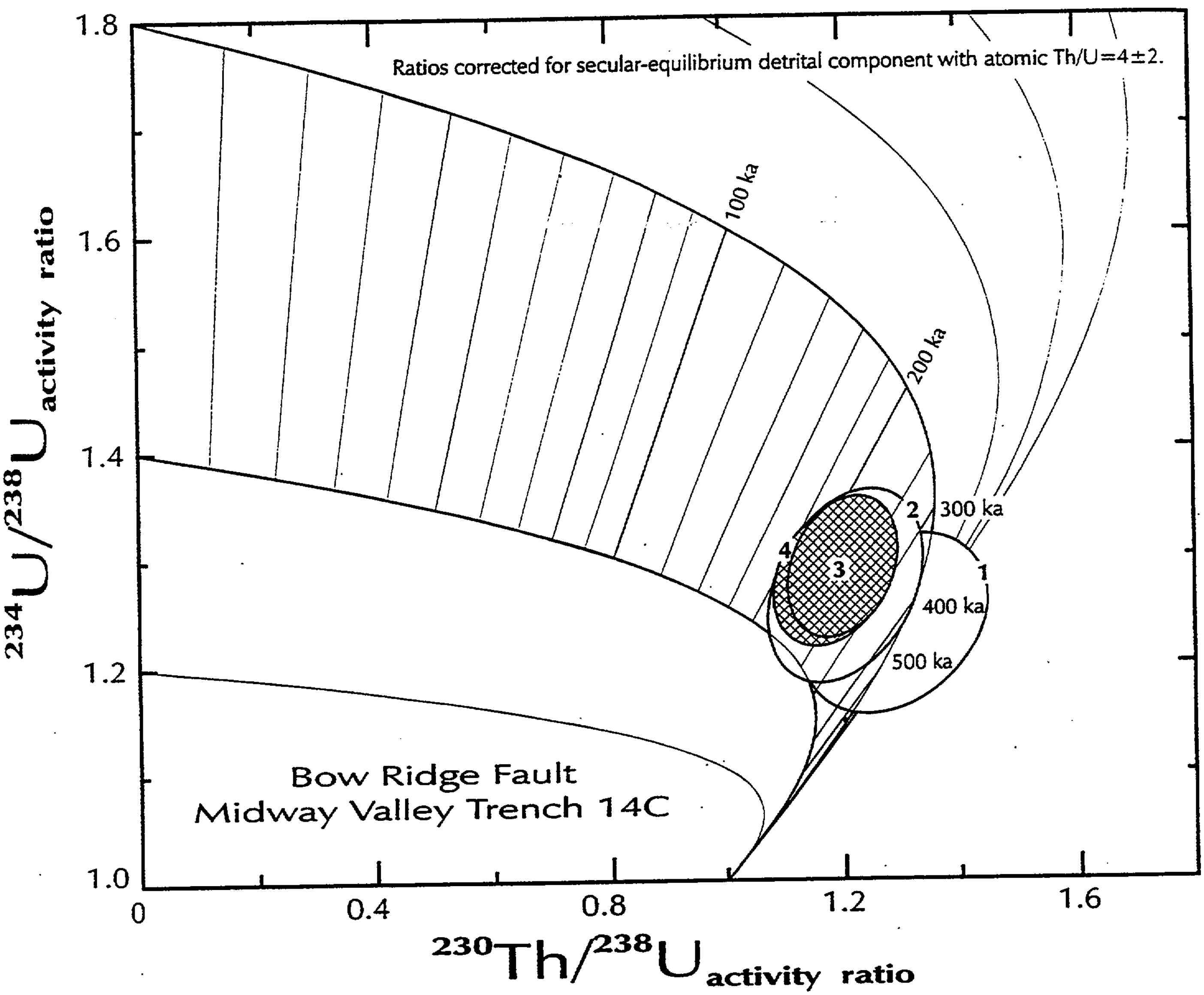

Figure 20: Uranium-series disequilibrium evolution diagram showing analyses of samples from Midway Valley Trench 14C. Error ellipses for aliqouts of the same sample are shaded in the same pattern. Data are given in Table 13 and correspond to the following numbers: 1=HD965-AL/R sum; 2=HD965-BL/R sum; 3=HD966-AL/R sum; 4=HD966-BL/R sum.

d:\ym\data\tecton\mwv\t14-ccrd.cdr
date updated: 8/11/95

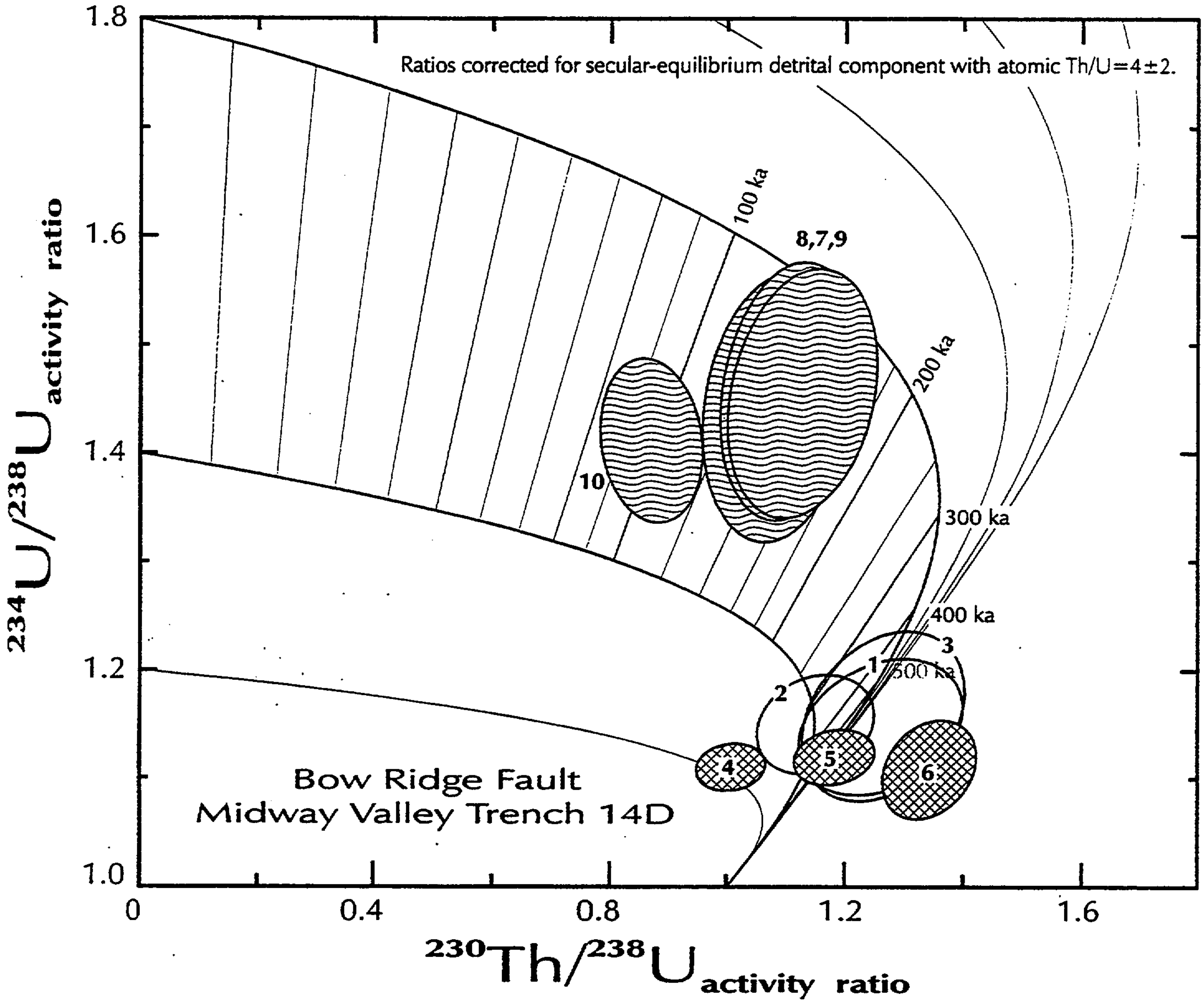

Figure 21: Uranium-series disequilibrium evolution diagram showing analyses of samples from Midway Valley Trench 14D. Error ellipses for aliqouts of the same sample are shaded in the same pattern. Data are given in Table 13 and correspond to the following numbers: 1=HD969-AW; 2=HD969-BW; 3=HD969-BL/R sum; 4=HD970-AW; 5=HD970-BW; 6=HD970-BL/R sum; 7=HD971-AL/R sum; 8=HD971-CL/R sum; 9=HD971-AW; 10=HD971-BW.

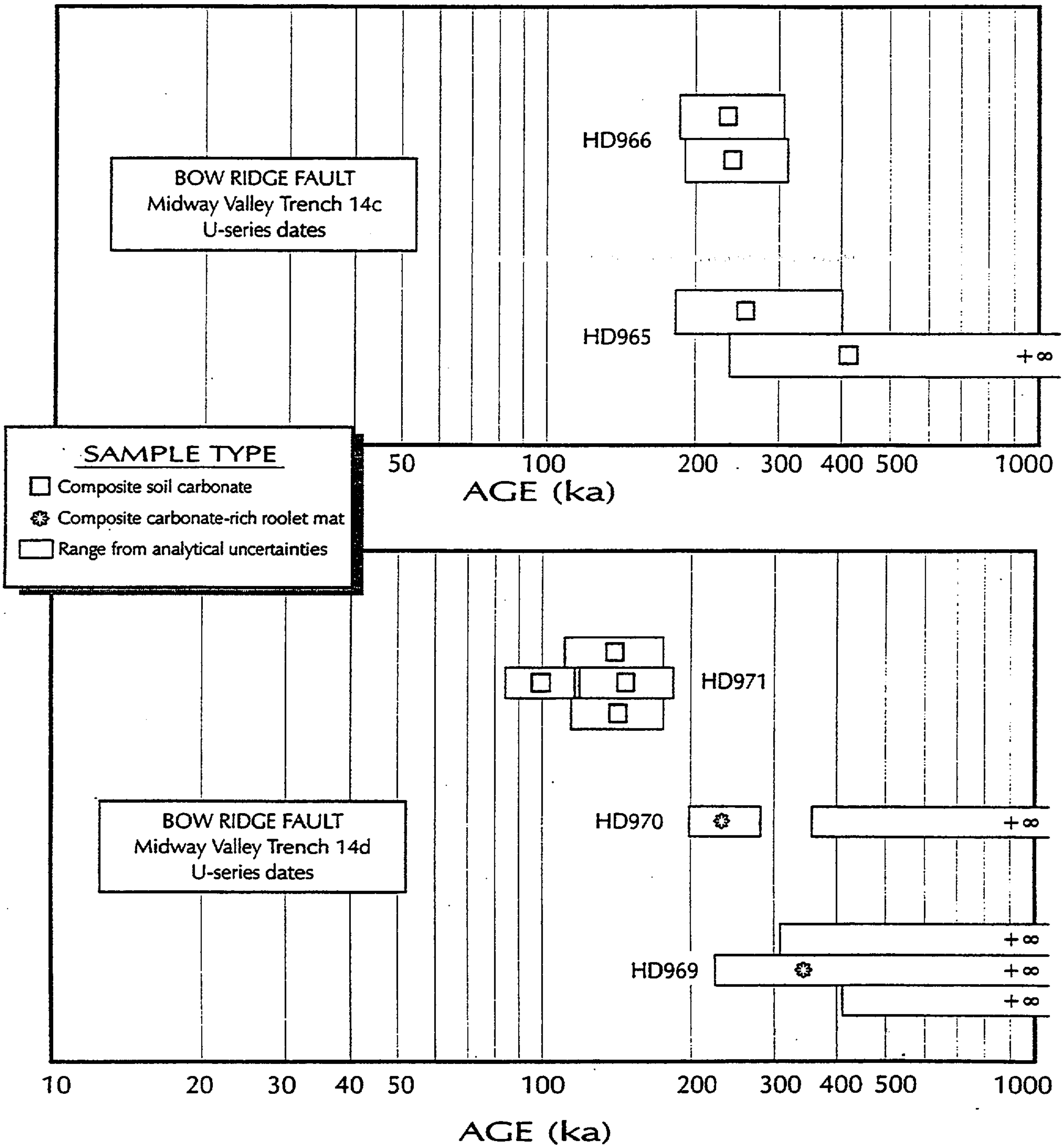

Figure 22: Distribution of uranium-series disequilibrium ages for samples from Midway Valley Trenches 14C and 14D. Data are given in Table 13.

d:\ym\data\tecton\mwv\t14-ages.cdr
updated 9/21/95

Table 14: Thermoluminescence results from Midway Valley Trench 14D. All errors given at the 95% confidence limit.

Sample Name	Field Moist. (%)	Saturation Moist. (%)	Dose Rate (Gy/ka) Field H_2O	Dose Rate (Gy/ka) Saturation H_2O	Total Bleach Eqivalent Dose (Gy)	Total Bleach Age (ka) for field moisture H_2O	Total Bleach Age (ka) for saturation moisture H_2O	Total Bleach Age (ka) Total Range	Partial Bleach Eqivalent Dose (Gy)	Partial Bleach Age (ka) for field moisture H_2O	Partial Bleach Age (ka) for saturation moisture H_2O	Partial Bleach Age (ka) Total Range
TL-06	*[North Wall, northern box trench, Unit 10 of Menges: Compact clay-rich, reddened B horizon]*											
	0.5	25	6.8±0.9	5.4±0.8	327 ± 125	48 ± 20	60 ± 25	28-85	302 ± 174	45 ± 26	55 ± 33	19-88
TL-09	*[Southern wall, northern box trench, Unit 4 of Menges: Silty-loam rich unit underlying K horizon]*											
	2.3	22	7.8±1.2	6.2±1.0	1026 ± 88	132 ± 23	165 ± 29	109-194	708 ± 305	91 ± 41	114 ± 52	50-166

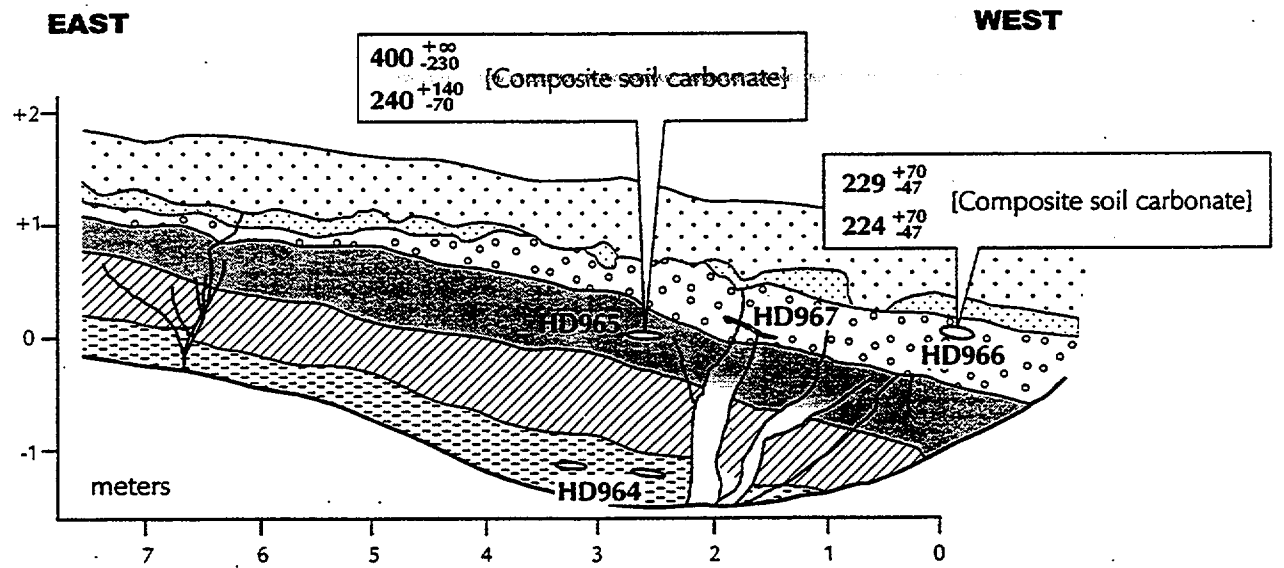

Figure 23: Generalized geological log of the south wall of Midway Valley Trench 14C exposing the Bow Ridge Fault (after Menges et al., 1994) and showing geochronological data. Uranium-series disequilibrium data (HD sample names) are from Table 13. See section 5.1 in text for explanations.

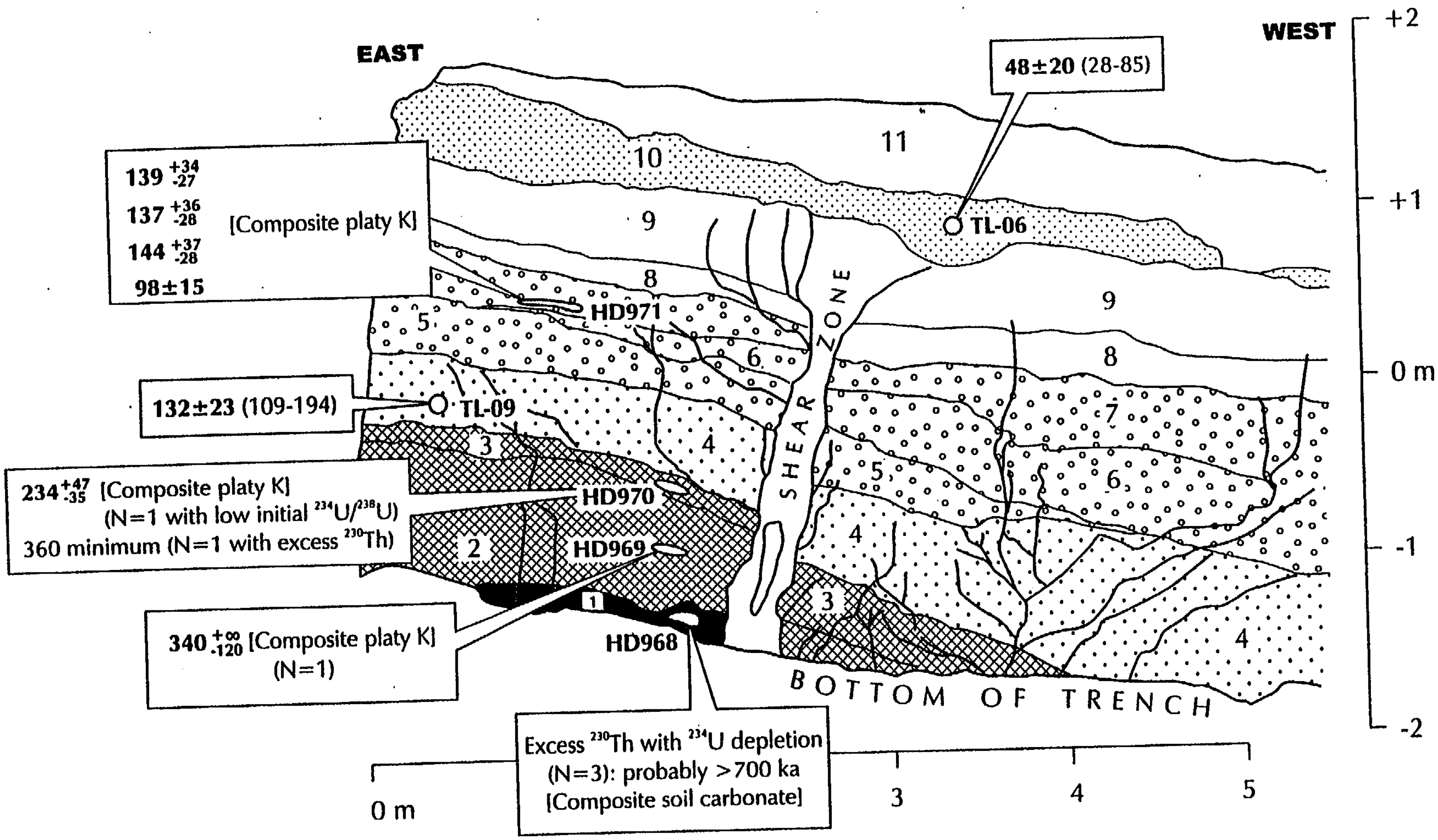

Figure 24: Generalized geological log of the south wall of the inner box of Midway Valley Trench 14D exposing the Bow Ridge Fault (after Menges et al., 1995) and showing geochronological data. Uranium-series disequilibrium data (HD sample names) are from Table 13, and thermoluminescence data are from Table 14. See section 5.1 in text for explanations.

5.2.4 Ghost Dance Fault

Whale Back Ridge Trench, Drill Hole Wash Trench 2, Spit Wash Trench 4

Table 15: Mass spectrometric U-series results from Ghost Dance Fault trenches

Figure 25: U-series concordia plot for samples from Whale Back Ridge trench

Figure 26: U-series concordia plot for samples from Drill Hole Wash Trench 2

Figure 27: U-series concordia plot for samples from Split Wash Trench 4

Figure 28: Distribution of U-series ages from Ghost Dance Fault trenches

Figure 29: Schematic log of Whale Back Ridge trench showing dating results

Figure 30: Schematic log of Drill Hole Wash Trench 2 showing dating results

Figure 31: Schematic log of Split Wash Trench 4 showing dating results

Table 15: Uranium-series disequilibrium results from Trenches along the Ghost Dance Fault. Data are determined by mass spectrometry. The detrital component is assumed to be in secular equilibrium with an atomic TH/U of 4±2. See trench logs in Taylor and others (1995) for specific sample locations. All errors given at the 95% confidence level.

Sample Name	Sample wt. (g)	Concentration		$^{230}Th/^{232}Th$ activity ratio	Detritus-corrected		Sample Type
		U ppm	Th ppm		Age (ka)	$^{234}U/^{238}U_{initial}$	
South wall, east end, Whale Back Ridge Trench: Densely-cemented (Si+Cc) colluvium directly overlying brecciated bedrock							
HD1721-A1	0.100	10.8	0.352	47.5	42.7 ± 0.6	1.593 ± 0.009	Si-rich matrix lamina
HD1721-A3	0.104	12.4	0.301	98.4	81 ± 2	1.57 ± 0.02	Si-rich matrix lamina
HD1721-B1	0.120	10.5	1.03	24.8	83 ± 2	1.559 ± 0.013	Si-rich matrix lamina
HD1721-C1	0.188	15.7	0.031	928.7	53.4 ± 0.5	1.581 ± 0.008	Si-rich matrix lamina
South wall, east end, Whale Back Ridge Trench: Densely-cemented (Si+Cc) colluvium directly overlying brecciated bedrock							
HD1722-A1	0.106	4.18	2.06	2.0	17 ± 6	1.56 ± 0.05	Si-rich matrix lamina
HD1722-A2	0.143	21.4	0.161	53.5	9.64 ± 0.12	1.553 ± 0.007	Si-rich matrix lamina
South wall, east end, Whale Back Ridge Trench: Densely-cemented (Si+Cc) colluvium near top of unit (overlying HD1721)							
HD1723-A1	0.144	65.6	0.129	1303	90.9 ± 1.0	1.556 ± 0.008	Si-rich matrix lamina
HD1723-B1	0.141	20.6	1.77	28.6	84.8 ± 1.8	1.557 ± 0.014	Si-rich matrix lamina
HD1723-C1	0.079	7.79	0.622	11.3	21.8 ± 0.9	1.573 ± 0.010	Si-rich matrix lamina
South wall, east end, Whale Back Ridge Trench: Cobble-sized clast with well-developed Si-rich rind from within fault breccia.							
HD1724-B1	0.101	0.68	0.0896	24.7	270 +inf/-220	1.28 ± 0.09	Silica-rich clast rind
HD1724-B2	0.216	0.88	0.0580	60.4	392 ± +70/-48	1.79 ± 0.14	Silica-rich clast rind
HD1724-B3	0.063	6.98	0.0403	973	Excess Th	Undetermined	Silica-rich clast rind
HD1724-C1	0.147	0.68	0.0475	50.8	420 +inf/-110	1.47 ± 0.08	Silica-rich clast rind
HD1724-C2	0.258	1.06	0.0375	112	392 ± 29	1.77 ± 0.07	Silica-rich clast rind
South wall, east end, Trench 2, Drill Hole Wash: 20 cm diameter cobble with well-developed rind from Unit 2 K horizon							
HD1717-A1	0.136	4.27	3.07	3.9	95 ± 12	1.64 ± 0.08	Silica-rich clast rind
HD1717-B1	0.114	5.04	3.71	3.7	88 ± 12	1.63 ± 0.08	Silica-rich clast rind
HD1717-C1	0.175	2.19	2.28	1.6	26 ± 13	1.80 ± 0.16	Si-rich matrix lamina
HD1717-E1	0.169	2.24	1.86	2.1	33 ± 10	1.75 ± 0.11	Si-rich matrix lamina
South wall, east end, Trench 2, Drill Hole Wash: 0.5 cm diameter rhizoliths from Unit 2 K horizon							
HD1718-A1	0.184	3.13	0.348	19.8	66.9 ± 1.5	1.619 ± 0.013	Individual rhizolith
HD1718-B1	0.150	6.16	0.662	20.6	67.0 ± 1.5	1.635 ± 0.013	Individual rhizolith
HD1718-C1	0.312	5.42	0.377	32.1	67.5 ± 1.1	1.644 ± 0.011	Individual rhizolith
South wall, east end, Trench 2, Drill Hole Wash: Sub-horizontal lens of soil carbonate from Unit 2 K horizon							
HD1719-A1	0.217	4.14	0.638	5.8	19.6 ± 1.6	1.64 ± 0.02	Carbonate-rich rootlet mass
HD1719-A2	0.405	5.50	0.528	11.0	24.6 ± 1.0	1.656 ± 0.013	Si-rich stringer in rootlet mass

Table 15: Continued.

Sample Name	Sample wt. (g)	Concentration		$^{230}Th/^{232}Th$	Detritus-corrected		Sample Type
		U ppm	Th ppm	activity ratio	Age (ka)	$^{234}U/^{238}U_{initial}$	
South wall, east end, Trench 2, Drill Hole Wash: Large (2-3 cm diameter), horizontally-oriented rhizolith from Unit 2 K horizon							
HD1720-A1	0.223	3.96	0.745	12.9	71 ± 3	1.71 ± 0.02	Individual rhizolith
HD1720-B1	0.116	4.35	1.12	9.4	73 ± 3	1.68 ± 0.03	Individual rhizolith
South wall, west end, Trench 4a, Split Wash: Slope-parallel lens of soil carbonate from Unit 3 K horizon							
HD1829-A1	0.369	14.2	1.02	25.1	49.6 ± 1.0	1.655 ± 0.011	Si-rich stringer in rootlet mass
HD1829-B1	0.293	14.5	0.317	76.6	45.2 ± 0.5	1.667 ± 0.010	Si-rich stringer in rootlet mass
North wall, west end, Trench 4a, Split Wash: Banded Si-rich fracture filling between blocks of pryed-apart bedrock							
HD1830-A1	0.162	5.35	0.591	36.1	253 ± 13	1.75 ± 0.03	Shallow bedrock vein
HD1830-A2	0.177	7.99	0.856	39.2	265 ± 12	1.87 ± 0.04	Shallow bedrock vein
HD1830-A4	0.365	7.11	2.50	9.2	132 ± 7	1.67 ± 0.04	Shallow bedrock vein
North wall, west end, Trench 4a, Split Wash: Slope-parallel platy soil carbonate from 10 to 20 cm below Quaternary/bedrock interface.							
HD1831-A1	0.190	5.02	0.431	11.3	22.2 ± 0.9	1.675 ± 0.012	Si-rich stringer in rootlet mass
HD1831-A1b	0.357	5.02	0.452	11.1	23.0 ± 1.0	1.669 ± 0.011	Si-rich stringer in rootlet mass
HD1831-B2	0.291	5.55	0.955	8.9	37 ± 2	1.69 ± 0.02	Si-rich stringer in rootlet mass

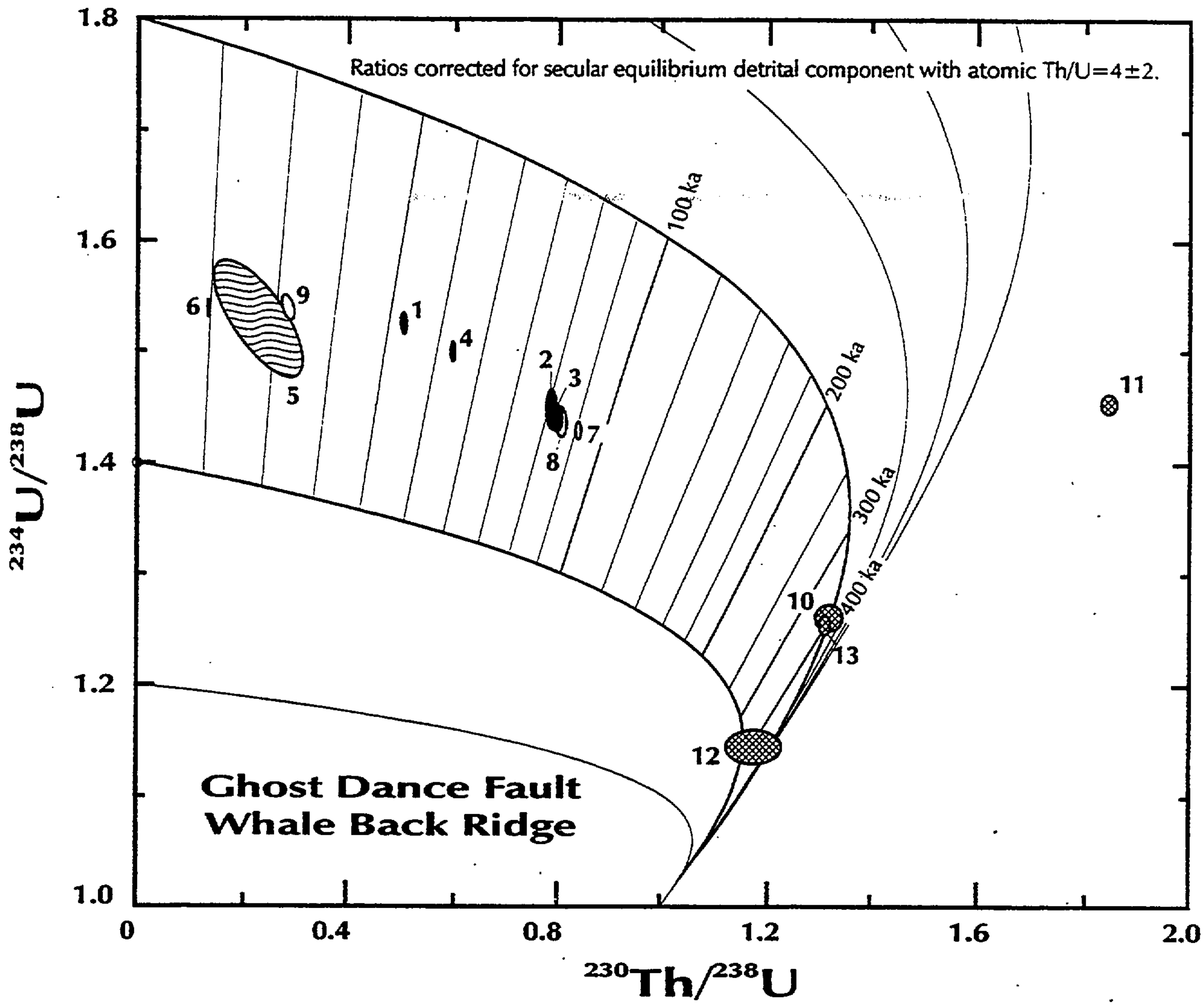

Figure 25: Uranium-series disequilibrium evolution diagram showing analyses of samples from the Whale Back Ridge Trench across the Ghost Dance Fault. Error ellipses for aliquots of the same sample are shaded with the same pattern. Data are given in Table 15 and correspond to the following numbers: 1=HD1721-A1; 2=HD1721-A3; 3=HD1721-B1; 4=HD1721-C1; 5=HD1722-A1; 6=HD1722-A2; 7=HD1723-A1; 8=HD1723-B1; 9=HD1723-C1; 10=HD1724-B2; 11=HD1724-B3; 12=HD1724-C1; 13=HD1724-C2.

d:\ym\data\tecton\gdf\gdf-ccrd.cdr
updated: 9/21/95

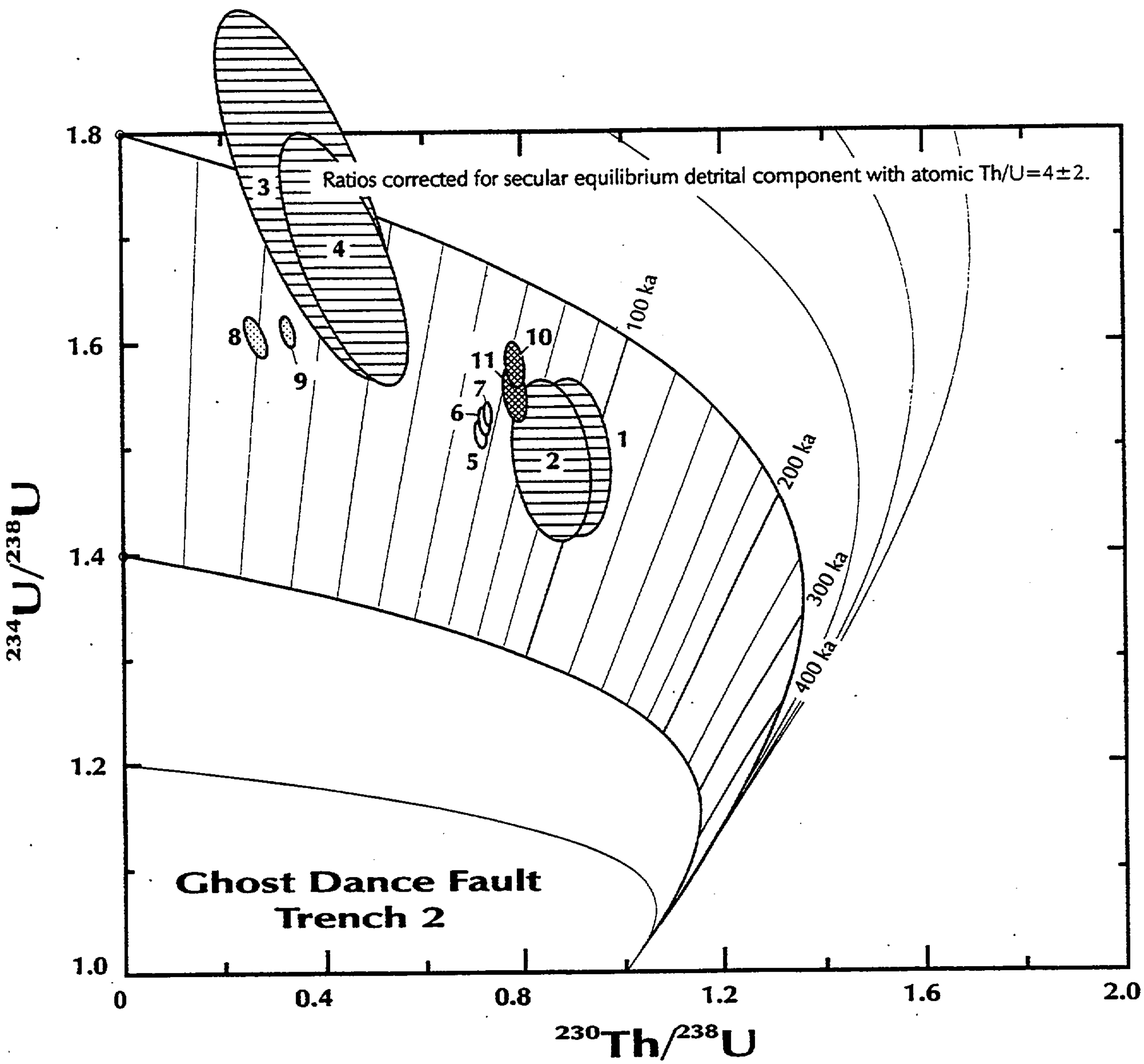

Figure 26: Uranium-series disequilibrium evolution diagram showing analyses of samples from Drill Hole Wash Trench 2 across the Ghost Dance Fault. Error ellipses for aliquots of the same sample are shaded with the same pattern. Data are given in Table 15 and correspond to the following numbers: 1=HD1717-A1; 2=HD1717-B3; 3=HD1717-C1; 4=HD1717-E1; 5=HD1718-A1; 6=HD1718-B1; 7=HD1718-C1; 8=HD1719-A1; 9=HD1719-A2; 10=HD1720-A1; 11=HD1724-B1.

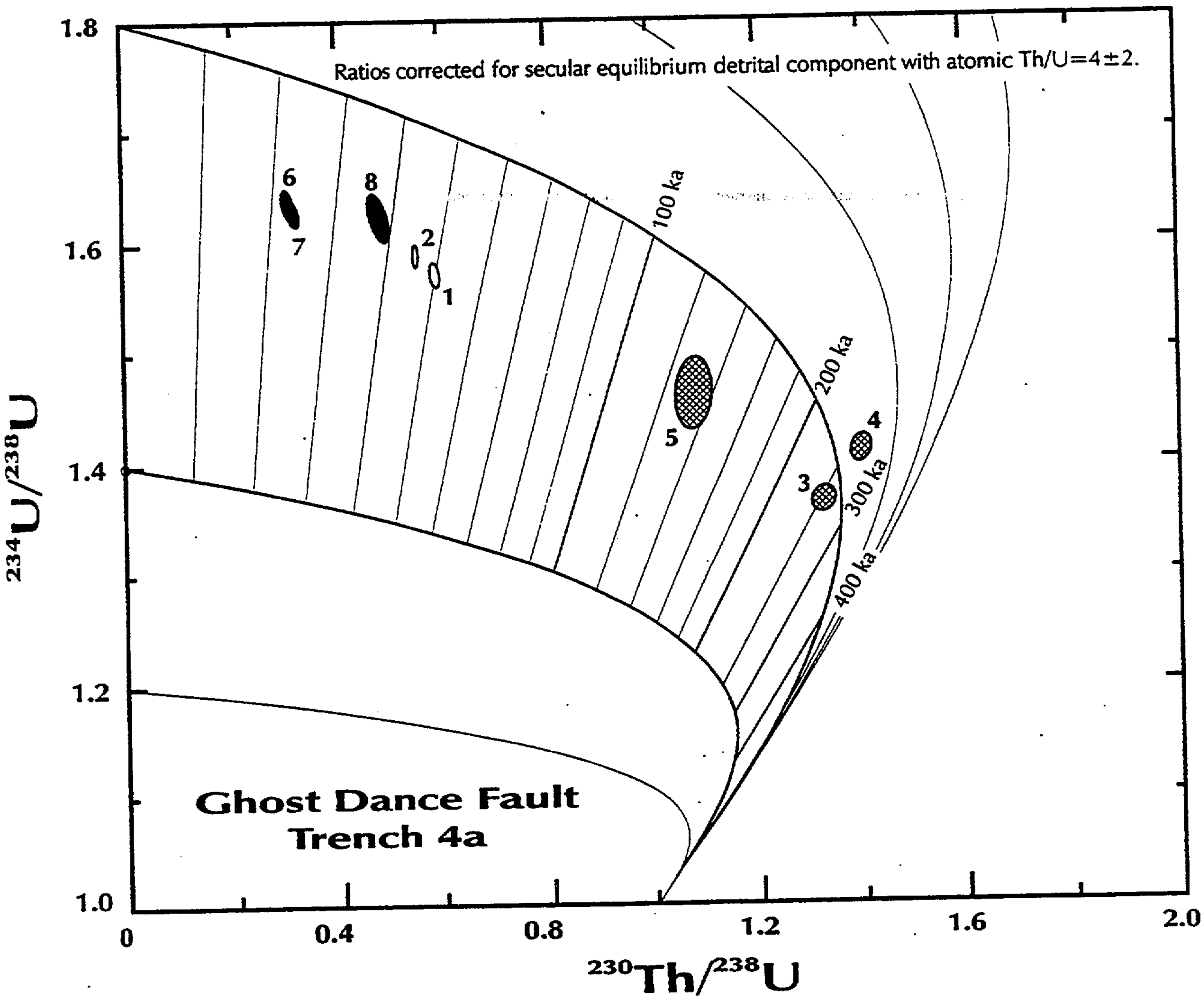

Figure 27: Uranium-series disequilibrium evolution diagram showing analyses of samples from Split Wash Trench 4a across the Ghost Dance Fault. Error ellipses for aliquots of the same sample are shaded with the same pattern. Data are given in Table 15 and correspond to the following numbers: 1=HD1829-A1; 2=HD1829-B1; 3=HD1830-A1; 4=HD1830-A2; 5=HD1830-A4; 6=HD1831-A1; 7=HD1831-A1b; 8=HD1831-B2.

d:\ym\data\tecton\gdf\gdf-ccrd.cdr
updated: 9/21/95

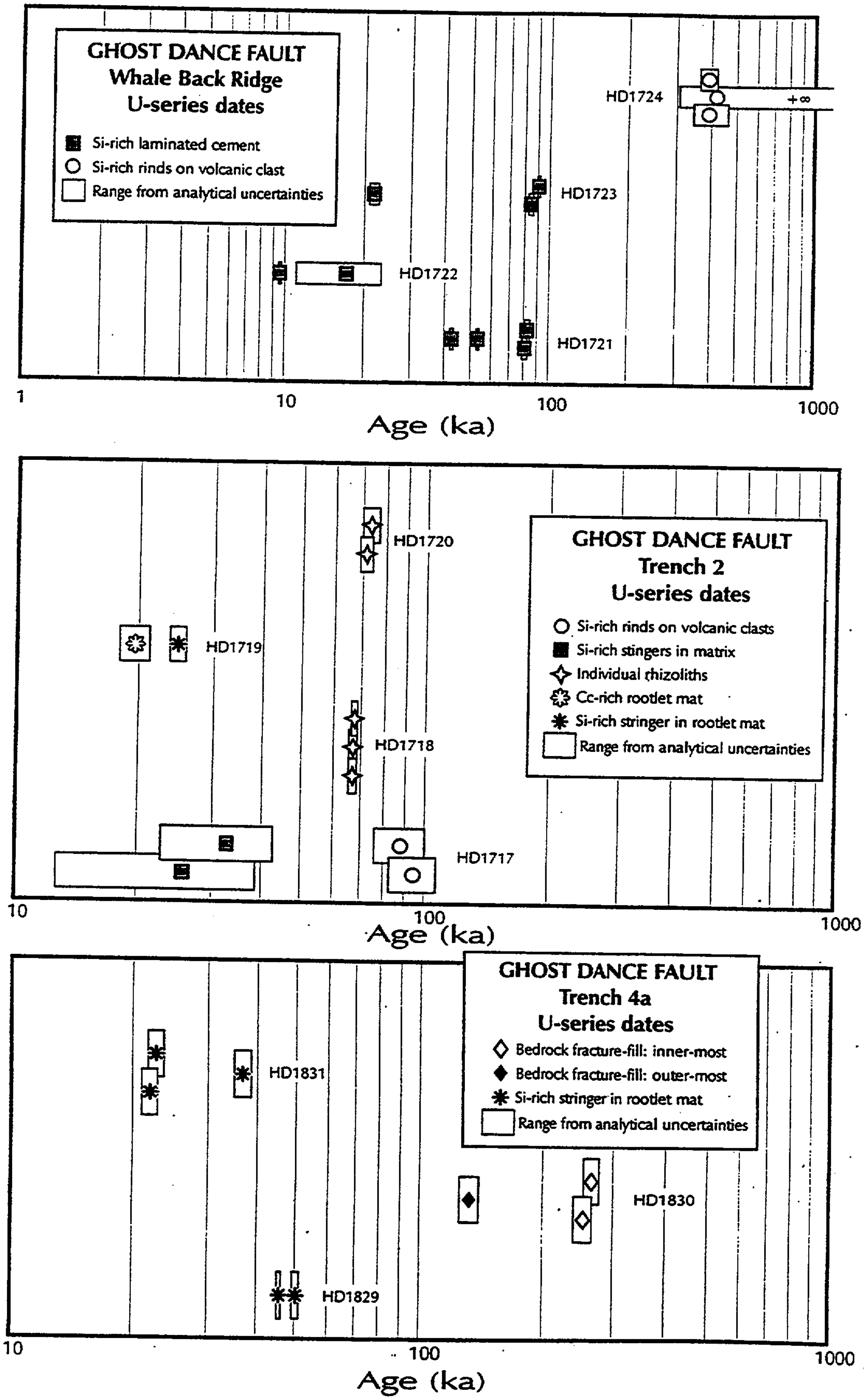

Figure 28: Distribution of uranium-series disequilibrium ages for samples from Ghost Dance Fault Trenches. Data are given in Table 15.

d:\ym\data\tecton\gdf\gdageplt.cdr

Note: Only oldest U-series disequilibrium dates for each sample are reported

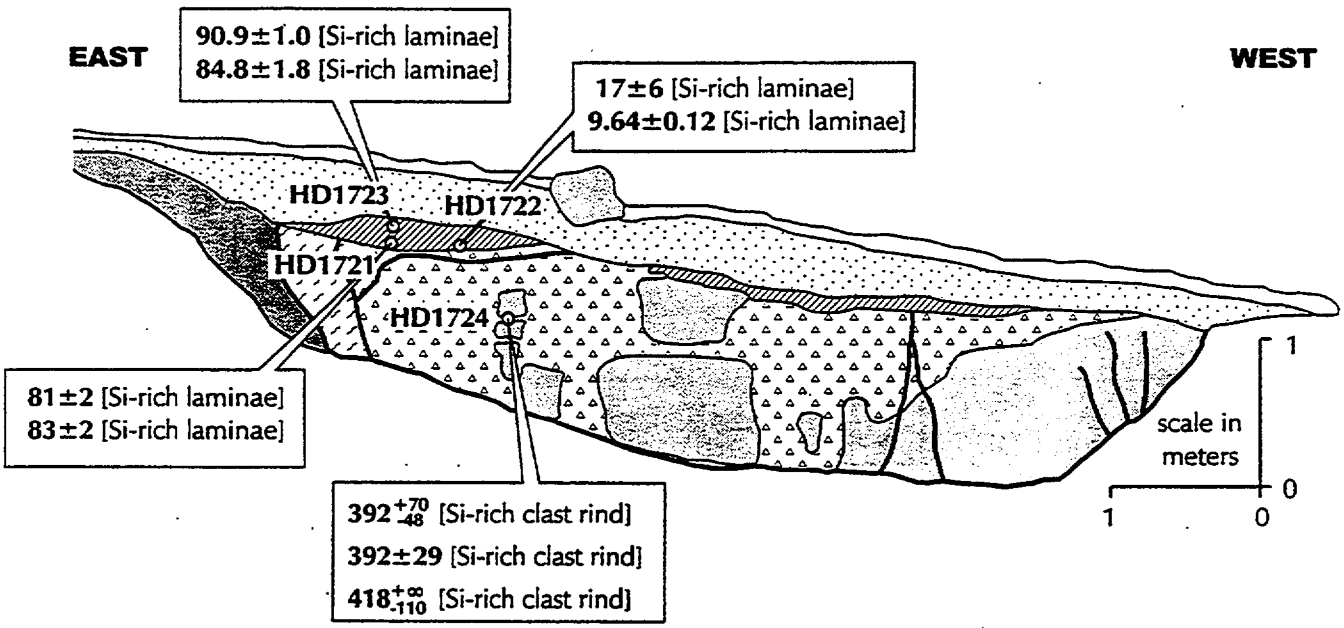

Figure 29: Generalized geological log showing geochronological data of the south wall, east end, of the trench on Whale Back Ridge exposing the Ghost Dance Fault (after Taylor, et al., 1995). Uranium-series data (HD sample names) are from Table 15. See section 5.1 in text for explanations.

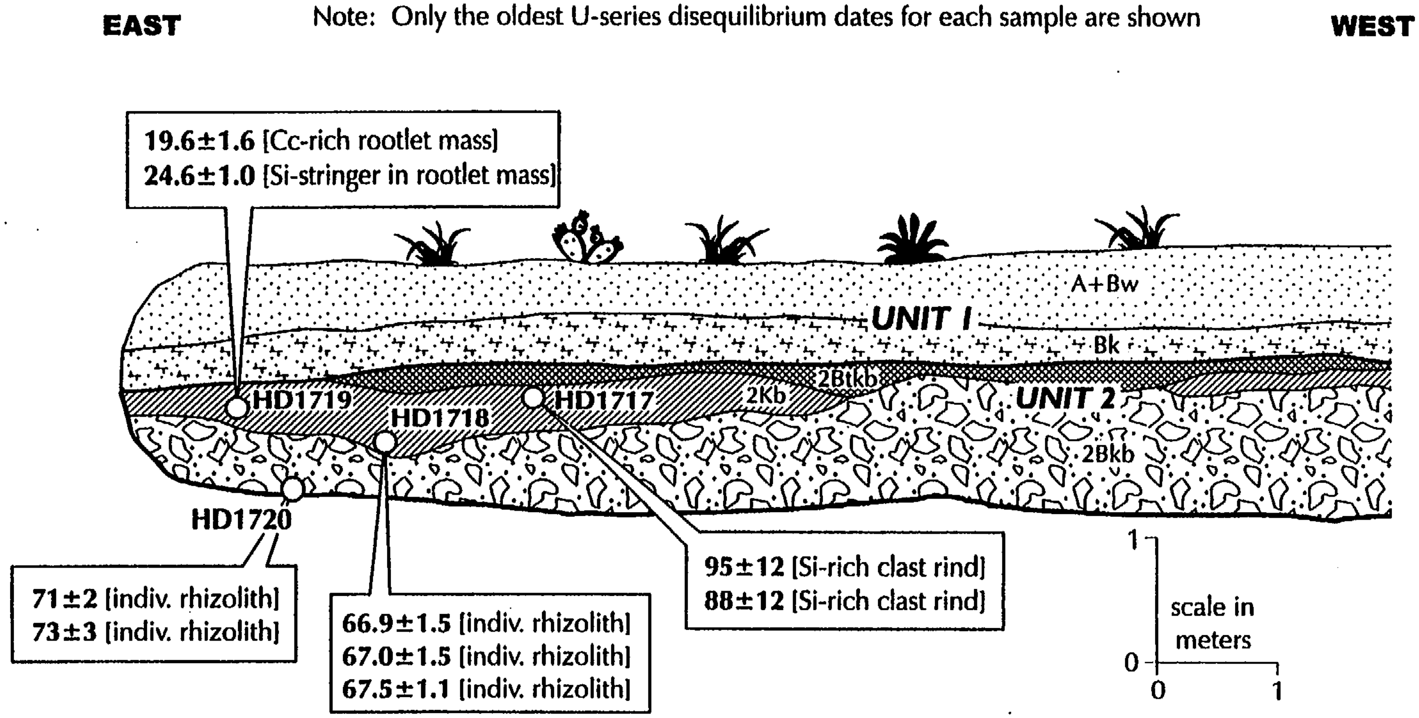

Figure 30: Generalized geological log showing geochronological data of the south wall, east end, of Drill Hole Wash Trench 2 exposing the Ghost Dance Fault (after Taylor, et al., 1995). Uranium-series data (HD sample names) are from Table 15. See section 5.1 in text for explanations.

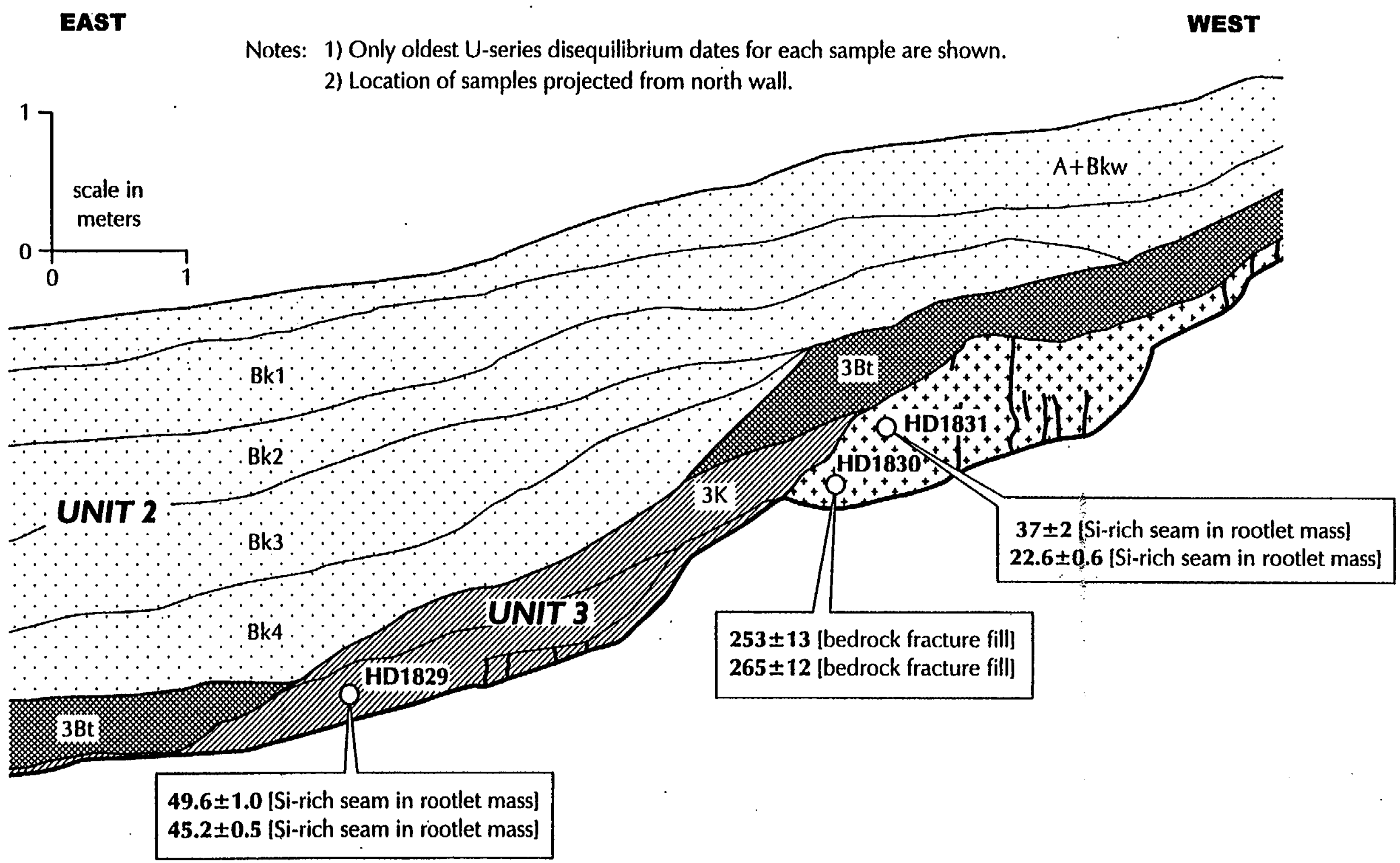

Figure 31: Generalized geological log showing geochronological data of the south wall, west end, of Split Wash Trench 4a exposing the Ghost Dance Fault (after Taylor, et al., 1995). Uranium-series data (HD sample names) are from Table 15. See section 5.1 in text for explanations.

5.2.5 Stagecoach Road Fault

SCR-T1/SCR-T3

Table 16: Mass spectrometric U-series results from Stagecoach Road Trenches

Table 17: Alpha spectrometric U-series results from Stagecoach Road Trenches

Figure 32: U-series concordia plot for samples from Stagecoach Road trench

Figure 33: Distribution of U-series ages for Stagecoach Road trench samples

Table 18: Thermoluminescence dating results from Stagecoach Road trench samples

Figure 34: Schematic log of Stagecoach Road Trench 1 showing dating results

Figure 35: Schematic log of Stagecoach Road Trench 3 showing dating results

Table 16: Uranium-series disequilibrium results from Stagecoach Road Trenches 1 and 3. Data are determined by mass spectrometry. The detrital component is assumed to be in secular equilibrium with an atomic TH/U of 4±2. See trench logs in Menges and others (1995) for specific sample locations. All errors given at the 95% confidence level.

Sample Name	Sample wt. (g)	Concentration		$^{230}Th/^{232}Th$ activity ratio	Detritus-corrected		Sample Type
		U ppm	Th ppm		Age (ka)	$^{234}U/^{238}U_{initial}$	
Trench SCR-T1, south wall adjacent to main fault trace: Verically-oriented rhizolith in sandy matrix							
HD1439A	0.294	6.96	0.730	5.9	13.7 ± 1.2	1.545 ± 0.014	Individual Rhizolith
HD1439B	0.345	6.24	2.61	1.9	13 ± 5	1.58 ± 0.04	Individual Rhizolith
HD1439C	0.244	5.03	0.599	5.5	14.7 ± 1.3	1.52 ± 0.02	Individual Rhizolith
HD1439C-2	0.079	4.94	0.645	7.4	23 ± 4	1.59 ± 0.02	Individual Rhizolith
HD1439C-3	0.117	5.09	0.608	5.8	15.6 ± 1.3	1.54 ± 0.02	Individual Rhizolith
HD1439D(#5)	0.119	1.60	0.182	6.4	16.1 ± 1.4	1.59 ± 0.03	Individual Rhizolith
Trench SCR-T1, north wall, Unit F of Menges et al. (1995): Unconsolidated sandy horizon with 5 to 10% basaltic ash.							
HD1826-BA	0.095	1.97	7.37				Basalt ash concentrate
Trench SCR-T3, north wall, unit G2 of Menges et al., (1995): Composite sample of carbonate-rich soil of trench gently crushed and seived.							
HD1447-D	0.133	5.47	2.86	6.0	57 ± 15	2.7 ± 0.5	Composite massive soil carbonate

Table 17: Uranium-series disequlibrium results from Stagecoach Road Trenches 1 and 3. Data collected previously by alpha spectrometry (Paces et al., 1994). Criteria for calculating age estimates includes: 1) Whole rock analyses (either total digestion or leach/residue recombination; 2) Suffiently small detrital component correction (i.e., 230Th/232Th >~2); 3) Reasonable initial 234U/238U composition (i.e., 1.6±2). Analyses given in boldface below meet these critera. The detrital comonent is assumed to be in secular equilibrium with an atomic Th/U of 4±2. All uncertainties are given at the 95% confidence level.

Sample Name	Sample wt. (g)	Concentrations U (ppm)	Concentrations Th (ppm)	Measured $^{230}Th/^{232}Th$ activity ratio	Detritus-Corrected Activity Ratios $^{234}U/^{238}U$	Detritus-Corrected Activity Ratios $^{230}Th/^{238}U$	Corr.Coef. ρ(08-48)	AGE (ka)	Initial $^{234}U/^{238}U$ activity ratio	Aliquot Type
Trench 1, north wall, down-thrown block, Unit D of Menges et al. (1995): Composite rhizolith sample from lower rhizolith zone; cleaned of sandy sheaths, gently crushed and sieved.										
HD1067-AL	2.19	9.77	0.786	13.2	1.587 ± 0.020	0.335 ± 0.016	0.003			<325 mesh; 0.3N HNO3 leach
HD1067-AR	0.99	9.75	1.46	8.7	1.581 ± 0.031	0.409 ± 0.021	-0.011			<325 mesh; 0.3N HNO3 residue
HD1067-AL/R sum	***3.19***	9.76	1.00	***11.1***	***1.585 ± 0.033***	***0.358 ± 0.015***	***0.030***	***27.4 ± 1.4***	***1.63 ± 0.04***	***<325 mesh; math. recombination***
HD1067-AW	***3.02***	10.3	0.98	***10.6***	***1.567 ± 0.019***	***0.315 ± 0.015***	***-0.082***	***24.1 ± 1.3***	***1.61 ± 0.02***	***<325 mesh; total digestion***
HD1067-BW	***3.04***	11.8	1.34	***8.7***	***1.557 ± 0.019***	***0.306 ± 0.022***	***-0.120***	***23.5 ± 2.0***	***1.60 ± 0.02***	***200-325 mesh; total digestion***
HD1067-CW	***3.12***	11.0	3.28	***3.9***	***1.580 ± 0.031***	***0.328 ± 0.039***	***-0.525***	***25 ± 4***	***1.62 ± 0.03***	***100-200 mesh; total digestion***
Trench 1, north wall, down-thrown block, Unit F of Menges et al. (1995): Composite rhizolith sample from upper rhizolith zone; cleaned of sandy sheaths, gently crushed and sieved.										
HD1068-AL	1.21	7.01	0.616	8.7	1.501 ± 0.018	0.236 ± 0.027	-0.092			<325 mesh; 0.3N HNO3 leach
HD1068-AR	0.70	8.24	1.52	4.5	1.499 ± 0.061	0.236 ± 0.017	0.063			<325 mesh; 0.3N HNO3 residue
HD1068-AL/R sum	***1.91***	7.46	0.945	***6.2***	***1.500 ± 0.051***	***0.236 ± 0.019***	***0.003***	***18.4 ± 1.6***	***1.53 ± 0.05***	***<325 mesh; math. recombination***
HD1068-AW	***1.91***	7.54	0.928	***6.1***	***1.494 ± 0.019***	***0.221 ± 0.016***	***-0.230***	***17.2 ± 1.5***	***1.52 ± 0.02***	***<325 mesh; total digestion***
HD1068-BW	***2.17***	6.93	0.956	***6.3***	***1.509 ± 0.018***	***0.261 ± 0.101***	***-0.302***	***20.4 ± 1.7***	***1.54 ± 0.02***	***200-325 mesh; total digestion***
HD1068-CW	***1.95***	8.04	3.70	***1.8***	***1.519 ± 0.045***	***0.170 ± 0.011***	***-0.644***	***13 ± 6***	***1.54 ± 0.05***	***100-200 mesh; total digestion***
Trench 3, north wall, Unit G2 of Menges et al. (1995): Massive K soil at top of lower bench near west end of trench. Composite sample gently crushed and seived.										
HD1447-AL2	1.69	1.65	4.18	2.1	2.4 ± 1.3	3.10 ± 0.24	0.961			<325 mesh; 7.6N HNO3 leach
HD1447-AR2	0.90	15.4	3.01	12.1	1.53 ± 0.02	0.766 ± 0.033	0.027			<325 mesh; 7.6N HNO3 residue
HD1447-AL/R2	***2.58***	6.43	3.77	***4.8***	***1.59 ± 0.07***	***0.925 ± 0.046***	***-0.028***	***88 ± 9***	***1.76 ± 0.09***	***<325 mesh; math. recombination***
HD1447-AW	***1.58***	2.42	8.40	***7.2***	***1.53 ± 0.04***	***1.004 ± 0.090***	***0.151***	***107 ± 9***	***1.72 ± 0.06***	***<325 mesh; total digestion***
HD1447-BW	***1.23***	6.50	2.75	***13.1***	***1.52 ± 0.02***	***0.978 ± 0.069***	***0.093***	***104 ± 7***	***1.69 ± 0.03***	***200-325 mesh; total digestion***
HD1447-CW	2.31	12.9	2.93	1.5	1.7 ± 0.4	0.937 ± 0.073	-0.097			100-200 mesh; total digestion
HD1447-EW	***4.15***	4.64	8.89	***1.9***	***1.59 ± 0.22***	***0.968 ± 0.108***	***-0.032***	***94 +40/-29***	***1.8 ± 0.3***	***>100 mesh; total digestion***

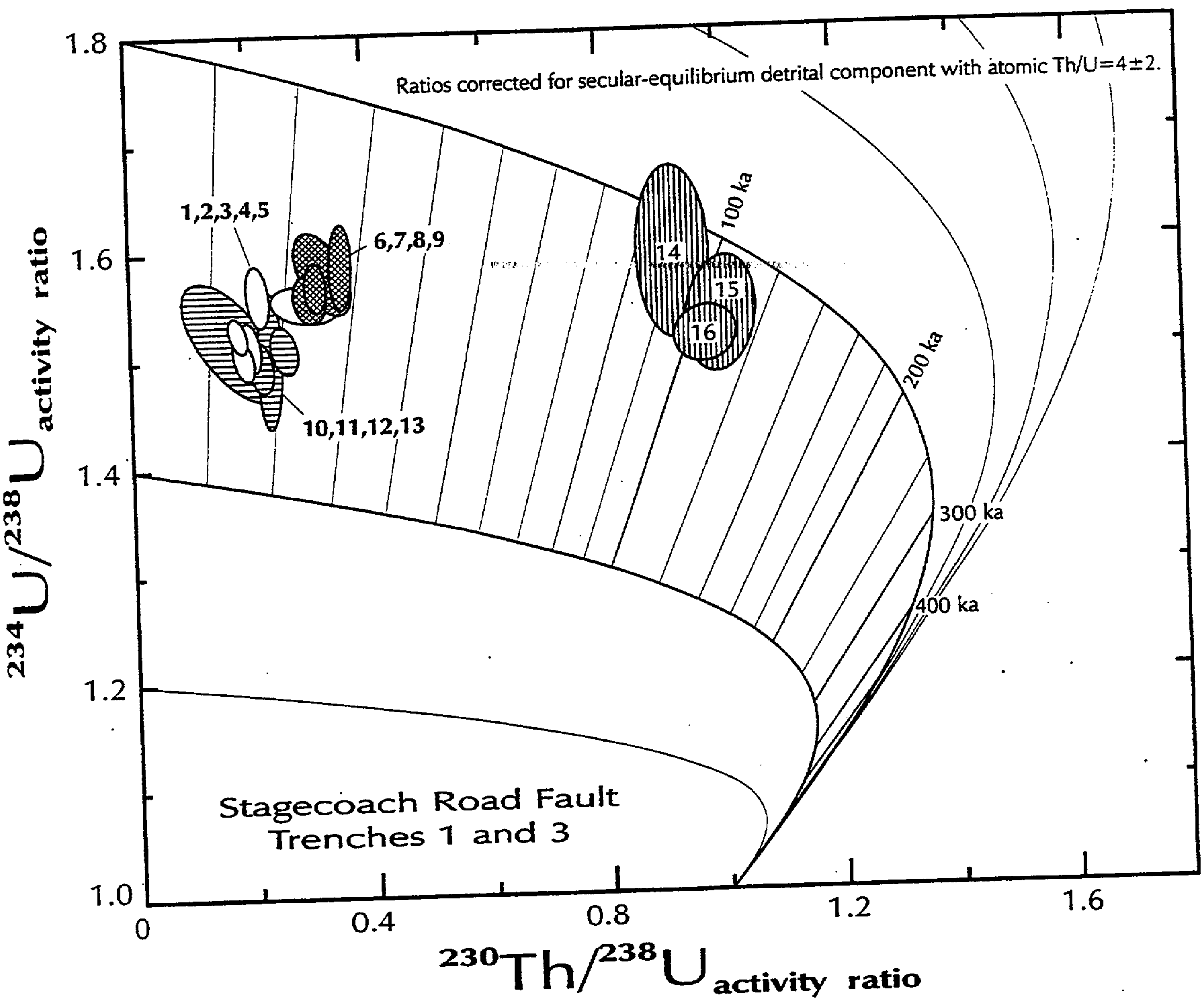

Figure 32: Uranium-series disequilibrium evolution diagram showing analyses of samples from Stagecoach Road Fault Trenches 1 and 3. Error ellipses for aliquots of the same sample are shaded with the same pattern. Data are given in Tables 16 and 17 and correspond to the following numbers: 1=HD1439A; 2=HD1439C; 3=HD1439C-2; 4=HD1439C-3; 5=HD1439D(#5); 6=HD1067-AL/R sum; 7=HD1067-AW: 8=HD1067-BW; 9=HD1067-CW; 10=HD1068-AL/R sum; 11=HD1068-AW; 12=HD1068-BW; 13=HD1068-CW; 14=HD1447-AL/R2 sum; 15=HD1447-AW; 16=HD1447-BW.

d:\ym\data\tecton\scr\scr-ccrd.cdr
date updated: 9/21/95

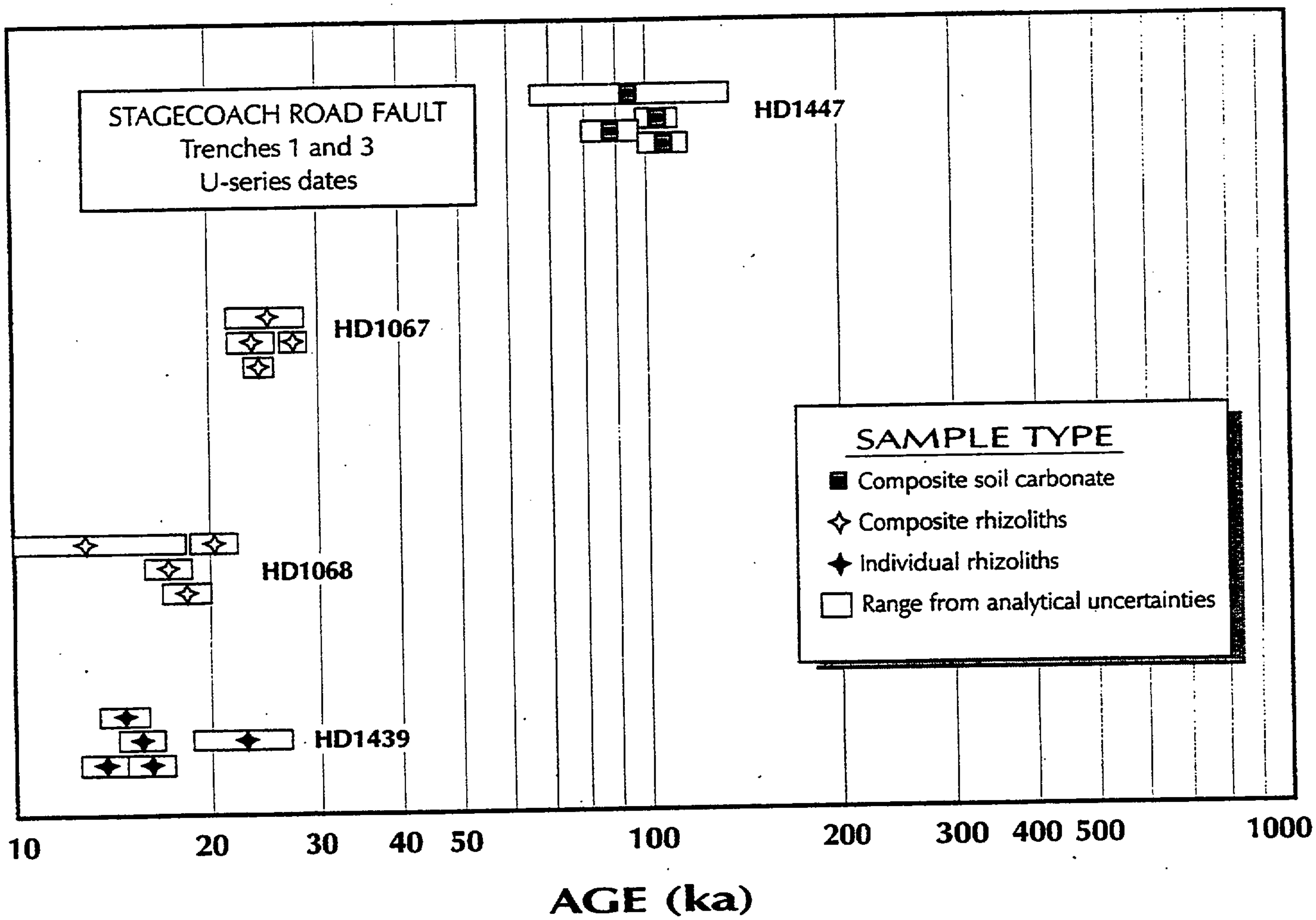

Figure 33: Distribution of uranium-series disequilibrium ages for samples from Stagecoach Road Fault Trenches 1 and 3. Data are given in Tables 16 and 17.

d:\ym\data\tecton\scr\scr-ages.cdr
updated 9/21/95

Table 18: Thermoluminescence results from Stagecoach Road Trenches 1 and 3. All errors given at the 95% confidence limit. See logs in Menges and others (1995) for specific sample locations.

Sample Name	Field Moist. (%)	Saturation Moist. (%)	Dose Rate (Gy/ka)		Total Bleach Eqivalent Dose (Gy)	Total Bleach Age (ka)			Partial Bleach Eqivalent Dose (Gy)	Partial Bleach Age (ka)		
			Field H_2O	Saturation H_2O		for field moisture H_2O	for saturation moisture H_2O	Total Range		for field moisture H_2O	for saturation moisture H_2O	Total Range
TL-02	*[North wall, Trench 1, Unit H of Menges: Vesicular A horizon.]*											
	5	15	8.6±1.2	8.2±1.2	95 ± 46	12 ± 6	13 ± 6	6-19	115 ± 60	14 ± 7.5	16 ± 8.4	6.5-24
TL-15	*[North wall, Trench 1, Unit G of Menges: Reddish-brown, sandy unit.]*											
	0.5	20	7.7±1.0	6.2±0.9	26 ± 0.3	3.4 ± 0.5	4.2 ± 0.6	3.0-4.8				
TL-16	*[North wall, Trench 1, Unit F of Menges: Sandy unit with abundant gravel clasts and carbonate rhizoliths.]*											
	0.8	15	7.5±1.0	6.0±0.9	210 ± 42	28 ± 4	35 ± 7	24-42	184 ± 59	25 ± 3.2	31 ± 10	21-41
TL-25	*[Resample of TL-15]*											
	3.8	13	8.8±1.2	7.9±1.1	103 ± 4	12 ± 1.7	13 ± 1.9	10-15	111 ± 29	13 ± 3.8	14 ± 4.2	9-18
TL-26	*[Resample of TL-02]*											
	4.7	15	8.4±1.1	7.5±1.0	75 ± 3	8.9 ± 1.2	10 ± 1	8-11	73 ± 4	8.8 ± 1.2	9.8 ± 1.5	7.6-11
TL-27	*[North wall, Trench 1, Unit D of Menges: Sandy unit with abundant carbonate rhizoliths.]*											
	4.7	14	8.0±1.1	7.2±1.0	392 ± 67	49 ± 11	54 ± 12	38-66	265 ± 117	33 ± 15	37 ± 17	18-54
TL-17	*[North wall, Trench 3, Unit J of Menges: Silty vesicuar A horizon]*											
	5	19	8.5±1.1	6.8±0.9	318 ± 17	38 ± 5	47 ± 7	33-54	387 ± 26	46 ± 6.8	57 ± 8.8	39-66
TL-16	*[North wall, Trench 3, Unit I of Menges: Silty unit]*											
	3	16	8.3±1.1	6.6±0.9	185 ± 31	22 ± 4.8	28 ± 6.2	17-34	154 ± 88	19 ± 11	23 ± 14	8-37
TL-19	*[North wall, Trench 3, Unit G of Menges: Sandy unit]*											
	0	20	8.0±1.0	6.4±0.9	691 ± 110	87 ± 18	108 ± 23	69-131	565 ± 123	71 ± 18	89 ± 23	53-112
TL-28	*[Resample of TL-17]*											
	4.7	19	8.4±1.1	7.2±1.0	20 ± 2	2.4 ± 0.4	2.8 ± 0.4	2.0-3.2	20 ± 4.5	2.4 ± 0.6	2.8 ± 0.7	1.6-3.5
TL-29	*[North wall, Trench 3, Unit C of Menges: Sandy unit]*											
	5.4	27	12±2	9.3±1.3	476 ± 124	40 ± 12	51 ± 15	28-66	241 ± 170	21 ± 15	26 ± 19	6-45

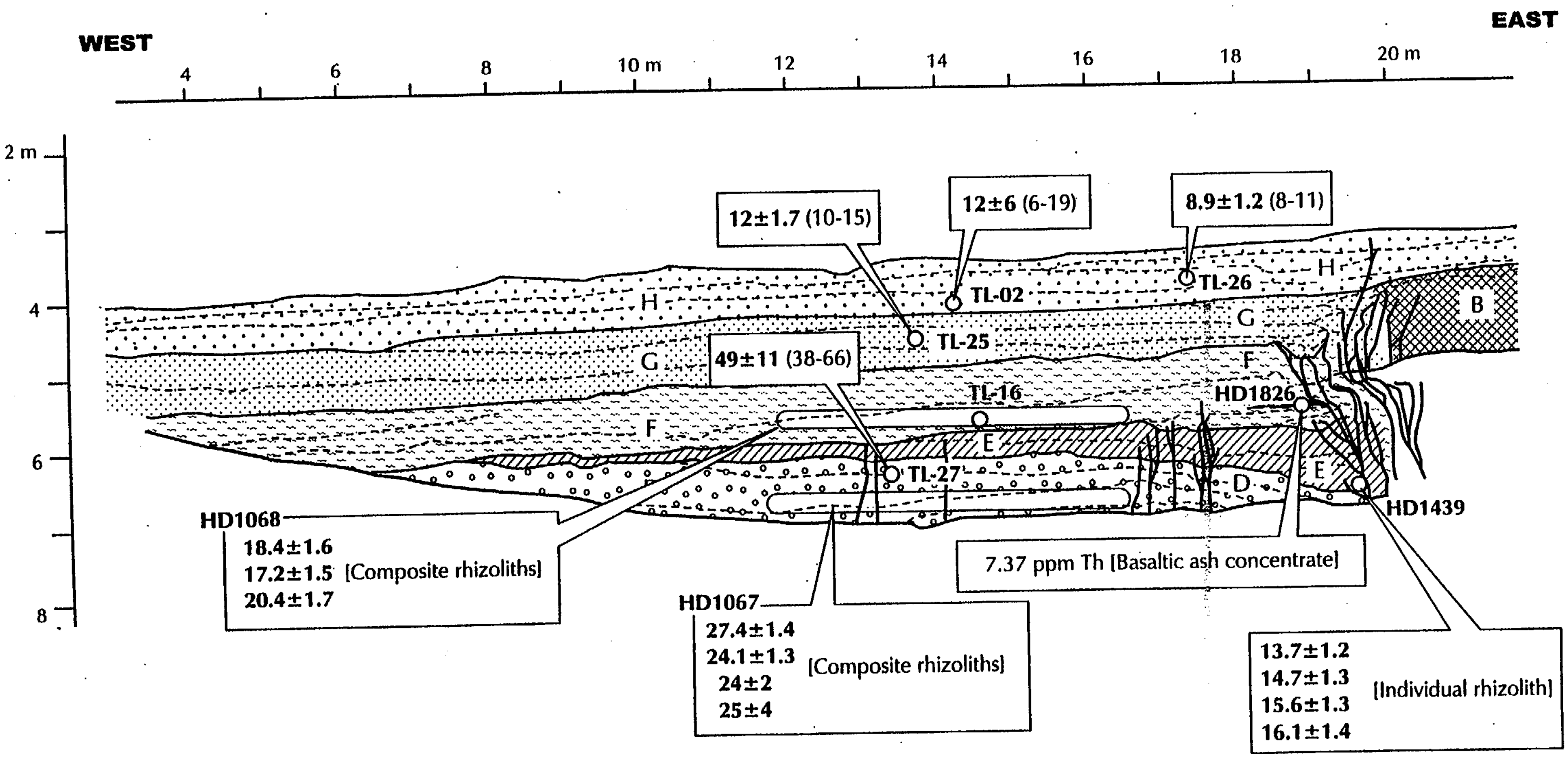

Figure 34: Generalized geologic log showing geochronological data of the north wall, west end of Stagecoach Road Fault Trench 1 (after Menges, et al., 1995). Uranium series data (HD sample names) are from Tables 16 and 17, and thermoluminescence data (TL sample names) are from Table 18. See section 5.1 in text for further explanation.

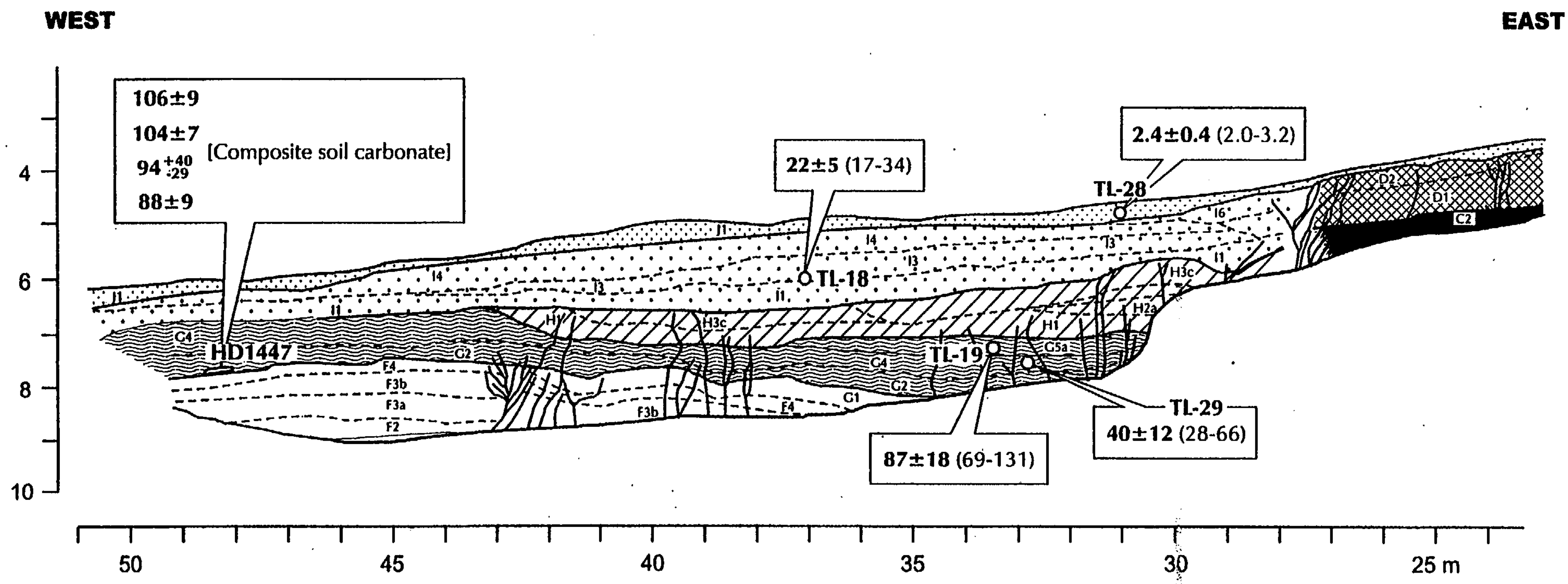

Figure 35: Generalized geologic log showing geochronological data of the north wall, west end of Stagecoach Road Fault Trench 3 (after Menges, et al., 1995). Uranium series data (HD sample names) are from Tables 16 and 17, and thermoluminescence data (TL sample names) are from Table 18. See section 5.1 in text for further explanation.

5.2.6 Solitario Canyon Fault

5.2.6.1 Trench 8

Table 19: Mass spectrometric U-series results from Solitario Canyon Fault Trench 8

Table 20: Alpha spectrometric U-series results from Solitario Canyon Fault Trench 8

Figure 36: U-series concordia plot for samples from Solitario Canyon Fault Trench 8

Figure 37: Distribution of U-series ages for samples from Solitario Canyon Fault Trench 8

Table 21: Thermoluminescence dating results from Solitario Canyon Fault Trench 8 samples

Figure 38: Schematic log of Solitario Canyon Fault Trench 8 showing dating results

Table 19: Uranium-series disequilibrium results from Solitario Canyon Fault Trench 8. Data are determined by mass spectrometry. The detrital component is assumed to be in secular equilibrium with an atomic TH/U of 4±2. See trench logs in Ramelli and others (1995) for specific sample locations. All errors given at the 95% confidence level.

Sample Name	Sample wt. (g)	Concentration		$^{230}Th/^{232}Th$ actvity ratio	Detritus-corrected		Sample Type
		U ppm	Th ppm		Age (ka)	$^{234}U/^{238}U_{Initial}$	
South wall, base of large fissure: Unconsolidated black ashy sand. Ash concentrated magnetically and hand-picked.							
HD1070-BA	0.071	2.12	7.39				Basalt ash concentrate
South wall, base of large fissure: Rhizoliths from ash-rich pocket							
HD1070-M1	0.127	6.67	0.102	96.9	39.3 ± 1.4	1.64 ± 0.02	Individual Rhizolith
HD1070-M2	0.129	15.6	0.482	34.9	26.5 ± 1.2	1.65 ± 0.02	Individual Rhizolith
South wall, in large fissure, ~30 cm from surface: Dispersed carbonate soil developed on fissure fill material							
HD1465-M2 mx	0.128	4.10	5.38	1.9	66 ± 23	1.70 ± 0.19	Composite Soil Carbonate
HD1465-M2 rd	0.108	9.56	5.71	2.9	47 ± 9	1.45 ± 0.05	Composite Soil Carbonate
South wall, in large fissue, ~85 cm below surface: Dispersed carbonate soil developed on fissure fill material							
HD1466-M1	0.164	16.1	2.63	15.7	101 ± 4	1.45 ± 0.03	Composite Soil Carbonate
HD1466-M2	0.135	4.63	3.10	7.3	Excess ^{230}Th	Undefined	Composite Soil Carbonate

Table 20: Uranium-series disequlibrium results from Solitario Canyon Fault Trench 8. Data collected previously by alpha spectrometry (Paces et al., 1994). Criteria for calculating age estimates includes: 1) Whole rock analyses (either total digestion or leach/residue recombination; 2) Suffiently small detrital component correction (i.e., 230Th/232Th >~2); 3) Reasonable initial 234U/238U composition (i.e., 1.6±2). Analyses given in boldface below meet these critera. The detrital comonent is assumed to be in secular equilibrium with an atomic Th/U of 4±2. All uncertainties are given at the 95% confidence level.

Sample Name	Sample wt. (g)	Concentrations U (ppm)	Concentrations Th (ppm)	Measured $^{230}Th/^{232}Th$ activity ratio	Detritus-Corrected Activity Ratios $^{234}U/^{238}U$	Detritus-Corrected Activity Ratios $^{230}Th/^{238}U$	Corr.Coef. ρ(08-48)	AGE (ka)	Initial $^{234}U/^{238}U$ activity ratio	Aliquot Type
Trench 8: Rhizoliths from within pocket of basaltic ash near base of fissure. Composite sample cleaned of sandy sheaths, gently crushed and seived.										
HD1070-AW	***1.24***	***8.77***	***0.86***	***13.4***	***1.429 ± 0.017***	***0.420 ± 0.014***	***0.011***	***37 ± 2***	***1.48 ± 0.02***	***<325 mesh; total digestion***
HD1070-BW	***1.82***	***6.53***	***1.03***	***11.7***	***1.431 ± 0.024***	***0.589 ± 0.023***	***0.078***	***56 ± 3***	***1.51 ± 0.03***	***200-325 mesh; total digestion***
HD1070-CW	***1.58***	***7.04***	***2.73***	***4.74***	***1.543 ± 0.041***	***0.562 ± 0.041***	***-0.357***	***48 ± 5***	***1.62 ± 0.05***	***100-200 mesh; total digestion***
HD1070-DW	***1.24***	***10.05***	***1.88***	***7.52***	***1.388 ± 0.023***	***0.437 ± 0.023***	***-0.117***	***40 ± 3***	***1.44 ± 0.03***	***>100 mesh; total digestion***
Trench 8: Carbonate-rich, ash-bearing vein material w/in fissure fill near base. Composite sample gently crushed and seived.										
HD1071-AW	***1.10***	***4.64***	***1.04***	***3.49***	***1.557 ± 0.034***	***0.211 ± 0.030***	***-0.339***	***16 ± 3***	***1.58 ± 0.04***	***<325 mesh; total digestion***
HD1071-BW	***1.58***	***5.04***	***1.26***	***3.13***	***1.540 ± 0.034***	***0.207 ± 0.033***	***-0.404***	***16 ± 3***	***1.56 ± 0.04***	***200-325 mesh; total digestion***
HD1071-CW	***1.11***	***5.50***	***3.05***	***1.73***	***1.568 ± 0.060***	***0.202 ± 0.079***	***-0.651***	***15 ± 7***	***1.59 ± 0.06***	***100-200 mesh; total digestion***
HD1071-DW	***1.39***	***6.25***	***2.39***	***2.24***	***1.553 ± 0.043***	***0.203 ± 0.052***	***-0.553***	***15 ± 4***	***1.58 ± 0.05***	***>100 mesh; total digestion***
Trench 8: Carbonate-rich, sub-vertical vein material, adjacent, but exterior, to fissure fill. Plant microfossils. Composite sample gently crushed and seived.										
HD1072-AW	***2.13***	***6.65***	***0.37***	***53.9***	***1.456 ± 0.017***	***0.987 ± 0.024***	***0.272***	***114 ± 5***	***1.63 ± 0.02***	***<325 mesh; total digestion***
HD1072-BW	***1.98***	***5.95***	***0.38***	***48.3***	***1.459 ± 0.022***	***1.020 ± 0.029***	***0.301***	***119 ± 6***	***1.64 ± 0.03***	***200-325 mesh; total digestion***
HD1072-CW	***1.82***	***6.65***	***0.50***	***41.9***	***1.466 ± 0.021***	***1.046 ± 0.029***	***0.290***	***124 ± 6***	***1.66 ± 0.03***	***100-200 mesh; total digestion***
HD1072-DW	***1.45***	***7.68***	***0.40***	***59.5***	***1.467 ± 0.019***	***1.011 ± 0.025***	***0.298***	***117 ± 5***	***1.65 ± 0.03***	***>100 mesh; total digestion***

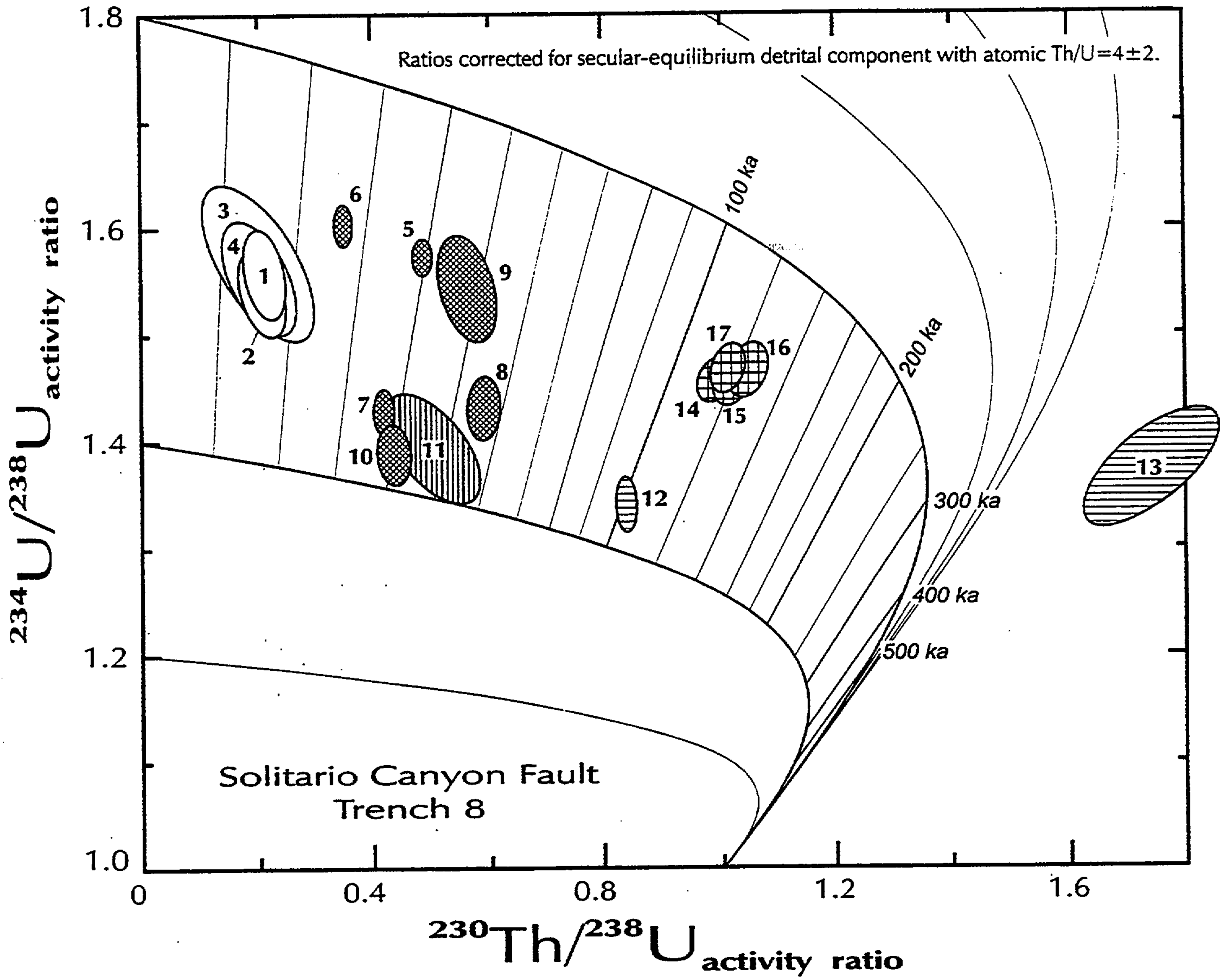

Figure 36: Uranium-series disequilibrium evolution diagram showing analyses of samples from Solitario Canyon Fault Trench 8. Error ellipses for aliquots of the same sample are shaded in the same pattern. Data are given in Tables 19 and 20 and correspond to the following numbers: 1=HD1071-AW; 2=HD1071-BW; 3=HD1071-CW; 4=HD1071-DW; 5=HD1070-M1; 6=HD1070-M2; 7=HD1070-AW; 8=HD1070-BW; 9=HD1070-CW; 10=HD1070-DW; 11=HD1465-M2; 12=HD1466-M1; 13=HD1466-M2; 14=HD1072-AW; 15=HD1072-BW; 16=HD1072-CW; 17=HD1071-DW.

d:\ym\data\tecton\sc\sc-ccrd.cdr
date updated: 9/21/95

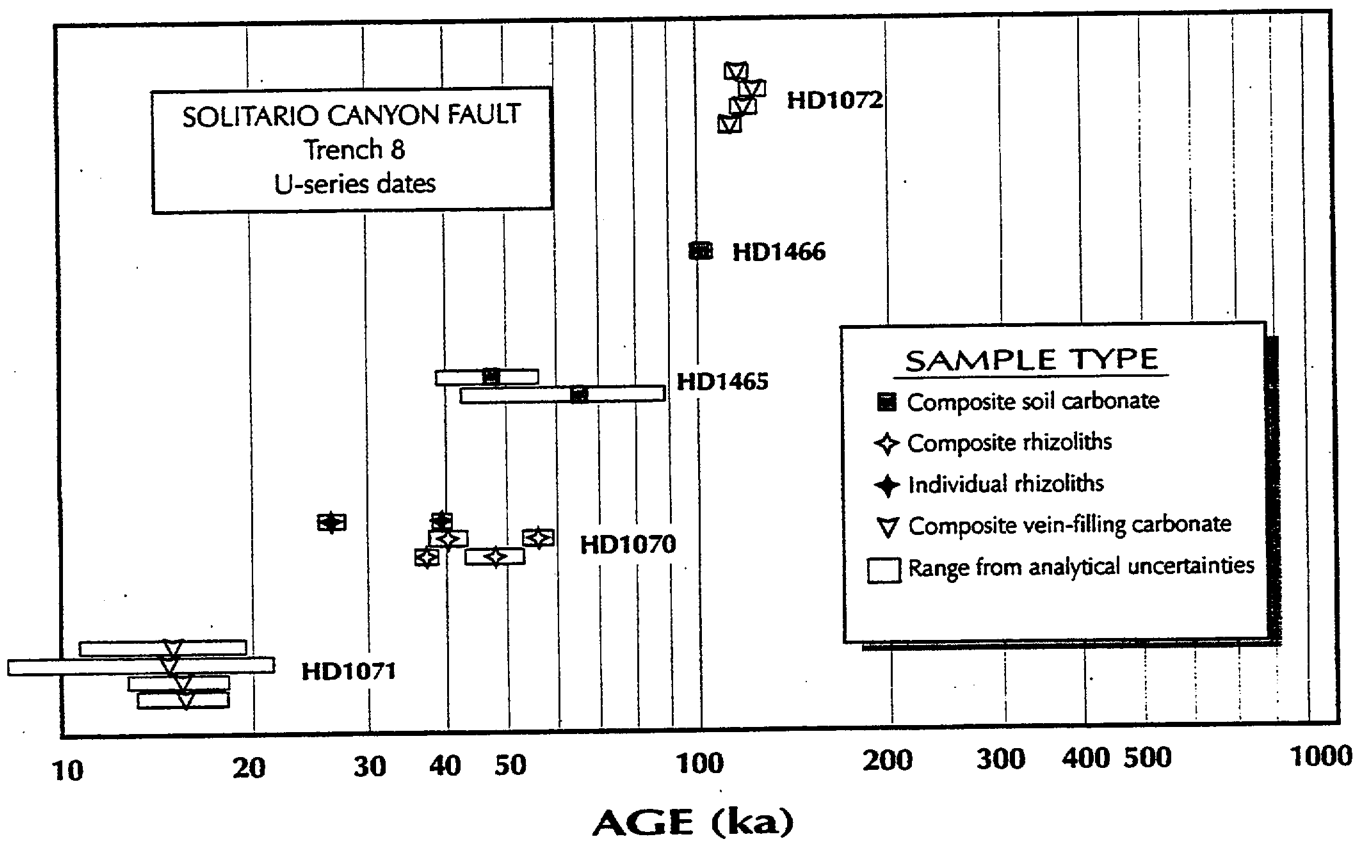

Figure 37: Distribution of uranium-series ages for samples from Solitario Canyon Fault Trench 8. Data are given in Tables 19 and 20.

d:\ym\data\tecton\sc\sc-age.cdr
updated 8/11/95

Table 21: Thermoluminescence results from Solitario Canyon Fault Trench 8a. All errors given at the 95% confidence limit. See logs in Ramelli and others (1995) for specific sample locations.

Sample Name	Field Moist. (%)	Saturation Moist. (%)	Dose Rate (Gy/ka)		Total Bleach Eqivalent Dose (Gy)	Total Bleach Age (ka)			Partial Bleach Eqivalent Dose (Gy)	Partial Bleach Age (ka)		
			Field H_2O	Saturation H_2O		for field moisture H_2O	for saturation moisture H_2O	Total Range		for field moisture H_2O	for saturation moisture H_2O	Total Range
TL-10	*[North wall, Trench 8a: Vesicular A horizon, upper portion]*											
	0.5	25	6.5±0.9	5.3±0.8	74 ± 2	11 ± 1.7	14 ± 2.1	10-16	67 ± 5	10 ± 1.7	13 ± 2.1	9-15
TL-11	*[North wall, Trench 8a: Vesicular A horizon, lower portion]*											
	0.5	31	7.1±1.0	5.2±0.7	98 ± 5	14 ± 2	19 ± 2.3	12-22				
TL-30	*[North wall, Trench 8: Fissure-filling material about half-way between bottom and top of fissure.]*											
	5.3	25	7.2±0.9	5.8±0.8	259 ± 11	36 ± 4.7	44 ± 6	31-50	306 ± 31	42 ± 6.8	52 ± 8.7	35-61

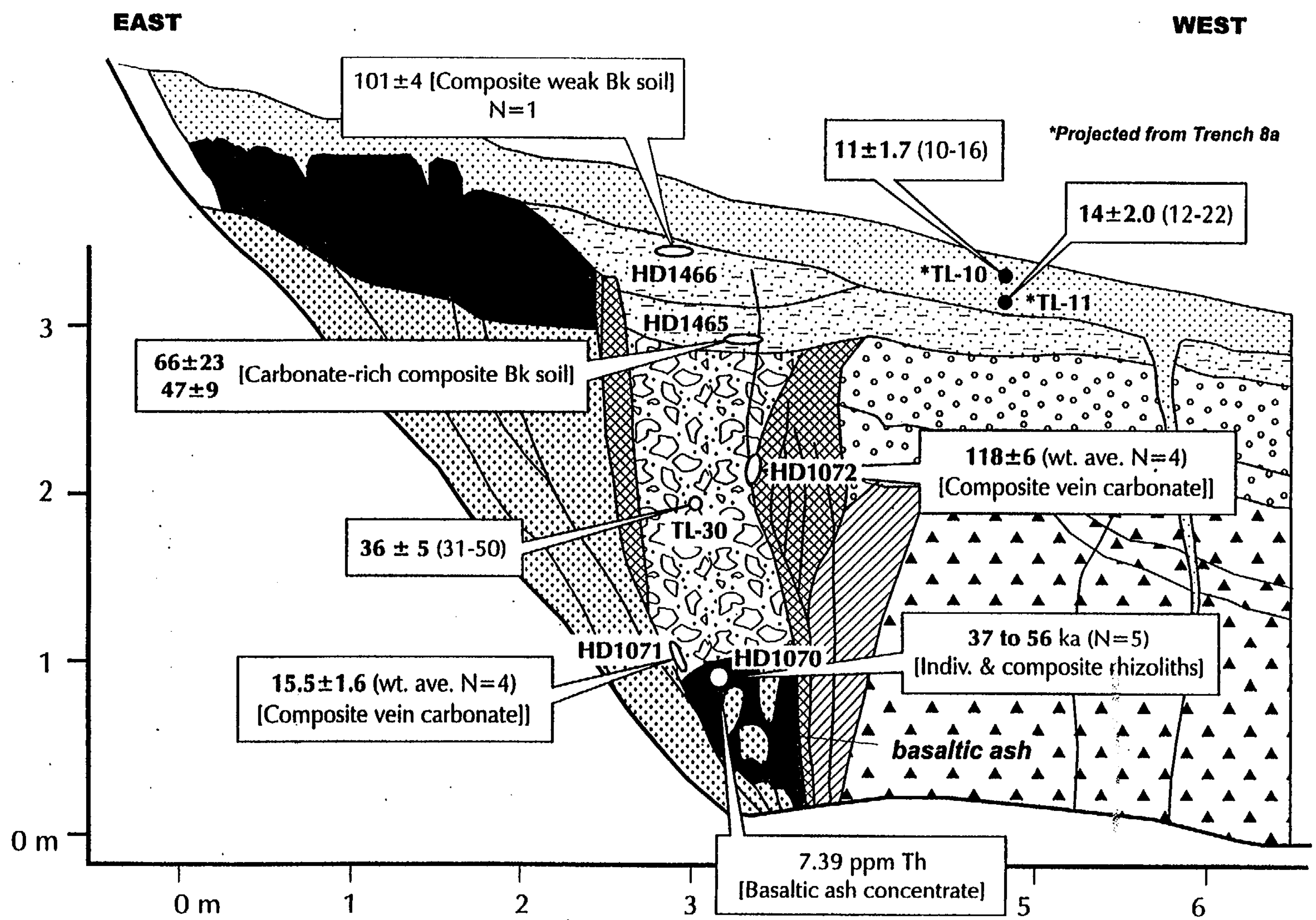

Figure 38: Generalized geologic log showing geochronological data available for the south wall, of Solitario Canyon Fault Trench 8 (modified from Ramelli, et al., 1995). Uranium-series disequilibrium data (HD sample names) are from Tables 19 and 20. Thermoluminescence data (TL sample names) are from Table 21. See section 5.1 in text for further explanation.

5.2.6.2 Trench 3

Table 22: Mass spectrometric U-series results from Solitario Canyon Fault Trench 3

Figure 39: U-series concordia plot for samples from Solitario Canyon Fault Trench 3

Figure 40: Distribution of U-series ages for samples from Solitario Canyon Fault Trench 3

Figure 41: Schematic log of Solitario Canyon Fault Trench 3 showing dating results

Table 22: Uranium-series disequilibrium results from Solitario Canyon Fault Trench 3. Data are determined by mass spectrometry. The detrital component is assumed to be in secular equilibrium with an atomic TH/U of 4±2. See trench logs in Ramelli and others (1995) for specific sample locations. All errors given at the 95% confidence level.

Sample Name	Sample wt. (g)	Elemental Concentration U (ppm)	Elemental Concentration Th (ppm)	Measured $^{230}Th/^{232}Th$ Activity Ratio	Detritus-corrected (secular equilibrium detrital component with Th/U=4) $^{230}Th/U$ Age (ka)	$^{234}U/^{238}U_{initial}$	Min. ^{230}Th Age	Max. ^{230}Th Age	$^{234}U/^{238}U$ Age (ka)	Sample Type
South wall, just west of main fissure within dense, Stage IV+ K horizon: Volcanic cobble with well-developed rind										
HD1726-a1	0.117	17.3	4.30	13.6	144 ± 4	1.68 ± 0.02			165 ± 94	Si-rich rind; outer layer
HD1726-a2	0.118	8.50	3.92	6.9		1.19 ± 0.07	340	inf.	950 ± 140	Si-rich rind; adjacent to clast
HD1726-b1	0.205	5.45	3.45	5.1	infinite		400	inf.	880 ± 160	Si-rich rind; adjacent to clast
HD1726-b2	0.269	18.0	1.32	54.1	324 ± 7	1.723 ± 0.013			323 ± 93	Si-rich rind; intermediate layer
South wall, west end of trench: Laminated "cap" in the upper portion of Stage IV+ K horizon densely cemented with carbonate and silica (unit 8 on original logs of Ramelli)										
HD1730-b1	0.113	19.9	0.037	530	25.0 ± 0.1	1.605 ± 0.002				Si-rich clast rind; whole rind
HD1730-c1	0.092	18.5	0.037	544	27.6 ± 0.2	1.607 ± 0.002				Si-rich clast rind; whole rind
South wall, west end of trench: Si-rich rinds from clasts in the upper portion of Stage IV+ K horizon (unit 8 on original logs of Ramelli)										
HD1731-a1	0.161	8.78	4.41	7.1	infinite		400	inf.	590 ± 110	Si-rich rind; outer layer
HD1731-a2	0.112	7.95	3.49	7.4	infinite		450	inf.	900 ± 140	Si-rich rind; intermediate layer
HD1731-b1	0.130	16.5	1.99	29.0	170 ± 3	1.620 ± 0.011				Si-rich clast rind; whole rind
HD1731-e1	0.314	4.39	2.70	5.3	infinite		400	inf.	870 ± 150	Si-rich rind; intermediate layer
HD1731-e2	0.157	4.10	5.34	2.3		1.10 ± 0.10	188	1050	970 ± 450	Si-rich rind; intermediate layer
South wall, west end of trench: Densely cemented matrix containing carbonate and silica lenses in the upper portion of Stage IV+ K horizon (unit 8 on original logs of Ramelli)										
HD1732-b1	0.131	3.45	0.085	168	233 ± 4	1.828 ± 0.008				Si-rich rind; outer layer
HD1732-b2	0.201	8.59	0.617	55.7	320 ± 7	1.746 ± 0.014			310 ± 90	Si-rich rind; outer layer
HD1732-b3	0.314	10.0	2.54	13.3		1.39 ± 0.20	368	inf.	700 ± 100	Si-rich rind; adjacent to clast
HD1732-c1	0.365	5.12	0.099	200	245 ± 4	1.655 ± 0.007				Si-rich seam in matrix
HD1732-c2	0.034	7.34	2.03	11.9		1.33 ± 0.24	400	inf.	840 ± 110	Si-rich seam in matrix
HD1732-d1	0.045	9.63	3.60	9.8	394 ± 69	1.59 ± 0.10			470 ± 100	Si-rich seam in matrix
HD1732-d2	0.177	8.15	1.99	15.7	199 ± 10	1.75 ± 0.03				Si-rich seam in matrix

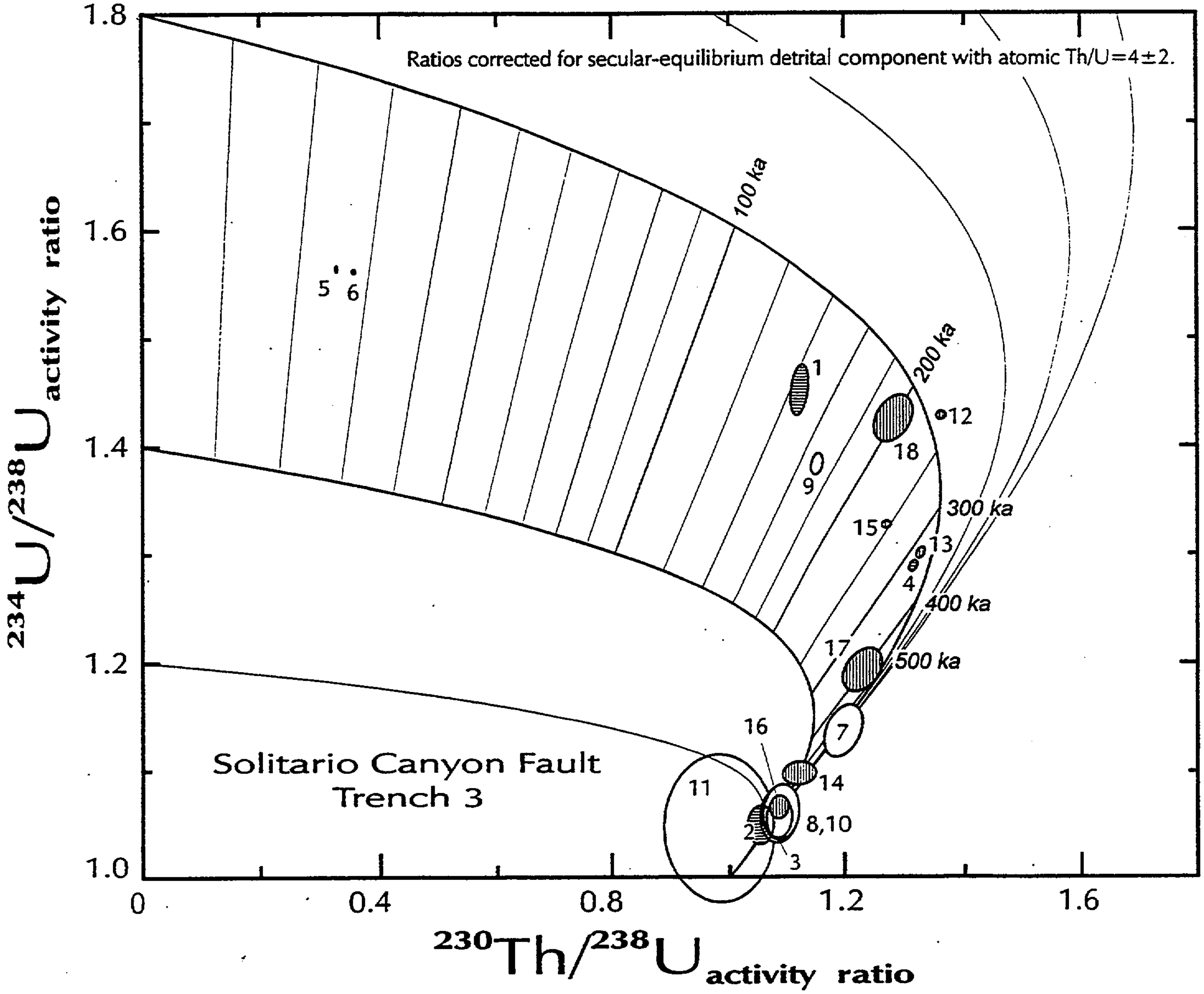

Figure 39: Uranium-series disequilibrium evolution diagram showing analyses of samples from Solitario Canyon Fault Trench 3. Error ellipses for aliquots of the same sample are shaded in the same pattern. Data are given in Table 22 and correspond to the following numbers: 1=HD1726-A1; 2=HD1726-A2; 3=HD1726-B1; 4=HD1726-B2; 5=HD1730-B1; 6=HD1730-C1; 7=HD1731-A1; 8=HD1731-A2; 9=HD1731-B1; 10=HD1731-E1; 11=HD1731-E2; 12=HD1732-B1; 13=HD1732-B2; 14=HD1732-B3; 15=HD1732-C1; 16=HD1732-C2; 17=HD1732-D1; 18=HD1732-D2.

d:\ym\data\tecton\sc\sc-ccrd.cdr
date updated: 9/21/95

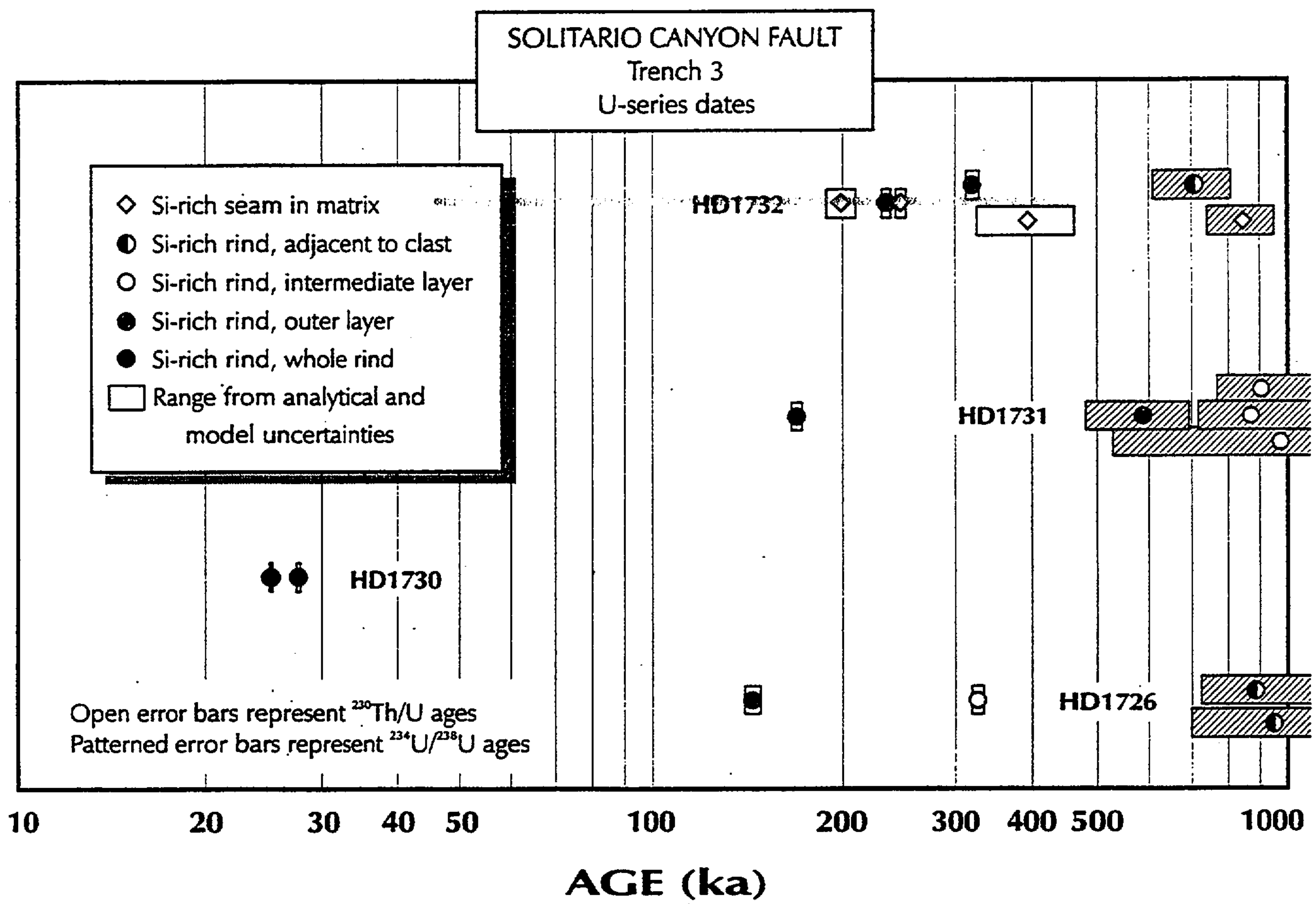

Figure 40: Distribution of uranium-series ages for samples from Solitario Canyon Fault Trench 3. Data are given in Table 22.

d:\ym\data\tecton\sc\sc3-ages.cdr
updated 8/19/95

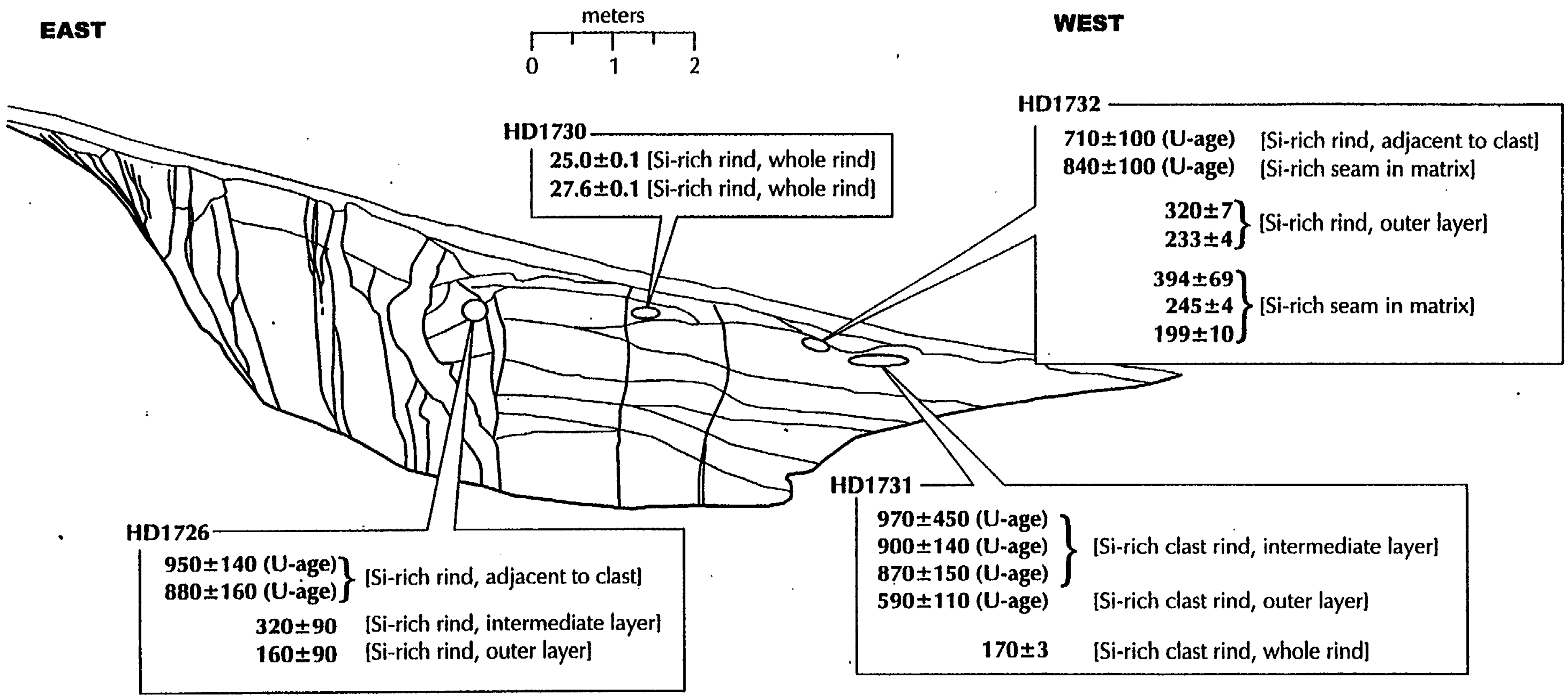

Figure 41: Generalized geologic log showing geochronological data available for the south wall of Solitario Canyon Fault Trench 3 (modified from Ramelli et al., 1995). Uranium-series data (HD sample names) are from Table 22. See section 5.1 in text for further explanation.

5.2.7 Fatigue Wash Fault

Trench CF1

Table 23: Mass spectrometric U-series results from Fatigue Wash Trench CF1

Figure 42: U-series concordia plot for samples from Fatigue Wash Trench CF1

Figure 43: Distribution of U-series ages for samples from Fatigue Wash Trench CF1

Table 24: Thermoluminescence dating results from Fatigue Wash Trench CF1 samples

Figure 44: Schematic log of Fatigue Wash Trench CF1 showing dating results

Table 23: Uranium-series disequilibrium results from Fatigue Wash Fault Trench CF1. Data are determined by mass spectrometry. The detrital component is assumed to be in secular equilibrium with an atomic TH/U of 4±2. See trench logs in Coe and others (1995) for specific sample locations. All errors given at the 95% confidence level.

Sample Name	Sample wt. (g)	Elemental Concentration		Measured $^{230}Th/^{232}Th$ Activity Ratio	Detritus-corrected (secular equilibrium detrital component with Th/U=4)					Sample Type
		U (ppm)	Th (ppm)		$^{230}Th/U$ Age (ka)	$^{234}U/^{238}U_{initial}$	Min. ^{230}Th Age	Max. ^{230}Th Age	$^{234}U/^{238}U$ Age (ka)	
South wall, up-thrown block, upper 10 cm of the buried soil near base of trench (Unit 1 of Coe et al., 1995): Clasts with thin carbonate/silica rinds in a well-cemented matrix										
HD 1608-a1	0.113	5.48	3.49	4.8	infinite		1000	inf.		Si-rich rind adjacent to clast
HD 1608-b1	0.065	9.30	2.44	11.2	511 ± 204	0.92 ± 0.07	423	inf.		Si-rich rind; adjacent to clast
HD 1608-c1	0.114	3.95	1.86	6.3	377 ± 102	1.00 ± 0.04	300	520		Si-rich seam in matrix
South wall, up-thrown block, upper K soil within 30-80 cm of the surface (Unit 4 of Coe et al., 1995): Clasts with carbonate/silica rinds in a Stage IV calcrete										
HD1729-A1	0.109	18.2	2.71	18.2	102 ± 2	1.544 ± 0.011				Si-rich seam in matrix
HD1729-B1	0.073	17.4	0.749	70.8	141.2 ± 1.4	1.484 ± 0.004				Si-rich clast rind; whole rind
HD1729-D1	0.107	16.7	1.55	30.4	115.3 ± 1.5	1.509 ± 0.007				Si-rich rind; intermediate layer
HD1729-H1	0.145	13.8	0.167	206	88.5 ± 1.1	1.557 ± 0.004				Si-rich rind; adjacent to clast
HD1729jbp	0.133	25.0	0.510	127.1	93.05 ± 1.2	1.560 ± 0.010				Si-rich rind; adjacent to clast
South wall, down-thrown block, upper K soil developed in thin fault-wedge Unit 5 of Coe et al., 1995): Large single clast with thick carbonate/silica rind.										
HD1610-C1	0.095	20.0	2.86	27.8	449 ± 35	1.89 ± 0.08			347 ± 101	Si-rich rind; adjacent to clast
HD1610-C1	0.051	19.3	2.65	26.7	474 ± 46	1.63 ± 0.07			496 ± 101	Si-rich rind; adjacent to clast
HD1610-C2	0.157	24.6	2.22	44.3	331 ± 10	1.75 ± 0.02			293 ± 100	Si-rich rind; intermediate layer
HD1610-C2	0.071	26.3	2.23	47.2	325 ± 21	1.75 ± 0.04			287 ± 100	Si-rich rind; intermediate layer
HD1610-C3	0.218	50.2	5.24	12.2	65 ± 4	1.61 ± 0.03				Si-rich rind; outer layer
HD1610-C3	0.050	5.31	6.19	3.1	329 ± 117	1.64 ± 0.20	199	inf.	347 ± 147	Si-rich rind; intermediate layer
HD1610-C4	0.188	16.5	3.97	10.1	79 ± 3	1.59 ± 0.02				Si-rich rind; outer layer
HD1610-C5	0.041	16.0	3.16	18.8	infinite		590	inf.	507 ± 101	Si-rich rind; adjacent to clast
South wall, down-thrown block, upper K soil developed in Unit 7 of Coe et al. (1995): Sandy to gravelly matrix containing stringers, thin layers and pods of carbonate/silica										
HD1611-A2	0.089	13.3	4.28	4.7	38 ± 4	1.58 ± 0.03				Si-rich seam in matrix
HD1611-A3	0.100	12.5	2.84	15.7	172 ± 7	1.66 ± 0.02			176 ± 101	Si-rich seam in matrix
HD1611-A5	0.171	11.2	3.30	12.6	189 ± 7	1.70 ± 0.03			175 ± 102	Si-rich seam in matrix

Table 23: Continued

Sample Name	Sample wt. (g)	Elemental Concentration U (ppm)	Elemental Concentration Th (ppm)	Measured $^{230}Th/^{232}Th$ Activity Ratio	Detritus-corrected (secular equilibrium detrital component with Th/U=4) $^{230}Th/U$ Age (ka)	$^{234}U/^{238}U_{Initial}$	Min. ^{230}Th Age	Max. ^{230}Th Age	$^{234}U/^{238}U$ Age (ka)	Sample Type
South wall, down-thrown block, upper K soil developed in Unit 7 of Coe et al. (1995): Sandy to gravelly matrix containing stringers, thin layers and pods of carbonate/silica										
HD1612-5a	0.123	9.78	1.45	21.0	115.5 ± 2.3	1.69 ± 0.01				Si-rich seam in matrix
HD1612-A2	0.356	13.4	0.519	81.1	118.8 ± 1.4	1.683 ± 0.006				Si-rich seam in matrix
HD1612-A3	0.331	12.6	0.517	73.9	112.0 ± 1.3	1.667 ± 0.005				Si-rich seam in matrix
HD1612-A4	0.126	11.0	0.774	44.2	116.2 ± 1.6	1.671 ± 0.008				Si-rich seam in matrix
HD1612-B4	0.143	10.1	1.12	26.7	107.4 ± 1.5	1.670 ± 0.010				Si-rich seam in matrix
HD1612-B2	0.541	12.8	0.528	72.8	110.9 ± 1.0	1.654 ± 0.005				Si-rich seam in matrix
HD1612-B3	0.324	12.6	0.884	39.7	169.4 ± 2.4	1.211 ± 0.004				Si-rich seam in matrix
HD1612-B3	0.263	13.1	0.627	67.2	124.5 ± 1.2	1.680 ± 0.005				Si-rich seam in matrix
HD1612-B4	0.195	10.9	0.890	37.7	115.6 ± 2.1	1.659 ± 0.008				Si-rich seam in matrix
HD1612-5c	0.076	19.3	1.65	34.2	101.6 ± 1.3	1.691 ± 0.008				Si-rich seam in matrix
HD1612-5d	0.106	10.8	3.05	11.7	128 ± 4	1.72 ± 0.03				Si-rich seam in matrix
HD1612-5e	0.134	11.1	1.32	25.6	111.6 ± 1.8	1.677 ± 0.011				Si-rich seam in matrix
HD1612-5e2	0.081	4.07	0.591	35.3	269 ± 9	2.45 ± 0.04				Si-rich seam in matrix

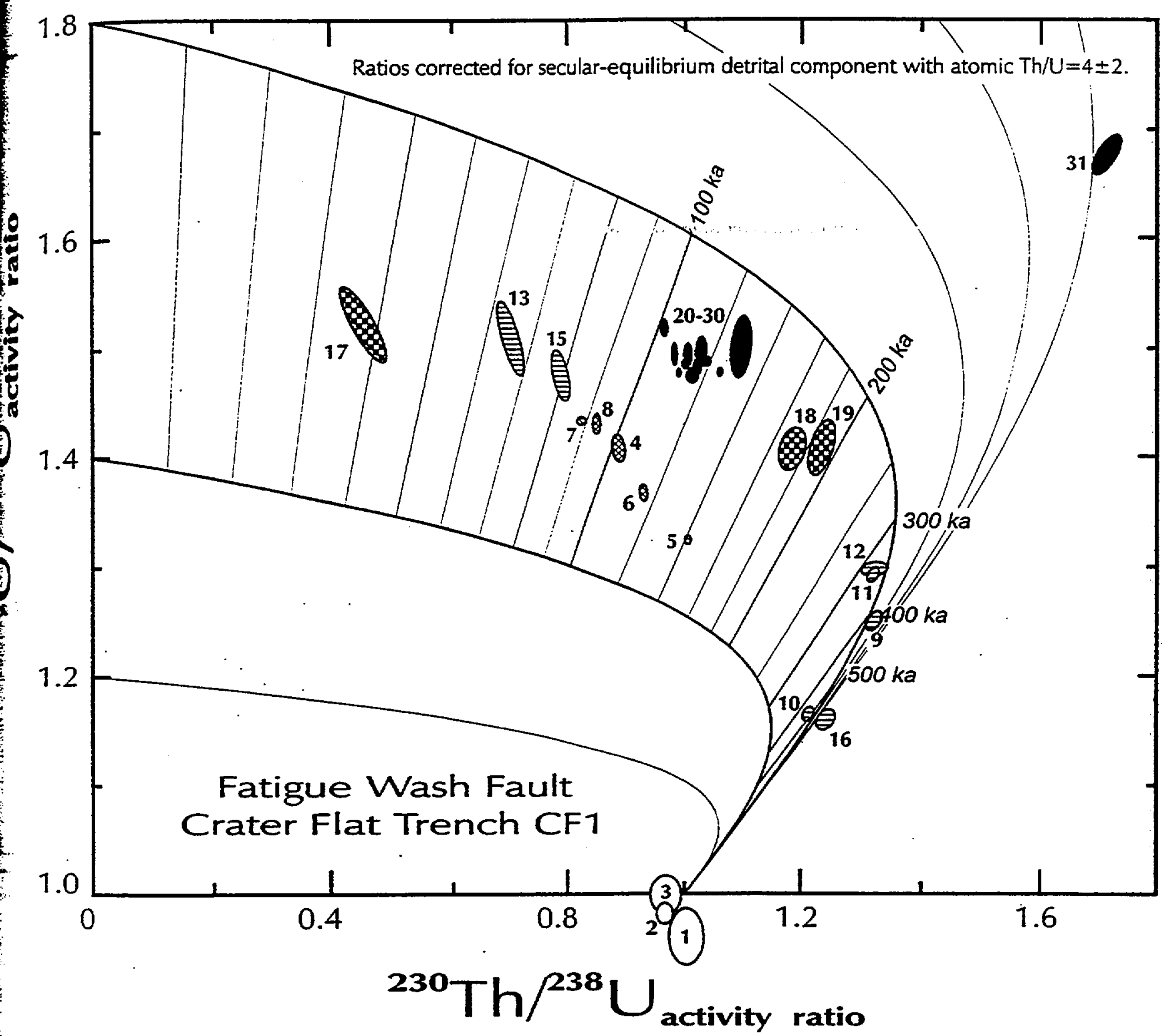

Figure 42: Uranium-series disequilibrium evolution diagram showing analyses of samples from Fatigue Wash Fault Trench CF1. Error ellipses for aliqouts of the same sample are shaded in the same pattern. Data are given in Table 23 and correspond to the following numbers: 1=HD1608-A1; 2=HD1608-B1; 3=HD1608-C1; 4=HD1729-A1; 5=HD1729-B1; 6=HD1729-D1; 7=HD1729-H1; 8=HD1729-jbp; 9=HD1610-C1sum; 10=HD1610-C1; 11=HD1610-C2sum; 12=HD1610-C2; 13=HD1610-C3sum; 14=HD1610-C3; 15=HD1610-C4; 16=HD1610-C5; 17=HD1611-A2sum; 18=HD1611-A3sum; 19=HD1611-A5sum; 20=HD1612-A; 21=HD1612-A2sum; 22=HD1612-A3sum; 23=HD1612-A4sum; 24=HD1612-B4; 25=HD1612-B2sum; 26=HD1612-B3sum; 27=HD1612-B3; 28=HD1612-B4sum; 29=HD1612-C; 30=HD1612-D; 31=HD1612-E.

d:\ym\data\tecton\cf\cf1-ccrd.cdr
date updated: 9/21/95

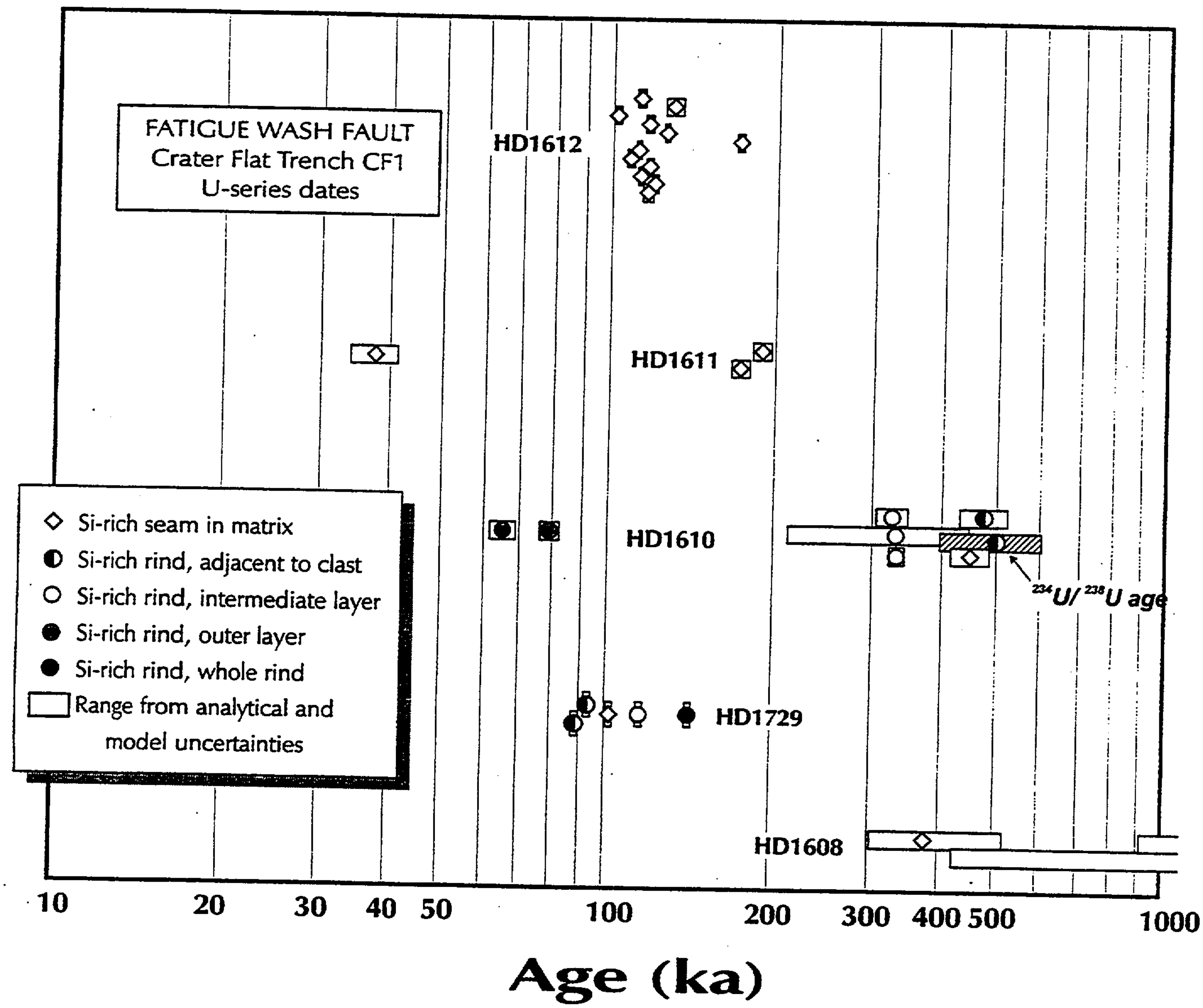

Figure 43: Distribution of uranium-series ages for samples from Fatigue Wash Fault Trench CF1. Data are given in Table 23.

d:\ym\data\tecton\cf\cf1-ages.cdr
updated 9/22/95

Table 24: Thermoluminescence results from Fatigue Wash Fault Trench CF1. All errors given at the 95% confidence limit. See logs in Coe and others (1995) for specific sample locations.

Sample Name	Field Moist. (%)	Saturation Moist. (%)	Dose Rate (Gy/ka) Field H_2O	Dose Rate (Gy/ka) Saturation H_2O	Total Bleach Eqivalent Dose (Gy)	Total Bleach Age (ka) for field moisture H_2O	Total Bleach Age (ka) for saturation moisture H_2O	Total Bleach Age (ka) Total Range	Partial Bleach Eqivalent Dose (Gy)	Partial Bleach Age (ka) for field moisture H_2O	Partial Bleach Age (ka) for saturation moisture H_2O	Partial Bleach Age (ka) Total Range
TL-12	*[South wall, shallow excavation south of main Trench CF1: Vesicular A horizon.]*											
	0.5	25	7.0±1.0	5.7±0.9	64 ± 3	9.2 ± 1.4	11.3 ± 1.8	7.8-13	46 ± 3	6.6 ± 1.1	8.2 ± 1.4	5.5-10

*Note: Analyses of HD1729 suggest mixing relations between late Pleistocene and early Pleistocene (400-500 ka) components

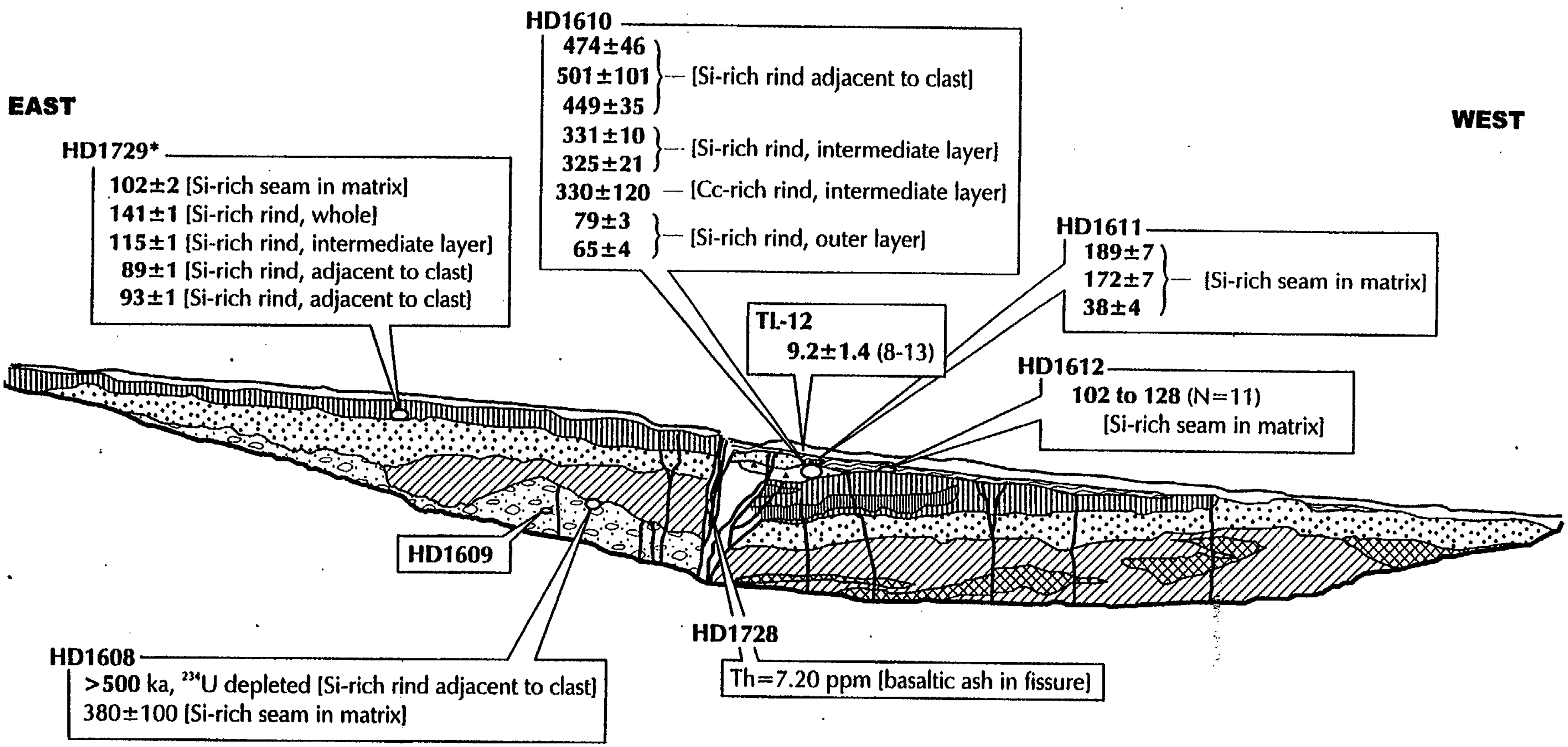

Figure 44: Generalized geological log showing geochronological data available for the south wall of Fatigue Wash Fault Trench CF1 (modified after Coe et al., 1995). Uranium-series data (HD sample names) are from Table 25. Thermoluminescence data (TL sample name) are from Table 26 and location is projected from shallow excavation to immediately south of the main trench. See section 5.1 in text for further explanation.

5.2.8 Windy Wash Fault

Trench CF2/CF3

Table 25: Mass spectrometric U-series results from Windy Wash Trench CF2

Figure 45: U-series concordia plot for samples from Windy Wash Trench CF2

Table 26: Mass spectrometric U-series results from Windy Wash Trench CF3

Figure 46: U-series concordia plot for samples from Windy Wash Trench CF3

Figure 47: Distribution of U-series ages for samples from Windy Wash Trenches CF2 and CF3

Table 27: Thermoluminescence dating results from Windy Wash Trench CF3 samples

Figure 48: Schematic log of Windy Wash Trench CF2 showing dating results

Figure 49: Schematic log of Windy Wash Trench CF3 showing dating results

Table 25: Uranium-series disequilibrium results from Windy Wash Fault Trench CF2. Data are determined by mass spectrometry. The detrital component is assumed to be in secular equilibrium with an atomic TH/U of 4±2. See trench logs in Whitney and others (1995) for specific sample locations. All errors given at the 95% confidence level.

Sample Name	Sample wt. (g)	Elemental Concentration		Measured $^{230}Th/^{232}Th$ Activity Ratio	Detritus-corrected (secular equilibrium detrital component with Th/U=4)					Sample Type
		U (ppm)	Th (ppm)		$^{230}Th/U$ Age (ka)	$^{234}U/^{238}U_{Initial}$	Min. ^{230}Th Age	Max. ^{230}Th Age	$^{234}U/^{238}U$ Age (ka)	
South wall, west end; lower portion of Unit M (Whitney et al., 1995): Cobble from below main K accumulation with well-developed rind on underside										
HD1617-A1	0.155	12.5	11.4	4.7	333 ± 62	2.20 ± 0.24	223	1010		Si-rich rind adjacent to clast
South wall, west end; lower portion of Unit J (Whitney et al., 1995): Gravel-free sandy unit well-cemented with carbonate & silica that grades into soil of underlying gravel unit										
HD1618-a2-1	0.137	10.4	13.4	4.4	excess Th230					Si-rich seam in matrix
HD1618-a2-1	0.107	12.1	9.26	4.8	153 ± 13	1.87 ± 0.11				Si-rich seam in matrix
HD1618-a2-1	0.150	15.7	2.02	22.7	104.5 ± 1.7	1.657 ± 0.012				Si-rich seam in matrix
HD1618-b1	0.122	13.6	8.20	17.2	excess Th230					Si-rich seam in matrix
South wall, west end; upper portion of Unit M (Whitney et al., 1995): Matrix and clasts from main K accumulation in gravelly unit										
HD-1619-a1	0.030	7.88	2.17	14.6	278 ± 13	1.79 ± 0.03			220 ± 102	Si-rich rind adjacent to clast
HD-1619-b1	0.018	10.7	4.24	8.8	159 ± 7	1.68 ± 0.04				Si-rich rind; intermediate layer
HD-1619-b2	0.013	3.51	1.61	8.7	277 ± 22	1.78 ± 0.06			222 ± 105	Si-rich rind; adjacent to clast
HD-1619-c1	0.114	24.8	3.32	19.7	91.2 ± 1.9	1.608 ± 0.011				Si-rich clast rind; whole rind
HD-1619-d1	0.053	29.6	3.72	21.8	96.4 ± 1.7	1.618 ± 0.011				Si-rich clast rind; whole rind
HD-1619-e1	0.032	9.06	2.79	13.0	264 ± 12	1.78 ± 0.04				Si-rich rind; outer layer
HD-1619-e2	0.025	7.74	2.39	13.3	331 ± 33	1.87 ± 0.08			239 ± 102	Si-rich rind; adjacent to clast
South wall, west end; lower portion of Unit M (Whitney et al., 1995): Clasts with rinds showing varying amounts of development in a porous, but well-indurated, matrix										
HD-1620-a1-1	0.116	11.5	2.03	23.3	287 ± 13	1.83 ± 0.03				Si-rich rind; adjacent to clast
HD-1620-b1	0.087	7.94	8.87	3.5	270 ± 135	1.94 ± 0.28	172	560		Si-rich rind; intermediate layer
HD-1620-c1	0.089	12.3	4.36	11.0	214 ± 22	1.78 ± 0.05				Si-rich rind; adjacent to clast
South wall, west end; lower portion of Unit M (Whitney et al., 1995): Clasts with rinds showing varying amounts of development in a porous, but well-indurated, matrix										
HD 1621 a1	0.135	13.5	2.18	24.8	267 ± 14	1.76 ± 0.03			225 ± 101	Si-rich rind; adjacent to clast
HD 1621 e1	0.053	7.78	3.71	8.4	311 ± 56	1.83 ± 0.09			235 ± 105	Si-rich rind; adjacent to clast

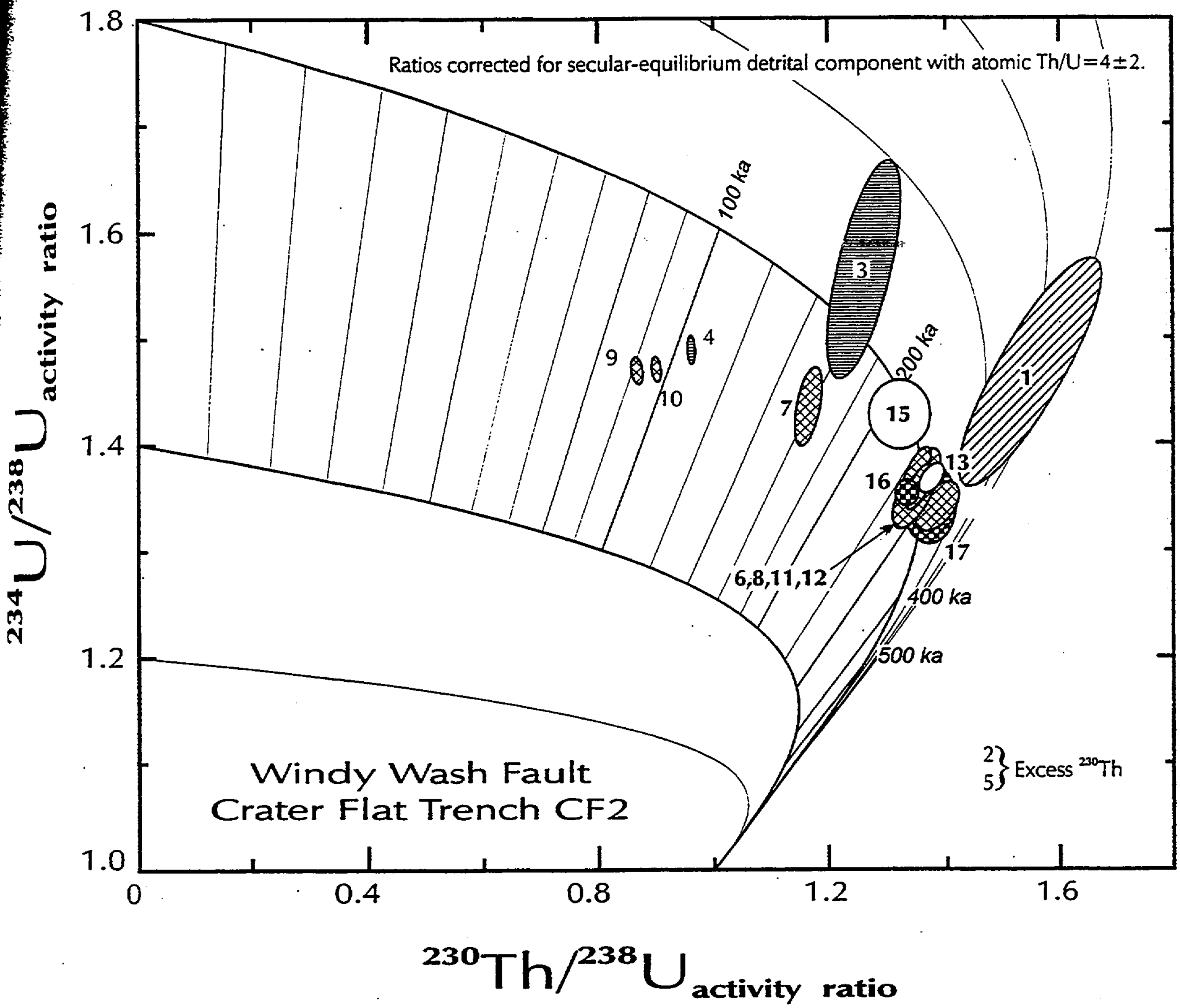

Figure 45: Uranium-series disequilibrium evolution diagram showing analyses of samples from Windy Wash Fault Trench CF2. Error ellipses for aliqouts of the same sample are shaded in the same pattern. Data are given in Table 25 and correspond to the following numbers: 1=HD1617-A1; 2=HD1618-A2-1; 3=HD1618-A2-1dup#1; 4=HD1618-A2-1dup#2; 5=HD1618-B1; 6=HD1619-A1; 7=HD1619-B1; 8=HD1619-B2; 9=HD1619-C1; 10=HD1619-D1; 11=HD1619-E1; 12=HD1619-E2; 13=HD1620-A1-1; 14=HD1620-B1; 15=HD1620-C1; 16=HD1621-A1; 17=HD1621-E1.

d:\ym\data\tecton\cf\cf1-ccrd.cdr
date updated: 9/21/95

Table 26: Uranium-series disequilibrium results from Windy Wash Fault Trench CF3. Data are determined by mass spectrometry. The detrital component is assumed to be in secular equilibrium with an atomic TH/U of 4±2. See trench logs in Whitney and others (1995) for specific sample locations. All errors given at the 95% confidence level.

Sample Name	Sample wt. (g)	Concentration		$^{230}Th/^{232}Th$	Detritus-corrected		Sample Type
		U (ppm)	Th (ppm)	Activity Ratio	$^{230}Th/U$ Age (ka)	$^{234}U/^{238}U_{Initial}$	
South wall, west end of trench; near top of Unit E (Whitney et al., 1995): Volcanic clasts containing thin, carbonate/silica coatings on undersides.							
HD1615-a1	0.095	7.64	2.65	5.7	52 ± 4	1.68 ± 0.03	Si-rich rind adjacent to clast
HD1820-A1	0.125	8.11	2.47	8.3	78 ± 5	1.69 ± 0.03	Si-rich rind adjacent to clast
HD1820-B1	0.306	3.50	0.974	7.8	62 ± 4	1.66 ± 0.03	Si-rich rind adjacent to clast
HD1820-C1	0.071	7.37	2.43	8.0	86 ± 5	1.65 ± 0.04	Si-rich rind adjacent to clast
South wall, west end of trench; near top of Unit E (Whitney et al., 1995): Poorly-cemented matrix sample with distinct sub-horizontal stringers of opal							
HD1821-A	0.225	12.6	0.789	9.1	12.7 ± 0.7	1.599 ± 0.011	Si-rich stringer in matrix
HD1821-B	0.323	11.8	0.223	27.3	12.0 ± 0.2	1.602 ± 0.009	Si-rich stringer in matrix
HD1821-D1	0.085	6.77	0.123	97.7	46.8 ± 0.7	1.717 ± 0.011	Individual rhizolith

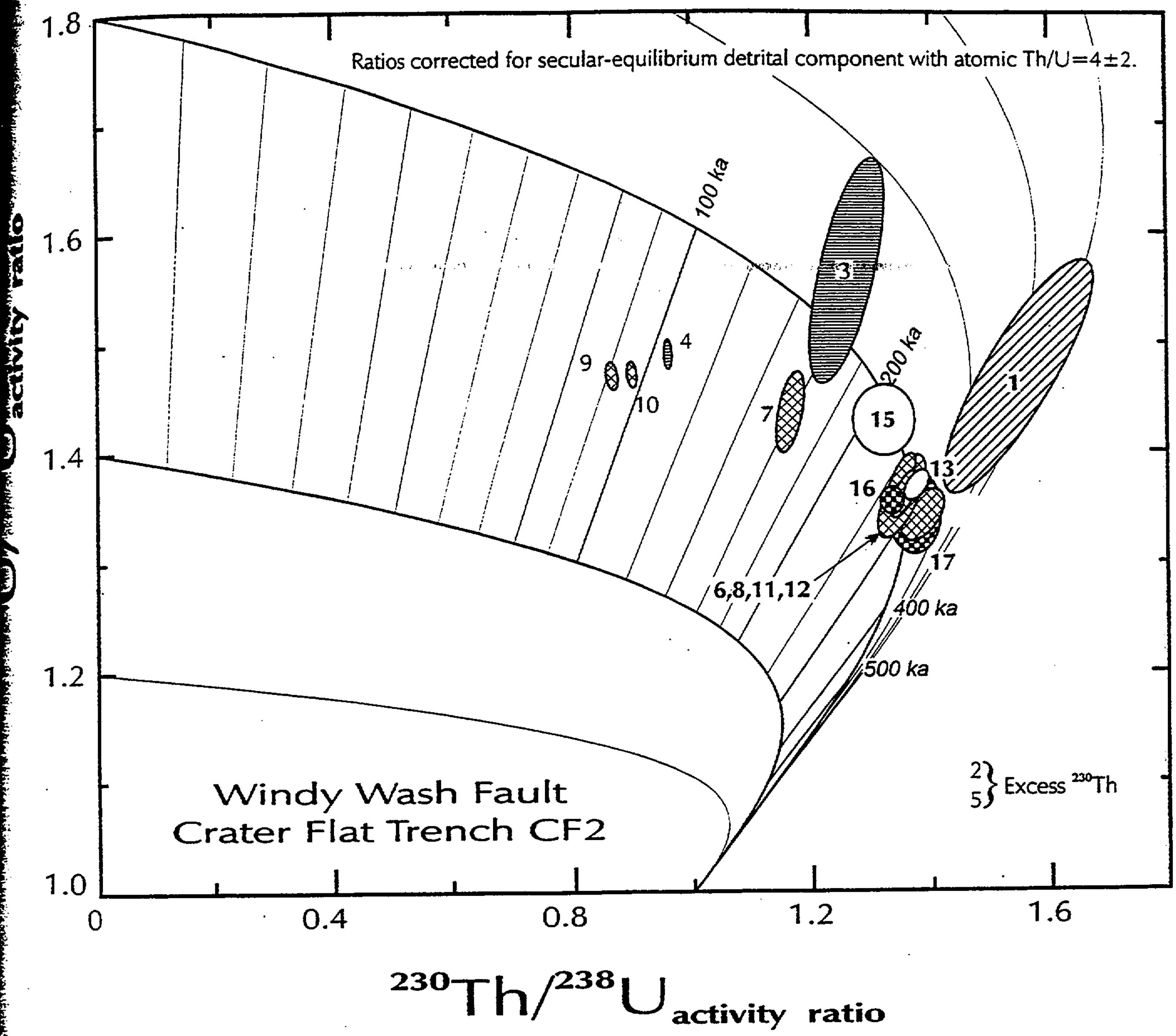

Figure 45: Uranium-series disequilibrium evolution diagram showing analyses of samples from Windy Wash Fault Trench CF2. Error ellipses for aliqouts of the same sample are shaded in the same pattern. Data are given in Table 25 and correspond to the following numbers: 1=HD1617-A1; 2=HD1618-A2-1; 3=HD1618-A2-1dup#1; 4=HD1618-A2-1dup#2; 5=HD1618-B1; 6=HD1619-A1; 7=HD1619-B1; 8=HD1619-B2; 9=HD1619-C1; 10=HD1619-D1; 11=HD1619-E1; 12=HD1619-E2; 13=HD1620-A1-1; 14=HD1620-B1; 15=HD1620-C1; 16=HD1621-A1; 17=HD1621-E1.

d:\ym\data\tecton\cf\cf1-ccrd.cdr
date updated: 9/21/95

Table 26: Uranium-series disequilibrium results from Windy Wash Fault Trench CF3. Data are determined by mass spectrometry. The detrital component is assumed to be in secular equilibrium with an atomic TH/U of 4±2. See trench logs in Whitney and others (1995) for specific sample locations. All errors given at the 95% confidence level.

Sample Name	Sample wt. (g)	Concentration		$^{230}Th/^{232}Th$	Detritus-corrected		Sample Type
		U (ppm)	Th (ppm)	Activity Ratio	$^{230}Th/U$ Age (ka)	$^{234}U/^{238}U_{Initial}$	
South wall, west end of trench; near top of Unit E (Whitney et al., 1995): Volcanic clasts containing thin, carbonate/silica coatings on undersides.							
HD1615-a1	0.095	7.64	2.65	5.7	52 ± 4	1.68 ± 0.03	Si-rich rind adjacent to clast
HD1820-A1	0.125	8.11	2.47	8.3	78 ± 5	1.69 ± 0.03	Si-rich rind adjacent to clast
HD1820-B1	0.306	3.50	0.974	7.8	62 ± 4	1.66 ± 0.03	Si-rich rind adjacent to clast
HD1820-C1	0.071	7.37	2.43	8.0	86 ± 5	1.65 ± 0.04	Si-rich rind adjacent to clast
South wall, west end of trench; near top of Unit E (Whitney et al., 1995): Poorly-cemented matrix sample with distinct sub-horizontal stringers of opal							
HD1821-A	0.225	12.6	0.789	9.1	12.7 ± 0.7	1.599 ± 0.011	Si-rich stringer in matrix
HD1821-B	0.323	11.8	0.223	27.3	12.0 ± 0.2	1.602 ± 0.009	Si-rich stringer in matrix
HD1821-D1	0.085	6.77	0.123	97.7	46.8 ± 0.7	1.717 ± 0.011	Individual rhizolith

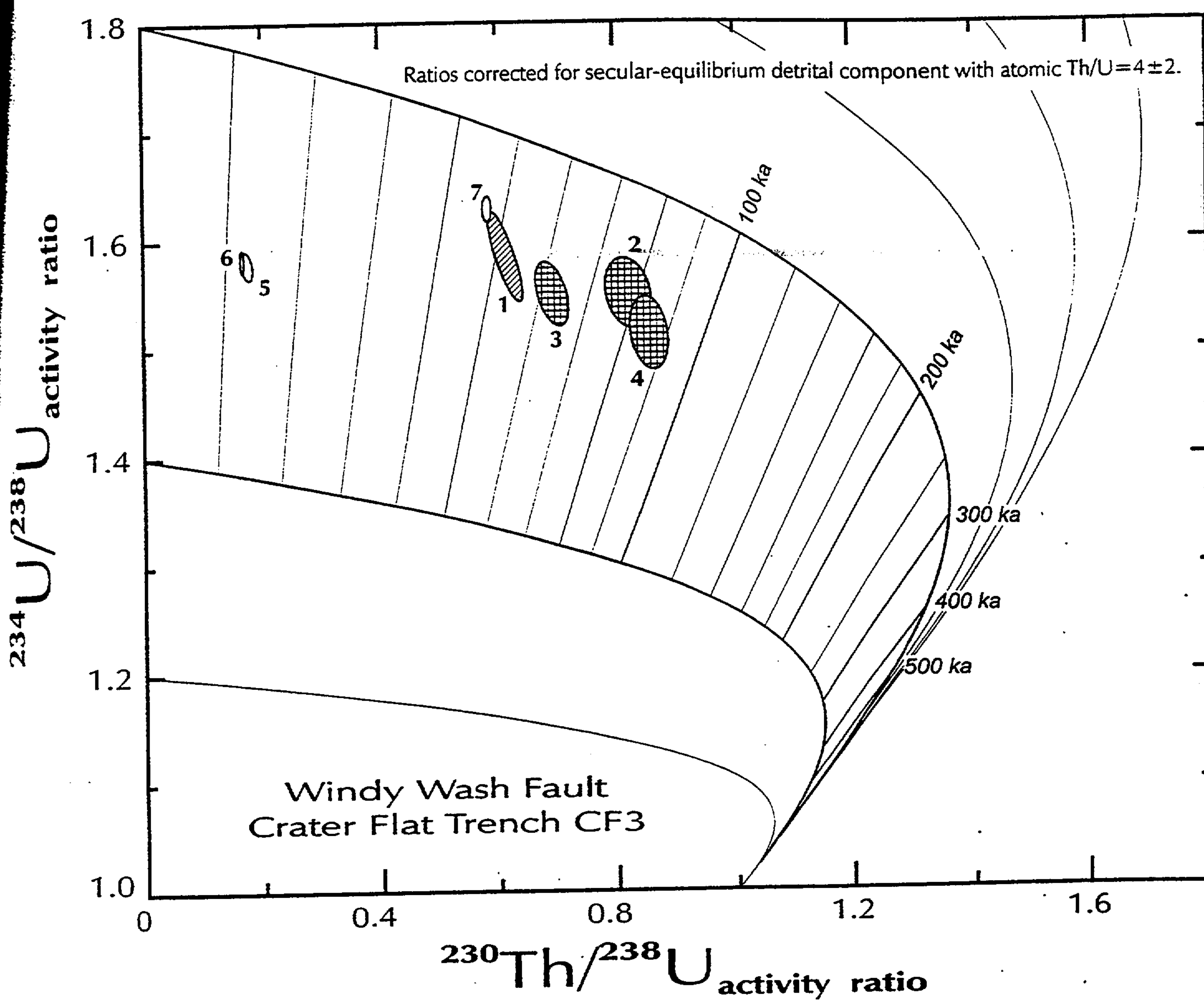

Figure 46: Uranium-series disequilibrium evolution plot showing analyses from Windy Wash Fault Trench CF3. Error ellipses for aliqouts from the same sample are shaded in the same pattern. Data are given in Table 26 and coresond to the following numbers: 1=HD1615-A1; 2=HD1820-A1; 3=HD1820-B1; 4=HD1820-C1; 5=HD1821-A; 6=HD1821-B; 7=HD1821-D1.

d:\ym\data\tecton\cf\cf3-ccrd.cdr
date updated: 9/21/95

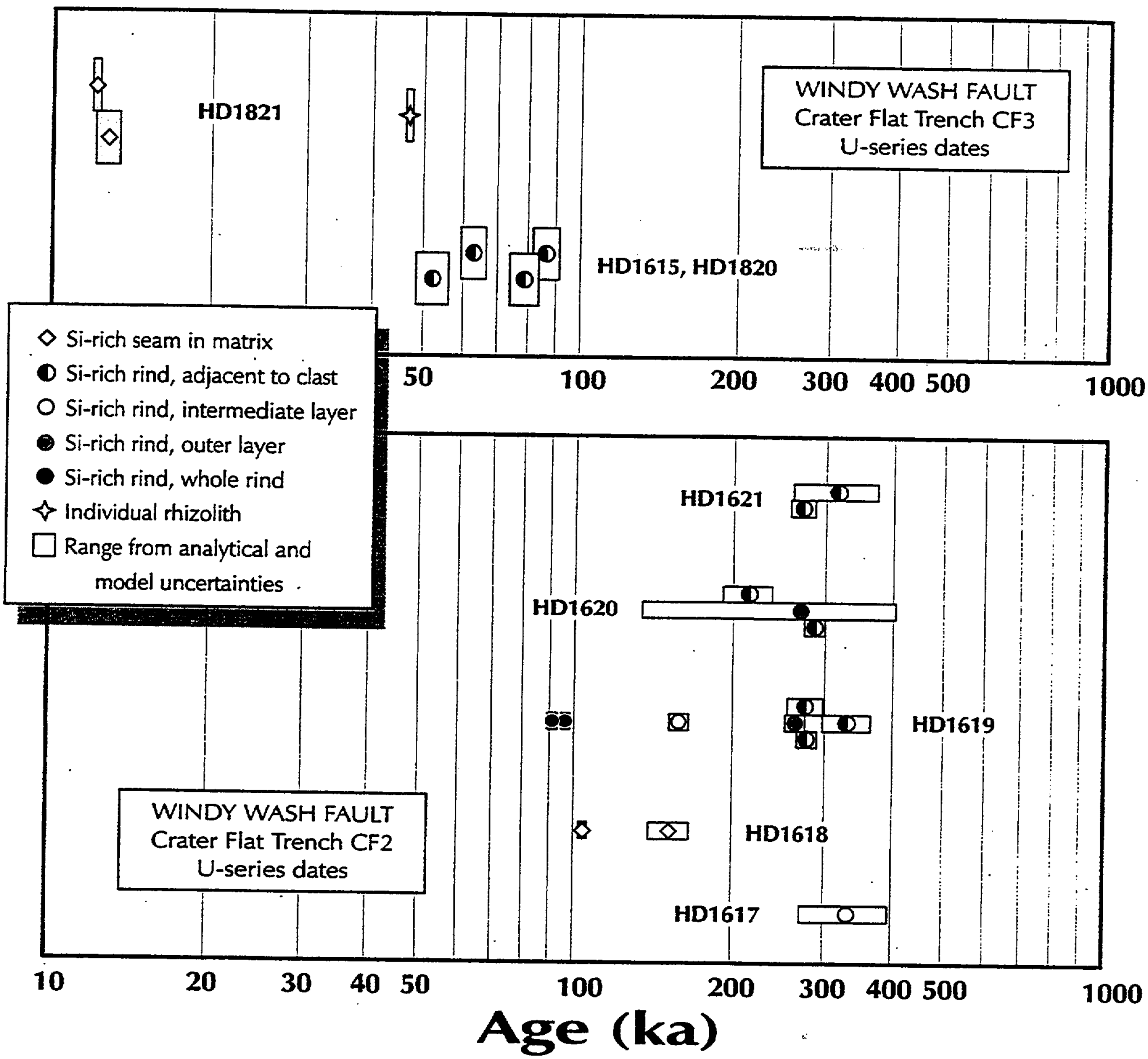

Figure 47: Distribution of uranium-series ages from Windy Wash Fault Trenches CF2 and CF3. Data are given in Tables 25 and 26.

d:\ym\data\tecton\cf\ww-age.cdr
updated 8/19/95

Table 27: Thermoluminescence results from Windy Wash Fault Trench CF3. All errors given at the 95% confidence limit. See logs in Whitney and others (1995) for specific sample locations.

Sample Name	Field Moist. (%)	Saturation Moist. (%)	Dose Rate (Gy/ka)		Total Bleach Eqivalent Dose (Gy)	Total Bleach Age (ka)			Partial Bleach Eqivalent Dose (Gy)	Partial Bleach Age (ka)		
			Field H_2O	Saturation H_2O		for field moisture H_2O	for saturation moisture H_2O	Total Range		for field moisture H_2O	for saturation moisture H_2O	Total Range
TL-59	*[South wall, west end, Unit C of Whitney and others (1995): Gray-brown eolian unit with abundant volcanic clasts in fine-sand matrix. Directly overlies reddened Bt unit.]* DATA NOT AVAILABLE AT PRESENT											
TL-60	*[South wall, west end, Unit F of Whitney and others (1995): Pebble-gravel alluvial unit with sand-rich matrix.]* DATA NOT AVAILABLE AT PRESENT											

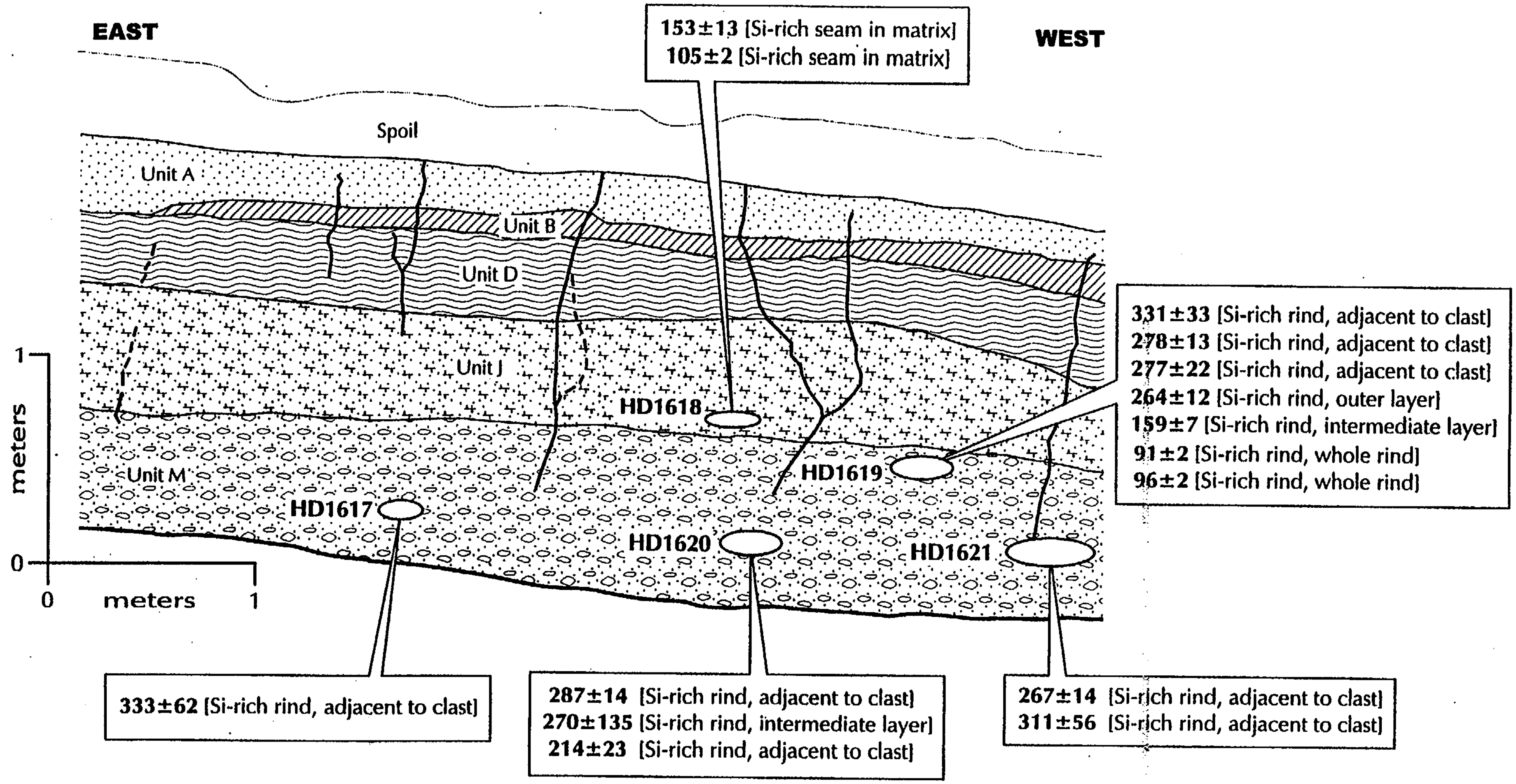

Figure 48: Generalized geologic log showing geochronological data available for the south wall, west end of Windy Wash Fault Trench CF2 (modified after Whitney, et al., 1995). Uranium-series data (HD sample names) are from Table 25. See section 5.1 in text for further explanation.

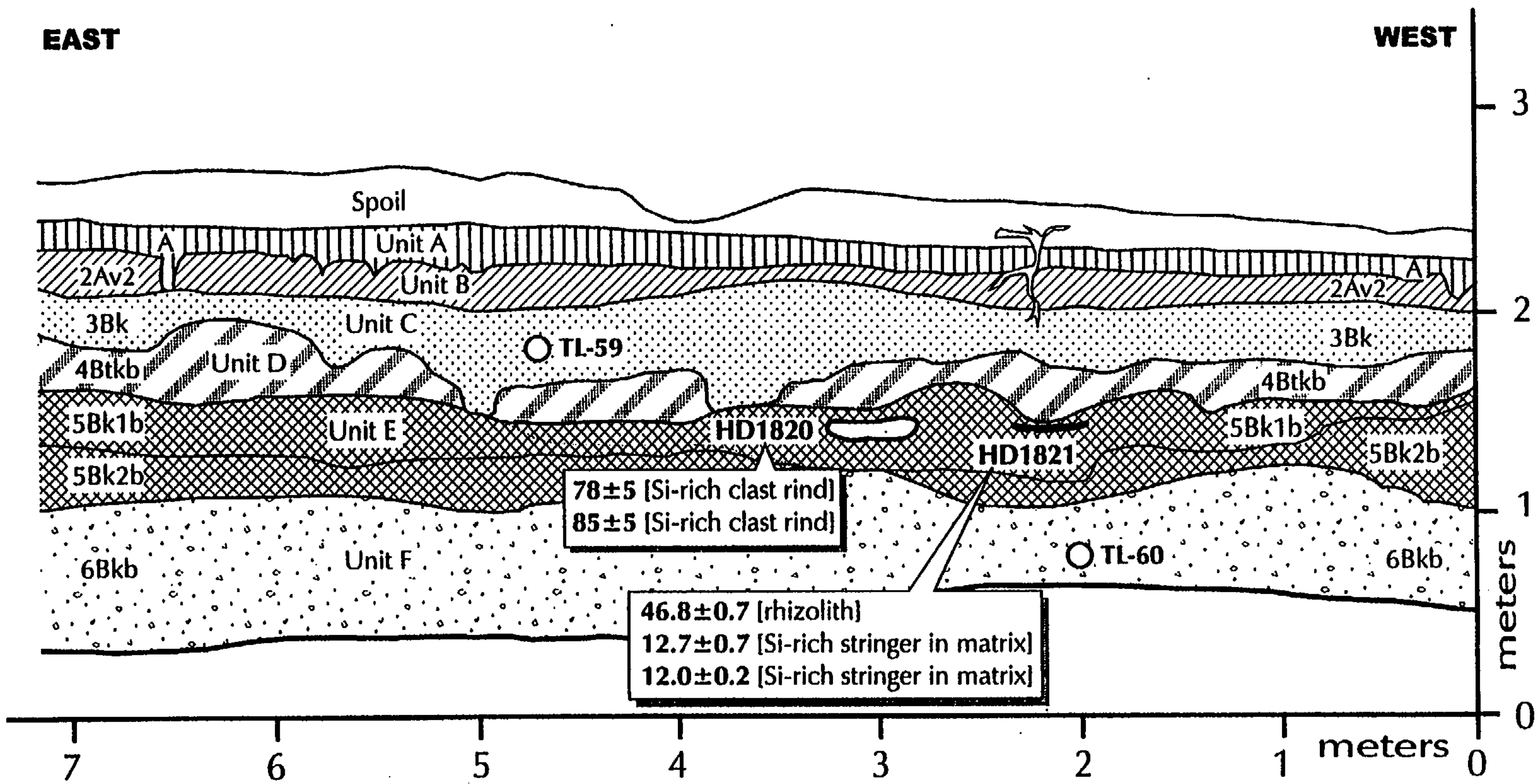

Figure 49: Generalized geologic log showing geochronological data available for the south wall, west end of Windy Wash Fault Trench CF3 (modified after Whitney, et al., 1995). Uranium-series data (HD sample names) are from Table 26. See section 5.1 in text for further explanation.

5.2.9 Bare Mountain Fault

Trenches BMT-1/BMT-2

Table 28: Mass spectrometric U-series results from Trench BMT-1

Table 29: Thermoluminescence dating results from Bare Mountain Trenches

Figure 50: Schematic log of Trench BMT-1 showing dating results

Figure 51: Schematic log of Trench BMT-2 showing dating results

Table 28: Uranium-series disequilibrium results from Bare Mountain Fault Trench BM-T1. Data are determined by mass spectrometry. The detrital component is assumed to be in secular equilibrium with an atomic TH/U of 4±2. See trench logs in Anderson and Klinger (1994) for specific sample locations. All errors given at the 95% confidence level.

Sample Name	Sample wt. (g)	Concentration		$^{230}Th/^{232}Th$ activity	Detritus-corrected		Sample Type
		U ppm	Th ppm		$^{230}Th/U$ Age (ka)	$^{234}U/^{238}U_{Initial}$	
Trench BMT-1, north wall: Laminated carbonate/silica sheet draping footwall block on top of Unit 2 of Anderson & Klinger (1994) and fault scarp.							
HD1379-M1	0.101	2.32	7.03	0.72	Excessive detrital correction	Undefined	Carbonate/opal lamina
HD1379-M2	0.096	2.39	4.87	0.98	Excessive detrital correction	Undefined	Carbonate/opal lamina

Table 29: Thermoluminescence results from Bare Mountain Fault Trenches BM-T1 and BM-T2. All errors given at the 95% confidence limit. See logs in Anderson and Klinger (1994), and Klinger and others (1994) for specific sample locations.

Sample Name	Field Moist. (%)	Saturation Moist. (%)	Dose Rate (Gy/ka) Field H_2O	Dose Rate (Gy/ka) Saturation H_2O	Total Bleach Eqivalent Dose (Gy)	Total Bleach Age (ka) for field moisture H_2O	Total Bleach Age (ka) for saturation moisture H_2O	Total Bleach Age (ka) Total Range	Partial Bleach Eqivalent Dose (Gy)	Partial Bleach Age (ka) for field moisture H_2O	Partial Bleach Age (ka) for saturation moisture H_2O	Partial Bleach Age (ka) Total Range
TL-31	*[North wall, Trench BM-T1, in Unit 4 of Anderson and Klinger (1994): Vesicular A horizon.]*											
	4.8	31	5.6±0.7	4.3±0.6	34 ± 4.7	6.2 ± 1.2	8.0 ± 1.5	5.0-10	53 ± 9	9.4 ± 2	12 ± 2.7	7.4-15
TL-32	*[South wall, Trench BM-T1, in Unit 3 of Anderson and Klinger (1994): Gravelly silt-rich unit within pleistocene colluvium.]*											
	6.4	35	5.5±0.7	4.2±0.5	88 ± 4.5	16 ± 2.1	21 ± 2.9	14-24	91 ± 7	17 ± 2.4	22 ± 3.3	15-25
TL-33	*[North wall, Trench BM-T2, in Unit 3 of Klinger and others (1994): Colluvial wedge containing dispersed pedogenic carboante.]*											
	4.8	33	3.4±0.55	2.6±0.04	22 ± 1.9	6.6 ± 1.1	8.6 ± 1.5	5.5-10	22 ± 7.6	6.5 ± 2.4	6.5 ± 3.2	4.1-12

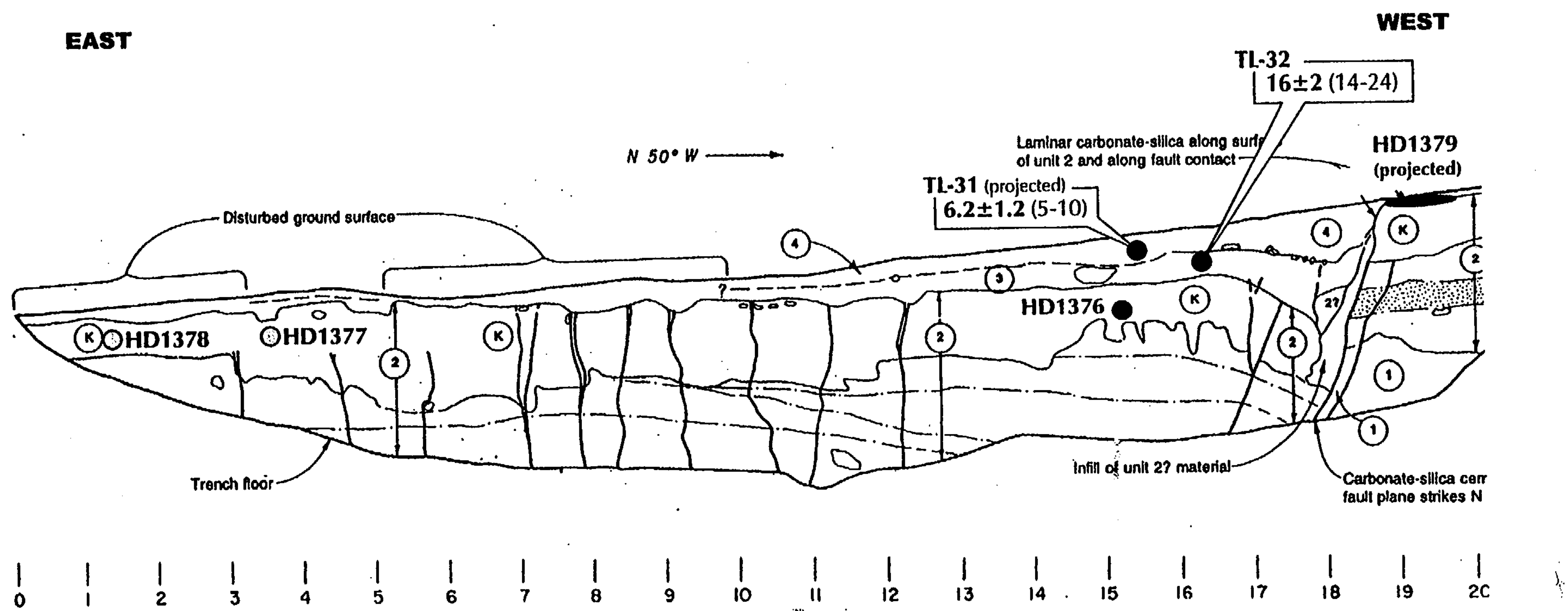

Figure 50: Generalized geologic log showing geochronological data available for Bare Mountain Fault Trench BM-T1 (after Anderson and Klinger, 1994). Uranium-series data (HD sample names) are from Table 28. Thermoluminescence data (TL sample names) are from Table 29. See section 5.1 in text for further explanation.

5.2.10 Lathrop Wells Cone

Table 30: Mass spectrometric U-series results from Lathrop Wells samples

Table 31: Thermoluminescence dating results from Lathrop Wells samples

Figure 52: Schematic diagrams of Lathrop Wells sites showing dating results

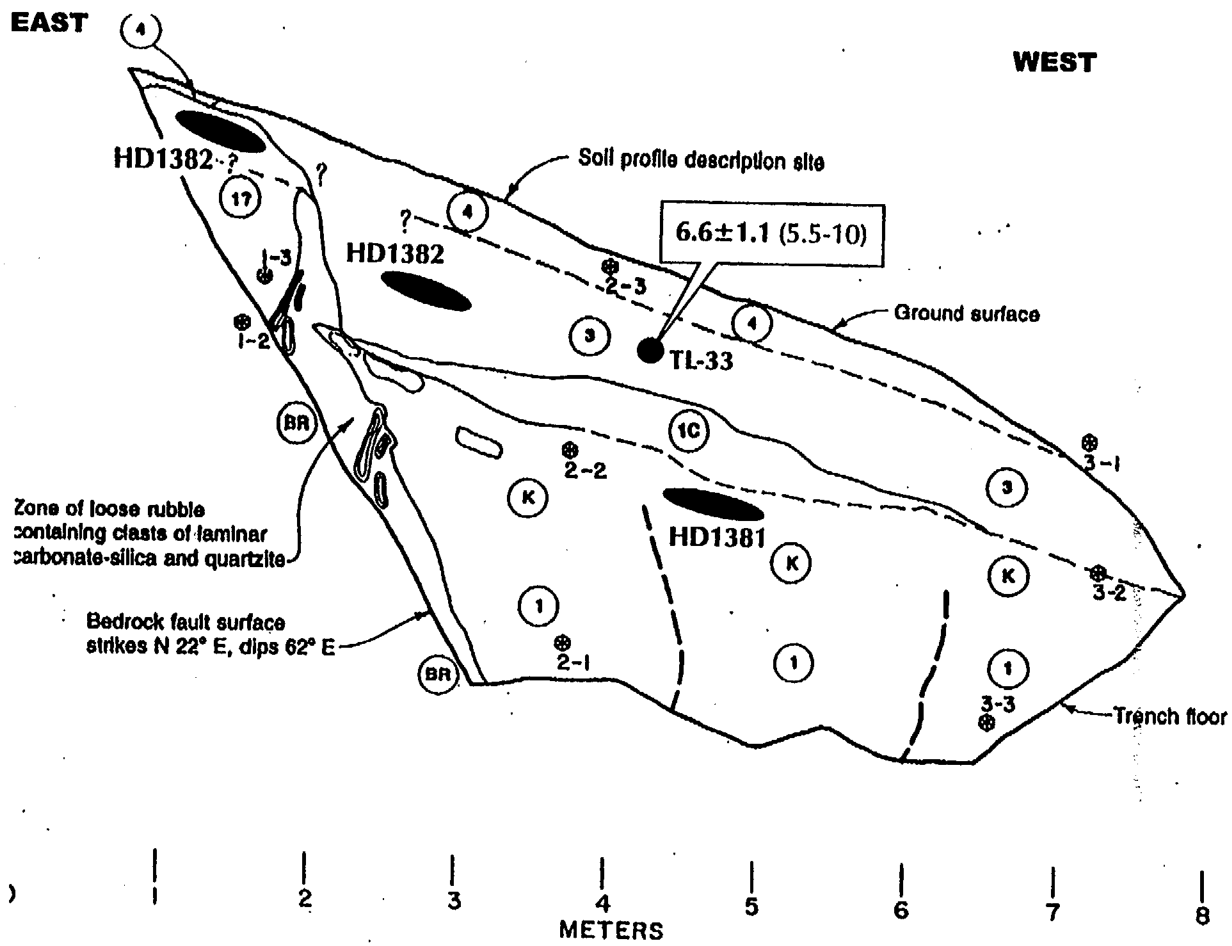

Figure 51: Generalized geologic log showing geochronological data available for Bare Mountain Fault Trench BM-T2 (after Klinger, et al., 1994). Thermoluminescence data (TL sample names) are from Table 29. See section 5.1 in text for further explanation.

Table 30: Uranium-series disequilibrium results from Lathrop Wells cinder cone area. Data are determined by mass spectrometry. The detrital component is assumed to be in secular equilibrium with an atomic TH/U of 4±2. All errors given at the 95% confidence level.

Sample Name	Sample wt. (g)	Concentration		$^{230}Th/^{232}Th$ activity ratio	Detritus-corrected		Sample Type
		U ppm	Th ppm		$^{230}Th/U$ Age (ka)	$^{234}U/^{238}U_{initial}$	
Freshly-excavated pit ~400 m west of cone (36°41.767'N; 116°30.894'W): Rhizoliths in Event 2 airfall tephra about 40-60 cm above base.							
HD1632-A	0.185	2.99	0.17	9.9	12.2 ± 0.8	1.641 ± 0.011	Composite small rhizoliths
HD1632-C	0.224	1.86	6.67	0.9			Basalt Ash
HD1632-D	0.175	3.76	0.241	11.2	16.3 ± 1.0	1.62 ± 0.02	Composite small rhizoliths
HD1632-E	0.226	3.23	1.01	2.4	12 ± 3	1.62 ± 0.03	Composite small rhizoliths
HD1632-G	0.172	3.19	0.106	15.3	11.4 ± 0.4	1.616 ± 0.011	Individual rhizolith
Exposure in wash ~750 m E-NE of cone (36°41.634'N; 116°29.924'W): Basaltic airfall tephra from beneath thick lava flow.							
LW122-FVP BA	0.123	1.97	7.83				Basalt Ash
LANL "working standard" for analytical comparisons of Th determinations by isotope dilution and INAA.							
LW27-FVP-P7A	0.086	2.02	7.01				Basalt Ash
LW27-FVP-P7B	0.165	2.02	6.99				Basalt Ash

Table 31: Thermoluminescence results from Lathrop Wells cinder cone area. All errors given at the 95% confidence limit. Experiments were duplicated with different types of disk normalization procedures. See section 4.3.2 in text for further explanation.

Sample/ *Type of Normal.*	Field Moist. (%)	Saturation Moist. (%)	Dose Rate (Gy/ka) Field H_2O	Dose Rate (Gy/ka) Saturation H_2O	Total Bleach Eqivalent Dose (Gy)	Total Bleach Age (ka) for field moisture H_2O	Total Bleach Age (ka) for saturation moisture H_2O	Total Bleach Age (ka) Total Range	Partial Bleach Eqivalent Dose (Gy)	Partial Bleach Age (ka) for field moisture H_2O	Partial Bleach Age (ka) for saturation moisture H_2O	Partial Bleach Age (ka) Total Range
TL-38 *[Exposure in wash ~750 m E-NE of cone (36°41.634'N; 116°29.924'W): Sandy eolian material beneath basaltic Event#2 airfall tephra, in turn, buried by thick lava flow.*												
IRSL	4	22	7.1±1.1	5.9±0.8	340 ± 16	48 ± 17	58 ± 20	31-78	368 ± 17	52 ± 20	63 ± 24	32-87
TL	4	22	7.1±1.1	5.9±0.8	178 ± 21	25 ± 4.8	30 ± 5.8	20-36	164 ± 30	23 ± 5.4	28 ± 6.6	18-35
TL-39A *[Freshly-excavated pit ~750 m SE of cone (36°40.813'N; 116°30.423'W): Sandy eolian material immediately underlying thick sheet of Event#2 basaltic airfall tephra.]*												
IRSL	0.1	29	5.9±1.0	4.3±0.7	537 ± 49	92 ± 17	124 ± 24	75-148	415 ± 89	71 ± 19	96 ± 26	52-122
TL	0.1	29	5.9±1.0	4.3±0.7	377 ± 38	64 ± 12	87 ± 17	52-105	302 ± 63	51 ± 14	70 ± 19	38-89
TL-39B *[Duplicate sample from the same site about 3 m to the east.]*												
IRSL	0.1	29	5.9±1.0	4.3±0.7	302 ± 124	52 ± 23	70 ± 31	29-101	147 ± 72	25 ± 13	34 ± 18	12-52
TL	0.1	29	5.9±1.0	4.3±0.7	203 ± 160	34 ± 19	47 ± 22	15-69				
TL-40 *[Freshly-excavated pit ~400 m west of cone (36°41.767'N; 116°30.894'W): Sandy eolian material immediately underlying thick sheet of Event#2 basaltic airfall tephra.]*												
IRSL	1.3	26	7.4±1.2	5.6±0.9	404 ± 82	55 ± 14	72 ± 19	41-91	499 ± 141	68 ± 22	89 ± 29	46-118
TL	1.3	26	7.4±1.2	5.6±0.9	212 ± 26	29 ± 6	37 ± 8	23-45	225 ± 57	31 ± 9	40 ± 12	22-52

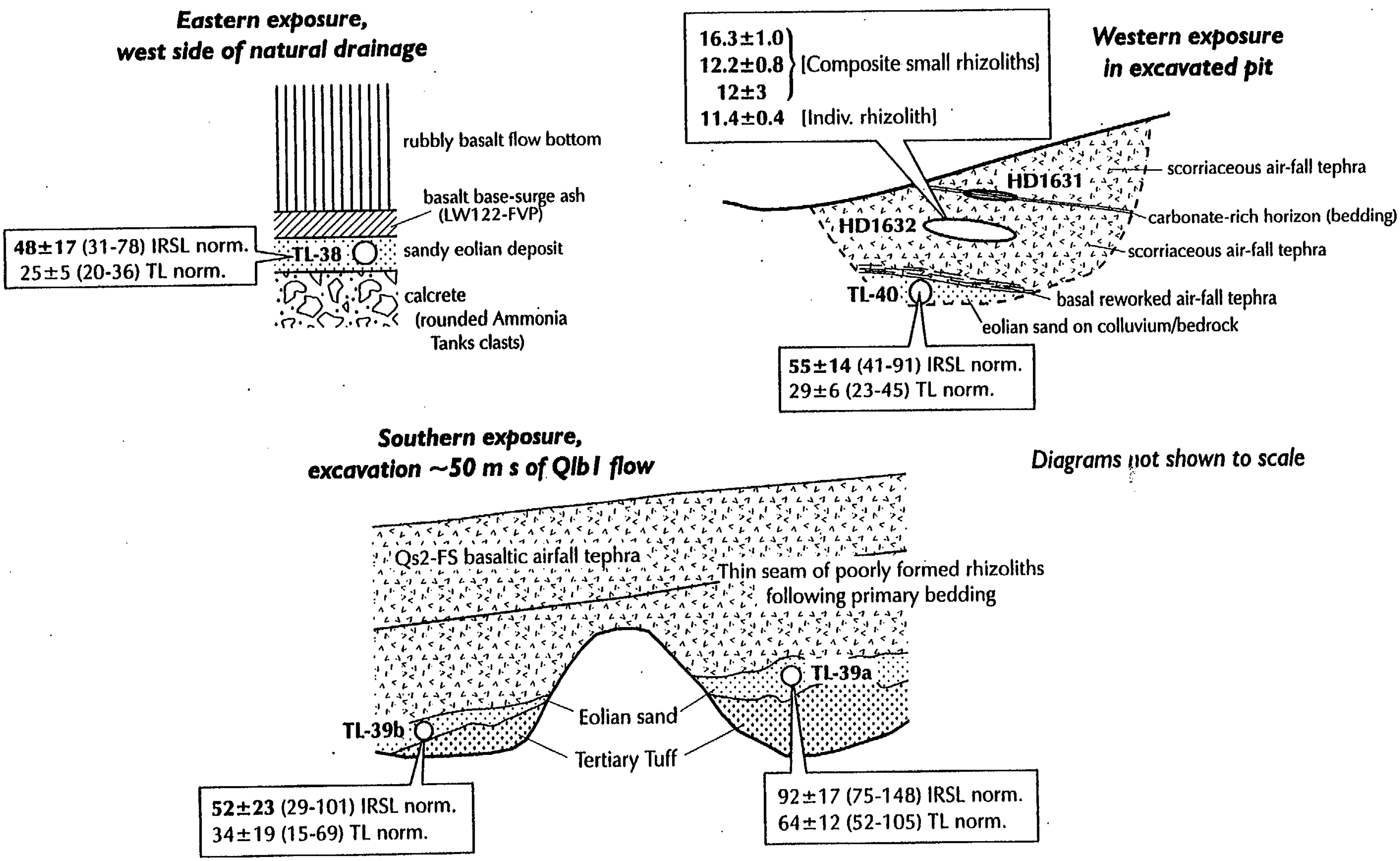

Figure 52: Schematic diagrams showing sample relations associated with Unit Qs2-FS (basaltic airfall tephra event number 2) proximal to Lathrop Wells cinder cone. Samples collected from three locatities described as the Eastern, Western and Southern exposures. Data and location information are given in Tables 30 and 31. See section 5.1 in text for further explanations of data presentation.

5.2.11 Fortymile Wash

Table 32: Mass spectrometric U-series results from Fortymile Wash samples

Table 33: Alpha spectrometric U-series results from Fortymile Wash samples

Figure 53: U-series concordia plot for samples from Fortymile Wash

Table 34: Thermoluminescence dating results from Fortymile Wash samples

Figure 54: Schematic diagrams of Fortymile Wash sites showing dating results

Table 32: Uranium-series disequilibrium results from the Fortymile Wash area. Data are determined by mass spectrometry. The detrital component is assumed to be in secular equilibrium with an atomic TH/U of 4±2. All errors given at the 95% confidence level.

Sample Name	Sample wt. (g)	Concentration		$^{230}Th/^{232}Th$ activity ratio	Detritus-corrected		Sample Type
		U ppm	Th ppm		$^{230}Th/U$ Age (ka)	$^{234}U/^{238}U_{initial}$	
West side of FMW, top of terrace exposure at USW-UZ-N85 site: Carbonate-cemented gravelly alluvium within upper-most calcrete (90 cm from terrace surface).							
HD1375-A1	0.092	9.06	4.67	3.8	51 ± 7	1.65 ± 0.06	Si-rich stringer in detrital matrix
East side of FMW, south wall near top of tributary arroyo (36°49.66'N; 116°23.24'W): Sandy eolian unit with rhizoliths and carbonate seams from cut-back below overlying calcrete.							
HD1742-B2	0.149	8.06	0.205	95.3	79.1 ± 1.0	1.614 ± 0.010	Individual Rhizolith
HD1742-B3	0.239	6.94	0.449	31.7	61.5 ± 1.2	1.608 ± 0.014	Individual Rhizolith
East side of FMW, south wall near top of tributary arroyo (36°49.66'N; 116°23.24'W): Well-cemented, resistive calcrete ledge representing upper-most carbonate accumulation.							
HD1743-A1	0.068	7.24	0.667	15.7	39.1 ± 1.1	1.568 ± 0.012	Si-rich stringer in rootlet Mass
HD1743-A2	0.117	4.61	1.65	5.3	52 ± 5	1.59 ± 0.03	Si-rich stringer in rootlet Mass
HD1743-A4	0.047	11.6	0.077	225	42.1 ± 0.5	1.550 ± 0.009	Si-rich stringer in rootlet Mass

Table 33: Uranium-series disequlibrium results from Fortymile Wash eolianite deposit. Data collected previously by alpha spectrometry (Paces et al., 1994). Criteria for calculating age estimates includes: 1) Whole rock analyses (either total digestion or leach/residue recombination; 2) Suffiently small detrital component correction (i.e., 230Th/232Th >~2); 3) Reasonable initial 234U/238U composition (i.e., 1.6±2). Analyses given in boldface below meet these critera. The detrital comonent is assumed to be in secular equilibrium with an atomic Th/U of 4±2. All uncertainties are given at the 95% confidence level.

Sample Name	Sample wt. (g)	Concentrations U (ppm)	Concentrations Th (ppm)	Measured $^{230}Th/^{232}Th$ activity ratio	Detritus-Corrected Activity Ratios $^{234}U/^{238}U$	Detritus-Corrected Activity Ratios $^{230}Th/^{238}U$	Corr.Coef. ρ(08-48)	AGE (ka)	Initial $^{234}U/^{238}U$ activity ratio	Aliquot Type
Southwest wall of tributary, east side of Fortymile Wash beneath powerline (36°50.19'N; 116°23.34'W): Composite rhizoliths in eolian sand deposit.										
HD1079-AL	1.966	3.61	2.06	4.90	1.128 ± 0.040	0.910 ± 0.059	0.184			<325 mesh; 0.3N HNO3 leach
HD1079-AR	1.076	4.87	6.79	3.08	1.154 ± 0.087	1.65 ± 0.25	0.461			<325 mesh; 0.3N HNO3 residue
HD1079-AL/R sum	***3.042***	***4.06***	***3.73***	***3.73***	***1.137*** ± 0.054	***1.173*** ± 0.092	***0.243***	***460 +inf/-180***	***1.50 ± 0.3***	***<325 mesh; math. recombination***

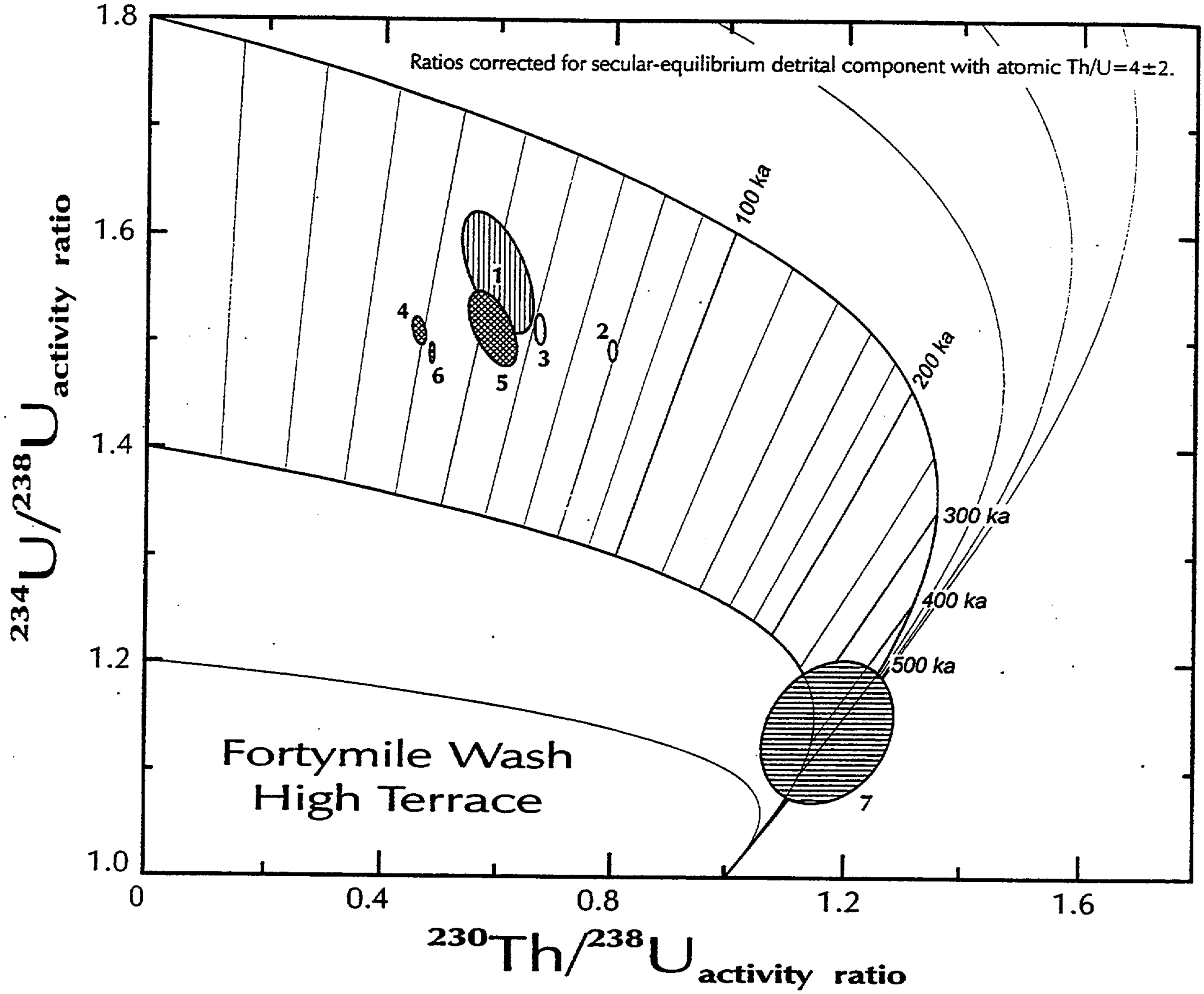

Figure 53: Uranium-series disequilibrium evolution diagram showing analyses from the Fortymile Wash area. Error ellipses for aliquots from the same sample are shaded in the same pattern. Data are given in Tables 32 and 33 and correspond to the following numbers: 1=HD1375-A1; 2=HD1742-B2; 3=HD1742-B3; 4=HD1742-A1; 5=HD1742-A2; 6=HD1742-A4; 7=HD10792-AL/Rsum.

d:\ym\data\tecton\fmw\fmw-ccrd.cdr
date updated: 9/23/95

Table 34: Thermoluminescence results from the Fortymile Wash area. All errors given at the 95% confidence limit.

Sample Name	Field Moist. (%)	Saturation Moist. (%)	Dose Rate (Gy/ka) Field H_2O	Dose Rate (Gy/ka) Saturation H_2O	Total Bleach Eqivalent Dose (Gy)	Total Bleach Age (ka) for field moisture H_2O	Total Bleach Age (ka) for saturation moisture H_2O	Total Bleach Age (ka) Total Range	Partial Bleach Eqivalent Dose (Gy)	Partial Bleach Age (ka) for field moisture H_2O	Partial Bleach Age (ka) for saturation moisture H_2O	Partial Bleach Age (ka) Total Range
TL-08												
	2.2	25	7.9±1.1	6.2±0.9	95 ± 4	12 ± 1.7	15 ± 2.4	10-18	96 ± 9.4	12 ± 2.1	15 ± 2.8	10-18
TL-13	*[West side, Forymile Wash high terrace just south of Fran Ridge-Alice Ridge water gap. Homogeneous fine-grained sandy unit, upper portion.]*											
	0.5	18	7.4±0.9	6.1±0.8	54 ± 6.9	7.3 ± 1.3	8.9 ± 1.7	6-11	66 ± 11	9.0 ± 1.9	11 ± 2.3	7.1-13
TL-14	*[West side, Forymile Wash high terrace just south of Fran Ridge-Alice Ridge water gap. Homogeneous fine-grained sandy unit, lower portion.]*											
	0.5	19	7.8±0.9	6.3±0.9	64 ± 2.3	8.3 ± 1.1	10 ± 1.5	7.2-12	52 ± 2.4	6.7 ± 0.9	8.3 ± 1.2	5.8-10
TL-47	*[West side, Fortymile Wash high terrace at Sever Wash gooseneck, west of highway (36°49.605'N; 116°24.025'W): Well-cemented, reddened sand unit beneath uppermost soil.]*											
	4.9	25	7.8±0.9	6.3±0.9	799 ± 117	103 ± 20	127 ± 25	83-152				
TL-49	*[East side, Fortymile Wash high terrace south of powerline to Midway Valley (36°49.661'N; 116°23.244'W): Brown sandy unit underlying capping ledge of calcrete of surface soil.]*											
	4.4	24	7.4±0.9	6.0±0.8	780 ± 120	105 ± 23	131 ± 30	82-160				

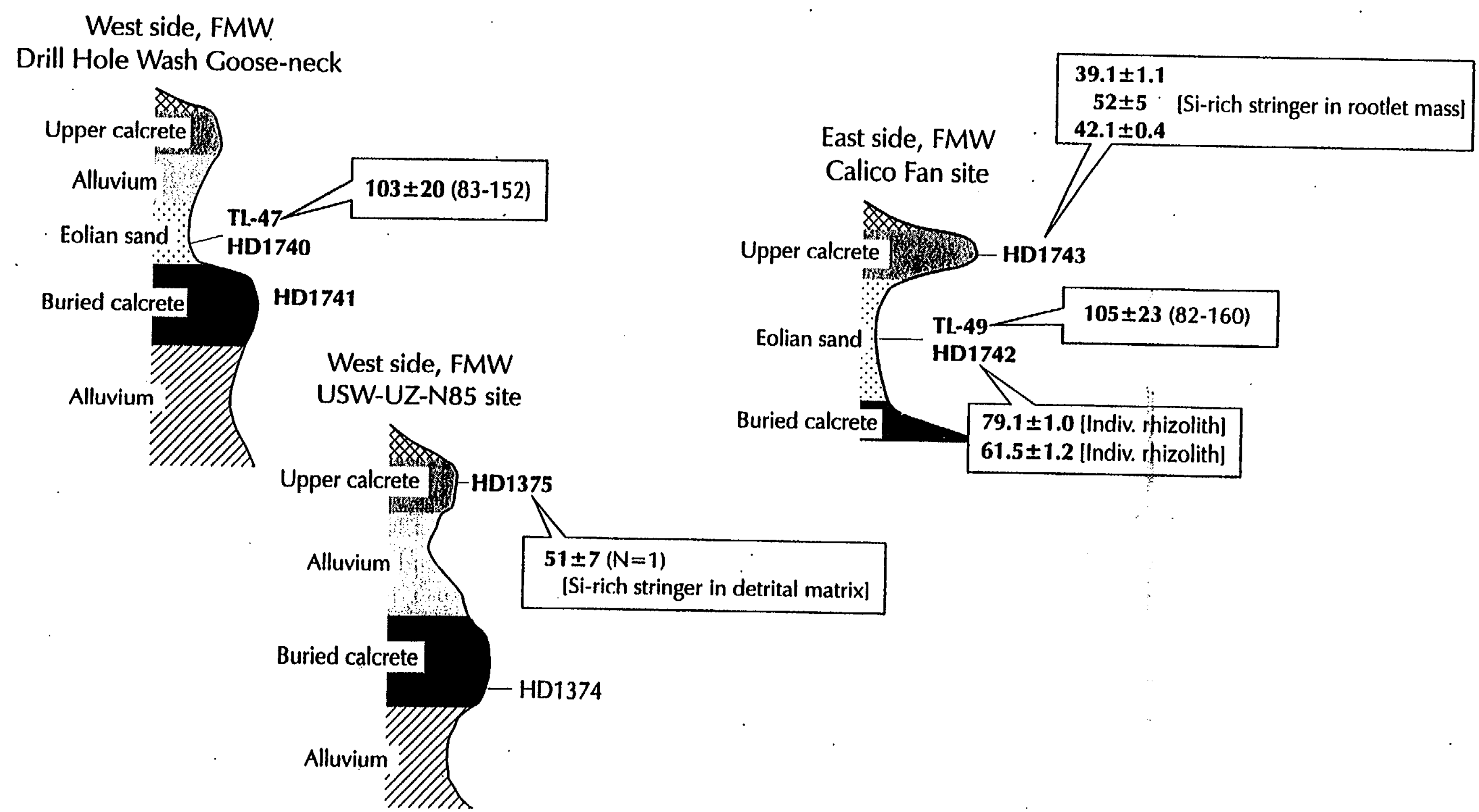

Figure 54: Schematic stratigraphic columns from the upper portions of the Fortymile Wash high terrace showing the relations between samples collected from natural exposures in the Fran/Alice ridge vicinity. Sketches not shown to scale. Uranium-series data (HD sample names) are from Table 32. Thermoluminescence data (TL sample names) are from Table 34. See section 5.1 in the text for further explanations of the data presentation.

5.2.12 Midway Valley Soil Pits/Trenches

Table 35: Alpha spectrometric U-series results from Midway Valley soil pit/trench samples

Table 36: Thermoluminescence dating results from Midway Valley soil pit/trench samples

Figure 55: Schematic log of Midway Valley Pit 10 showing dating results

Figure 56: Schematic log of Midway Valley Pit 14 showing dating results

Table 35: Uranium-series disequlibrium results from Midway Valley Trenches 5a and 7. Data collected previously by alpha spectrometry (Paces et al., 1994). Criteria for calculating age estimates includes: 1) Whole rock analyses (either total digestion or leach/residue recombination; 2) Suffiently small detrital component correction (i.e., 230Th/232Th >~2); 3) Reasonable initial 234U/238U composition (i.e., 1.6±2). Analyses given in boldface below meet these critera. The detrital comonent is assumed to be in secular equilibrium with an atomic Th/U of 4±2. All uncertainties are given at the 95% confidence level.

Sample Name	Sample wt. (g)	Concentrations U (ppm)	Th (ppm)	Measured $^{230}Th/^{232}Th$ activity ratio	Detritus-Corrected Activity Ratios $^{234}U/^{238}U$	$^{230}Th/^{238}U$	Corr.Coef. ρ(08-48)	$^{230}Th/U$ AGE (ka)	Initial $^{234}U/^{238}U$ activity ratio	$^{234}U/^{238}U$ Age (ka)	Aliquot Type
Trench 5a: Soil carbonate from upper platy K horizon near west end of trench. Unit is fractured but not offset. Composite sample gently crushed and seived.											
HD972-AL	1.97	4.76	1.81	4.29	1.550 ± 0.043	0.487 ± 0.044	-0.357				<325 mesh; 0.3N HNO3 leach
HD972-AR	1.23	7.84	6.61	2.25	1.592 ± 0.096	0.520 ± 0.102	-0.526				<325 mesh; 0.3N HNO3 residue
HD972-AL/R sum	***3.20***	***5.94***	***3.65***	***2.87***	***1.570 ± 0.068***	***0.502 ± 0.069***	***-0.495***	***41 ± 8***	***1.640 ± 0.078***		<325 mesh; math. recombination
Trench 7: Carbonate rhizoliths w/in sandy horizon near bedrock/Quaternary boundary. Composite sample gently crushed and seived.											
HD1083-AL	1.70	4.51	1.86	10.02	1.097 ± 0.026	1.409 ± 0.060	0.315				<325 mesh; 0.3N HNO3 leach
HD1083-AR	1.14	10.0	4.20	7.75	1.085 ± 0.026	1.081 ± 0.054	0.211				<325 mesh; 0.3N HNO3 residue
HD1083-AL/R sum	2.84	6.71	2.80	8.66	1.090 ± 0.028	1.213 ± 0.046	0.243	Excess Th	Undefined	$670^{+120}/_{-90}$	<325 mesh; math. recombination

Table 36: Thermoluminescence results from soil pits in Midway Valley. All errors given at the 95% confidence limit.

Sample Name	Field Moist. (%)	Saturation Moist. (%)	Dose Rate (Gy/ka)		Total Bleach Eqivalent Dose (Gy)	Total Bleach Age (ka)			Partial Bleach Eqivalent Dose (Gy)	Partial Bleach Age (ka)		
			Field H_2O	Saturation H_2O		for field moisture H_2O	for saturation moisture H_2O	Total Range		for field moisture H_2O	for saturation moisture H_2O	Total Range
TL-41	*[Sandy lens in alluvial gravel deposit in upper, Q5 soil package]*											
	3.4	21	9.1±1.3	7.4±1.1	36 ± 3	4.0 ± 0.7	4.9 ± 0.8	3.3-5.7	45 ± 5.8	4.9 ± 1	6.0 ± 1.2	3.9-7.2
TL-42	*[Coarse gravely alluvium with abundant sandy matrix within upper, Q5 soil package.]*											
	0.1	27	9.3±1.4	7.0±1.1	65 ± 5	6.9 ± 1.2	9.3 ± 1.6	5.7-10.9	98 ± 9	11.0 ± 1.8	14 ± 2.5	9.2-17
TL-48	*[Reddened, argillic Bt horizon buried by Q5 soil package. Provides maximum age for overlying Q5 sedimentation.]*											
	4.4	22	9.4±1.4	7.8±1.2	254 ± 20	27 ± 4.6	33 ± 5.6	22-39				

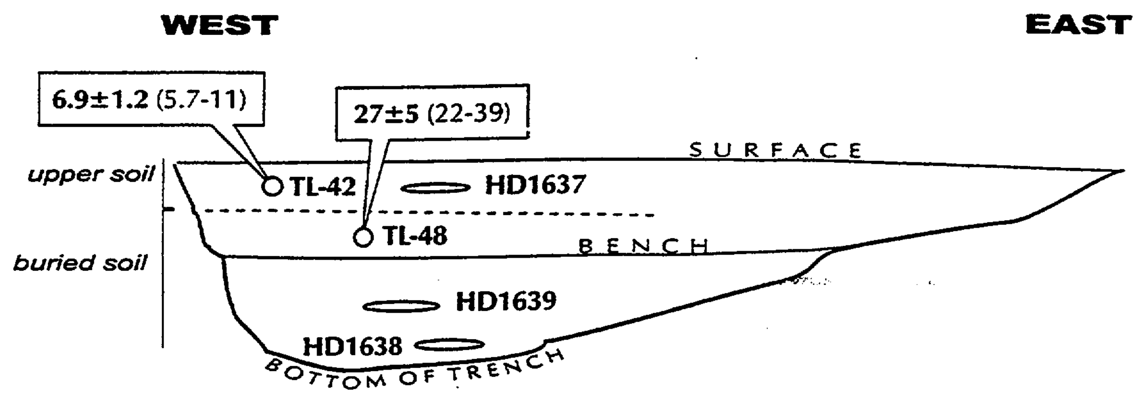

Figure 55: Schematic log showing physical relations and data for geochronology samples from Midway Valley Pit 10. Thermoluminescence data (TL sample names) are from Table 36. Uranium-series data (HD sample names) are unavailable. See section 5.1 in text for further explanation.

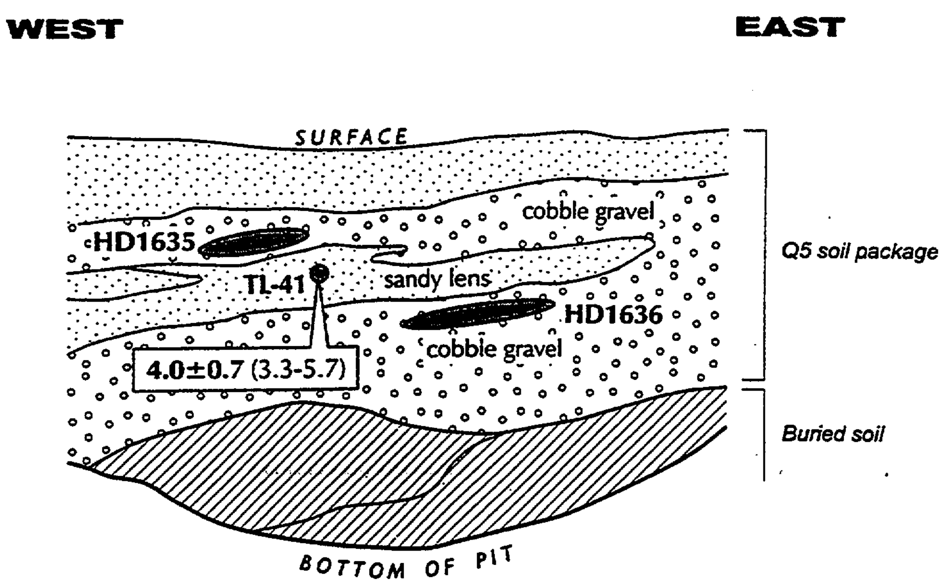

Figure 56: Schematic log showing physical relations and data for geochronology samples from Midway Valley Pit 14. Thermoluminescence data (TL sample names) are from Table 36. Uranium-series data (HD sample names) are unavailable. See section 5.1 in text for further explanation.

5.2.12 Coyote Wash Trenches

Table 37: Thermoluminescence dating results from Coyote Wash Trenches

Figure 57: Schematic log of Coyote Wash trenches showing dating results

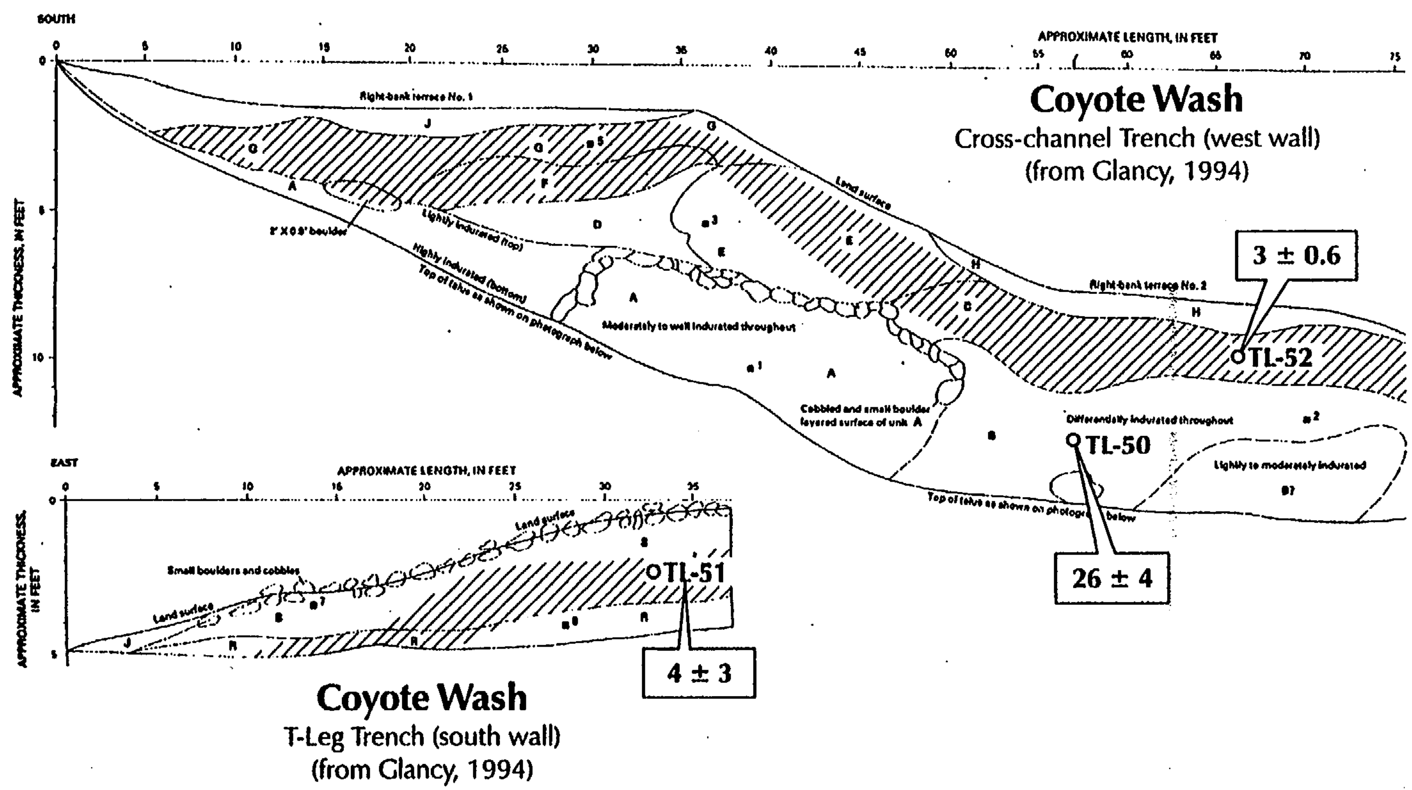

Figure 57: Generalized geologic log showing geochronological data in west wall of the Coyote Wash Cross-Channel Trench and south wall of the Coyote Wash T-Leg Trench (modified from Glancy, 1994). Thermoluminescence data (TL sample names) are from Table 37. See section 5.1 in text for further explanation.

Table 37: Thermoluminescence results from Coyote Wash Trenches. All errors given at the 95% confidence limit.

Sample Name	Field Moist. (%)	Saturation Moist. (%)	Dose Rate (Gy/ka)		Total Bleach Eqivalent Dose (Gy)	Total Bleach Age (ka)			Partial Bleach Eqivalent Dose (Gy)	Partial Bleach Age (ka)		
			Field H_2O	Saturation H_2O		for field moisture H_2O	for saturation moisture H_2O	Total Range		for field moisture H_2O	for saturation moisture H_2O	Total Range
TL-50	*[West wall, Cross-channel Trench, Unit B of Glancy (1994): Coarse cobble alluvium with abundant fine-sandy matrix of likely eolian origin.]*											
	3.8	25.7	10.1±0.8	8.0±0.6	257 ± 13	26 ± 4	32 ± 5	21-38	267 ± 17	26 ± 4	33 ± 6	22-39
TL-51	*[South wall, T-Leg Trench, Unit S of Glancy (1994): Cobble alluvium with distinctly abundant, fine-sand matrix of likely eolian origin; "seive deposit".]*											
	0.8	23.4	9.9±0.7	8.3±0.6	40 ± 30	4 ± 3	5 ± 4	1-9	15 ± 41	2 ± 4	2 ± 5	0-7
TL-52	*[West wall, Cross-channel Trench, Unit C of Glancy (1994): Cobble alluvium with abundant fine-sandy matrix of likely eolian origin.]*											
	2.3	21.8	15.2±1.1	12.2±0.9	43 ± 6	2.9 ± 0.6	3.6 ± 0.8	2-4	41 ± 18	2.7 ± 1.3	3.4 ± 1.6	1-6

REFERENCES

Atkins, M., 1986, A geochemical and geochronological study of U and Th radioisotopes in paleosols, loess and tephra: a Middle Rhine case study: Unpublished Ph.D thesis, University of Reading, 349 pp.

Balescu, S. and Lamonthe, M., 1992, The blue emission of K-feldspar coarse grains and its potential for overcoming TL age Underestimation, Quaternary Science Reviews, v. 11, p. 45-51.

Berger, G.W., 1985, Thermoluminescence dating of volcanic ash: Journal of Volcanology and Geothermal Research v. 25, p. 333-347.

Berger, G.W., 1987, Thermoluminescence dating of the Pleistocene Old Crow Tephra and adjacent loess, near Fairbanks, Alaska: Canadian Journal of Earth Sciences, v. 24, p. 1975-1984.

Berger, G.W., 1992, Dating volcanic ash by use of thermoluminescence: Geology, v. 20, p. 11-14.

Bischoff, J.L., Fitzpatrick, J.A., 1991, Uranium-series dating of impure carbonates: An isochron technique using total sample dissolution: Geochimica et Cosmochimica. Acta, v. 55, p. 543-554.

Christensen, J.N., and DePaolo, D.J., 1993, Time scales of large volume silicic magma systems: Sr isotopic systematics of phenocrysts and glass from the Bishop Tuff, Long Valley, California: Contributions to Mineralogy and Petrology, v. 113, p. 100-114.

Forman, S. L., 1988, Assessment of the Applicability of the Thermoluminescence Dating Technique to Natural Hazard Evaluations at the high-level Nuclear Waste Repository Site, Yucca Mountain, Nevada: Nevada Bureau of Mines RMS SL# 026901, 15 p.

Forman, S.L., Wintle, A.G., Thorleston, L.H., and Wyatt, P.H., 1987, TL Properties and age estimates for Quaternary raised marine sediments, Hudson Bay Lowland, Canada: Canadian Journal of Earth Sciences, v. 24, p. 2405-2411.

Halliday, A.N., Fallick, A.E., Hutchinson, J., and Hildreth, W., 1984, A Nd, Sr and O isotopic investigation into the causes of chemical and isotopic zonation in the Bishop Tuff, California: Earth and Planetary Science Letters, v. 68, no. 3, p. 379-391.

Halliday, A.N., Mahood, G.A., Holden, P., Metz, J.M., Dempster, T.J., and Davidson, J.P., 1989, Evidence for long residence times of rhyolitic magma in the Long Valley magmatic system: the isotopic record in precaldera lavas of Glass Mountain: Earth and Planetary Science Letters, v. 94, p. 274-290.

Izett, G.A., Obradovich, J.D., and Mehnert, H.H., 1988, The Bishop ash bed (Middle Pleistocene) and some older (Pliocene and Pleistocene) chemically and mineralogically similar ash beds in California, Nevada, and Utah: U.S. Geological Survey Bulletin 1675, 37 p.

Kaufman, A., 1971, U-series dating of Dead Sea Basin carbonates: Geochimica et Cosmochimica Acta, v. 35, p. 1269-1281.

Ku T.-L., and Joshi, L.U., 1980, Dating terrestrial carbonate cementation with uranium-series isotopes: in Patel, B., ed., Management of Environment: Bombay, Wiley Eastern Ltd., p. 551-557.

Ku, T.-L., and Liang, Z.C., 1984, The dating of impure carbonates with decay-series isotopes: Nuclear Instruments and Methods in Physics Research, v. 223, p. 563-571.

Ku, T.-L., Bull, W.B., Freeman, S.T., and Knauss, K.G., 1979, ^{230}Th-^{234}U dating of pedogenic carbonates in gravelly desert soils of Vidal Valley, southern California: Geological Society of America Bulletin, v. 90, p. 1063-1073.

Latham, A.G., (unpublished manuscript) On the principles of the U-trend method for dating Quaternary sediments.

Ludwig, K.R., Titterington, D.M., 1994, Calculation of $^{230}Th/U$ isochrons, ages, and errors: Geochimica et Cosmochimica. Acta, v.58, n. 22, p. 5031-5042.

Luedke, R.G., and Smith, R.L., 1991, Quaternary volcanism in the western conterminous United States, in Morrison, R.B., ed., Quaternary nonglacial geology: Conterminous U.S.: Boulder, Geological Society of America, The Geology of North America, v. K-2, p. 75-92.

Luo, S., and Ku, T.-L., 1991, U-series isochron dating: A generalized method employing total-sample dissolution: Geochimica et Cosmochimica. Acta, v. 55, p. 555-564.

Millard, H.T., and Maat, P.B., 1994, Thermoluminescence Dating Procedures in Use at the U.S. Geological Survey, Denver, Colorado: U.S. Geological Survey Open-File Report 94-249, 112 p.

Morrison, R.B., 1991, Quaternary stratigraphic, hydrologic, and climatic history of the Great Basin, with emphasis on Lakes Lahontan, Bonneville, and Tecopa, in Morrison, R.B., ed., Quaternary nonglacial geology: Conterminous U.S.: Boulder, Geological Society of America, The Geology of North America, v. K-2, p. 13-44.

Muhs, D.R., Rosholt, J.N., and Bush, C.A., 1989, The uranium-trend dating method: principles and application for southern California marine terrace deposits. Quaternary International, v. 1, pp. 19-34.

Muhs, D.R., Szabo, B.J., Bush, C.A., Shroba, R.R., Taylor, E.M., and Whitney, J.W., (unpublished manuscript) 238U-234U-230Th systematics and the origin of near-surface secondary carbonates in the Yucca Mountain area.

Muhs, D.R., Whitney, J.W., Shroba, R.R., Taylor, E.M., and Bush, C.A., 1990, Uranium-series dating of secondary carbonates near Yucca Mountain, Nevada: Applications to tectonic, paleoclimatic and paleohydrologic problems: *in* Conference on High-Level Radioactive Waste Management, 1st, Las Vegas, NV, 1990, Proceedings, American Society of Civil Engineers, p. 924-929.

Osmond, J.K., May, J.P., and Tanner, W.F., 1970, Age of the Cape Kennedy barrier-and-lagoon complex: Journal of Geophysical. Research, v. 75, p. 5459-5468.

Paces, J.B., Menges, C.M., Widmann, B., Wesling, J.R., Bush, C.A., Futa, K., Millard, H.T., Maat, P.B., and Whitney, J.W., 1994, Preliminary U-series disequilibrium and thermoluminescence ages of surficial deposits and paleosols associated with Quaternary faults, eastern Yucca Mountain: *in* Conference on High-Level Radioactive Waste Management, 5th, Las Vegas, NV, 1994, Proceedings, American Society of Civil Engineers, p. 2391-2401.

Peterson, F.F., Bell, J.W., Dorn, R.I., Ramelli, A.R., and Ku, T.-L., 1995, Late Quaternary geomorphology and soils in Crater Flat, Yucca Mountain area, southern Nevada: Geological Society of America Bulletin, v. 107, no. 4, p. 379-395.

Rosholt, J.N., 1976, $^{230}Th/^{234}U$ dating of travertine and caliche rinds (abstr.): Geological Society of America Abstracts with Program, v. 8, p. 1076.

Rosholt, J.N., 1980, Uranium-trend dating of Quaternary sediments: U.S. Geological Survey Open-File Report 80-1087, 65 p.

Rosholt, J.N., 1985, Uranium-trend systematics for dating Quaternary sediments: U.S. Geological Survey Open-File Report 85-298, 48 p.

Rosholt, J.N., Bush, C.A., Carr, W.J., Hoover, D.L., Swadley, W.C., and Dooley, J.R., Jr., 1985b, Uranium-trend dating of Quaternary deposits in the Nevada Test Site area, Nevada and California: U.S. Geological Survey Open-File Report 85-540, 72 p.

Rosholt, J.N., Bush, C.A., Shroba, R.R., Pierce, K.L., and Richmond, G.M., 1985a, Uranium-trend dating and calibrations for Quaternary sediments: U.S. Geological Survey Open-File Report 85-299, 48 p.

Rosholt, J.N., Colman, S.M., Stuiver, Minze, Damon, P.E., Naeser, C.W., Naeser, N.D., Szabo, B.J., Muhs, D.R., Liddicoat, J.C., Forman, S.L., and others, 1991, Dating methods applicable to the Quaternary, in Morrison, R.B., ed., Quaternary nonglacial geology: Conterminous U.S.: Boulder, Geological Society of America, The Geology of North America, v. K-2, p. 45-74.

Rosholt, J.N., Downs, W.R., and O'Malley, P.A., 1986, Uranium-trend ages of surficial deposits in the central Grand Canyon National Park, Arizona (abstr.). Geological Society of America Abstracts with Program, v. 18, p. 408.

Rosholt, J.N., Swadley, W.C., and Bush, C.A., 1988, Uranium-trend dating of fluvial and fan deposits in the Beatty area, Nevada: in Carr, M.D., and Yount, J.C., eds., Investigations of a Potential Nuclear Waste Disposal Site at Yucca Mountain, Southern Nevada. U.S. Geological Survey Bulletin 1790, p. 129-147.

Sarna-Wojcicki, A.M., and Davis, J.O., 1991, Quaternary tephrochronology, in Morrison, R.B., ed., Quaternary nonglacial geology: Conterminous U.S.: Boulder, Geological Society of America, The Geology of North America, v. K-2, p. 93-116.

Sarna-Wojcicki, A.M., Lajoie, K.R., Meyer, C.E., Adam, D.P., and Rieck, H.J., 1991, Tephrochronologic correlation of upper Neogene sediments along the Pacific margin, conterminous United States, in Morrison, R.B., ed., Quaternary nonglacial geology: Conterminous U.S.: Boulder, Geological Society of America, The Geology of North America, v. K-2, p. 117-140.

Schwarcz, H.P., Latham, A.G., 1989, Dirty calcites I. Uranium-series dating of contaminated calcite using leachates alone: Chemical Geology, v. 80, p. 34-43.

Singhvi, A.K., Sharma, Y.P., and Agrawal, D.P., 1982, TL dating of dune sands in Rajasthana, India: Nature, v. 295; p. 313-315.

Szabo, B.J., and O'Malley, P.A., 1985, Uranium-series dating of secondary carbonate and silica precipitates relating to fault movements in the Nevada Test Site Region and of caliche and travertine samples from the Amargosa Desert: U.S. Geological Survey Open-File Report 85-47, 12 p.

Szabo, B.J., and Rosholt, J.N., 1982, Surficial continental sediments: in Ivanovich, M., and Harmon, R.S., eds., Uranium Series Disequilibrium: Applications to Environmental Problems: Oxford, Claredon Press, p. 246-267.

Szabo, B.J., and Sterr, H., 1978, Dating caliches from southern Nevada by $^{230}Th/^{232}Th$ versus $^{234}U/^{232}Th$ and $^{234}U/^{232}Th$ versus $^{238}U/^{232}Th$ isochron-plot method. U.S. Geological Survey Open File Report 78-701, p. 416-418.

Szabo, B.J., CARR, W.J., and GOTTSCHALL, W.C., 1981, Uranium-thorium dating of Quaternary carbonate accumulations in the Nevada Test Site region, southern Nevada: U.S. Geol. Survey Open-file Report 81-119, 35 p.

Templer, R. H., 1985, The removal of anomalous fading in zircons: Nuclear Tracks, v. 10 (4-6), p. 531-537.

Wintle, A.G. and Huntley, D.J., 1980, TL dating of ocean sediments: Canadian Journal of Earth Sciences, v. 17, p. 348-360.

Wintle, A.G. and Huntley, D.J., 1982, Thermoluminescence Dating of Sediments: Quaternary Science Reviews v. 1, p. 31-53.

Wintle, A.G., 1973, Anomalous fading of thermoluminescence in mineral samples: Nature, v. 245, p. 143-144.

Wintle, A.G., 1977, Detailed study of a thermoluminescent mineral exhibiting anomalous fading: Journal of Luminescence, v. 15, p. 385-393.

Wintle, A.G., 1985, Stability of TL signal in fine-grains from loess: Nuclear Tracks, v. 10 (4-6), p. 725-730.

Zeller, E. J., 1955, Thermoluminescence of carbonate sediments: in Nuclear Geology, John Wiley and Sons, New York; p. 180-188.

CHARACTERISTICS AND DEVELOPMENT OF ALLUVIAL SOILS OF THE YUCCA MOUNTAIN AREA, SOUTHERN NEVADA

by Lundstrom, S.C., McDaniel, S.M., Guertal, W., Nash, M.H., Wesling, J.R., Cidziel, J., Cox, S., and Coe, J.

ABSTRACT

The imprint of pedogenesis and associated surface characteristics provide basic criteria for distinguishing and mapping surficial alluvial units in the Yucca Mountain area, and for developing a soil-stratigraphic framework for geochronologic studies. In this paper, we discuss field characteristics and laboratory data on particle size distribution and carbonate content from alluvial soils in and near Midway Valley, and the relation of soil characteristics to climate history and paleohydrology. Age control, documented in a companion paper (Paces and others) for young alluvial units is predominantly based on thermoluminescence ages on eolian material associated with soils that formed on or underlie surficial alluvium, and on U series ages on pedogenic carbonate and silica.

Eolian addition is a predominant initial pedogenic modification of freshly deposited alluvium; in soils as young as late Holocene, the fine fraction (< 2mm) predominated by sand size decreases downward from the surface, and is interpreted to be the result of eolian addition, infiltration and pedoturbation. Fine sand is a ubiquitous peak mode of the fine fraction, whereas particle size distribution within the gravel fraction is more variable. It is likely that much of the eolian input closely follows episodes of alluviation from distal areas of freshly deposited alluvial sand. The episodes of alluviation relate to climates with runoff events larger than observed historically. Alluvial depositional morphology on younger alluvium (largely Holocene) is subdued by the eolian mantle but is still apparent, while surface pavement is loosely packed and little varnished. A reddenned argillic horizon observed in older soils is not observed in Holocene alluvium of this area. Carbonate content of the fine fraction is generally less than 5 percent and is associated with stage I-II carbonate/silica morphology consisting of thin coats on clast undersides. This type of surface and soil morphology is developed on units from as old as 12 ka to younger than 4 ka.

Climates effectively wetter than during the past 8000 years have impacted soils formed on older (Pleistocene) alluvium covered and mixed with an eolian mantle. Though a fine sand mode attributed to an eolian origin exists in older soils as well, the eolian-dominated upper part of Pleistocene soils are reddenned, and clay and silt contents are higher than in younger soils; in the upper part of older soils, an additional silt peak is typically present. Late Pleistocene soils are distinctly more cemented by carbonate and silica than Holocene soils and have stage II-III morphology generally at >30 cm depth, with a maximum carbonate content of less than 10 percent of the fine fraction. This type of soil morphology is developed on alluvium as young as 25 ka (?) and as old as 40-100 ka, and in this area is associated with a well-packed, smooth, and varnished desert pavement. Though desert pavements are known to occur on alluvium of Holocene age where clay and silt rich eolian dust is abundant (such as near exposures of marsh and playa deposits), well-developed pavements at Yucca Mountain are predominantly associated with underlying Av horizons and reddenned argillic horizons indicative of Pleistocene age. However, alluvial surfaces possessing well packed, varnished pavements near Midway Valley grade southward to poorly varnished and developed pavements in the Amargosa Desert where there is a higher eolian sand flux.

Progressive addition of clay, silt, silica, and carbonate cements during repeated wet climates impedes infiltration and enhances surface runoff and erosion, especially during intense rainfall events. Thus, soils are transformed to rounded erosional surfaces, underlain by a laminar K horizon at typically less than 50 cm depth. Maximum carbonate content in the fine fraction of the K horizon ranges from 20-40 percent. The surface pavement of these erosional surfaces incorporates fragments of pedogenic calcite and silica originally formed in subsurface K horizons, but left as fragments at the surface during subsequent erosional periods. We interpret the silt and clay rich eolian mantle that underlies the surface pavement as having developed since the latest erosional period at that location. This type of soil and surface morphology occurs on alluvial units younger than 700 ka, but probably not on alluvium as young as late Pleistocene. Such erosional morphology can occur on any alluvium older than that in which soil development has reached an erosional threshold, including pre-Quaternary alluvium.

Buried soils are common in alluvium at Yucca Mountain and are recognized by increases in fine fraction, and differences in color and carbonate content relative to overlying material, especially where erosionally truncated during deposition of overlying alluvial unit. Buried soils are typically at least partially eroded, and may include truncated examples of any of the above morphology. Where the eolian rich top is preserved in the buried soil, it provides a source for thermoluminescence dates as maximum age constraints on the overlying alluvium.

INTRODUCTION

The study of soils is essential to the understanding of Quaternary stratigraphy and climate change. The characteristics and distribution of soils, in conjunction with geochronologic data, provide a basis for deciphering the paleoenvironmental history of Yucca Mountain. Because there is typically no inherent radiometric clock set with alluvial deposition analogous to the crystallization of igneous rocks, geochronologic studies of Quaternary alluvium commonly must tie into some relationship to soil development and surface history. The purpose of this report is to present results of field and laboratory characterization of an alluvial soil-stratigraphic framework done in collaboration with geochronologic studies presented in a companion report (Paces and others), and to discuss and interpret alluvial soil development as a basis for further work. In combination with the geochronological co-report, this preliminary progress report will serve as a basis for interim age estimation. It must be recognized that soil development is extremely complex, resulting from hydrologic, geologic, biologic and other processes occurring at the interface between land and atmosphere during highly variable climates of the Quaternary.

PREVIOUS WORK

Taylor (1986) completed the initial quantitative soils characterization of the Yucca Mountain area, using a sequence of pits along Fortymile Wash and Yucca Wash. She recognized and established the importance of pedogenic silica in this setting, and defined a chronosequence (Harden and others, 1991a, 1991b) through correlation of alluvial terraces to uranium trend dates (Rosholt, 1985) on surficial deposits elsewhere in the area. The U-trend ages are no longer considered to be reliable (see co-report) and geochronologic studies since 1992 (Paces and others, 1992; co-paper) provide a more defensible basis for understanding soil development. A large amount of work relating to the pedogenic origin of calcite and silica exposed in Trench 14 (Quade and Cerling, 1990; Taylor and Huckins, 1994; Vaniman, 1994) was done in response to proposed alternative models. Later, as part of studies to address pre-closure seismic hazards, pits in Midway Valley were excavated in conjunction with mapping of surficial geology (Wesling and others, 1992). Faulds and others (1994) and Peterson and others (1995) discuss alluvial soils in Crater Flat, to the west of Yucca Mountain. Subsequent mapping of surficial deposits of a larger area on and around Yucca Mountain (Lundstrom and others, in press) adapted map units from Wesling and others (1982). Here, we report on laboratory analyses of samples collected from alluvial soils of Midway Valley and nearby sites. Using these results, we discuss processes important to the pedogenesis of surficial deposits and stratigraphic framework of the area, and the relation of alluvial soils to paleoclimate.

ENVIRONMENTAL SETTING

Most of soil pit sites considered in this report occur in Midway Valley, immediately east of Yucca Mountain (Plate 1), a complex fault block ridge in the southern Great Basin. This area, set within the southern Basin and Range province, presently has a warm dry climate, with estimated mean annual temperature of 14 C and mean annual precipitation of 15 cm. The sites range in altitude from 3400 to 4180 feet. All but one (SWG-1) of the sites for which results are included in this report are from soils developed in gravelly alluvium derived from Yucca Mountain. The predominant lithology of alluvial clasts, is rhyolitic to trachytic ash flow tuff of the Paintbrush Group, which is exposed at the surface of Yucca Mountain (Scott and Bonk, 1984; Buesch and others, in press). Most of the exposed section is moderately to densely welded tuff, with the Tiva Canyon Tuff dominating the surface exposure. Because densely welded tuff is relatively resistant to comminution during alluvial transport, the gravel clast lithologies are dominated by welded Tiva Canyon Tuff. In northern Midway Valley, alluvium of pits MWV 13,14, and 22-28 also includes clasts derived from the rhyolite flows of Fortymile Canyon from Pinnacles Ridge, a high relief area on the north side of the Yucca Wash (Christiansen and Lipman, 1968). Though Yucca Wash is presently incised along the northern margin of Midway Valley, in earlier aggradational episodes, the Yucca Wash basin provided alluvium that included non-Paintbrush rhyolitic lithologies to northern Midway Valley. Though site SWG-1 is along present lower Sever Wash, which is only derived from Yucca Mountain and Midway Valley, alluvial unit 3f (Lundstrom and others, in press) at this site was deposited by Fortymile Wash. Alluvium of Fortymile Wash is characterized by the common occurence of rounded basaltic clasts that do not occur within the drainage where alluvium has been derived solely from Yucca Mountain or Yucca Wash.

METHODS

Soil pits excavated for previous studies in Midway Valley (Wesling, 1992), Coyote Wash (Glancy, 1994), and Crater Flat were used in this study (Plate 1). The sites in Midway Valley were emphasized because they provide the best exposures of alluvium derived from the main part of Yucca Mountain. In addition, trench CF-1 in Crater Flat and site SWG-1 near Fortymile Wash were sampled to complement geochronological work (Paces co-report).

Soils were described following Birkeland (1984) and Harden (1986). Stages of carbonate and silica morphology follow Gile and others (1966) and Taylor (1986), respectively. Horizons were sampled by collection of approximately 15-20 kg of material from each horizon. The coarse fraction (>2mm) was washed and separated from the fine fraction and analyzed by dry sieving. The fine fraction was pretreated using sodium hexametaphosphate as a dispersing agent, and was analyzed for sand, silt and clay fractions by sedimentation using the hydrometer method (Black, 1965). The sand fraction was further analyzed for 5 size fractions by dry sieving. The percent mass of $CaCO_3$ in the fine fraction was determined by acid/base titration, while pH was determined on soil pastes.

RESULTS

Field soil profile descriptions by site are in Table 1; Table 2 lists laboratory data. Surficial characteristics for each site are shown in Table 3, and the vegetation observed at sites is listed in Table 4. Alluvial map units referred to in this report follow descriptions of Lundstrom and others (in press), which were based on surficial characteristics and soil morphology as observed in field only. Laboratory results presented below provide a more quantitative basis for distinguishing units and for interpretation of soil development.

In all soils, the fine fraction (<2 mm) dominated by sand generally decreases downward from the surface (Figures 1-6). At most sites, the horizon having the greatest fine fraction occurs at the surface. The fine fraction generally decreases downward until a buried soil is reached, where the fine fraction can increase relative to overlying alluvium. The fine fraction is predominated by sand (Table 3) with a nearly ubiquitous mode (peak) of fine sand (0.25-0.10 mm). On younger alluvial soils (units 5 and 6), fine sand is the only peak mode in the fine fraction, and silt is subordinate in mass. In contrast to the fine fraction of soils of younger alluvium (units 5 and 6), the size distribution of the coarse fraction is more variable over depth. (figures 7-12). The decrease in the fine fraction with depth in combination with its predominant fine sand mode are stong evidence for eolian sand deposition and mixing with coarse gravelly alluvium. The greater variability of the modality of the coarse fraction is consistent with the spatially and temporally variable energy during fluvial processes involved in the transport and deposition of alluvium. There is no covariance of the mode of the fine fraction with the more variable modality of the coarse fraction, which is evidence of differing depositional processes in the fine and coarse fractions.

In the upper part (typically less than 0.5 m depth) of soils on alluvial units older than unit 5 (on map units 1,2,and 3; figs. 10-12), there is substantially more silt and clay in the fine fraction than occurs in the upper horizons of soils of unit 5 (figs. 8 and 9). Though the fine sand peak observed in the younger soils is still present, a silt peak (0.05-.002 mm) also occurs in the fine fraction of the upper part of soils on units 3, 2 and 1 that does not occur in unit 5, as well as more clay. In the upper horizons of older soils, silt typically ranges from 15-40% of the fine fraction, and clay ranges from 8-20%, compared to values less than 15% and 8% respectively in the fine portion of unit 5 soils. The relatively high amounts of silt and clay generally correspond to Av and Bt horizons distinguished by structure, color, and consistence that were the basis for sampling (Table 1). Though Av horizons are distinctive from Bt horizons in their morphology, these associated horizons show more similarities than differences in their particle size distributions, particularly the relatively high silt and clay contents (Figs 10-12).

Distinctive carbonate morphology (Table 1)and content (Table 2) of soil horizons are associated with certain map units. The younger alluvial map units 6 and 5 in all cases observed are associated with stage I-II morphology on non-cemented Bk horizons in which thin (< 1mm) carbonate and silica coats occur on the undersides of clasts, and with a carbonate content of less than 5 percent of the fine fraction of non buried soil horizons. On intermediate-age alluvial units 3 and 4, stage II-III carbonate morphology of more cemented Bkq horizons is associated with slightly elevated maximum carbonate contents. Map unit 1 has Kqm horizons with laminar stage IV carbonate and silica morphology, typically within 30 cm of the surface and with carbonate contents of 20-40 percent of the fine fraction.

Buried soils are observed at most of the sites (figs 1-6). Horizons interpreted to be buried soils have similar characteristics to some surface soil horizons. Buried soils are recognized by changes in particle size, carbonate content, color, or other morphologic or stratigraphic indications that are not consistent with pedogenic formation in their present stratigraphic position. Examples of properties suggestive of a buried soil are increases in the fine fraction, clay or silt content, a distinctly redder color, or discontinuities in carbonate morphology and content. As shown above, these features in surface soils decrease from the surface downward, so their occurrence at depth indicate a former surface soil buried by subsequent alluvial deposition. However, soils buried by alluvial gravels are usually partially eroded because streamflow energetic enough to transport gravel before deposition is competent to erode the fine-rich upper part of a surface soil. Erosional discontinuity of sand and silt rich reddenned horizons by an overlying alluvial gravel with few fines is a typical relationship interpreted to be a buried soil. In support of this interpretation, thermoluminescence results from 5 of 5 hypothesized and sampled buried alluvial soils have yielded ages significantly older than eolian material or pedogenic material from the surface soil of alluvium that overlies the buried soil.

Surface characteristics used to distinguish and map alluvial units are strongly associated with the various stages of soil development described above (Table 3). On younger alluvial units 5 and 6, weakly developed soils are associated with depositional bar and swale microtopography muted through eolian addition, absent to weak surface rock varnish, and loose surface concentration of gravel clasts, not the well packed desert pavement seen on older units.

Soils on intermediate-age alluvium with reddenned Bt horizons are associated with moderately to well developed desert pavements and rock varnish on smooth surfaces in which bar and swale depositional morphology is absent for non- bouldery alluvium. Alluvial unit 1 with a near-surface laminar stage IV petrocalcic horizon is associated with erosional whaleback (convex rounded ridges) morphology, and a varnished desert pavement that includes and is lightened by carbonate/silica chips. There does not appear to be a strong association between the vegetation occurrence and map unit (Table 4) though grass is more abundant on soils of alluvial units 5 and 6 than on older units.

DISCUSSION

We propose a model for alluvial soil evolution (figure 13) in the Yucca Mountain area that takes into account the above soil data, field relationships observed during mapping of surficial deposits (Lundstrom and others, in press), geochronology (Paces and others, co-report,) and other paleoclimatic and stratigraphic records.

Coarse gravelly alluvium in which soils develop is deposited during rainfall events of sufficient intensity to generate runoff competent to entrain surficial material, including hillslope colluvium and pre-existing alluvium in and along channels. Because the highest precipitation events observed historically have had relatively little geomorphic impact relative to the distribution of mappable alluvial units (Lundstrom and others, in press) it is likely that episodes of alluviation relate to climates wetter than present. As discussed by Bull (1991), it is also possible that episodes of aggradation relate to climatic transitions disturbing previous equilibrium conditions of fluvial systems. Cumulatively over such episodes, areas much larger than active channels are affected. Aggradation during these alluvial episodes is indicated by the common occurrence of buried soils in natural and man-made exposures throughout the YM area. Freshly deposited alluvium is characterized by fluvial micromorphology that includes boulder and cobble bars, and relatively sparse to no vegetation.

The predominant initial modification of freshly deposited alluvial gravels is the addition, mixing, and infiltration of eolian material dominated by sand, particularly fine sand which is a ubiquitous mode in all surface soils (figures 7-12). Fine sand is the most common sand size of many sand dunes and sand seas (Ahlbrandt, 1979). Because the fine fraction dominated by sand with a persistent fine sand mode decreases downward from the surface as a component added to more variably sorted gravelly alluvium, it is apparent that translocation and mixing processes occur. One process is inferred to be downward washing of fine material through larger pores during infiltration of precipitation. Another process, bioturbation through the burrowing activities of the creatures that live in the desert, is also likely to be important to the mixing of alluvial deposits and eolian mantles. These creatures include a variety of insects, especially ants, reptiles, and mammals (MacMahon, 1985) and the abundance of their burrowing activity is readily observed on most alluvial surfaces, especially that of units 5 and 6. Eolian addition to alluvial surfaces and subsequent infiltration and mixing tend to obliterate original fluvial surface micromorphology and bedding, especially in alluvium of pebble size or smaller. However, there is also evidence that some originally deposited surface clasts remain at the surface, despite these mixing processes. Bars composed of coarse cobbles to boulders are apparent on alluvial units 5 and 6 (Table 3) in which eolian material has been mixed into the original alluvium (Figures 1,2) Another line of evidence for the persistent exposure of surface clasts is the recognition that clasts in desert pavements occuring over lava flows must have remained at the surface during the deposition, infiltration and pedogenesis of eolian material underlying the pavements (McFadden and others, 1987), which has recently been substantiated by cosmogenic dating (Wells et al, 1995) and extended to surface alluvium.

Given a lack of other sources, we consider it likely that a dominant source for eolian sand is recently deposited alluvium, especially more distal finer grained parts of alluvial systems. Average particle size typically decreases down any given alluvial system (Bull, 1991), but this trend is accentuated in influent arid fluvial systems where stream discharge and competence decrease downwash from channel losses. Downwash loss of streamflow along Fortymile Wash for historic and channel-forming discharge is due to infiltration along the channel (Savard, 1995; Osterkamp and others, 1994); this process is also implied during 17-10 ka by Claasen (1985, 1986). The Central Amargosa Desert, especially the lower southern portion of the Fortymile Wash alluvial fan is the largest area of distal alluvium and is a likely source of eolian sand following episodes of alluviation. This hypothesis is supported by the distribution of eolian sand ramps in the Yucca Mountain area (Fig. 0, Lundstrom and others, in press; Swadley, 1983) which increase from north to south and from west to east toward the lower part of the alluvial fan of Fortymile Wash, Fresh non-vegetated alluvium, especially distal sand rich portions of alluvial fans, is readily entrained by eolian processes. Rough microtopography (boulder bars, stone stripes, and lava flows) and macro topography (separation eddys at sand ramp concavity on lower slopes of bedrock highs) are favorable sites for eolian deposition. Most unit 5 and younger alluvial sand caps appear to have experienced no noticable pedogenesis between alluvial deposition and eolian sand infiltration. Episodes of eolian sand deposition may be largely controlled by sediment supply, which in this area, are coeval with or immediately follow episodes of alluviation. This hypothesis implies that themoluminescence dates on eolian silt of surficial alluvial soils may provide close minimum ages on alluvial deposition. This model also invokes significant recyling of sand from erosion of older soils to distal alluvium, which can then be blown onto surfaces subject to more erosion. However, an increase in total sand content with time is possible from erosion of bedrock uplands (especially nonresistant nonwelded bedded tuffs, comminution of clasts during weathering and transport, and regional eolian sand input and ashfalls. Net sinks for sand include deposition in an aggrading, subsiding basin, and transport out of the basin system.

We also consider as eolian the higher silt and clay content and additional silt mode of soil epipedons formed on alluvial map units 3, 2,and 1. However, the source of this greater eolian silt component is less readily apparent. These soils occur on alluvium older than that of unit 5 (which has close minimum TL ages from 7-12 ka; co-report), and their significantly different morphology, including a reddenned Bt horizon and more cemented nature, are interpreted to indicate these soils were impacted by significantly wetter climates of the late Pleistocene. The higher silt and clay content could be simply a consequence of a longer period to accumulate these fine materials which can be transported globally. However, marine (Rea, 1994) and ice core records (Patterson and Hammer, 1987; Taylor and others, 1993) show pronounced (1-2 orders of magnitude) increases in eolian dust flux in the late Pleistocene, particularly during peak glacial and during some rapidly fluctuating climatic transitions. The higher silt and clay contents of older soils could have been added to soils of late Pleistocene alluvium at higher rates than the silt and clay component of Holocene soils,and perhaps originated from more widespread sources. A plausible alternative to higher global dust flux during full glacial conditions is higher regional dust flux during wet-to-dry climatic transitions that expose lake sediments. A higher local silt flux into soils near newly exposed sediments of latest Pleistocene lakes in the Great Basin has been shown near Lake Lahontan (Chadwick and Davis, 1990; and Lake Mojave (Wells and others, 1987). Thermoluminescence dates of silt rich soil horizons provide age control on dust flux; the occurrence of 3 TL dates of 24-27 ka (Paces co- report)from reddened silt rich buried soils overlain by younger alluvium with weak soils and Holocene minimum ages is evidence of an episode of high dust flux capable of producing the silt peak observed in soils of unit 3 during or immediately preceding the last full glacial maximum.

The association of desert pavements having tightly packed clasts and smooth surfaces with the fine-rich epipedons of older alluvial soils of Yucca Mountain suggests a causal relation. McFadden and others (1987) and Wells and others (1995) show evidence that surface clasts of other similarly tightly packed pavements have remained exposed throughout eolian deposition and infiltration. Workers invoke a shrink/swell process during wetting and drying to facilitate the translocation of additional eolian material through the otherwise tightly packed pavement. If the proportion of expansive clay is insufficient in near-surface matrix, a well packed pavement is not present. Though the presence of a well-developed pavement is associated with reddened Bt horizons indicating Pleistocene alluvium for all sites of this study, a well-developed pavement is not necessarily a robust Pleistocene age indicator. Well packed desert pavements are known to occur on alluvium of Holocene age where clay and silt rich eolian dust is abundant, such as near badland exposures of marsh and playa deposits in the Las Vegas Valley. On the other hand, alluvial surfaces possessing well packed, varnished pavements such as map unit 3f forming a high terrace along Fortymile Wash with a minimum age of 40 ka (Paces co-report) grade continuously southward to surfaces near and in the Amargosa Desert where poorly developed pavements immediately overly a sand mantle lacking an Av or argillic horizon. However, Peterson and others (1995) and Faulds and others (1994) description of soil development, surface characteristics and late Pleistocene age estimates for the Black Cone unit is similar to the association of surface and soil characteristics of soils in Midway Valley of this report.

Progressive addition of clay, silt, silica and carbonate cements during repeated wet climates impedes infiltration, and enhances surface runoff and erosion, especially during intense rainfall events. With reduced infiltration and more runoff capable of rill and gully development, the stable surface of a well developed soil may begin to erode to form an eroding surface. Carbonate and silica horizons that originally developed at depth are eroded and temporarily stored as clasts incorporated in the surface pavement over a fine-rich, eolian mantle. A soil profile in dynamic equilibrium is maintained as a rounded surface lowers through erosion into succesively lower depositional layers below the original depositional top of the alluvium. The surface pavement has a lighter tone by incorporating fragments of eroded pedogenic silica originally formed in subsurface K horizons, but left as fragments at the surface during subsequent erosional periods. The silt and clay rich eolian mantle that underlies the surface pavement is interpreted as having developed subsequent to the latest erosional period at that location. This type of soil and surface morphology occurs on surface alluvial units that overlie or include the 760 ka Bishop ash, but probably not on alluvium as young as late Pleistocene. Such erosional morphology can occur on any alluvium older than that in which soil development has reached an erosional threshold, including pre-Quaternary alluvium.

An implication of this model is that one cannot use an integrated mass of pedogenic material, such as carbonate, silica, silt or clay as a means to estimate age, even if it is possible to independently determine the age of alluvial deposits in which soils have formed, particularly when the soils have reached an erosional stage.

CONCLUSIONS

1. Eolian addition is a predominant initial pedogenic modification of freshly deposited alluvium. In soils formed in Holocene and Pleistocene alluvium, the fine fraction is predominated by or includes a fine sand mode which decreases downward from the surface. This distribution of the fine fraction is interpreted to be the result of eolian addition, infiltration and pedoturbation. Little subsequent pedogenesis has been superimposed on soils formed on Holocene alluvium other than eolian addition and development of thin calcitic coats on clast undersides.

2. Stable alluvial surfaces that were exposed to climatic change during the late Pleistocene are markedly more cemented by calcite and silica. These soils include a reddenned Bt horizon characterized by higher silt and clay contents, including an additional silt mode not observed in Holocene alluvium.

3. An erosional stage of soil development can be reached in which net additions of pedogenic materials are unlikely.

4. There is a strong association between surface characteristics and soil development, which facilitates mapping and delineation of alluvial soils.

5. Buried soils, particularly those which include eolian material suitable for TL dating, can provide maximum ages on overlying alluvial units.

REFERENCES

Ahlbrandt, T.S., 1979, Textural parameters of eolian deposits IN McKee, E.D., A study of global sand seas, U.S. Geological Survey Professional Paper 1052, p. 21-51

Birkeland, P.W., 1984, Soils and Geomorphology: New York, Oxford University Press

Bull, W.B., 1991, Geomorphic responses to climatic change: New York, Oxford University Press

Buesch, D.C., Spengler, R.W., Moyer, T.C., and Geslin, J.K., in press, Revised stratigraphic nomenclature and macroscopic identification of lithostratigraphic units of the Paintbrush Group exposed at Yucca Mountain, Nevada: U.S. Geological Survey Open-File Report 94-469.

Chadwick, O.A., and Davis, J.O., 1990, Soil-forming intervals caused by eolian sediment pulses in the Lahontan basin, northwestern Nevada: Geology, v. 18, p. 243-246

Christiansen, R.L., and Lipman, P.W., 1965, Geologic map of the Topopah Spring NW Quadrangle, Nye, County, Nevada: U.S. Geological Survey Geologic Quadrangle Map GQ-444, scale 1:24,000.

Claassen, H.C., 1985, Sources and mechanisms of recharge for ground water in the west-central Amargosa Desert, Nevada - a geochemical interpretation: U.S. Geological Survey Professional Paper 712-F, 31 p.

Claassen, H.C., 1986, Late-Wisconsin paleohydrology of the west-central Amargosa Desert, Nevada, U.S.A.: Chemical Geology, v. 58, p. 311-323

Faulds, J.E., Bell, J.W., Feuerbach, D.L., and Ramelli, A.R., 1994, Geologic Map of the Crater Flat area, Nevada: Nevada Bureau of Mines and Geology Map 101

Gile, L.H., Peterson, F.F., and Grossman, R.B., 1966, Morphological and genetic sequences of carbonate accumulation in desert soils: Soil Science, v. 101, p. 347-360.

Glancy, P.A., 1994, Evidence of prehistoric flooding and the potential for future extreme flooding at Coyote Wash, Yucca Mountain, Nye County, Nevada: U.S. Geological Survey Open-File Report 92-458

Harden, J., 1986, Field Methods, IN Singer, M.J., and Janitzky, editors, Field and laboratory procedures used in a soil chronosequence study: U.S. Geological Survey Bulletin 1648

Harden, J.W., Taylor, E.M., Hill, C., Mark, R.K., McFadden, L.D., Reheis, M.C., Sowers, J.M., and Wells, S.G., 1991, Rates of soil development from four soil chronosequences in the southern Great Basin: Quaternary Research, V. 35, p. 383-399

Harden, J.W., Taylor, E.M., Reheis, M.C. McFadden, L.D., 1991, Calcic, gypsic, and siliceous soil chronosequences in arid and semiarid environments, in Occurrence, Characteristics and genesis of Carbonate, gypsum, and silica accumulations in Soils: Soil Science Society of America Special Publication n. 26, p. 1-16

Lundstrom, S.C., Wesling, J.R., Taylor, E.M., and Paces, J.B., in press, Preliminary Surficial Deposits Map of the Northeast 1/4 of the Busted Butte 7.5-minute Quadrangle: United States Geological Survey Open-File Report 94-341, scale 1:12,000.

Lundstrom, S.C., Mahan, S.A. and Paces, J.B., in press, Preliminary Surficial Deposits Map of the Northwest 1/4 of the Busted Butte 7.5-minute Quadrangle: United States Geological Survey Open-File Report 95-133, scale 1:12,000.

Lundstrom, S.C., and Taylor, E.M., in press, Preliminary Surficial Deposits Map of the Southern Half of the Topopah Spring NW 7.5-minute Quadrangle: United States Geological Survey Open- File Report 95-132, scale 1:12,000.

Lundstrom, S.C., Whitney, J.W., Paces, J.B., Mahan. S.A., and Ludwig, K.R., in press, Preliminary Surficial Deposits Map of the southern half of the Busted Butte 7.5-minute Quadrangle: United States Geological Survey Open-File Report 95-311, scale 1:12,000.

McFadden, L.D., Wells, S.G., and Jercinovich, M.J., 1987, Influence of eolian and pedogenic processes on the origin and evolution of desert pavements: Geology, v. 15, p. 504-508

Osterkamp, W.R., Lane, L.J., and Savard, C.S., 1994, Recharge estimates using a geomorphic/distributed-parameter simulation approach, Amargosa River Basin: Water Resources Bulletin, v. 30, p. 493-507

Paces, J.B., Menges, C.M., Widmann, B., Wesling, J.R., Bush, C.A., Futa, K., Millard, H.T., Maat, P.B., Whitney, J.W., 1994, Preliminary U-series disequilibrium and thermoluminescence ages of surficial deposits and paleosols associated with Quaternary faults, eastern Yucca Mountain, Proceedings of the Fifth International Conference on High Level Radioactive Waste Management, p. 2391-2401.

Paterson, W.S.B., 1987, Ice core and other glaciological data IN Ruddiman, W.F., and Wright, H.E., Jr., North America and adjacent oceans during the last deglaciation: Geological Society of America DNAG volume K-3, p. 91-111

Peterson, F.F., Bell, J.W., Dorn, R.I., Ramelli, A.R., and Ku, T.L., 1995, Late Quaternary geomorphology and soils in Crater Flat, Yucca Mountain area, southern Nevada: Geological Society of America Bulletin, v. 107,p. 379-395

Quade, J., and Cerling, T.E., 1990, Stable isotopic evidence for a pedogenic origin of carbonates in trench 14 near Yucca Mountain, Nevada: Science, v. 250, p. 1549-1552

Rea, D.K., 1994, The paleoclimatic record provided by eolian deposition in the deep sea: the geologic history of wind: Reviews of Geophysics, v. 32, p. 159-195

Rosholt, J.N., Bush, C.A., Carr, W.J., Hoover, D.L., Swadley, WC, and Dooley, J.R., 1985, Uranium-trend dating of Quaternary deposits in the Nevada Test Site are, Nevada and California: U.S. Geological Survey Open-file Report 85-540

Savard, C.S., 1995, Selected hydrologic data from Fortymile Wash in the Yucca Mountain area, Nevada, Water Year 1992: U.S. Geological Survey Open-File Report 94-317

Scott, R.B., and Bonk, Jerry, 1984, Preliminary geologic map of Yucca Mountain with geologic sections, U.S. Geological Survey Open-File Report 84-494: scale 1:12,000.

Swadley, WC, 1983, Map showing surficial geology of the Lathrop Wells Quadrangle, Nye County, Nevada: U.S. Geological Survey mpa I-1361

Taylor, E.M., 1986, Impact of time and climate on Quaternary soils in the Yucca Mountain Area of the Nevada Test Site, Boulder, University of Colorado, M.S. thesis, 217 p.

Taylor, E.M., and Huckins, H.E., 1995, Lithology, fault displacement, and origin of secondary calcium carbonate and opaline silica at Trenches 14 and 14D on the Bow Ridge Fault at Exile Hill, Nye, County, Nevada: U.S. Geological Survey Open-File Report 93-477

Taylor, K.C., Lamorey, G.W., Doyle, G.A., Alley, R.B., Grootes, P.M., Mayewski, P.A., White, J.W.C., and Barlow, L.K., 1993, The flickering switch of late Pleistocene climatic change: Nature, v. 361, p. 432-436

Vaniman, D.T., 1994, Pedogenesis of siliceous calcretes at Yucca Mountain, Nevada: Geoderma, v. 63, p. 1-17

Wesling, J.R., Bullard, T.F., Swan, F.H., Perman, R.C., Angell, M.M., Gibson, J.D., 1992, Preliminary mapping of surficial geology of Midway Valley, Yucca Mountain Project, Nye County, Nevada: Sandia Report Sand91-0607, scale 1:6000, 55 p.

Wells, S.G., McFadden, L.D., and Dohrenwend, J.C., 1987, Influence of late Quaternary climatic changes on geomorphic and pedogenic processes on a desert piedmont, Eastern Mojave Desert, California: Quaternary Research, v. 27, p. 130-146

Wells, S.G., McFadden, L.D., Poths, J., and Olinger, C.T., 1995, Cosmogenic He surface-exposure dating of stone pavements: implications for landscape evolution in deserts: Geology, v. 23, p. 613-616

PLATE CAPTIONS

Plate 1 Compiled map of surficial deposits with site locations

FIGURE CAPTIONS

Figure 1. Soil sites on map unit 6. Fine fraction (<2mm) is portion of whole soil sample, whereas silt, clay and $CaCO_3$ components are portions of fine fraction. In MWV-P14, note horizon 2CBk, an eolian unit from which TL-41 was collected, underlying gravel of unit 6. In NCW-TX1, TL-52 was collected from infiltrated eolian cap in surface alluvial unit 6, whereas TL-50 was collected from buried soil underlying alluvial unit 6

Figure 2. Soil sites on map unit 5. Fine fraction (<2mm) is portion of whole soil sample, whereas silt, clay and $CaCO_3$ components are portions of fine fraction. In MWV-P10, TL-42 was collected from infiltrated eolian cap in surface alluvial unit 5, whereas TL-48 was collected from buried soil underlying alluvial unit 5. In NCW-TT1, TL-51 was collected from infiltrated eolian unit within sieve deposit spanned by upper four soil horizons.

Figure 3. Soil sites on map unit 4. Fine fraction (<2mm) is portion of whole soil sample, whereas silt, clay and $CaCO_3$ components are portions of fine fraction. In MWV-P6 horizon 3Kqb represents shallowly buried unit 1.

Figure 4a,b,c. Soil sites on map unit 3 and 3f. Fine fraction (<2mm) is portion of whole soil sample, whereas silt, clay and $CaCO_3$ components are portions of fine fraction. In Fig. 4c, at site SWG-1, TL-47 was collected from buried soil in horizon 2Btjb.

Figure 5. Soil sites on map unit 2. Fine fraction (<2mm) is portion of whole soil sample, whereas silt, clay and $CaCO_3$ components are portions of fine fraction.

Figure 6. Soil sites on map unit 1. Fine fraction (<2mm) is portion of whole soil sample, whereas silt, clay and $CaCO_3$ components are portions of fine fraction.

Figure 7. Histograms of particle size distribution of horizons in MWV-P14, unit 6. Note ubiquitous mode of fine sand (0.25-0.10 mm) which decreases with depth, with higher variability in coarse fraction (>2mm)

Figure 8. Histograms of particle size distribution of horizons in MWV-P7, unit 5. Note ubiquitous mode of fine sand (0.25-0.10 mm) which decreases with depth, with higher variability in coarse fraction (>2mm)

Figure 9. Histograms of particle size distribution of selected horizons in MWV-P20, unit 4. Note ubiquitous mode of fine sand (0.25-0.10 mm) which decreases with depth, with higher variability in coarse fraction (>2mm)

Figure 10. Histograms of particle size distribution of horizons in MWV-P8, unit 3. Note bimodality of fine fraction which decreases with depth, one mode of fine sand (0.25-0.10 mm), and additional mode of silt (0.053-.002mm), with clay values above 10 % in the top 3 horizons. Also note higher variability in coarse fraction (>2mm)

Figure 11. Histograms of particle size distribution of horizons in MWV-P28, unit 2. Note bimodality of fine fraction which decreases with depth, one mode of fine sand (0.25-0.10 mm), and additional mode of silt (0.053-.002mm). Also note higher variability in coarse fraction (>2mm)

Figure 12. Histograms of particle size distribution of horizons in MWV-P25, unit 1. Note bimodality of fine fraction which decreases with depth, one mode of fine sand (0.25-0.10 mm), and additional mode of silt (0.053-.002mm). Also note higher variability in coarse fraction (>2mm)

Figure 13. Proposed conceptual model of alluvial soil evolution with stages in evolution corresponding to map units and age increasing from bottom to top. See discussion section of text.

Table 1: Soil Field Descriptions

Horizon	Top	Bot.	Dry Color	Texture	Structure	Consistence Wet	Consistence Dry	Clayfilms	CaCO3	HCl Rxn	Boundary
MWV-P5 Unit 3											
Avk	0	8	10YR 7/3	sicl	3vc pl	ss-s, p	sh	N.O.	N.O.	ve	as
Bwk	8	15	10YR 6/3	l	2f-m sbk	ss, ps	so	N.O.	I	es	cs
Bwk2	15	28	10YR 6/3	fsl	1f sbk	ss, ps	so	N.O.	I	es	aw
2Bwkb	28	40	10YR 6/4	fsl	1-2f c	ss, ps	sh	1n co	I-	es	as
3Btkqmb2	40	80	10YR 7/6	sl	3m-c pl	so, po	vh	3mk pf	I+	ve	cs
					2- 1c abk						
3Btkqm2b2	80	99	10YR 7/6	sl	1m-c pl	so, po	vh	vln pf	I+	ve	cw
3Bkqb2	99	128	10YR 4/4	sl	m	so, po	h	N.O.	I	ve	as
4Bkqb3	128	168	10YR 8/4	ls	1m sbk	sh, h	so, po	N.O.	II-III+	ev	cw
4Bkq2b3	168	20	10YR 2/3	s	m	so, po	lo	N.O.	I	ev	cs
4BCkqb3	200	235	10YR 8/4	m-cs	sg	so, po	lo-so	N.O.	I-	es	cs
5Bkqb4	235	268+	10YR 7/4	ls	m 1fm gr	so, po	so	N.O.	I+	es	--
MWV-P6 Unit 4											
Avk	0	6	10YR 7/3	l	3m-c pl	ss, ps	so	N.O.	N.O.	es	cs
2Btjkq	6	10	10YR 7/3	l	3f sbk	ss, ps-p	sh	1n pf	N.O.	es	cs
2Btkq	10	20	7.5YR 7/4	cl	2m sbk	ss-s, p	so-sh	1n pf	I	es	cs
								2-1n po			
2Btjkq	20	28	7.5YR 7/4	l	1m sbk	ss, ps	so	v1n pf, po	I	es	cs
2Btjkq2	28	37	7.5YR 6/6	sl	2f-m sbk	ss, ps	so	v1n pf	I	es	aw
3Kqb	37	90	10YR 8/3	sl	v1m pl	so, po	vh	N.O.	III+IV	ev	gs
3Bkqb	90	120	10YR 8/3	cls	sg	so, po	lo	N.O.	II+	ev	gw
3Bkq2b	120	138	10YR 7/2	cs	sg	so, po	lo	N.O.	II	ev	cw
3BCkqb	185	205	10YR 7/3	cls	sg	so, po	lo	N.O.	I	es	aw
4Bkqb2	205	235	7.5YR 7/4	ls	1m-c sbk	so, po	sh	N.O.	I+	ve	cb
4Bkq2b2	235	275	10YR 7/3	ls	sg	so, po	lo	N.O.	I+	ev	cw
4CBkqb2	27	285+	10YR 7/4	cs	sg	so	lo	N.O.	I+	ve	--
MWV-P7 Unit 5											
A	0	5	10YR 5/3	fsl	1f gr	so, ps-p	lo-so	N.O.	N.O.	eo	as
Bw	5	20	10YR 6/3	sl	1f sbk	so, ps	so	N.O.	N.O.	eo	cw
Bwk	20	33	10YR 6/3	ls	1f sbk	so, ps	so	N.O.	N.O.	vve	cw
Bwk2	33	49	10YR 6/3	fsl	1f gr	so, ps	lo-so	N.O.	I	es	gs
Bk	49	112	10YR 6.5/3	fsl	sg	so, ps	lo	N.O.	I+	es-ev	aw
2Bkqb	112	154	10YR 6/3	mls	2m sbk	so, po	h	1n pf	I	es	cs
2Bkq2b	154	192	10YR 6/4	fls	m	so, vps	h	N.O.	I-	ve	cw
2Bkqb	192	218	10YR 7/4	ls	sg	so, po	lo	N.O.	I	e-es	cw
2Cqb	218	237	10YR 7/4	mls	sg	so, po	lo	N.O.	N.O.	eo	aw
3Bkqb2	237	307	10YR 7/3	m-cls	m	so, po	h	N.O.	I+	ev	aw
4Bkqb3	307	332+	10YR 7/3	ls	m	so, po	h	N.O.	I-	ev	--
MWV-P8 Unit 3											
Av	0	10	10YR 6/3	sl	1f pl	so, ps	so	N.O.	N.O.		cs
BAtj	10	22	10YR 7/3	scl	2m sbk	ss, p	so	1n co	N.O.		gs
					2f gr			N.O.	N.O.		
Bt	22	40	7.5YR 6/4	scl	3 f-m abk	s, p	h	-3mk-k pf b	N.O.		gs
Btqk	40	64	7.5YR 6/4	scl	1-2f abk	s, p	sh	-3 n-mk pf c	N.O.		gs
BCkq	64	95	10YR 8/1	s	1f-m sbk	so, po	lo	N.O.	II-III		ds
CBkq	95	145	10YR 7/3	s	sg	so, po	lo	N.O.	I-II		dw
Ck	145	200	10YR 7/3	s	sg	so, po	lo	N.O.	I-II		ci
2Btjkqb	200	220	10YR 7/3	s	m	so, po	sh	1n co	II-III		gs
2CBkb	220	300+	10YR 7/3	s	sg	so, po	lo	N.O.	I-II		--

Table 1: Soil Field Descriptions

Horizon	Top	Bot.	Dry Color	Texture	Structure	Consistence Wet	Consistence Dry	Clayfilms	CaCO3	HCl Rxn	Boundary
MWV-P9 Unit 3											
Av	0	5	10YR 7/3	l-sl	1m pl	ss, ps	sh	N.O.	N.O.	eo-ve	cs
Bt	5	35	7.5YR 5/4	scl-l	2-3m abk	s, p	h	2mk pf, po	N.O.	eo	gwb
2Bt	35	60	7.5YR 6/4	sl-l	2f-m abk	ss, ps	h	2mk pf, po	N.O.	eo-ve	gw
3Btkq	60	87	7.5YR 7/4	ls	1f-m bk	so, po	sh	2n pf, co	I-II	e	gs
3Bkq	87	110	7.5YR 6/6	s	m-sg	so, po	h	N.O.	II+	e-es	cw
4Bkq	110	220	10YR 6/3	s	sg	so, po	lo	N.O.	II	es	gw
5Kq	220	255	7.5YR 7/2	s	m	so, po	h	N.O.	III-	ev	cb
6BCkq	255	330	10YR 7/3	s	sg	so, po	lo-so	N.O.	II-	e-es	aw
7Bkqb	330	360+	7.5YR 7/3	s	m1m sbk	so, po	so-sh	N.O.	II-	e-es	--
MWV-P10 Unit 5											
A	0	5	10YR 5/4	s-ls	sg to 1 f gr	so, po	lo-so	N.O.	N.O.	eo	as
Bw	5	35	10YR 5/4	sl	1f-m sbk-sg	so, po	so	N.O.	N.O.	eo	cs
Bwk	35	68	10YR 6/4	ls-sl	1f-m sbk	so, po	so	N.O.	I	es	cs
2BCk	68	110	10YR 6/4	s-ls	sg	so, po	lo	N.O.	I	es	acw
2CBk	110	138	10YR 6/4	s-ls-sl	sg	so, po	lo	N.O.	I	es	cb
3Btkqb	138	192	7.5YR 5/6	sl	2-3f-m abk	ss, ps	sh-h	n pf	I-II	es	cw
3Bkqb	192	210	10YR 5/4	ls	1 f sbk to sg	so, po	lo	N.O.	I	ve	cw
3CBkb	210	300	10YR 5/4	s-ls	sg to 1-2f sb	so, po	lo	N.O.	I	e	--
MWV-P13 Unit 1											
Avk	0	8	10YR 7/3	l	3c pl	ss, p	so-sh	N.O.	N.O.	es	as
Btkq	8	22	7.5YR 5/8	cl	2m sbk	ss, p	sh	3nmk pf 3n po	I	eo-ve	aw
2Kqb	22	51	10YR 8/3	ls	m	so, po	h	N.O.	III	ev	cs
2Bkqb	51	75	7.5YR 8/2	ls	1f-m pl	so, po	h	N.O.	II+	ev	cw
2Bkq2b	75	103	10YR 8/2	ls	sg	so, po	lo	N.O.	I+	ev	cw
2BCkqb	103	130	10YR 7/3	cs	sg	so, po	lo	N.O.	I	ev	aw
3Bkqb2	230	230	7.5YR 7/4	cs	1m pl 1f abk	so, po	vh	N.O.	I+	ev	gw
3Bkq2b2	230	260	10YR 8/4	m-cs	m	so, po	h	N.O.	N.O.	ev	cw
3Bqb2	260	314+	10YR 6/6	m-cs	m	so, po	h	N.O.	I	ve	--
MWV-P14 Unit 6											
A	0	7	10YR 6/4	ls	1f pl/sg	so, po	so	N.O.	N.O.	eo	as
Bw	7	23	10YR 4/4	ls	1-2m sbk	so, po	so	N.O.	N.O.	eo	cs
CBk	23	48	10YR 7/3	s	2f abk 1vf-f gr	so, po	sh	v1 b co	II	es	as
2CBk	48	82	10YR 6/3	sl	sg	so, po	so	N.O.	I-II	es	sg
3CBk1	82	115	10YR 7/3	s	sg	so, po	lo	N.O.	I-II	e	cs
3CBk2	115	140	10YR 7/3		sg	so, po	lo	N.O.	I-II	eo	w
4Btkqb1	140	185	8.5YR 7/4	ls	m1-2f abk	so, po	h	2n pf	I-II	eo-es	cw
5Btqb2	185	200	7.5YR 6/4	scl-sl	2-3m-c abk	so, po	h	2-3 mk-k pf	N.O.	eo-ve	--

Table 1: Soil Field Descriptions

Horizon	Top	Bot.	Dry Color	Texture	Structure	Consistence Wet	Consistence Dry	Clayfilms	CaCO3	HCl Rxn	Boundary
MWV-P15 Unit 3											
Avk	0	7	10YR 6/3	l	3c-vc pl	ss, ps-p	so	N.O.	N.O.	ev	as
BAtvk	7	11	10YR 7/4	–	1c pl 2m sbk	ss-s, p	sh	3n-mk pf	N.O.	ve	cs
Btk	11	19	10YR 7/3	scl	2m sbk	ss, p	sh	3n-mk pf, po	N.O.	e	cs
2Btkq	19	30	10YR 7/4	scl	2m skb	ss, p	sh	1n pf	I	es	aw
3Btkqb	30	44	10YR 6/4	scl	2f-m sbk	ss,p	sh	1n-mk pf 1n-mk co	I	ve	aw
4Bkqb2	44	80	7.5YR 7/4	mls	1-2m sbk	so, po	h	1n pf	II+	ev	gs
4Bkq2b2	80	125	10YR 7/4	cs	sg-1f sbk	so, po	lo	1n pf	I+	es	cw
4Bkq3b2	125	148	10YR 7/4	cs	sg	so, po	–	N.O.	I+	ve	cw
4BCkqb2	148	190	10YR 6/3	cs	sg	so, po	lo	N.O.	I+	ev	aw
5Bkqb3	190	245	10YR 7/2	cls	m	so, po	lo	N.O.	II+	ev	cs
5Bkq2b3	245	286+	10YR 7/3	ms	m	so, po	lo	N.O.	I+	ev	–
MWV-P20 Unit 4											
Avj	0-4	4	10YR 6/3	ls	sg, 1f pl	ss, po	lo-so	N.O.	N.O.	eo	as
ABvk	4	23	10YR 7/3	sl	m-1m sbk 1m pl	so-sh	ss, po –	N.O.	I+	e-es	cs
2Bwk	23	42	7.5YR 6/4	sl-l	1vf-m abk	ss, ps	so	v1n co	I-	ve	gs
2Btkq	42	85	7.5YR 6/5	sl-l	2f abk	ss, ps	sh-h	2n pf, po, co	I+	es	gss
2Btkq2	85	133	7.5YR 6/4	ls	m, sg 1f abk	so, po	h	ln co	II	es	cw
3Bkq	133	178	10YR 7/4	s	sg	so, po	so	N.O.	I-II	es	cw
4Bkqy	178	203	10YR 7/3	s	sg	so, po	lo	N.O.	II	es	cl
5Btkqb	203	225	10YR 6/4	ls	1m sbk	so, po	so-h	2n co	II-	eo	cw
6Bckqb	225	320+	10YR 7/2	s	sg	so, po	lo	N.O.	I	ev	–
MWV-P21 Unit 5											
A	0	7	10YR 5/3	ls	1f sbk	so, po	so	N.O.	N.O.	eo	as
Bw	7	23	10YR 6/3	ls	1-2 m, sbk	so, po	so	N.O.	N.O.	eo	cs
CBk	23	48	10YR 7/3	s	2f, abk	so, po	sh	v1n co	II	es	as
2CBk	48	82	10YR 6/30	sl	sg	so, po	so	N.O.	I-II	es	gs
3CBk	82	115	10YR 7/3	s	sg	so, po	lo	N.O.	I-II	e	cs
3CBk2	115	140	10YR 7/4		sg	so, po	lo	N.O.	I-II	eo	w
4Btkqb1	140	185	8.5YR 7/4	s-ls	m1-2f, abk	so, po	h	2n pf co	I-II	eo-e	cw
5Btqb2	185	200+	7.5TR 6/4	scl-sl	2-3m-c abk	ss, po	h	-3mk-k, pf b	N.O.	eo-ve	–
MWV-P22 Unit 3											
Avk	0	10	10YR 6/2	l	3vc pl	ss, vps	sh	N.O.	N.O.	es	aw
2Btjk	10	32	10YR 7/2	scl	2f-m sbk	ss, ps-p	so	v1n pf, co	N.O.	ve-e	aw
2Btkq	32	63	10YR 7/6	mls	3-fm sbk	so, po	h-vh	1npf 2n*mk po	I	ve	cw
2Bkq	63	80	10YR 6/4	m*cls*	1-2f sbk	so, po	sh-h sl	N.O.	I+*II	es-ev	cw
2Bkq2	80	130	10YR 7/4	mc/ss	m	so, po	sh-h	N.O.	I-	ve	cw
2Ckq	130	260+	10YR 7/3	cs	sg	so, po	lo	N.O.	N.O.	eo	–
MWV-P23 Unit 1											
Avk	0	10	10YR 7/3	sicl	2-3m-c pl	ss-s, ps	sh-h	N.O.	N.O.	ve-e	as
2Btkq	10	30	10YR 6/4	sl	2f-m sbk	ss, ps	so-sh	2npf, 2npo	I	e	aw
2Btkqm	30	68	10YR 7/6	cls	1cpl	so, po	h	2npf	I	ve	cw
2kqm	68	135	10YR 7/3	cls	m	so, po	sh-h	N.O.	III+	ev	cw
2Kq	135	175	10YR 8/2	cs	m	so, po	sh	N.O.	III	ev	cw
Bkq	175	195	10YR 8/2	cs	m	so, po	sh-h	N.O.	II+	e-es	aw
2Ck	195	300+	10YR 7/2	cs	sg	so, po	lo	N.O.	I-	e	[illegible]

Table 1: Soil Field Descriptions

Horizon	Top	Bot.	Dry Color	Texture	Structure	Consistence Wet	Consistence Dry	Clayfilms	CaCO3	HCl Rxn	Boundary
MWV-P24 Unit 3											
Av(k?)	0	8	10YR 7/3	fscl	3vc pl	s, p	sh	N.O.	N.O.	e	as
Btk	8	25	10YR 6/3.5	fscl	2f-m sbk	s, p	so-sh	1n pf	N.O.	ve	aw
								1n po			
2Btkq	25	48	7.5YR 6/4	mscl	3f sbk	s-s, ps-	vh	2n-mk pf	I	e	cw
2Btkq2	48	83	7.5YR 6/6	csl	1f-m pl	ss, ps	vh-eh	-3n-mk pf,p	I	e-es	acw
								3n co			
2Bkq1	83	132	10YR 7/4	ls	m	so, po	h	N.O.	II	ev	cw
2Bkq2	132	197	10YR 7/3	cs	sg	so, po	lo-so	N.O.	I	es	gs
2Cq	197	247	10YR 7/4	cs	sg	so, po	lo	N.O.	N.O.	eo	vaw
3Bkqb	247	287+	10YR 8/4	cs	1m pl	so, po	vh	N.O.	II	ev	–
MWV-P25 Unit 1											
Avk	0	10	10YR 7/3	fscl	2c pl	s, p	sh	N.O.	N.O.	ve	as
2Btkj	10	32	7.5YR 6/4	fscl	1f-m gr	ss, p	so	v1n pf	I-	ve	ci
3Bkq	32	50	7.5YR 8/2	cls	1f-m pl	so, po	vh	N.O.	II-III	es	ab
3Kqym	50	65	7.5YR 8/2	sl	m, 1c pl	so, po	eh	N.O.	IV	ev	cw
3Kqy	65	100	10YR 8/3	cls	m	so, po	h	N.O.	IV	ev	as
3Bkq1	100	136	10YR 8/2	cs	sg	so, po	lo	N.O.	II+ -III	ev	cw
3Bkq2	136	198	10YR 7/2	cs	sg	so, po	lo	N.O.	I-II+	ev	aw
4Bkq	198	245	7.5YR 8/6	cs	m-sg	so, po	sh	N.O.	I+ -II	ev	cw
4Ckq1	245	290	7.5YR 7/4	cs	m	so, po	so	N.O.	N.O.	ve	cw
4Ckq2	290	320+	10YR 8/3	cs	m	so, po	lo	N.O.	N.O.	ve	–
MWV-P26 Unit 2											
Avkq	0	7	10YR 7/3	fscl	3c pl	ss, p	sh	N.O.	N.O.	ve-e	as
Bw	7	18	7.5YR 7/4	fscl	2f-m gr	ss-s, p	so	N.O.	N.O.	eo	cw
2Btjq	18	33	5YR 7/4	l	2f-m gr	ss, p	sh	v1n pf	N.O.	eo	as
2Avkqmb	33	45	7.5YR 6/4	sl-l	3c pl	so, po	vh	N.O.	I	e	as
2Bwkqmb											
2Btkqb	45	53	7.5YR 7/4	scl	3f abk	ss, p	h	2n pf	I+	e-es	aw
2Btqb	53	83	5YR 7/6	scl	3f-m gr	s, p	sh	3n-mk pf	N.O.	eo-ve	a-cw
3Kqymb	83	123	10YR 8/3	cls	m	so, po	vh	N.O.	III+	es	cw
3Bkqyb	123	147	7.5YR 7/4	ls	sg	so, po	sh	N.O.	I+ -II	es	cw
3BCkqb	147	195	7.5YR 6/4	ls	sg, m	so, po	lo	N.O.	I-	e	cw
3Ckqb	195	270+	10YR 7/3	cs	sg	so, po	lo	N.O.	N.O.	ve	–
MWV-P28 Unit 2											
Avk	0	8	10YR 7/3	cl-l	3c pl	ss, p	sh	N.O.	N.O.	e	aw
BAtq	8	13	10YR 6/3	cl	1f pl	ss-s, p	sh	2n-mk pf	N.O.	eo-ve	cs
								2n-mk po			
Btq	13	26	7.5YR 6/4	scl	3f-m abk	s, p	h	3mk pf	I	eo	cs
								3mk po			
2Btkq	26	43	10YR 6/4	scl	3f-m abk	ss-s, p	h	3n-mk pf	I	ve-e	gs
					v1f pl			3n-mk po			
2Btkq2	43	66	7.5YR 7/6	sic	1-2m pl	s, p	h	3n-mk pf	I	ev	cs
					3f abk			3mk po			
3Btkqb	66	91	7.5YR 7/4	scl	1m pl	ss-s, ps	sh	2n pf	II	ev	aw
					2f-m sbk						
3BKqmb	91	130	10YR 8/4	ls	2m pl	so, po	vh	N.O.	III+	es	cw
3Bkqb	130	182	10YR 8/3	ls	1m pl	so, po	h	N.O.	II+	ev	cs
3BCkqb	182	208	10YR 7/3	ms	sg	lo	so, po	l	N.O.	es	aw
3Ckqb	208	246	10YR 7/3	ms	sg	so, po	lo	N.O.	I-	eo-ve	aw
4Bqb2	246	287	7.5YR 7/6	f-mls	2f abk	so, po	h	v1n pf	N.O.	eo	gs
4Bkqb2	287	340+	10YR 8/3	fls	m	so, po	h	N.O.	II	ev	–

Table 1: Soil Field Descriptions

NCW-TT1 Unit 5

Horizon	Top	Bot.	Dry Color	Texture	Structure	Consistence Wet	Consistence Dry	Clayfilms	CaCO3	HCl Rxn	Boundary
A	0	5	10YR 4/3	s-ls	1vf gr	so, po	so	N.O.	N.O.	eo	as
Bw	5	40	10YR 6/3	ls	sg	so,po	lo	N.O.	N.O.	eo	gs
BCk1	40	75	10YR 6/3	ls	sg	ss,ps	lo	N.O.	I	ve-e	ds
BCk2	75	115	10YR 5/3	s-ls	sg	ss, ps	lo	N.O.	I	e	cs
2CBk	115	140	10YR 5/3	s	sg	so, po	lo	N.O.	I	eo-ve	as
3CBk	140	170+	10YR 6/3	s	sg	so, po	lo	N.O.	I	e	–

NCW-TX1 Unit 5

Horizon	Top	Bot.	Dry Color	Texture	Structure	Consistence Wet	Consistence Dry	Clayfilms	CaCO3	HCl Rxn	Boundary
AO	0	5	10YR 3-4/2	ls	1f gr-sbk	so, po	so	N.O.	N.O.	eo-ve	cw
Bwk	5	30	10YR 5/3	s-ls	1m sbk	so, po	lo-so	N.O.	I	eo-ve	cgs
BCk	30	70	10YR 6/3	s-ls	2f sbk-abk	so, po	so	N.O.	I-II	e	cs
Ck	70	100	10YR 6/3	s	sg	so, po	lo	N.O.	I	es-ev	cw
2Btkqb	100	120	8-9TY 6/4	scl-sl	3m abk	so-ss, p	h-vh	2-3 n br-co	I	ve-e	cs
2Btkq2b	120	145	7.5YR 7/4	scl-sl	f-m sbk-abk	ss	h-vh	1n pf	I	ve-e	cs
2BCkqb	145	175	10YR 6/4	ls	sg	so, po	lo	N.O.	I	ve-e	cwb
3Btqb2	175	200	7.5YR 6/4	ls	3m sbk-abk	so, po	vh	1-2 n br-co	N.O.	eo	–

SWG-1 Unit 3f

Horizon	Top	Bot.	Dry Color	Texture	Structure	Consistence Wet	Consistence Dry	Clayfilms	CaCO3	HCl Rxn	Boundary
Bkq	50	100		s	m1c pl	so, po	h	1n co	II-III		cgs
K	100	280		s	sg	so, po	lo-so	N.O.	I-II		asw
2Btjb	280	340	7.5YR?	ls	m1c, sbk	so, po	sh	1n br co	I		gs
2Kqb	340	400		s	m	so, po	sh	1n co	N.O.		dw
3Bkqmb	400	500		s	m	so, po	h-vh	N.O.	II-III		gs
3CBkb	500	610+		s	sg	so, po	sh-h	N.O.	I-II		–

CFI-SPI Unit 1

Horizon	Top	Bot.	Dry Color	Texture	Structure	Consistence Wet	Consistence Dry	Clayfilms	CaCO3	HCl Rxn	Boundary
Avk	0	14	10YR 7/3	sil	2 vf-m sbk	so, po	so	N.O.	N/A	es	as
Bk	14	17	10YR 7/3	sil	1vf-f sbk	so, ps	sh	N.O.	I-II	em	aw
2kqmb1	17	34	10YR 8/1	N/A	m-1f pl	N/A	eh	N.O.	IV	es-ev	cw
3Kqmb1	34	65	10YR 8/1	N/A	m	N/A	eh	N.O.	III+	ev	ci
4Bkb1	65	130	10YR 8/1	N/A	sg-1f-m abk	N/A	lo-vh	N.O.	I-III	eo-es	cgw
5Bkb1	130	167	10YR 8/1	N/A	sg	N/A	lo-sh	N.O.	I-II	es	ci
6Bkb2	167	283+	10YR 7/2	sl	1 vf-c abk	so, po	h	N.O.	II-III	ev	–

CFI-SPII Unit 1

Horizon	Top	Bot.	Dry Color	Texture	Structure	Consistence Wet	Consistence Dry	Clayfilms	CaCO3	HCl Rxn	Boundary
Av	0	10	10YR 6/3	sil	1vf-m sbk	so, po	so	N.O.	N/A	eo-ve	cs
Bk1	10	26	10YR 7/3	sil	1-2f-vc bk	so, po	so-sh	N.O.	I-II	es	cw
Bk2	26	35	10YR 7/3	sil	2f-m sbk	so, po	vh	N.O.	II	es	aw
2Kqmb1	35	110	10YR 8/1	N/A	m1 f-c sbk	N/A	eh	N.O.	IV	es-ev	cgw
3Bkqmb2	110	150	10YR 8/1	N/A	1vf-c sbk	so, po	sh-vh	N.O.	II-III	em-es	cgw
4Bkb2	150	210	10YR 7/3	sl	sg	so, po	lo	N.O.	I-III-	em-es	
5Bkb3	210	260	10YR 8/1	sls	m1m abk	so, po	h-vh	N.O.	III		cw
6Bkb3	260	270+	10YR 7/3	s	sg	so, po	lo	N.O.	I-II		–

Key to Table 1: Soil Field Descriptions

Master horizons:

A - a surface horizon characterized by the accumulation of organic matter and typically as a zone of elluviation of clay, sesquioxides, silica, gypsum, and/or salts.

B - a subsurface horizon characterized as having a redder color, stronger structure development, and/or accumulation of secondary illuvial materials, such as clay, sesquioxide, silica, gypsum, and salts.

K - a subsurface horizon engulfed with carbonate to the extent that the morphology of the horizon is determined by the carbonate.

C - a subsurface horizon that may appear similar or dissimilar to the parent material and includes unaltered material and material in various stages of weathering. Modifiers of master horizons:

b - buried soil horizon
k - accumulation of carbonates
m - strong cementation.
q - accumulation of silica
t- accumulation of clay
v - vesicular structure
w - color or structural B
y - accumulation of gypsum

Top and Bot: The height in cm of the top and bottom contacts of horizon

Dry Color: color of dry sample from Munsell Soil Color Chart, Baltimore, Maryland.

Texture: From the sand (s), silt (si), and clay (c) triangle. fs-fine sand, ms - medium sand, cs- coarse sand, l - loam, fsl - fine sandy loam, sl - sandy loam, ls - loamy sand, lcos - loamy coarse sand, scl - sandy clay loam, sc - sandy clay, cl - clay loam, sil - silty loam, sicl - silty clay loam, sic - silty clay.

Structure: Grade: m - massive, sg - single grain; 1 - weak, 2 - moderate, 3 - strong. Size: f - fine, m - medium, c - coarse, vc - very coarse. Type: pl - platy, gr - granular, abk - angular blocky, sbk - subanguar blocky.

Consistence: Wet: so - nonsticky, ss - slightly sticky, s - sticky; po - nonplastic, ps - slightly plastic, p - plastic. Dry: lo - loose, so - soft, sh - slightly hard, h - hard, eh - extremely hard.

Clayfilms: Frequency: v1 - very few, 1 - few; 2 - common; 3 - many. Thickness: n - thin; mk - moderately thick. Location: pf - faces of peds, co - colloidal stains on mineral grains, po - aligned along pores, br - bridges between grains; N.O. - none observed.

$CaCO_3$: Carbonate morphology. N.O. - none observed, d - disseminate in matrix; Stages I, II, III, and IV are defined in Birkeland (1984).

HCL Rxn: Reaction to cold, dilute hydrochloric acid: eo - non-effervescent, ve - very slight, e - slight, es - strongly effervescent, ev - violent.

Boundary: boundary with lower horizon: Distinctness: va - very abrupt; a - abrupt; c - clear. Topography: s - smooth; w - wavy; b - broken.

Table 2: Soil Laboratory Analyses

Sample ID	Depth (cm) Top	Depth (cm) Bot.	Fine Fraction (ff) of total (<2.00mm)	portion of the FF Sand	portion of the FF Silt	portion of the FF Clay	fraction of Total (all sizes in mm) >76.2	76.2-38.1	38.1-19.0	19-9.5	9.5-4.75	4.75-2.00	2.00-1.00	1.00-0.50	0.50-0.25	0.25-0.10	0.10-0.053	pH	CaCO3 of the FF
MWV-P5-Avk	0	8	0.89	0.52	0.39	0.08	0.00	0.00	0.01	0.02	0.05	0.03	0.01	0.02	0.05	0.25	0.14	9.3	3.7%
MWV-P5-Bwk	8	15		0.62	0.33	0.05												8.6	4.4%
MWV-P5-Bwk2	15	28	0.88	0.65	0.33	0.03	0.00	0.00	0.00	0.02	0.05	0.04	0.03	0.08	0.12	0.25	0.09	8.3	4.1%
MWV-P5-2Bwkb	28	40	0.80	0.64	0.31	0.05	0.00	0.00	0.03	0.04	0.07	0.06	0.02	0.05	0.08	0.26	0.09	8.1	3.2%
MWV-P5-3Btkqmb2	40	80	0.25	0.69	0.26	0.04	0.07	0.05	0.19	0.17	0.16	0.11	0.02	0.02	0.03	0.08	0.03	7.8	3.6%
MWV-P5-3Btkqm2b2	80	99	0.26	0.83	0.15	0.03	0.00	0.10	0.23	0.18	0.13	0.10	0.02	0.03	0.04	0.10	0.03	7.7	4.0%
MWV-P5-3Bkqb2	99	128	0.31	0.88	0.09	0.03	0.00	0.25	0.14	0.14	0.09	0.07	0.03	0.04	0.05	0.13	0.03	7.5	2.5%
MWV-P5-4Bkqb3	128	168	0.34	0.88	0.07	0.06	0.00	0.08	0.10	0.17	0.17	0.15	0.07	0.06	0.06	0.09	0.02	8.1	12.7%
MWV-P5-4Bkq2b3	168	200	0.25	0.88	0.11	0.01	0.00	0.07	0.12	0.25	0.20	0.11	0.06	0.04	0.04	0.07	0.01	8.3	9.7%
MWV-P5-4BCkqb3	200	235	0.18	0.90	0.07	0.03	0.06	0.13	0.19	0.18	0.14	0.11	0.04	0.03	0.03	0.05	0.01	8.2	2.9%
MWV-P5-5Bkqb4	235	268	0.20	0.86	0.11	0.02	0.03	0.24	0.19	0.19	0.11	0.04	0.03	0.03	0.03	0.07	0.02	7.5	3.4%
MWV-P6-Avk	0	6	0.71	0.56	0.32	0.12	0.00	0.01	0.08	0.09	0.06	0.04	0.01	0.02	0.07	0.23	0.07	8.5	5.7%
MWV-P6-2Btjkq	6	10	0.90	0.53	0.32	0.15	0.00	0.00	0.01	0.03	0.040.02		0.01	0.02	0.09	0.27	0.08	8.2	4.1%
MWV-P6-2Btkq	10	20	0.89	0.54	0.35	0.11	0.00	0.00	0.01	0.03	0.04	0.03	0.02	0.03	0.08	0.25	0.11	8.6	3.1%
MWV-P6-2Btjkq12	20	28	0.71	0.55	0.35	0.10	0.00	0.15	0.04	0.03	0.03	0.04	0.02	0.02	0.07	0.20	0.08	8.8	37.8%
MWV-P6-2Btjkq22	28	37	0.69	0.62	0.32	0.07	0.00	0.15	0.05	0.03	0.04	0.04	0.02	0.05	0.11	0.17	0.08	8.7	4.6%
MWV-P6-3Kqb	37	90	0.16	0.85	0.11	0.04	0.41	0.19	0.08	0.07	0.05	0.04	0.02	0.02	0.03	0.06	0.01	8.4	14.6%
MWV-P6-3Bkqb	90	120	0.38	0.91	0.05	0.04	0.00	0.00	0.04	0.28	0.21	0.09	0.03	0.04	0.08	0.16	0.03	7.8	8.8%
MWV-P6-3Bkq2b	120	185	0.50	0.86	0.11	0.03	0.00	0.32	0.06	0.04	0.04	0.03	0.06	0.06	0.07	0.20	0.04	8.3	7.7%
MWV-P6-3BCkqb	185	205	0.27	0.73	0.25	0.02	0.08	0.23	0.18	0.10	0.08	0.05	0.03	0.03	0.04	0.08	0.02	8.3	4.4%
MWV-P6-4Bkqb2	205	235	0.26	0.92	0.07	0.02	0.11	0.13	0.10	0.19	0.13	0.09	0.03	0.04	0.04	0.10	0.03	7.9	2.1%
MWV-P6-4Bkq2b2	235	275	0.38	0.91	0.07	0.03	0.07	0.11	0.18	0.14	0.12	0.00	0.04	0.05	0.07	0.16	0.02	8.0	7.3%
MWV-P6-4CBkqb2	275	285	0.21	0.97	0.00	0.03	0.19	0.16	0.13	0.13	0.10	0.09	0.05	0.06	0.04	0.05	0.01	8.1	1.2%
MWV-P7-A	0	5	0.65	0.81	0.13	0.05	0.00	0.01	0.08	0.13	0.10	0.05	0.02	0.02	0.03	0.27	0.18	7.6	1.4%
MWV-P7-Bw	5	20	0.38	0.79	0.15	0.05	0.15	0.15	0.15	0.09	0.06	0.03	0.01	0.01	0.02	0.16	0.10	8.2	1.5%
MWV-P7-Bwk	20	33	0.25	0.78	0.15	0.08	0.00	0.10	0.23	0.29	0.10	0.02	0.01	0.01	0.01	0.10	0.06	8.2	3.3%
MWV-P7-Bwk2	33	49	0.20	0.81	0.12	0.07	0.00	0.29	0.26	0.19	0.04	0.01	0.00	0.01	0.02	0.09	0.04	8.6	3.2%
MWV-P7-Bk	49	112	0.20	0.85	0.10	0.05	0.07	0.15	0.26	0.19	0.08	0.04	0.02	0.02	0.02	0.08	0.04	8.7	2.5%
MWV-P7-2Bkqb	112	154	0.20	0.86	0.09	0.05	0.00	0.11	0.18	0.20	0.19	0.12	0.02	0.02	0.02	0.08	0.02	8.5	3.6%
MWV-P7-2Bkq2b	154	192	0.19	0.88	0.07	0.04	0.00	0.09	0.25	0.28	0.14	0.05	0.02	0.01	0.02	0.09	0.03	8.3	2.3%
MWV-P7-2Bkq3b	192	218	0.24	0.88	0.07	0.05	0.00	0.04	0.22	0.24	0.17	0.09	0.04	0.02	0.03	0.10	0.03	8.7	1.3%
MWV-P7-2Cqb	218	237	0.27	0.87	0.09	0.05	0.00	0.11	0.09	0.18	0.21	0.14	0.07	0.04	0.02	0.08	0.02	8.4	1.9%
MWV-P7-3Bkqb2	237	307	0.25	0.82	0.13	0.05	0.00	0.07	0.22	0.20	0.16	0.09	0.03	0.02	0.03	0.09	0.04	8.6	7.8%
MWV-P8-Av	0	10	0.87	0.50	0.36	0.14	0.00	0.00	0.01	0.05	0.04	0.02	0.02	0.02	0.04	0.28	0.08	7.9	1.7%
MWV-P8-BAtj	10	22	0.61	0.43	0.35	0.21	0.09	0.03	0.09	0.07	0.07	0.03	0.01	0.01	0.03	0.16	0.05	8.0	2.3%
MWV-P8-Bt	22	40	0.35	0.41	0.27	0.33	0.26	0.11	0.09	0.07	0.07	0.05	0.02	0.01	0.02	0.08	0.02	7.8	2.2%
MWV-P8-Btqk	40	64	0.30	0.54	0.32	0.15	0.23	0.23	0.14	0.05	0.02	0.02	0.02	0.01	0.02	0.09	0.02	8.1	2.7%

Table 2: Soil Laboratory Analyses

Sample ID	Depth (cm) Top	Depth (cm) Bot.	Fine Fraction (ff) of total (<2.00mm)	portion of the FF Sand	portion of the FF Silt	portion of the FF Clay	fraction of Total (all sizes in mm) >76.2	76.2-38.1	38.1-19.0	19-9.5	9.5-4.75	4.75-2.00	2.00-1.00	1.00-0.50	0.50-0.25	0.25-0.10	0.10-0.053	pH	CaCO3 of the FF
MWV-P8-BCkq	64	95	0.18	0.84	0.10	0.06	0.06	0.13	0.19	0.27	0.12	0.05	0.02	0.02	0.02	0.08	0.01	8.2	7.2%
MWV-P8-CBkq	95	145	0.15	0.86	0.09	0.06	0.05	0.30	0.30	0.11	0.06	0.03	0.09	0.04	0.00	0.00	0.00	8.1	4.5%
MWV-P8-Ck	145	200	0.19	0.92	0.05	0.03	0.14	0.12	0.16	0.20	0.13	0.07	0.04	0.02	0.02	0.07	0.02	8.2	2.8%
MWV-P8-2Btkqb	200	220	0.21	0.90	0.09	0.01	0.21	0.10	0.11	0.17	0.13	0.07	0.03	0.02	0.03	0.09	0.02	8.5	2.0%
MWV-P8-2CBkb	220	300	0.22	0.85	0.13	0.01	0.00	0.10	0.20	0.28	0.15	0.06	0.03	0.02	0.03	0.08	0.03	8.1	6.9%
MWV-P9-Av	0	5	0.57	0.53	0.34	0.13	0.00	0.00	0.03	0.04	0.30	0.06	0.01	0.01	0.03	0.17	0.08	8.8	1.7%
MWV-P9-Bt	5	35	0.53	0.54	0.24	0.22	0.16	0.08	0.08	0.05	0.06	0.04	0.01	0.02	0.04	0.16	0.06	7.6	1.2%
MWV-P9-2Bt	35	60	0.45	0.59	0.25	0.16	0.00	0.06	0.36	0.08	0.02	0.02	0.01	0.01	0.03	0.15	0.06	7.8	2.1%
MWV-P9-3Btkq	60	87	0.26	0.76	0.16	0.08	0.00	0.13	0.21	0.22	0.11	0.07	0.02	0.01	0.02	0.11	0.03	8.5	2.9%
MWV-P9-3Bkq	87	110	0.30	0.88	0.07	0.06	0.00	0.01	0.05	0.17	0.26	0.20	0.07	0.03	0.03	0.11	0.02	8.0	2.1%
MWV-P9-4Bkqi	110	180	0.25	0.89	0.04	0.07	0.00	0.10	0.18	0.25	0.15	0.07	0.02	0.02	0.03	0.12	0.03	8.3	4.8%
MWV-P9-4Bkq2	180	220	0.31	0.88	0.10	0.02	0.00	0.00	0.08	0.22	0.23	0.15	0.04	0.03	0.05	0.13	0.03	8.8	5.2%
MWV-P9-5Kq	220	255	0.20	0.86	0.08	0.06	0.00	0.34	0.21	0.10	0.08	0.06	0.03	0.02	0.02	0.08	0.03	8.7	11.8%
MWV-P9-6BCkq	255	330	0.22	0.85	0.12	0.03	0.00	0.00	0.17	0.23	0.24	0.13	0.04	0.02	0.02	0.08	0.02	NA	4.0%
MWV-P9-7Bkqb	330	360		0.90	0.07	0.03												7.8	3.1%
MWV-P10-A	0	5	0.57	0.80	0.16	0.04	0.00	0.00	0.08	0.17	0.13	0.05							1.3%
MWV-P10-BW	5	35	0.21	0.80	0.14	0.06	0.00	0.21	0.33	0.11	0.08	0.05							1.4%
MWV-P10-BWK	35	68	0.38	0.85	0.10	0.06	0.08	0.14	0.13	0.11	0.10	0.05							3.0%
MWV-P10-2BCK	68	110	0.18	0.88	0.08	0.04	0.32	0.07	0.12	0.14	0.11	0.06							3.0%
MWV-P10-2CBK	110	138	0.16	0.84	0.11	0.05	0.56	0.02	0.03	0.07	0.09	0.06							2.4%
MWV-P10-3BTKQB	138	192	0.33	0.78	0.15	0.07	0.00	0.13	0.22	0.18	0.13	0.01							2.6%
MWV-P10-3BKQB	192	210	0.39	0.89	0.07	0.04	0.00	0.03	0.07	0.17	0.22	0.12							1.7%
MWV-P10-3CBKB	210	300	0.23	0.91	0.05	0.04	0.00	0.04	0.20	0.24	0.21	0.09							1.6%
MWV-P13-Avk	0	8	0.92	0.53	0.37	0.11	0.00	0.00	0.02	0.02	0.03	0.02	0.01	0.03	0.12	0.25	0.08	8.7	5.0%
MWV-P13-Btkq	8	22	0.86	0.45	0.40	0.14	0.00	0.01	0.03	0.03	0.03	0.04	0.01	0.03	0.10	0.18	0.06	8.3	1.9%
MWV-P13-2Kqb	22	51	0.22	0.80	0.15	0.05	0.20	0.10	0.16	0.14	0.10	0.08	0.03	0.04	0.05	0.04	0.01	8.0	28.7%
MWV-P13-Bkqb	51	75	0.32	0.83	0.13	0.04	0.00	0.09	0.14	0.18	0.16	0.11	0.05	0.05	0.07	0.08	0.02	7.7	17.9%
MWV-P13-2Bkq2b	75	103	0.42	0.89	0.09	0.02	0.00	0.04	0.10	0.06	0.23	0.15	0.09	0.06	0.07	0.13	0.03	7.8	9.3%
MWV-P13-2BCkqb	103	139	0.19	0.92	0.06	0.02	0.22	0.13	0.16	0.14	0.09	0.07	0.04	0.04	0.03	0.05	0.01	8.0	5.0%
MWV-P13-3Bkqb2	139	230	0.27	0.82	0.12	0.06	0.12	0.16	0.11	0.11	0.13	0.10	0.05	0.05	0.05	0.06	0.01	7.9	14.5%
MWV-P13-3Bkq2b2	230	260	0.27	0.91	0.07	0.02	0.09	0.07	0.10	0.17	0.20	0.11	0.06	0.06	0.06	0.06	0.01	8.0	2.9%
MWV-P13-3Bqb2	260	314	0.38	0.70	0.27	0.03	0.05	0.00	0.03	0.14	0.23	0.17	0.06	0.06	0.07	0.07	0.01	7.6	1.1%
MWV-P14-A	0	7	0.67	0.88	0.09	0.04	0.00	0.10	0.07	0.06	0.05	0.04	0.05	0.05	0.10	0.30	0.09	8.0	1.3%
MWV-P14-Bw	7	23	0.45	0.83	0.09	0.08	0.07	0.11	0.11	0.11	0.09	0.06	0.04	0.03	0.09	0.18	0.03	8.3	1.4%
MWV-P14-CBk	23	48	0.19	0.90	0.05	0.05	0.24	0.27	0.12	0.08	0.05	0.04	0.02	0.02	0.03	0.08	0.03	8.5	3.1%
MWV-P14-2CBk	48	82	0.78	0.84	0.12	0.04	0.00	0.00	0.01	0.05	0.08	0.09	0.05	0.06	0.11	0.33	0.10	8.6	2.4%

Table 2: Soil Laboratory Analyses

Sample ID	Depth (cm) Top	Depth (cm) Bot.	Fine Fraction (ff) of total (<2.00mm)	portion of the FF: Sand	Silt	Clay	fraction of Total (all sizes in mm): >76.2	76.2-38.1	38.1-19.0	19-9.5	9.5-4.75	4.75-2.00	2.00-1.00	1.00-0.50	0.50-0.25	0.25-0.10	0.10-0.053	pH	CaCO3 of the FF
MWV-P14-3CBk1	82	115	0.24	0.91	0.06	0.03	0.12	0.15	0.17	0.11	0.10	0.10	0.05	0.04	0.05	0.07	0.01	8.4	2.3%
MWV-P14-3CBk2	115	140	0.27	0.90	0.05	0.05	0.00	0.02	0.07	0.16	0.27	0.22	0.07	0.05	0.05	0.07	0.01	8.6	1.8%
MWV-P14-4Btkqb1	140	185	0.60	0.90	0.01	0.10	0.00	0.00	0.01	0.04	0.14	0.20	0.10	0.12	0.15	0.14	0.02	8.5	0.8%
MWV-P14-5Btqb2	185	200	0.60	0.88	0.04	0.09	0.00	0.02	0.06	0.09	0.12	0.12	0.07	0.07	0.16	0.18	0.04	8.2	1.0%
MWV-P15-Avk	0	7	0.93	0.54	0.29	0.17	0.00	0.00	0.00	0.01	0.04	0.03	0.01	0.02	0.08	0.31	0.08	8.2	3.3%
MWV-P15-BAtvk	7	11	0.76	0.52	0.29	0.19	0.00	0.00	0.01	0.04	0.09	0.09	0.02	0.03	0.07	0.22	0.06	8.5	3.4%
MWV-P15-Btk	11	19	0.59	0.54	0.30	0.16	0.14	0.10	0.03	0.05	0.05	0.05	0.02	0.03	0.06	0.17	0.04	8.3	1.8%
MWV-P15-2Btkq	19	30	0.49	0.79	0.11	0.10	0.14	0.19	0.03	0.05	0.05	0.05	0.05	0.06	0.08	0.17	0.03	8.4	2.9%
MWV-P15-3Btkqb	30	44	0.54	0.72	0.17	0.11	0.00	0.13	0.10	0.06	0.08	0.08	0.04	0.03	0.06	0.20	0.06	8.5	2.7%
MWV-P15-4Bkqb2	44	80	0.32	0.83	0.06	0.11	0.00	0.10	0.20	0.16	0.12	0.10	0.04	0.05	0.06	0.09	0.02	8.7	5.0%
MWV-P15-4Bkq2b2	80	125	0.30	0.89	0.00	0.11	0.00	0.13	0.15	0.18	0.13	0.10	0.04	0.05	0.06	0.10	0.01	7.7	2.3%
MWV-P15-4Bkq3b2	125	148	0.34	0.79	0.12	0.09	0.00	0.06	0.19	0.16	0.15	0.11	0.03	0.04	0.06	0.12	0.02	7.9	3.5%
MWV-P15-4BCkqb2	148	190	0.24	0.90	0.03	0.07	0.00	0.11	0.15	0.18	0.18	0.13	0.02	0.04	0.04	0.10	0.02	8.0	3.5%
MWV-P15-5Bkqb3	190	245	0.28	0.89	0.04	0.07	0.00	0.13	0.14	0.21	0.14	0.10	0.04	0.05	0.05	0.10	0.02	7.8	13.6%
MWV-P15-5Bkq2b3	245	286		0.92	0.04	0.05												8.3	3.0%
MWV-P20-Avj	0	4	0.66	0.83	0.13	0.04	0.00	0.16	0.05	0.04	0.05	0.04	0.02	0.02	0.05	0.36	0.11	7.7	1.5%
MWV-P20-ABvk	4	23	0.62	0.71	0.16	0.12	0.20	0.05	0.04	0.03	0.03	0.03	0.01	0.01	0.05	0.30	0.07	8.3	2.3%
MWV-P20-2Bwk	23	42	0.44	0.65	0.18	0.17	0.13	0.20	0.10	0.05	0.04	0.04	0.01	0.01	0.03	0.18	0.05	8.0	2.5%
MWV-P20-2Btkq	42	85	0.32	0.79	0.08	0.13	0.00	0.11	0.19	0.15	0.12	0.10	0.03	0.02	0.03	0.14	0.04	8.1	3.1%
MWV-P20-2Btkq2	85	133	0.17	0.75	0.15	0.10	0.18	0.30	0.16	0.08	0.07	0.04	0.01	0.01	0.02	0.07	0.02	8.2	3.1%
MWV-P20-3Bkq	133	178	0.27	0.86	0.03	0.11	0.09	0.31	0.17	0.07	0.04	0.04	0.02	0.02	0.03	0.14	0.03	8.5	1.9%
MWV-P20-4Bkqy	178	203	0.04	0.89	0.08	0.03	0.14	0.31	0.29	0.11	0.06	0.06	0.00	0.00	0.00	0.02	0.00	8.9	1.2%
MWV-P20-5Btkqb	203	225	0.35	0.85	0.13	0.03	0.00	0.17	0.18	0.12	0.11	0.07	0.02	0.03	0.05	0.16	0.04	8.9	1.3%
MWV-P20-6BCkqb	225	320	0.23	0.89	0.08	0.03	0.13	0.25	0.15	0.10	0.08	0.06	0.02	0.03	0.04	0.10	0.02	8.4	2.8%
MWV-P21-A	0	5	0.54	0.89	0.10	0.02	0.00	0.00	0.14	0.16	0.11	0.06	0.02	0.02	0.04	0.28	0.11	7.6	0.2%
MWV-P21-Bw	5	35	0.46	0.84	0.12	0.04	0.22	0.03	0.13	0.06	0.06	0.04	0.02	0.01	0.04	0.26	0.06	7.8	0.7%
MWV-P21-2BCk	35	80	0.29	0.88	0.05	0.06	0.11	0.09	0.16	0.12	0.12	0.11	0.04	0.02	0.02	0.13	0.04	8.2	1.3%
MWV-P21-2BCk2	80	170	0.12	0.92	0.05	0.03	0.00	0.53	0.22	0.06	0.04	0.03	0.02	0.01	0.02	0.05	0.01	8.9	2.0%
MWV-P21-3Bkqb	170	260	0.11	0.90	0.08	0.02	0.32	0.38	0.09	0.04	0.03	0.02	0.01	0.01	0.02	0.05	0.01	9.1	6.6%
MWV-P21-4Btjkqb	260	295	0.78	0.89	0.09	0.03	0.00	0.05	0.06	0.04	0.03	0.03	0.01	0.13	0.22	0.28	0.05	9.0	2.4%
MWV-P21-5Bkqb	295	345	0.29	0.88	0.08	0.04	0.15	0.13	0.19	0.09	0.09	0.06	0.02	0.06	0.08	0.09	0.01	8.8	8.4%
MWV-P22-Avk	0	10	0.58	0.50	0.34	0.16	0.00	0.07	0.08	0.10	0.08	0.08	0.01	0.02	0.04	0.14	0.08	8.9	2.9%
MWV-P22-2Btjk	10	32	0.75	0.70	0.18	0.12	0.04	0.02	0.03	0.04	0.06	0.07	0.06	0.06	0.08	0.22	0.10	8.6	2.1%
MWV-P22-2Btkq	32	63	0.12	0.85	0.05	0.10	0.14	0.24	0.12	0.12	0.13	0.12	0.01	0.02	0.02	0.04	0.01	7.8	3.4%
MWV-P22-2Bkq	63	80	0.27	0.78	0.11	0.11	0.35	0.11	0.07	0.07	0.07	0.07	0.04	0.04	0.04	0.07	0.03	7.8	2.7%
MWV-P22-2Bkq2	80	130	0.45	0.88	0.02	0.10	0.00	0.01	0.08	0.15	0.15	0.17	0.09	0.11	0.08	0.09	0.02	7.6	1.5%
MWV-P22-3Ckq	130	260	0.45	0.91	0.07	0.02	0.00	0.01	0.11	0.14	0.13	0.16	0.12	0.11	0.07	0.08	0.02	8.1	3.4%

Table 2: Soil Laboratory Analyses

Sample ID	Depth (cm) Top	Depth (cm) Bot.	Fine Fraction (ff) of total (<2.00mm)	portion of the FF Sand	Silt	Clay	fraction of Total (all sizes in mm) >76.2	76.2-38.1	38.1-19.0	19-9.5	9.5-4.75	4.75-2.00	2.00-1.00	1.00-0.50	0.50-0.25	0.25-0.10	0.10-0.053	pH	CaCO3 of the FF
MWV-P23-Avk	0	10	0.77	0.46	0.44	0.10	0.00	0.07	0.03	0.03	0.06	0.05	0.01	0.03	0.04	0.17	0.11	8.7	3.1%
MWV-P23-2Btkq	10	30	0.75	0.75	0.20	0.05	0.00	0.00	0.06	0.06	0.07	0.05	0.04	0.09	0.09	0.23	0.11	8.0	3.4%
MWV-P23-2Btkqm	30	68	0.20	0.84	0.14	0.02	0.06	0.36	0.19	0.08	0.07	0.04	0.04	0.04	0.03	0.04	0.01	7.4	3.6%
MWV-P23-2Kqm	68	135	0.47	0.85	0.11	0.05	0.00	0.08	0.08	0.10	0.13	0.14	0.03	0.08	0.08	0.16	0.04	7.8	13.1%
MWV-P23-2Kq	135	175	0.38	0.85	0.10	0.04	0.00	0.20	0.13	0.11	0.10	0.09	0.05	0.06	0.06	0.11	0.04	7.8	13.3%
MWV-P23-2Bkq	175	195	0.24	0.88	0.09	0.03	0.00	0.08	0.08	0.22	0.22	0.15	0.06	0.05	0.04	0.05	0.02	8.4	5.3%
MWV-P23-2Ck	195	360	0.44	0.91	0.06	0.02	0.00	0.00	0.02	0.15	0.19	0.19	0.10	0.09	0.07	0.09	0.04	8.4	3.2%
MWV-P24-Av	0	8	0.80	0.47	0.37	0.16	0.00	0.09	0.04	0.00	0.04	0.03	0.01	0.03	0.05	0.19	0.09	8.4	2.4%
MWV-P24-Btk	8	25	0.64	0.66	0.21	0.13	0.08	0.04	0.05	0.05	0.07	0.07	0.03	0.04	0.06	0.19	0.10	8.4	1.5%
MWV-P24-2Btkq	25	48	0.46	0.69	0.16	0.15	0.00	0.16	0.11	0.10	0.10	0.07	0.03	0.04	0.06	0.14	0.05	7.6	3.0%
MWV-P24-2Btkq2	48	83	0.37	0.77	0.13	0.10	0.00	0.10	0.16	0.13	0.13	0.11	0.05	0.05	0.05	0.10	0.05	7.3	2.2%
MWV-P24-2Bkq1	83	132	0.28	0.92	0.03	0.04	0.00	0.11	0.17	0.16	0.14	0.14	0.08	0.07	0.05	0.05	0.01	8.8	3.4%
MWV-P24-2Bkq2	132	197	0.22	0.92	0.05	0.02	0.24	0.25	0.09	0.06	0.07	0.07	0.04	0.05	0.04	0.05	0.02	8.5	2.0%
MWV-P24-2Cq	197	247	0.35	0.90	0.02	0.08	0.00	0.00	0.03	0.15	0.24	0.23	0.08	0.08	0.05	0.08	0.03	7.8	1.1%
MWV-P24-3Bkqb	247	287	0.31	0.82	0.15	0.04	0.11	0.01	0.08	0.17	0.18	0.14	0.04	0.04	0.05	0.09	0.03	7.4	7.5%
MWV-P25-Avk	0	10	0.87	0.47	0.43	0.09	0.00	0.00	0.06	0.02	0.02	0.02	0.01	0.02	0.06	0.22	0.09	8.3	7.1%
MWV-P25-2Btkj	10	32	0.68	0.56	0.35	0.09	0.11	0.04	0.04	0.03	0.05	0.05	0.03	0.04	0.06	0.18	0.08	8.3	2.0%
MWV-P25-3Bkq	32	50	0.45	0.75	0.22	0.03	0.00	0.09	0.16	0.09	0.11	0.10	0.05	0.07	0.08	0.11	0.02	8.4	13.4%
MWV-P25-3Kqym	50	65	0.29	0.81	0.17	0.03	0.00	0.12	0.16	0.17	0.14	0.11	0.03	0.04	0.04	0.05	0.06	8.4	29.5%
MWV-P25-2Kqy	65	100	0.41	0.75	0.21	0.04	0.00	0.06	0.14	0.17	0.12	0.10	0.03	0.06	0.08	0.11	0.03	7.8	27.7%
MWV-P25-3Bkq1	100	136	0.32	0.83	0.15	0.02	0.06	0.20	0.09	0.13	0.10	0.09	0.04	0.05	0.06	0.09	0.03	8.3	12.6%
MWV-P25-3Bkq2	136	198	0.20	0.86	0.11	0.03	0.11	0.23	0.15	0.09	0.11	0.11	0.05	0.04	0.03	0.04	0.02	8.2	14.2%
MWV-P25-4Bkq	198	245	0.25	0.87	0.09	0.04	0.05	0.14	0.14	0.17	0.13	0.11	0.05	0.04	0.04	0.06	0.02	7.8	20.6%
MWV-P25-4Ckq1	245	290	0.24	0.91	0.06	0.03	0.21	0.08	0.17	0.12	0.11	0.08	0.04	0.04	0.04	0.08	0.02	7.8	1.6%
MWV-P25-4Ckq2	290	320		0.92	0.06	0.03												7.9	0.4%
MWV-P26-Avkq	0	7	0.90	0.53	0.29	0.18	0.00	0.00	0.03	0.03	0.02	0.02	0.02	0.03	0.08	0.25	0.09	8.3	1.9%
MWV-P26-Bw	7	18	0.91	0.58	0.26	0.16	0.00	0.00	0.01	0.02	0.03	0.04	0.02	0.02	0.09	0.30	0.09	7.8	1.4%
MWV-P26-2Btjq	18	33	0.89	0.58	0.31	0.11	0.00	0.02	0.00	0.02	0.03	0.04	0.02	0.03	0.10	0.27	0.10	7.0	1.4%
MWV-P26-2Bwkfqmb	33	45	0.89	0.79	0.08	0.13	0.00	0.00	0.01	0.02	0.04	0.04	0.09	0.11	0.14	0.28	0.07	8.8	47.7%
MWV-P26-2Btkqb	45	53	0.59	0.69	0.21	0.09	0.00	0.04	0.05	0.04	0.11	0.17	0.03	0.07	0.11	0.15	0.05	7.5	50.4%
MWV-P26-2Btqb	53	83	0.60	0.72	0.18	0.09	0.00	0.03	0.04	0.05	0.11	0.17	0.03	0.07	0.12	0.17	0.04	7.7	3.0%
MWV-P26-3Kqymb	83	123	0.40	0.79	0.16	0.05	0.17	0.07	0.06	0.10	0.10	0.11	0.08	0.08	0.07	0.06	0.01	7.5	25.4%
MWV-P26-3Bkqvb	123	147	0.43	0.88	0.07	0.05	0.00	0.02	0.05	0.15	0.19	0.16	0.07	0.08	0.09	0.11	0.03	7.9	8.0%
MWV-P26-3BCkqb	147	195	0.23	0.89	0.04	0.07	0.19	0.10	0.10	0.15	0.13	0.10	0.04	0.04	0.05	0.06	0.01	7.9	4.2%
MWV-P26-3Ckqb	195	270	0.31	0.88	0.02	0.10	0.00	0.03	0.06	0.15	0.22	0.22	0.09	0.07	0.05	0.06	0.02	8.5	1.8%
MWV-P28-Avk	235	275	0.93	0.53	0.37	0.10	0.00	0.00	0.00	0.02	0.02	0.02	0.01	0.03	0.08	0.31	0.07	8.9	1.6%
MWV-P28-BAtq	8	13	0.85	0.59	0.30	0.12	0.00	0.00	0.02	0.04	0.05	0.05	0.02	0.03	0.07	0.30	0.07	8.6	1.7%

Table 2: Soil Laboratory Analyses

Sample ID	Depth (cm) Top	Bot.	Fine Fraction (ff) of total (<2.00mm)	portion of the FF Sand	Silt	Clay	fraction of Total (all sizes in mm) >76.2	76.2-38.1	38.1-19.0	19-9.5	9.5-4.75	4.75-2.00	2.00-1.00	1.00-0.50	0.50-0.25	0.25-0.10	0.10-0.053	pH	CaCO3 of the FF
MWV-P28-Btq	13	26	0.82	0.28	0.64	0.08	0.00	0.02	0.01	0.05	0.06	0.05	0.01	0.01	0.03	0.13	0.04	8.4	1.9%
MWV-P28-Btkq	26	43	0.87	0.43	0.36	0.21	0.00	0.02	0.01	0.03	0.04	0.03	0.03	0.02	0.05	0.21	0.06	8.8	3.7%
MWV-P28-2Btkq2	43	66	0.35	0.48	0.38	0.14	0.12	0.18	0.05	0.09	0.11	0.10	0.01	0.01	0.02	0.10	0.02	8.9	6.6%
MWV-P28-3Btkqb	66	91	0.61	0.73	0.23	0.04	0.00	0.06	0.09	0.07	0.08	0.09	0.04	0.08	0.11	0.17	0.04	9.1	10.4%
MWV-P28-3Bkqmb	91	130	0.11	0.78	0.19	0.03	0.00	0.03	0.22	0.25	0.21	0.18	0.01	0.01	0.02	0.03	0.01	8.1	10.5%
MWV-P28-3Bkqb	130	182	0.27	0.83	0.14	0.04	0.03	0.06	0.16	0.22	0.15	0.11	0.04	0.05	0.05	0.07	0.02	8.9	12.8%
MWV-P28-3BCkqb	182	208	0.23	0.90	0.08	0.02	0.16	0.17	0.19	0.14	0.07	0.06	0.04	0.05	0.04	0.06	0.01	9.1	2.2%
MWV-P28-3Ckqb	208	246	0.36	0.88	0.10	0.02	0.03	0.13	0.11	0.10	0.14	0.12	0.06	0.07	0.06	0.11	0.02	9.1	1.3%
MWV-P28-4Bqb2	246	287	0.37	0.82	0.15	0.04	0.13	0.09	0.13	0.11	0.09	0.08	0.03	0.05	0.07	0.13	0.03	8.6	6.8%
MWV-P28-4Bkqb2	287	345	0.26	0.79	0.16	0.05	0.23	0.13	0.12	0.15	0.06	0.06	0.02	0.02	0.04	0.09	0.03	8.5	4.9%
CF1-SPI-Avk	0	14	NA	0.56	0.35	0.10												8.5	6.1%
CF1-SPI-Bk	14	17	0.55	0.48	0.39	0.13	0.00	0.15	0.17	0.07	0.05	0.03	0.01	0.01	0.02	0.15	0.07	8.6	7.5%
CF1-SPI-2Kqmb1	17	24	0.16	0.77	0.16	0.08	0.06	0.06	0.23	0.28	0.15	0.06	0.02	0.02	0.02	0.05	0.02	8.4	16.4%
CF1-SPI-3Kqmb1	34	65	0.09	0.75	0.16	0.09	0.25	0.24	0.17	0.13	0.08	0.04	0.01	0.01	0.01	0.03	0.01	8.1	23.8%
CF1-SPI-4Bkb1	65	130	0.18	0.87	0.11	0.03	0.29	0.18	0.12	0.10	0.08	0.06	0.04	0.02	0.02	0.05	0.02	8.4	15.1%
CF1-SPI-5Bkb1	130	167	0.21	0.87	0.10	0.03	0.14	0.17	0.11	0.12	0.14	0.11	0.04	0.03	0.02	0.07	0.03	8.4	15.9%
CF1-SPI-6Bkb2	167	280	0.51	0.81	0.14	0.05	0.05	0.03	0.11	0.14	0.08	0.06	0.07	0.05	0.05	0.17	0.07	8.2	23.9%
CF1-SPII-Av	0	10	0.71	0.80	0.14	0.06	0.00	0.11	0.08	0.03	0.04	0.03	0.01	0.01	0.04	0.39	0.12	8.2	3.4%
CF1-SPII-Bk1	10	26	0.68	0.68	0.20	0.13	0.00	0.04	0.10	0.06	0.07	0.05	0.02	0.02	0.04	0.27	0.11	8.5	6.7%
CF1-SPII-Bk2	26	35	0.49	0.67	0.22	0.11	0.00	0.09	0.14	0.11	0.10	0.07	0.03	0.03	0.04	0.16	0.07	8.4	9.9%
CF1-SPII-2Kqmb1	35	110	0.18	0.83	0.12	0.05	0.16	0.15	0.16	0.14	0.11	0.09	0.04	0.03	0.03	0.04	0.01	8.4	40.6%
CF1-SPII-3Bkqmb2	110	150	0.15	0.86	0.09	0.05	0.10	0.39	0.20	0.09	0.05	0.03	0.01	0.01	0.02	0.07	0.03	8.0	11.4%
CF1-SPII-4Bkb2	150	210	0.21	0.90	0.07	0.03	0.18	0.01	0.22	0.20	0.11	0.08	0.03	0.02	0.02	0.09	0.03	8.1	12.4%
CF1-SPII-5Bkb2	210	260	0.12	0.90	0.06	0.04	0.37	0.16	0.13	0.10	0.07	0.04	0.02	0.01	0.01	0.05	0.02	9.0	14.1%
CF1-SPII-6Bkb2	260	261	0.23	0.92	0.05	0.04	0.15	0.28	0.14	0.10	0.07	0.04	0.07	0.03	0.02	0.07	0.03	9.1	8.9%
FW-5-A	0	5	0.91	0.81	0.13	0.06	0.00	0.00	0.01	0.03	0.03	0.02	0.02	0.07	0.17	0.41	0.06	8.3	1.6%
FW-5-AB	5	20	0.88	0.78	0.13	0.10	0.00	0.00	0.01	0.03	0.04	0.04	0.03	0.06	0.12	0.36	0.12	8.4	2.4%
FW-5-Btk	20	45	0.72	0.76	0.14	0.09	0.00	0.15	0.01	0.04	0.04	0.04	0.02	0.06	0.14	0.24	0.08	8.6	2.7%
FW-5-2Btkv	45	56	0.59	0.83	0.12	0.05	0.00	0.18	0.06	0.04	0.07	0.06	0.03	0.05	0.11	0.21	0.08	8.6	1.7%
FW-5-2Btqmkb	56	106	0.18	0.87	0.08	0.05	0.10	0.26	0.13	0.14	0.10	0.08	0.02	0.03	0.04	0.06	0.02	8.5	4.8%
FW-5-2Kqb	106	164	0.23	0.91	0.06	0.03	0.00	0.13	0.18	0.15	0.16	0.16	0.09	0.06	0.04	0.02	0.01	8.5	2.7%
SWG-1-Bkq	50	100	0.31	0.87	0.07	0.05	0.10	0.14	0.12	0.10	0.11	0.12	0.05	0.07	0.08	0.06	0.01	8.4	1.7%
SWG-1-CBk	100	280	0.13	0.82	0.06	0.11	0.13	0.19	0.18	0.13	0.13	0.12	0.02	0.04	0.03	0.02	0.00	8.1	1.5%
SWG-1-2Btjb	280	340	0.76	0.89	0.05	0.05	0.00	0.00	0.06	0.07	0.06	0.05	0.03	0.05	0.21	0.34	0.06	8.3	2.4%
SWG-1-3Bkqmb	400	500	0.18	0.88	0.06	0.05	0.00	0.18	0.29	0.20	0.08	0.06	0.04	0.05	0.04	0.03	0.01	8.5	1.8%
SWG-1-3CBkb	500	610	0.85	0.87	0.09	0.04	0.00	0.00	0.01	0.03	0.05	0.06	0.18	0.13	0.14	0.27	0.03	8.2	1.0%

Table 2: Soil Laboratory Analyses

Sample ID	Depth (cm) Top	Depth (cm) Bot.	Fine Fraction (ff) of total (<2.00mm)	portion of the FF Sand	portion of the FF Silt	portion of the FF Clay	fraction of Total (all sizes in mm) >76.2	76.2-38.1	38.1-19.0	19-9.5	9.5-4.75	4.75-2.00	2.00-1.00	1.00-0.50	0.50-0.25	0.25-0.10	0.10-0.053	pH	CaCO3 of the FF
NCW-TT1-A	0	5	0.52	0.68	0.22	0.10	0.08	0.15	0.14	0.07	0.03	0.02	0.00	0.00	0.02	0.19	0.13	7.1	1.2%
NCW-TT1-Bw	5	40	0.26	0.63	0.27	0.10	0.40	0.24	0.06	0.03	0.00	0.00	0.00	0.00	0.01	0.09	0.07	7.7	1.6%
MCW-TT1-BCk1	40	75	0.28	0.62	0.29	0.09	0.11	0.48	0.10	0.02	0.01	0.01	0.00	0.00	0.01	0.10	0.06	8.4	3.3%
NCW-TT1-BCk2	75	115	0.33	0.65	0.26	0.09	0.27	0.35	0.02	0.01	0.01	0.01	0.01	0.01	0.01	0.12	0.07	8.4	5.2%
NCW-TT1-2CBk	115	140	0.38	0.81	0.15	0.04	0.00	0.03	0.06	0.13	0.25	0.15	0.06	0.04	0.05	0.12	0.03	8.9	1.6%
NCW-TT1-3CBk	140	170	0.38	0.79	0.18	0.03	0.00	0.05	0.18	0.16	0.13	0.11	0.05	0.05	0.05	0.12	0.03	9.6	2.0%
NCW-TX1-A0	0	5	0.52	0.73	0.22	0.05	0.00	0.14	0.09	0.09	0.10	0.05							3.3%
NCW-TX1-BWK	5	30	0.21	0.71	0.24	0.05	0.43	0.17	0.07	0.06	0.04	0.02							2.1%
NCW-TX1-BCK	30	70	0.35	0.82	0.14	0.04	0.22	0.15	0.11	0.08	0.06	0.04							1.5%
NCW-TX1-CK	70	100	0.23	0.89	0.07	0.04	0.14	0.22	0.14	0.10	0.09	0.06							3.3%
NCW-TX1-2BTKQB1	100	120	0.32	0.77	0.18	0.05	0.26	0.13	0.08	0.07	0.09	0.04							1.3%
NCW-TX1-2BTKQB2	120	145	0.20	0.77	0.19	0.05	0.25	0.11	0.20	0.16	0.15	0.05							1.3%
NCW-TX1-2BCKQB	145	175	0.18	0.85	0.12	0.04	0.23	0.10	0.18	0.14	0.13	0.05							1.0%
NCW-TX1-3BTQB	175	200	0.39	0.75	0.21	0.04	0.15	0.14	0.13	0.09	0.08	0.03							1.0%

Table 3: Surface Characteristics

Pit Name	Map Unit	Alluvial Surface Morphology	Pavement Packing	Main Varnish	CaCO3 chips
MWV-P14	6	muted bar and swale	loose-weak	absent-weak	
NCW-TX-	6	muted bar and swale	absent	absent-weak	
MWV-P10	5	muted bar and swale	loose-weak	absent-weak	no
MWV-P21	5	muted bar and swale	loose-weak	absent-weak	no
MWV-P7	5	muted bar and swale	loose-weak	absent-weak	
NCW-TT-	5	muted bar and swale	absent	relict-patchy-eroded	
MWV-P6	4/1	smooth-paved	weak-moderate	moderate	yes
MWV-P12	4	smooth-paved	weak-moderate	absent-weak	
MWV-P19	4	smooth-paved	moderate	moderate	no
MWV-P20	4	smooth-paved	weak-moderate	weak-moderate	no
SWG-1	3f	smooth-paved	tight-well developed	moderate	no
MWV-P15	3	smooth-paved	moderate	moderate	no
MWV-P16	3	smooth-paved	moderate -well	well developed	no
MWV-P17	3	smooth-paved	moderate -well	moderate	no
MWV-P22	3	smooth-paved	moderate	moderate	no
MWV-P24	3	smooth-paved	moderate	moderate	
MWV-P5	3	smooth-paved	moderate-well	moderate	no
MWV-P8	3	smooth-paved	moderate-tight	moderate	no
MWV-P9	3	smooth-paved	tight-well developed	moderate	
MWV-P26	2	smoothed paved- isolated	tight-well developed	moderate-well	no
MWV-P28	2	smooth-paved	moderate	well developed	no
CF-1	1	accordant rounded ridges	moderate	moderate	yes
MWV-P13	1	smooth-paved	moderate -well	moderate	yes
MWV-P23	1	accordant rounded ridges	moderate	moderate	
MWV-P25	1	accordant rounded ridges	tight-well developed	moderate	yes

able 4. Ve[illegible]tation

urfac	Map Unit	Ambrosia		Atriplex can.	Atriplex can.	Bromus	Colegyne	Ceratoides		Psorothamnu		Ephedra	Ephedra n.		Eriogonum f.	Eriogonum l.	Grass	Grayia		Happlopappus	Hymenoclea	Krameria	Larrea	Lycium	Menodora	Opuntia e.			Sarcobatus	Tetradymia	
'V-P14	6	X				X	X					X										X	X		X						
N-TX-1	6				X								X		X			X		X										X	
'V-P10	5					X																	X								
'V-P21	5	X				X						X					X								X						
'V-P7	5	X				X						X								X			X								
N-TT-1	5											X					X														
'V-P6	4/	X										X										X	X	X							
'V-P12	4	X										X					X						X		X				X		
V-P19	4	X						X				X				X							X		X					X	
V-P20	4	X				X		X					X					X							X				X	X	
G-1	3f																														
V-P15	3	X					X					X								X		X	X						X		
V-P16	3	X										X					X	X		X			X						X		
V-P17	3											X						X		X	X		X		X				X		
V-P22	3	X					X					X						X					X	X							
V-P24	3	X					X					X											X	X	X				X		
V-P5	3	X					X					X					X					X	X								
V-P8	3	X					X					X								X			X			X			X		
V-P9	3	X																		X									X		
V-P26	2	X					X					X											X	X	X				X		
V-P28	2	X			X		X					X					X						X	X							
	1	X		X						X		X				X						X	X	X							
V-P13	1	X										X												X							
V-P23	1	X				X	X					X										X	X	X	X				X		
V-P25	1	X					X						X										X	X	X						

Key to Table 4: Vegetation

Abbreviation	Genus	species	common name
Ambrosia	Ambrosia	dumosa	bursage
shadscale	Atriplex	confertifolia	shadscale
Atriplex can.	Atriples	canescens	four-wing saltbush
Bromus	Bromus	tectorum	cheatgrass
Coleogyne	Coleogyne	ramossissima	blackbrush
Ceratoides	Ceratoides	lanata	winterfat
Dalea	Dalea		indigobush
Ephedra n.	Ephedra	nevadansis	mormon tea
Eriogonum f.	Eriogonum	fasciculatum	desert buckwheat
Eriogonum i.	Eriogonum	inflatum	desert trumpet
Grass			unspecified grass
Grayia	Grayia	spinosa	hopsage
Happlopappus	Happlopappus	goldenbush	
Hymenoclea	Hymenoclea	salsola	cheeseweed
Krameria	Krameria	parviflora	ratany
Larrea	Larrea	diversiloba	creosotebush
Lycium	Lycium		wolfberry
Menodora	Menodora	spinescens	spiny menodora
Sarcobatus	Sarcobatus	baileyi	greasewood
Tetradymia	Tetradymia		horsebush

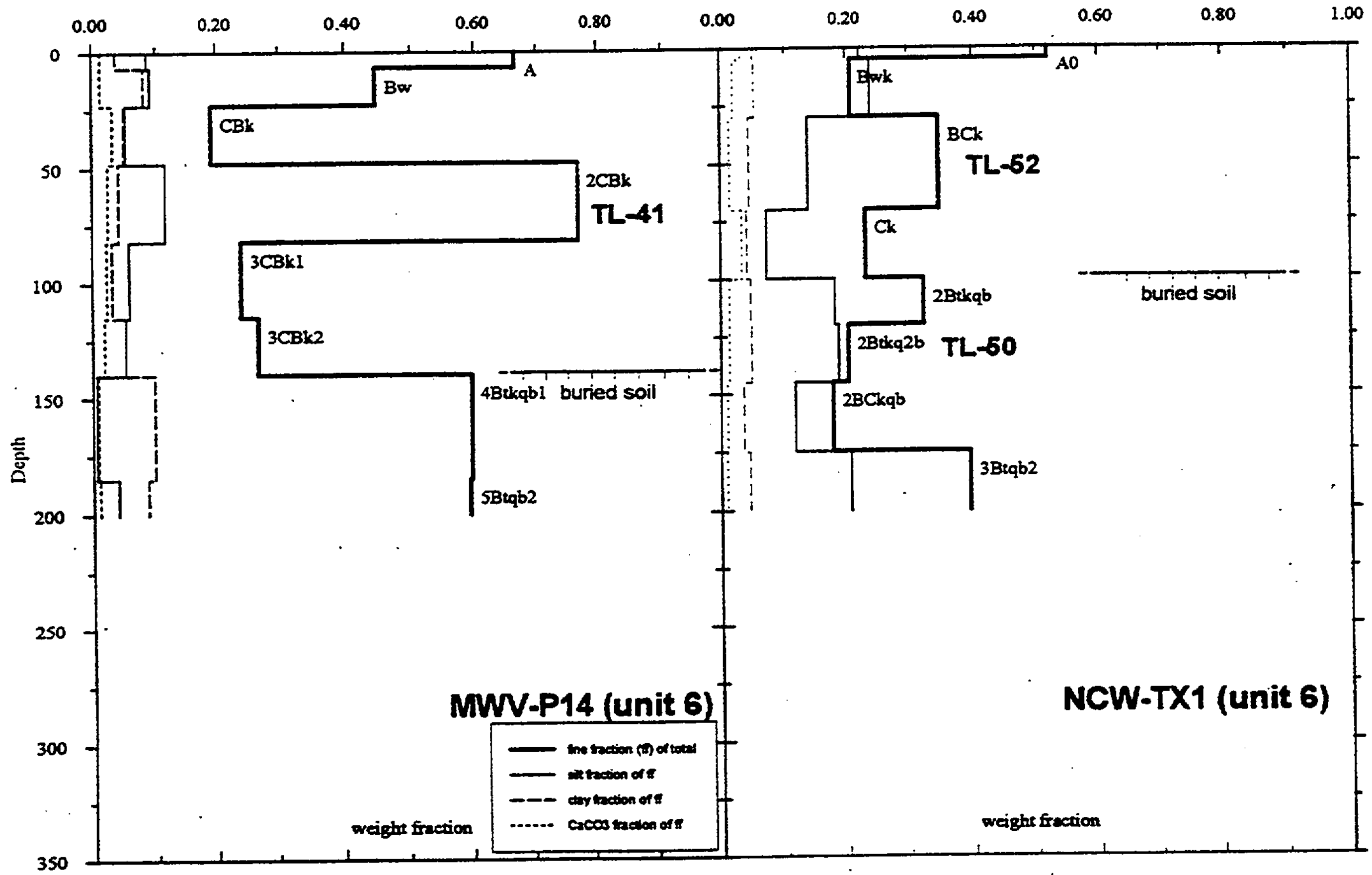

0.00
0.20
0.40
0.60
0.80
0.00
0.20
0.40
0.60
0.80
1.00
0
50
100
150
200
250
300
350
Depth
A
Bw
CBk
2CBk
TL-41
3CBk1
3CBk2
4Btkqb1
buried soil
5Btqb2
A0
Bwk
BCk
TL-52
Ck
2Btkqb
buried soil
2Btkq2b
TL-50
2BCkqb
3Btqb2
MWV-P14 (unit 6)
NCW-TX1 (unit 6)
fine fraction (ff) of total
silt fraction of ff
clay fraction of ff
CaCO3 fraction of ff
weight fraction
weight fraction

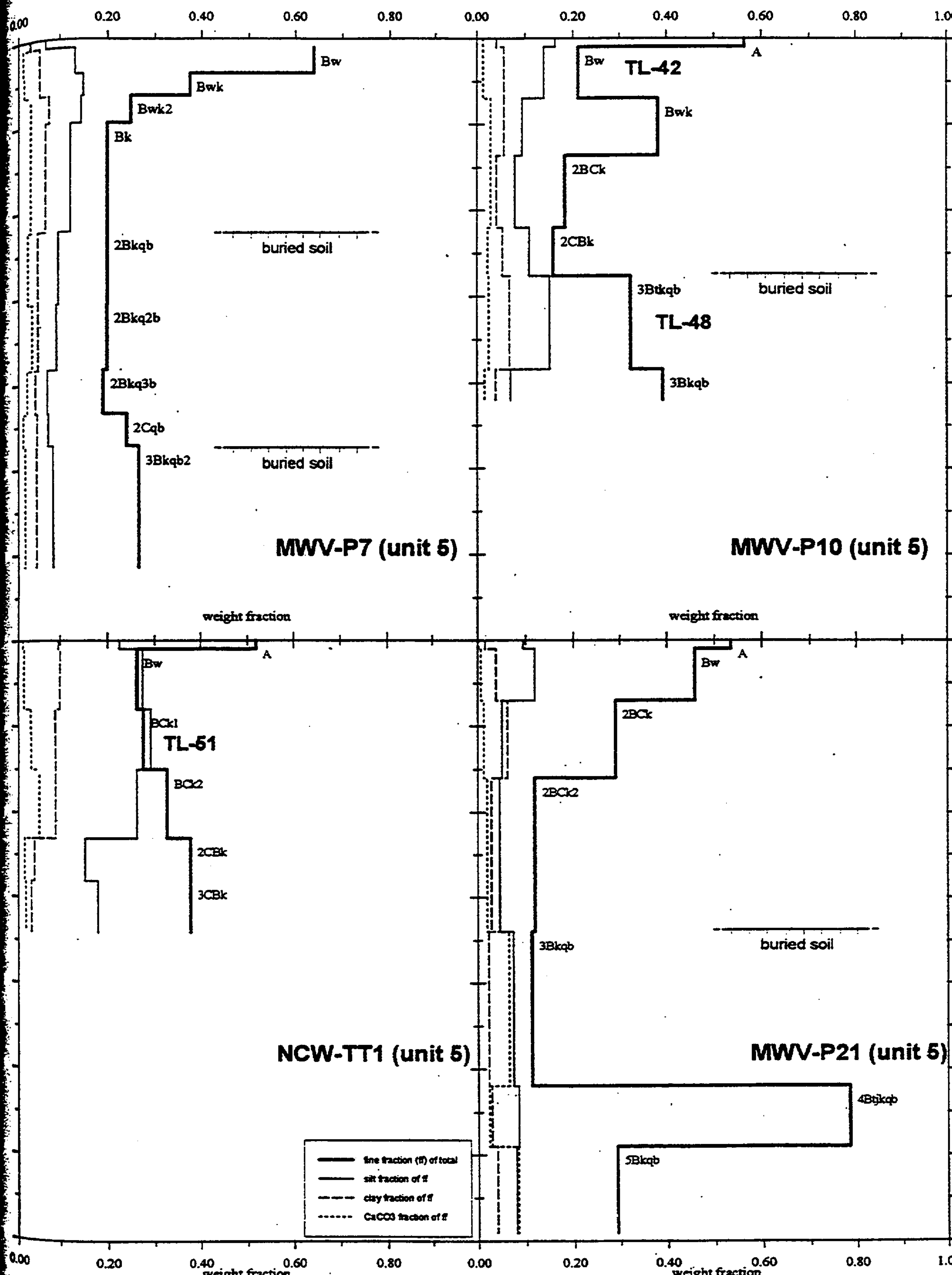

MWV-P7 (unit 5)
MWV-P10 (unit 5)
NCW-TT1 (unit 5)
MWV-P21 (unit 5)
TL-42
TL-48
TL-51
buried soil
weight fraction
fine fraction (ff) of total
silt fraction of ff
clay fraction of ff
CaCO3 fraction of ff

2

Figure 2

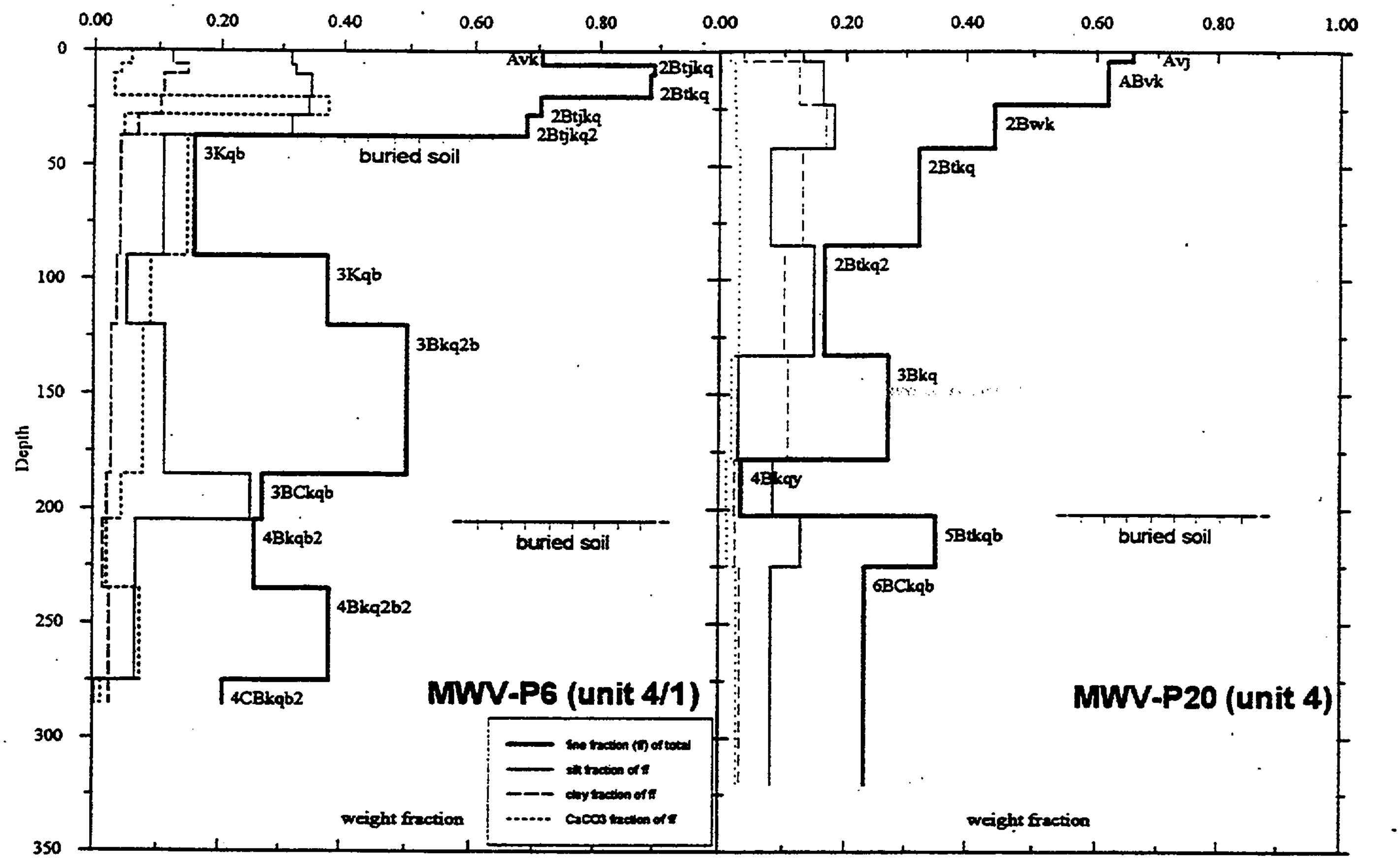

0.00
0.20
0.40
0.60
0.80
0.00
0.20
0.40
0.60
0.80
1.00
Depth
0
50
100
150
200
250
300
350
Avk
2Btjkq
2Btkq
2Btjkq
2Btjkq2
3Kqb
buried soil
3Kqb
3Bkq2b
3BCkqb
4Bkqb2
buried soil
4Bkq2b2
4CBkqb2
MWV-P6 (unit 4/1)
fine fraction (ff) of total
silt fraction of ff
clay fraction of ff
CaCO3 fraction of ff
weight fraction
Avj
ABvk
2Bwk
2Btkq
2Btkq2
3Bkq
4Bkqy
5Btkqb
buried soil
6BCkqb
MWV-P20 (unit 4)
weight fraction

3

Fig. 3

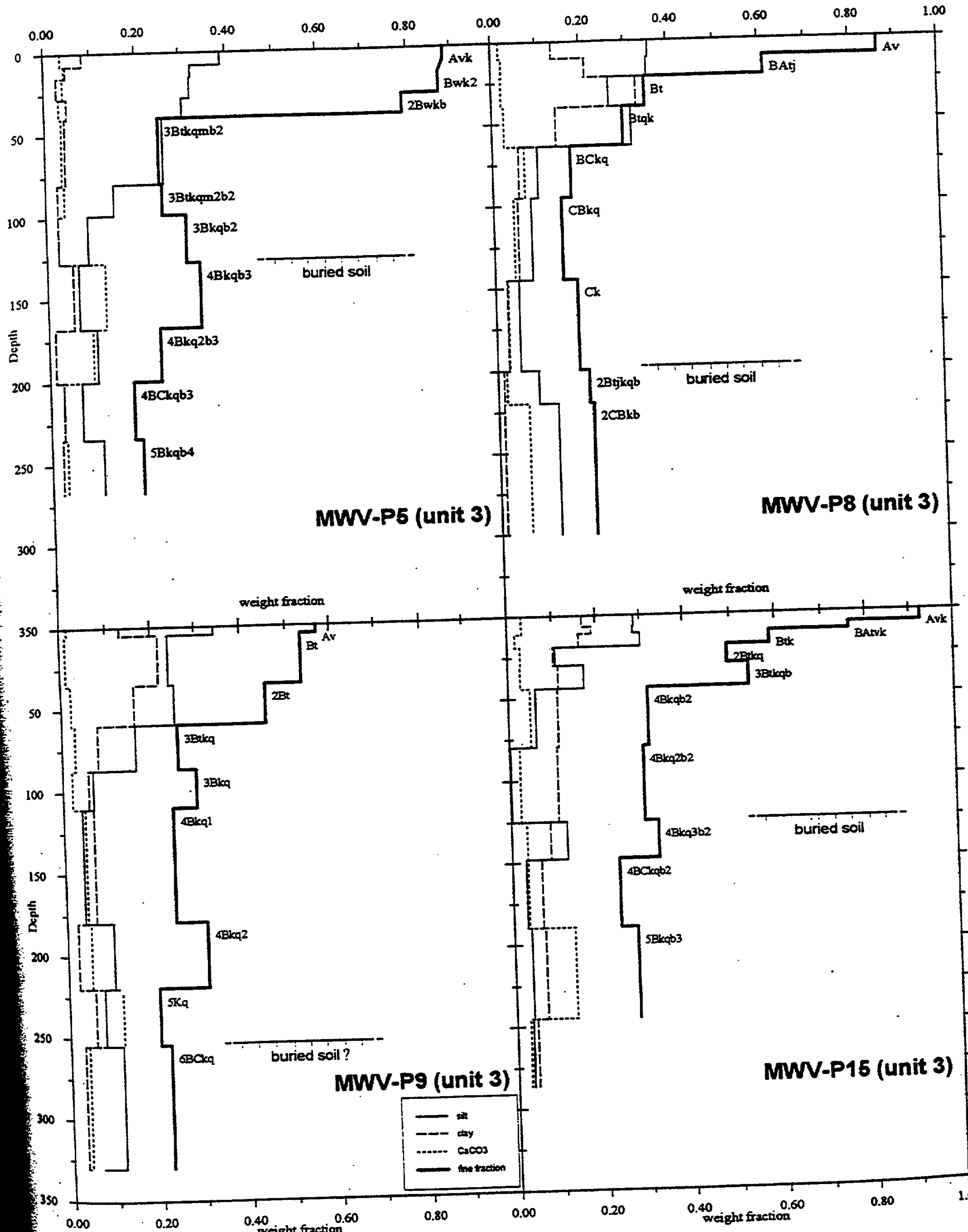
MWV-P5 (unit 3)
MWV-P8 (unit 3)
MWV-P9 (unit 3)
MWV-P15 (unit 3)
Depth
weight fraction
buried soil
buried soil ?
Avk
Bwk2
2Bwkb
3Btkqmb2
3Btkqm2b2
3Bkqb2
4Bkqb3
4Bkq2b3
4BCkqb3
5Bkqb4
Av
BAtj
Bt
Btqk
BCkq
CBkq
Ck
2Btjkqb
2CBkb
Av
Bt
2Bt
3Btkq
3Bkq
4Bkq1
4Bkq2
5Kq
6BCkq
Avk
BAtvk
Btk
2Btkq
3Btkqb
4Bkqb2
4Bkq2b2
4Bkq3b2
4BCkqb2
5Bkqb3
silt
clay
CaCO3
fine fraction

4a

Fig. 4

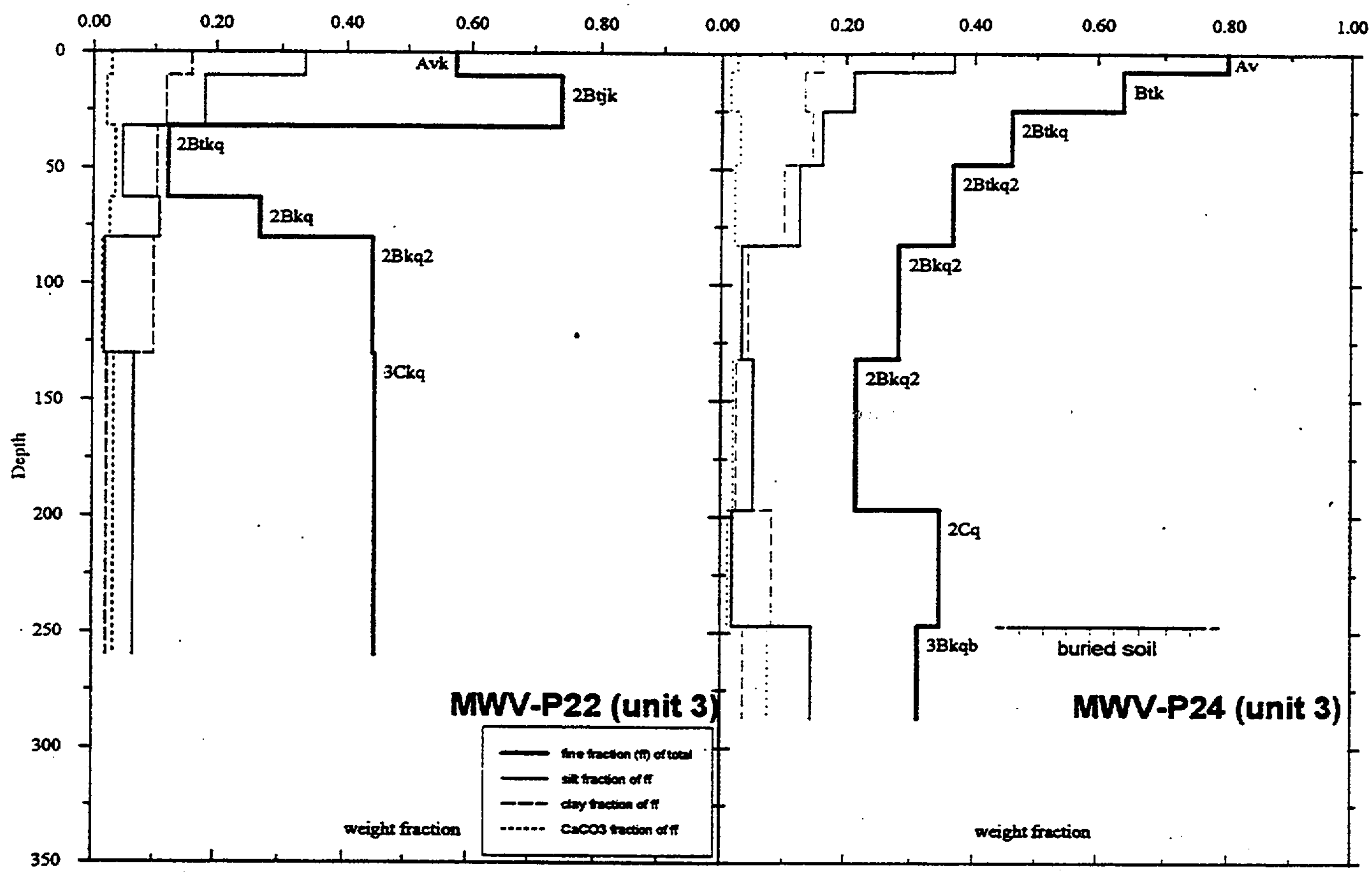

MWV-P22 (unit 3)
MWV-P24 (unit 3)
Depth
weight fraction
weight fraction
Avk
2Btjk
2Btkq
2Bkq
2Bkq2
3Ckq
Av
Btk
2Btkq
2Btkq2
2Bkq2
2Bkq2
2Cq
3Bkqb
buried soil
fine fraction (ff) of total
silt fraction of ff
clay fraction of ff
CaCO3 fraction of ff

46

F. 42

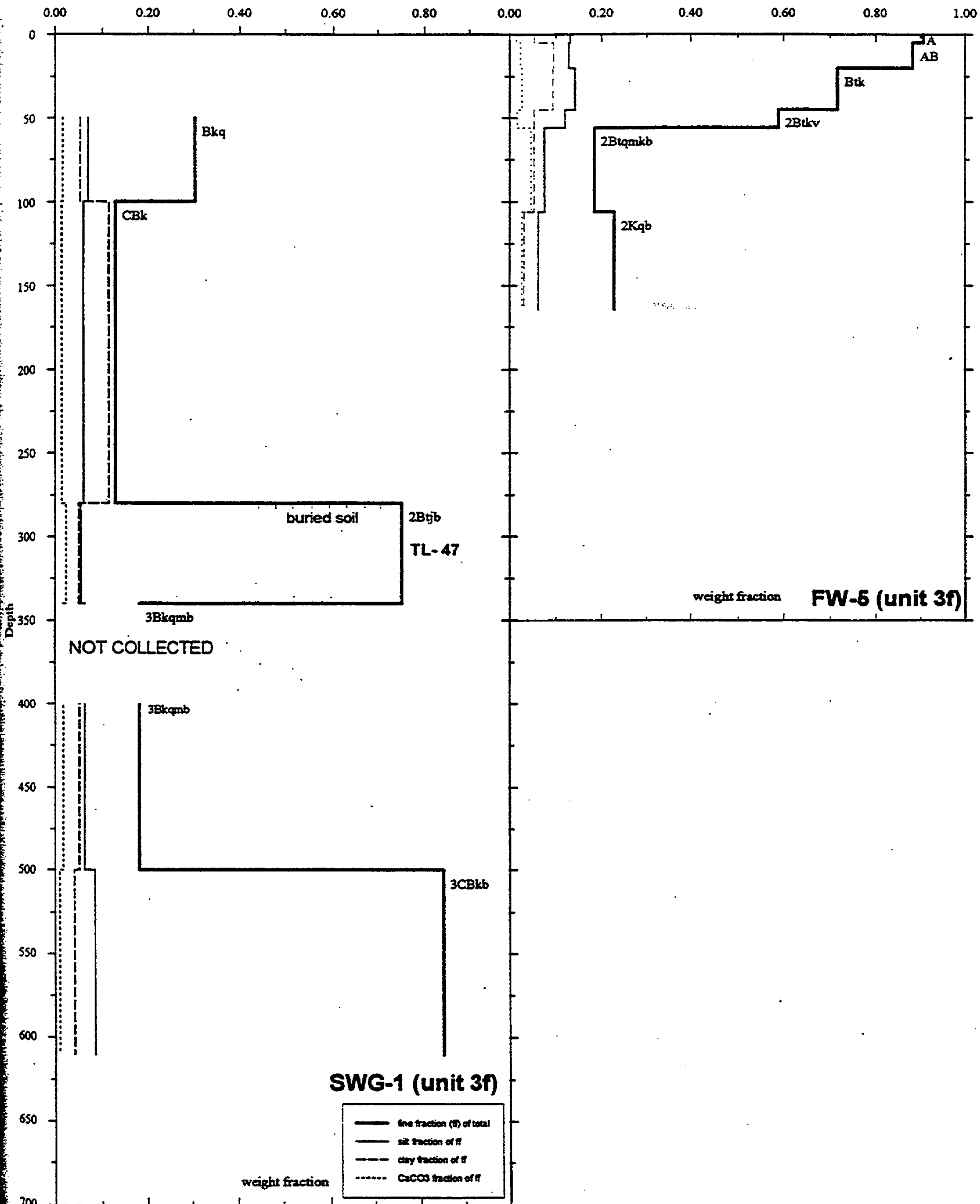

0.00
0.20
0.40
0.60
0.80
0.00
0.20
0.40
0.60
0.80
1.00
0
50
100
150
200
250
300
350
400
450
500
550
600
650
700
Depth
Bkq
CBk
buried soil
2Btjb
TL-47
3Bkqmb
NOT COLLECTED
3Bkqmb
3CBkb
SWG-1 (unit 3f)
fine fraction (ff) of total
silt fraction of ff
clay fraction of ff
CaCO3 fraction of ff
weight fraction
A
AB
Btk
2Btkv
2Btqmkb
2Kqb
weight fraction
FW-5 (unit 3f)

4c

Fig 4c

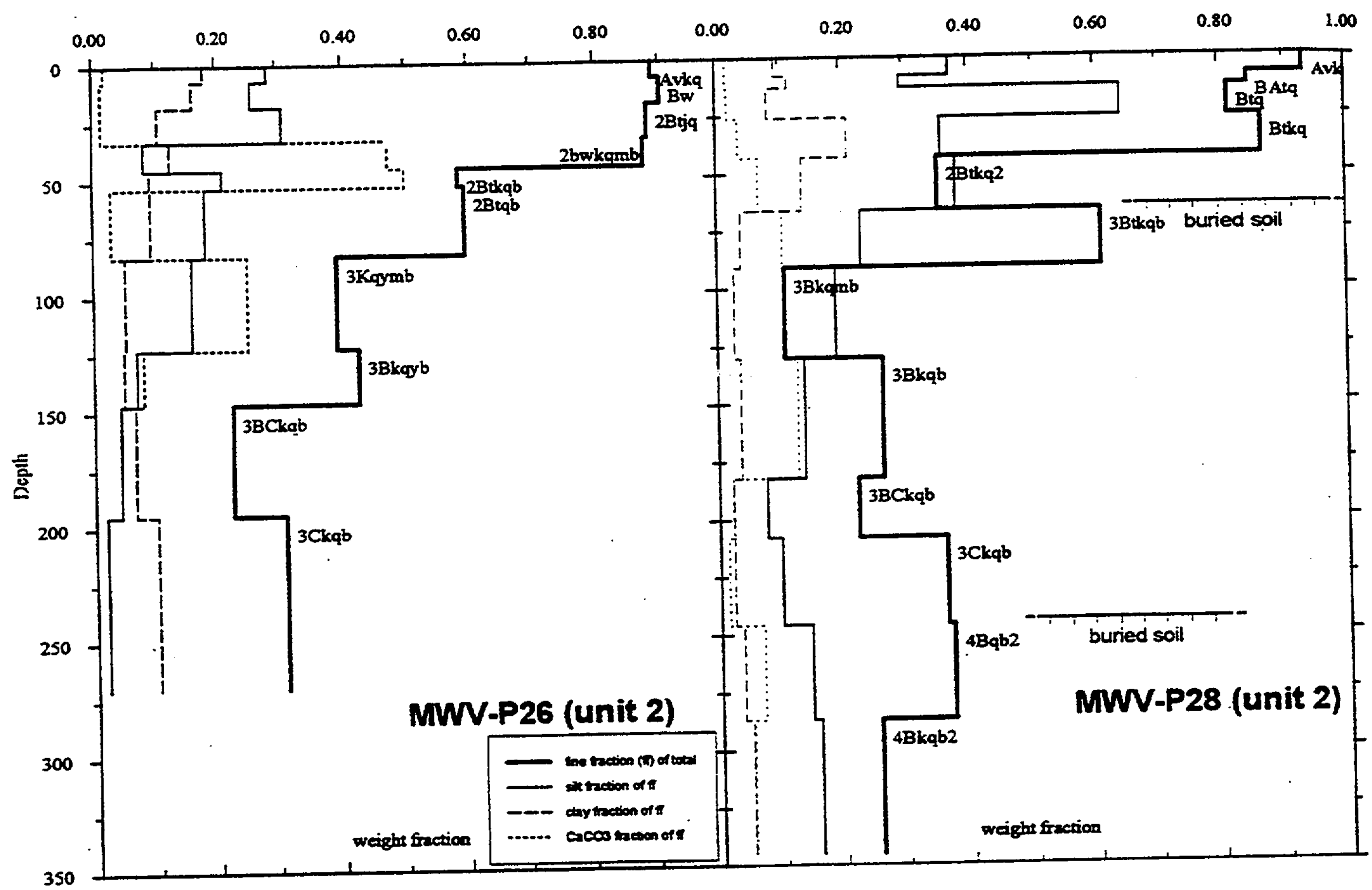

MWV-P26 (unit 2)
MWV-P28 (unit 2)
Depth
weight fraction
weight fraction
0.00
0.20
0.40
0.60
0.80
1.00
0
50
100
150
200
250
300
350
fine fraction (ff) of total
silt fraction of ff
clay fraction of ff
CaCO3 fraction of ff
Avkq
Bw
2Btjq
2bwkqmb
2Btkqb
2Btqb
3Kqymb
3Bkqyb
3BCkqb
3Ckqb
Avk
BAtq
Btq
Btkq
2Btkq2
3Btkqb
buried soil
3Bkqmb
3Bkqb
3BCkqb
3Ckqb
4Bqb2
buried soil
4Bkqb2

5

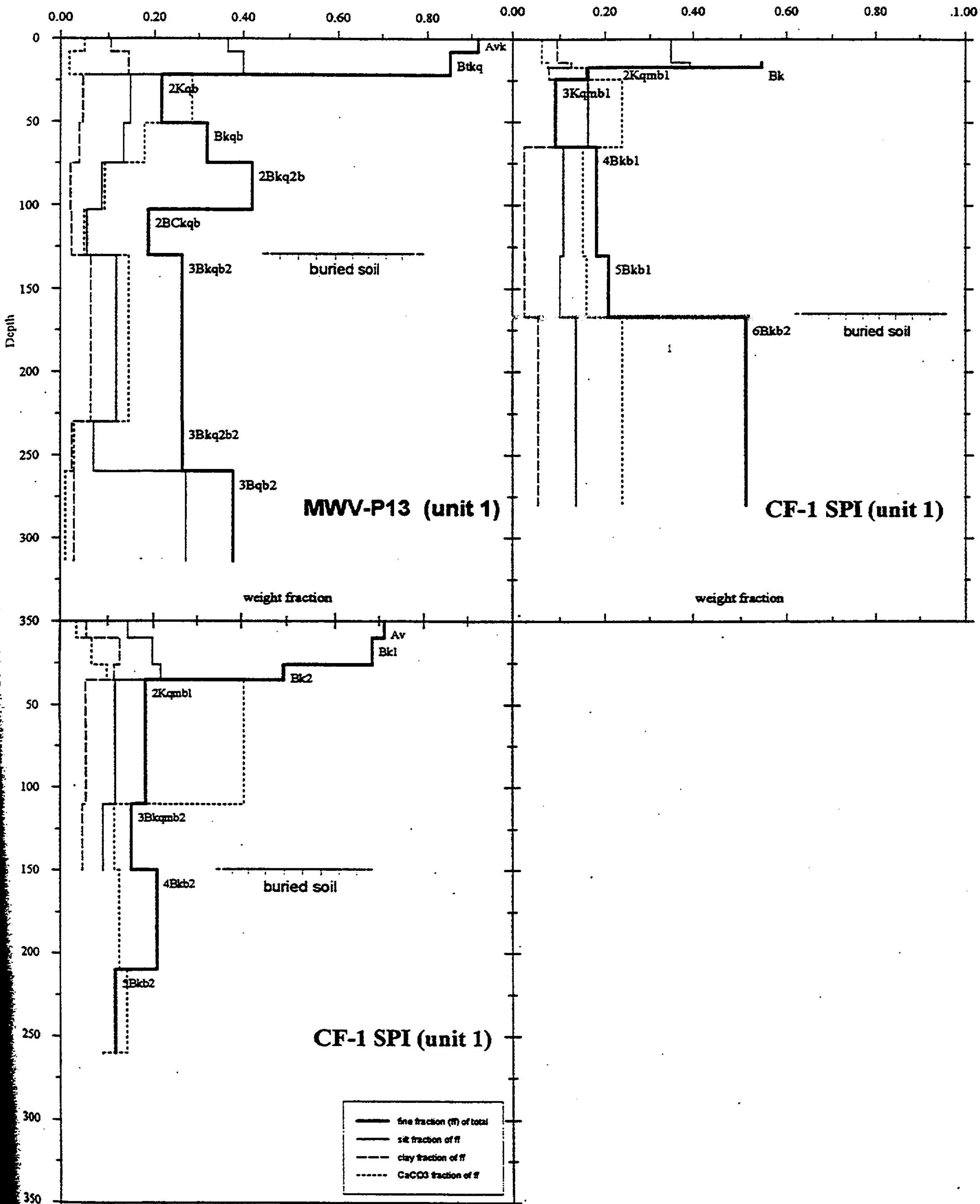
MWV-P13 (unit 1)
CF-1 SPI (unit 1)
CF-1 SPI (unit 1)
Depth
weight fraction
weight fraction
buried soil
buried soil
buried soil
Avk
Btkq
2Kqb
Bkqb
2Bkq2b
2BCkqb
3Bkqb2
3Bkq2b2
3Bqb2
Bk
2Kqmb1
3Kqmb1
4Bkb1
5Bkb1
6Bkb2
Av
Bk1
Bk2
2Kqmb1
3Bkqmb2
4Bkb2
5Bkb2
fine fraction (ff) of total
silt fraction of ff
clay fraction of ff
CaCO3 fraction of ff

6a

Fig 6a

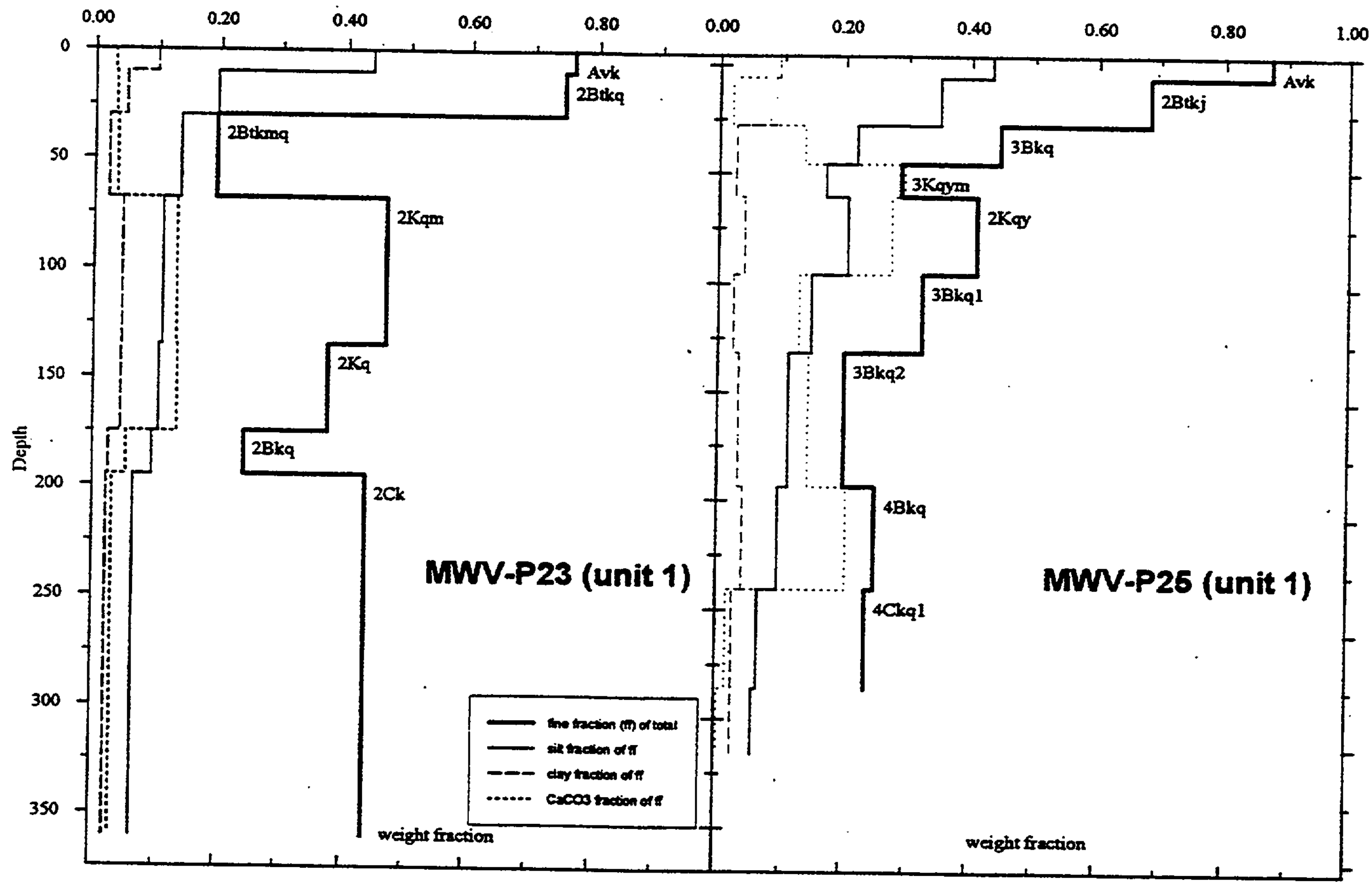

0.00
0.20
0.40
0.60
0.80
1.00
0
50
100
150
200
250
300
350
Depth
Avk
2Btkq
2Btkmq
2Kqm
2Kq
2Bkq
2Ck
MWV-P23 (unit 1)
fine fraction (ff) of total
silt fraction of ff
clay fraction of ff
CaCO3 fraction of ff
weight fraction
Avk
2Btkj
3Bkq
3Kqym
2Kqy
3Bkq1
3Bkq2
4Bkq
4Ckq1
MWV-P25 (unit 1)
weight fraction

66

Fig 6:

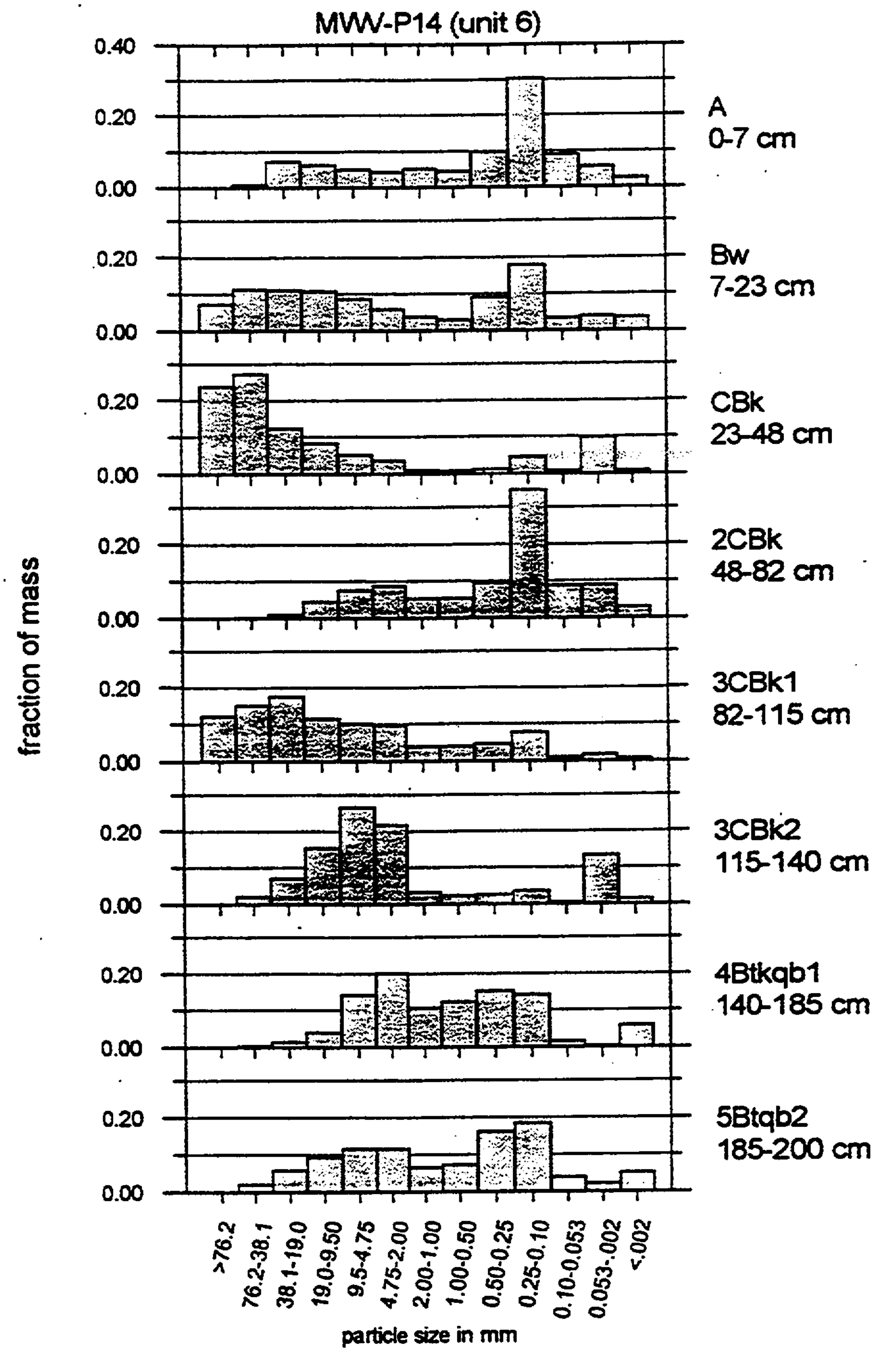
MWV-P14 (unit 6)
fraction of mass
0.40
0.20
0.00
A
0-7 cm
Bw
7-23 cm
CBk
23-48 cm
2CBk
48-82 cm
3CBk1
82-115 cm
3CBk2
115-140 cm
4Btkqb1
140-185 cm
5Btqb2
185-200 cm
>76.2
76.2-38.1
38.1-19.0
19.0-9.50
9.5-4.75
4.75-2.00
2.00-1.00
1.00-0.50
0.50-0.25
0.25-0.10
0.10-0.053
0.053-.002
<.002
particle size in mm

7

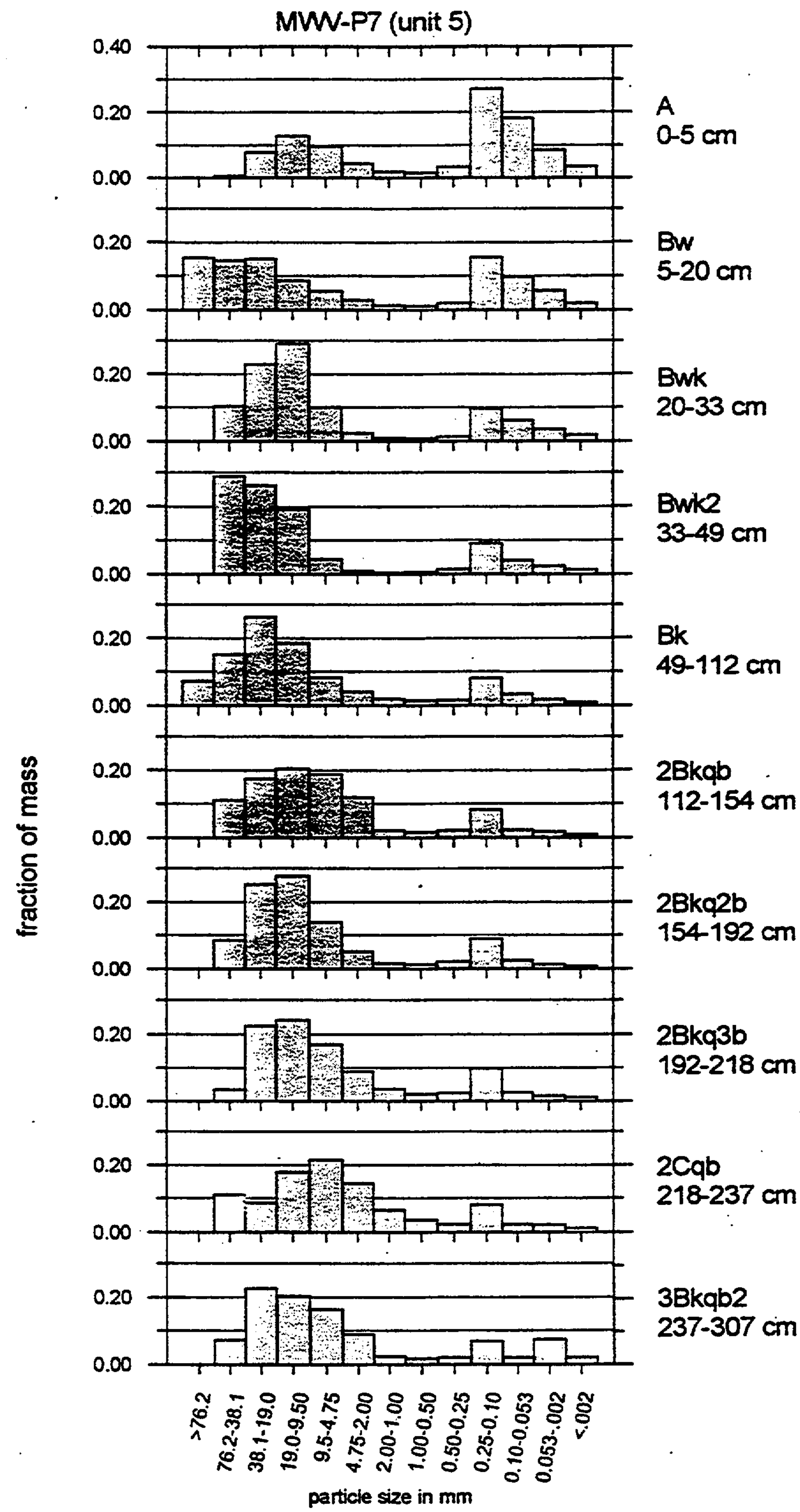
MWV-P7 (unit 5)
fraction of mass
0.40
0.20
0.00
A
0-5 cm
Bw
5-20 cm
Bwk
20-33 cm
Bwk2
33-49 cm
Bk
49-112 cm
2Bkqb
112-154 cm
2Bkq2b
154-192 cm
2Bkq3b
192-218 cm
2Cqb
218-237 cm
3Bkqb2
237-307 cm
>76.2
76.2-38.1
38.1-19.0
19.0-9.50
9.5-4.75
4.75-2.00
2.00-1.00
1.00-0.50
0.50-0.25
0.25-0.10
0.10-0.053
0.053-.002
<.002
particle size in mm

89

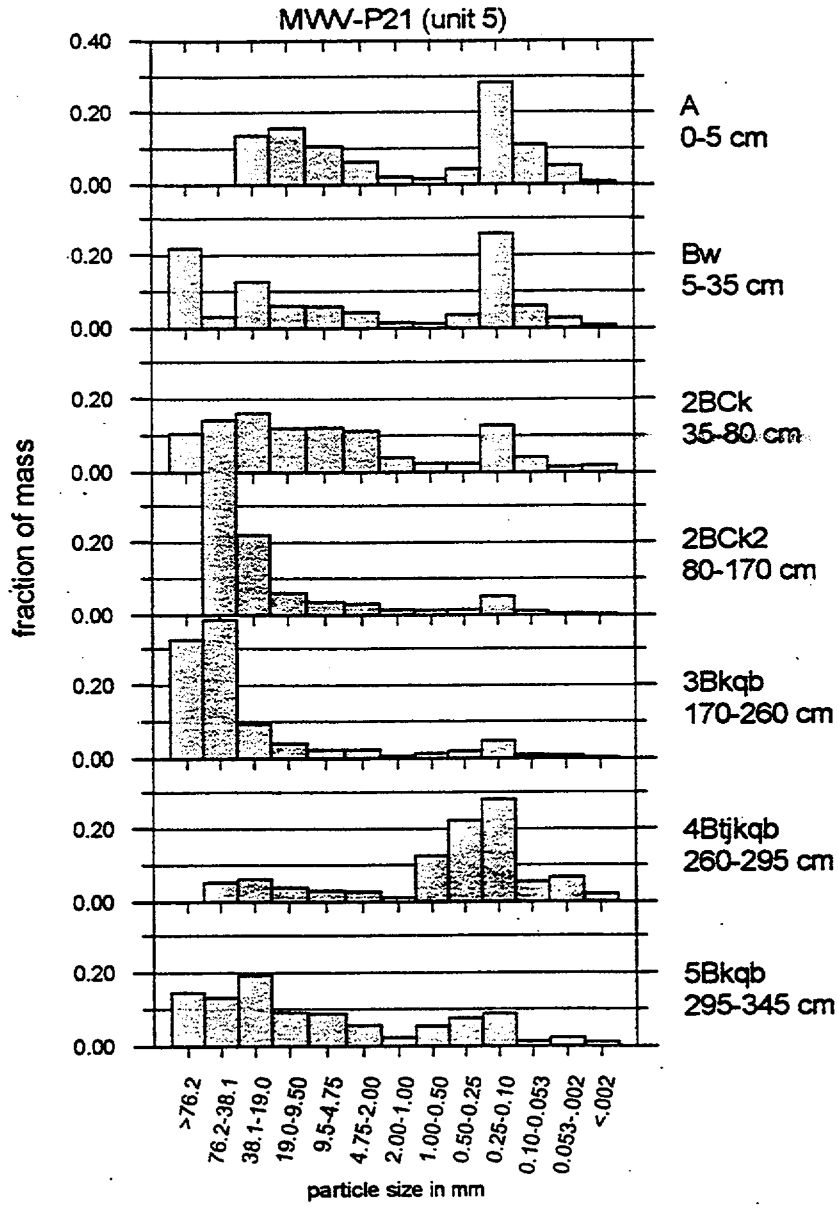

MWV-P21 (unit 5)
fraction of mass
0.40
0.20
0.00
A
0-5 cm
Bw
5-35 cm
2BCk
35-80 cm
2BCk2
80-170 cm
3Bkqb
170-260 cm
4Btjkqb
260-295 cm
5Bkqb
295-345 cm
>76.2
76.2-38.1
38.1-19.0
19.0-9.50
9.5-4.75
4.75-2.00
2.00-1.00
1.00-0.50
0.50-0.25
0.25-0.10
0.10-0.053
0.053-.002
<.002
particle size in mm

8b

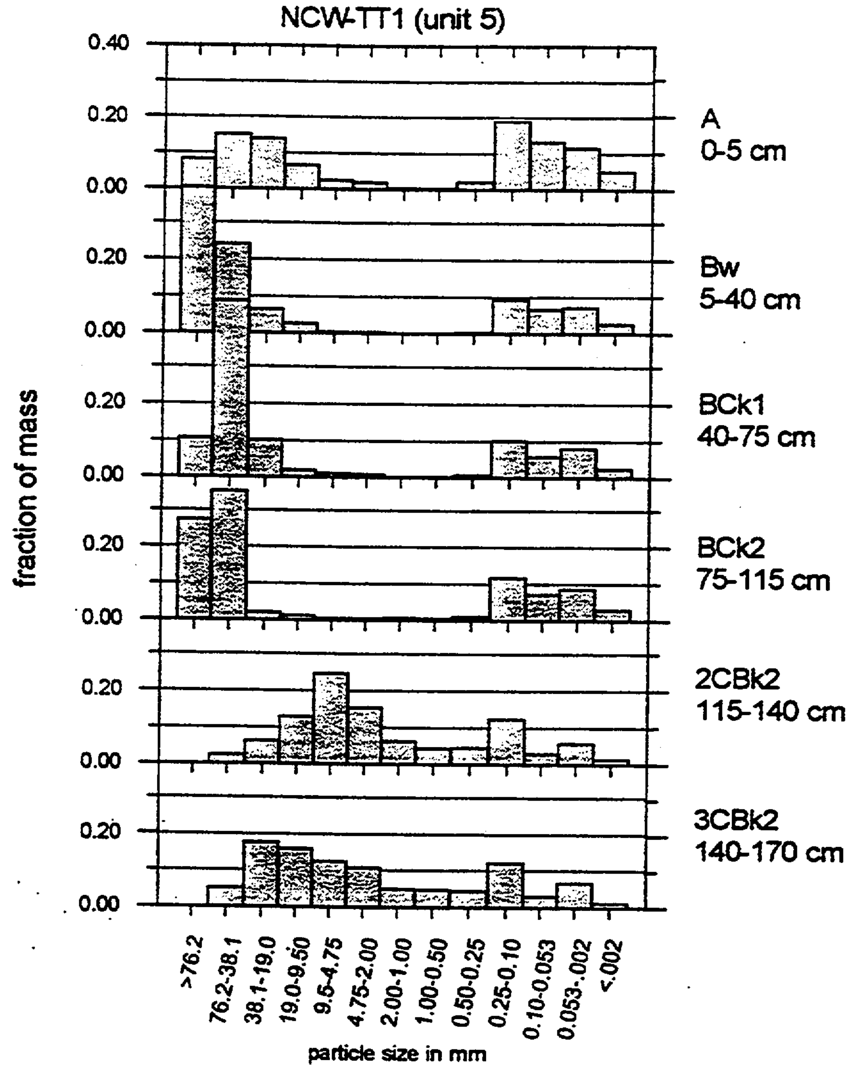
NCW-TT1 (unit 5)
0.40
0.20
0.00
0.20
0.00
0.20
0.00
0.20
0.00
0.20
0.00
0.20
0.00
fraction of mass
A
0-5 cm
Bw
5-40 cm
BCk1
40-75 cm
BCk2
75-115 cm
2CBk2
115-140 cm
3CBk2
140-170 cm
>76.2
76.2-38.1
38.1-19.0
19.0-9.50
9.5-4.75
4.75-2.00
2.00-1.00
1.00-0.50
0.50-0.25
0.25-0.10
0.10-0.053
0.053-.002
<.002
particle size in mm

8c

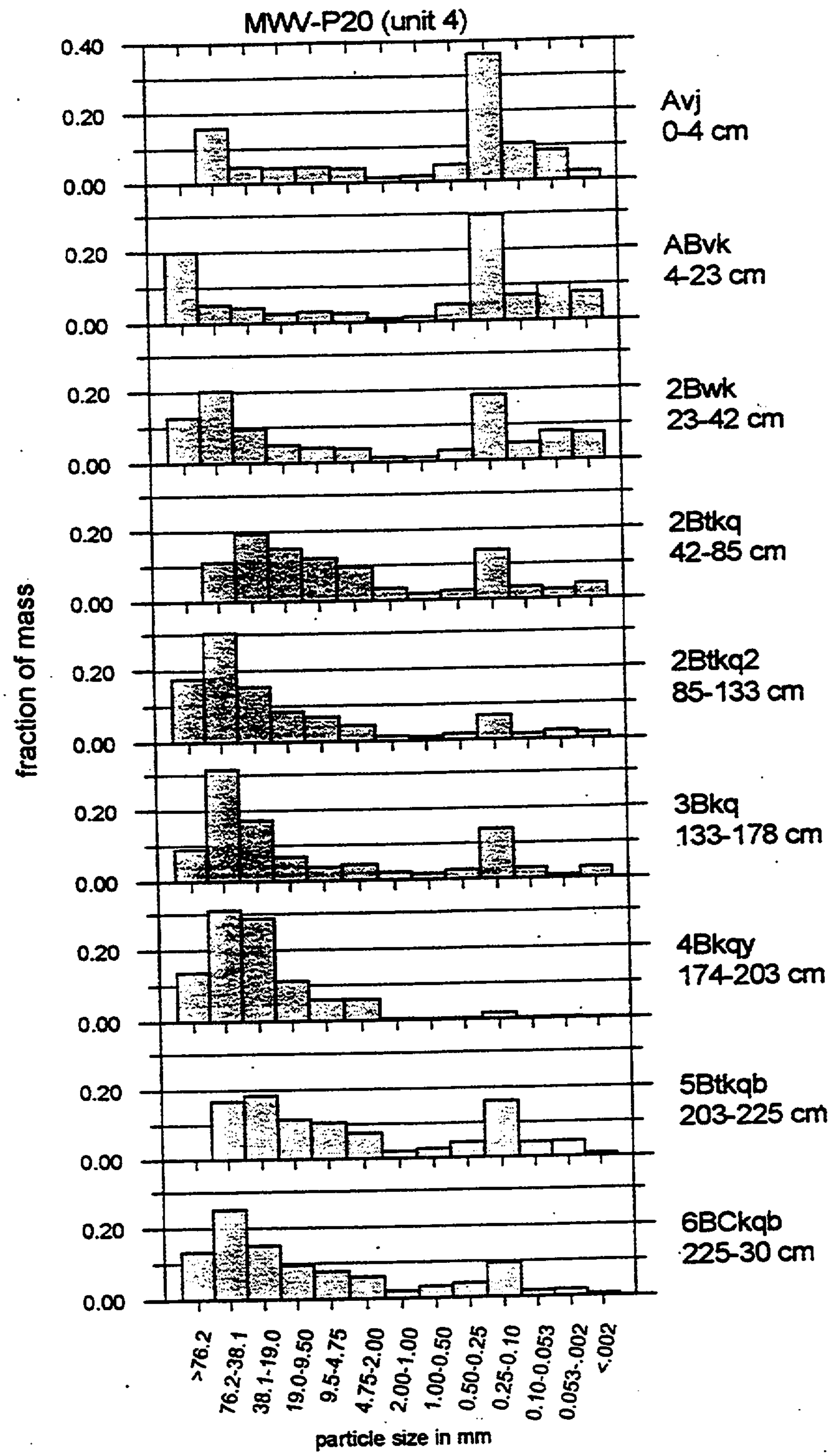

MWV-P20 (unit 4)
0.40
0.20
0.00
fraction of mass
Avj
0-4 cm
ABvk
4-23 cm
2Bwk
23-42 cm
2Btkq
42-85 cm
2Btkq2
85-133 cm
3Bkq
133-178 cm
4Bkqy
174-203 cm
5Btkqb
203-225 cm
6BCkqb
225-30 cm
>76.2
76.2-38.1
38.1-19.0
19.0-9.50
9.5-4.75
4.75-2.00
2.00-1.00
1.00-0.50
0.50-0.25
0.25-0.10
0.10-0.053
0.053-.002
<.002
particle size in mm

9a

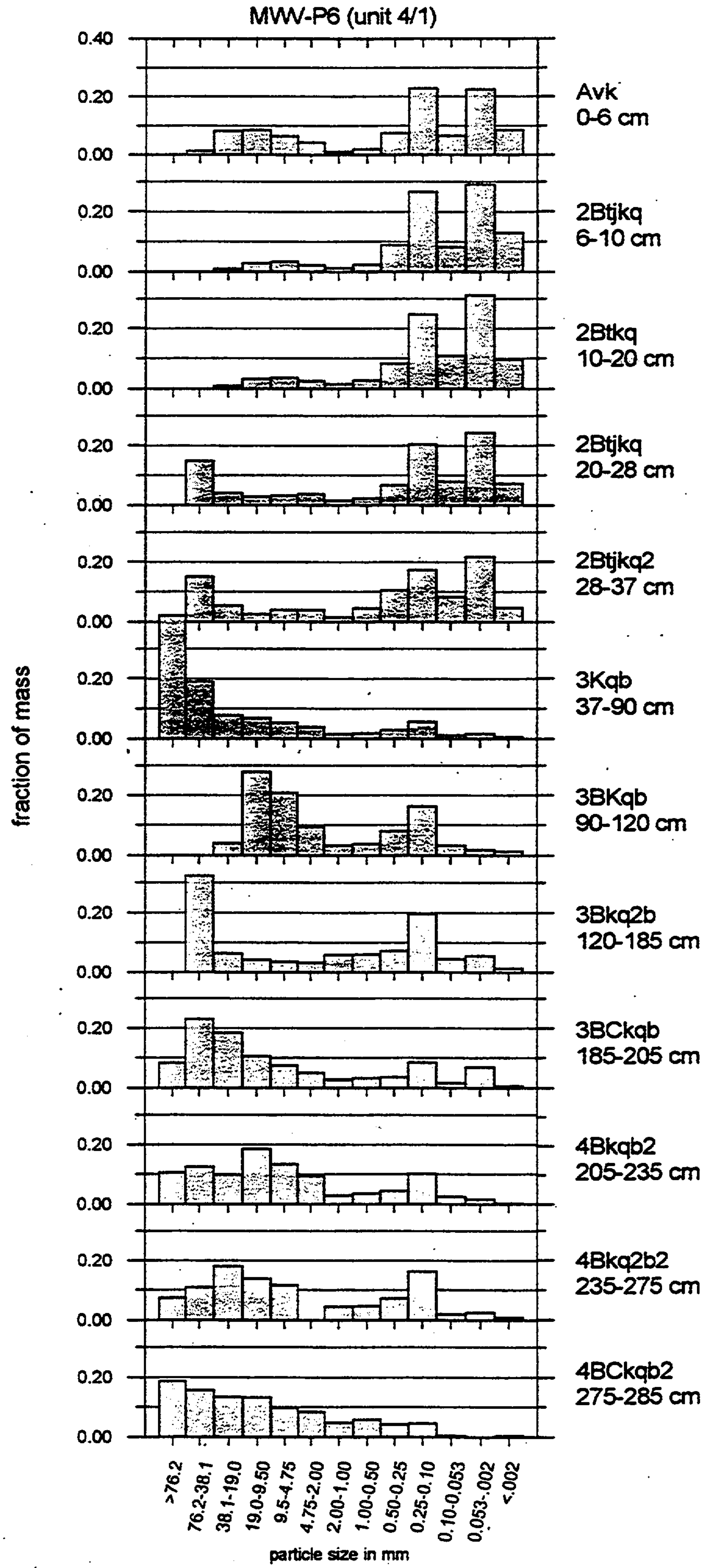

MWV-P6 (unit 4/1)
fraction of mass
0.40
0.20
0.00
Avk
0-6 cm
2Btjkq
6-10 cm
2Btkq
10-20 cm
2Btjkq
20-28 cm
2Btjkq2
28-37 cm
3Kqb
37-90 cm
3BKqb
90-120 cm
3Bkq2b
120-185 cm
3BCkqb
185-205 cm
4Bkqb2
205-235 cm
4Bkq2b2
235-275 cm
4BCkqb2
275-285 cm
>76.2
76.2-38.1
38.1-19.0
19.0-9.50
9.5-4.75
4.75-2.00
2.00-1.00
1.00-0.50
0.50-0.25
0.25-0.10
0.10-0.053
0.053-.002
<.002
particle size in mm

96

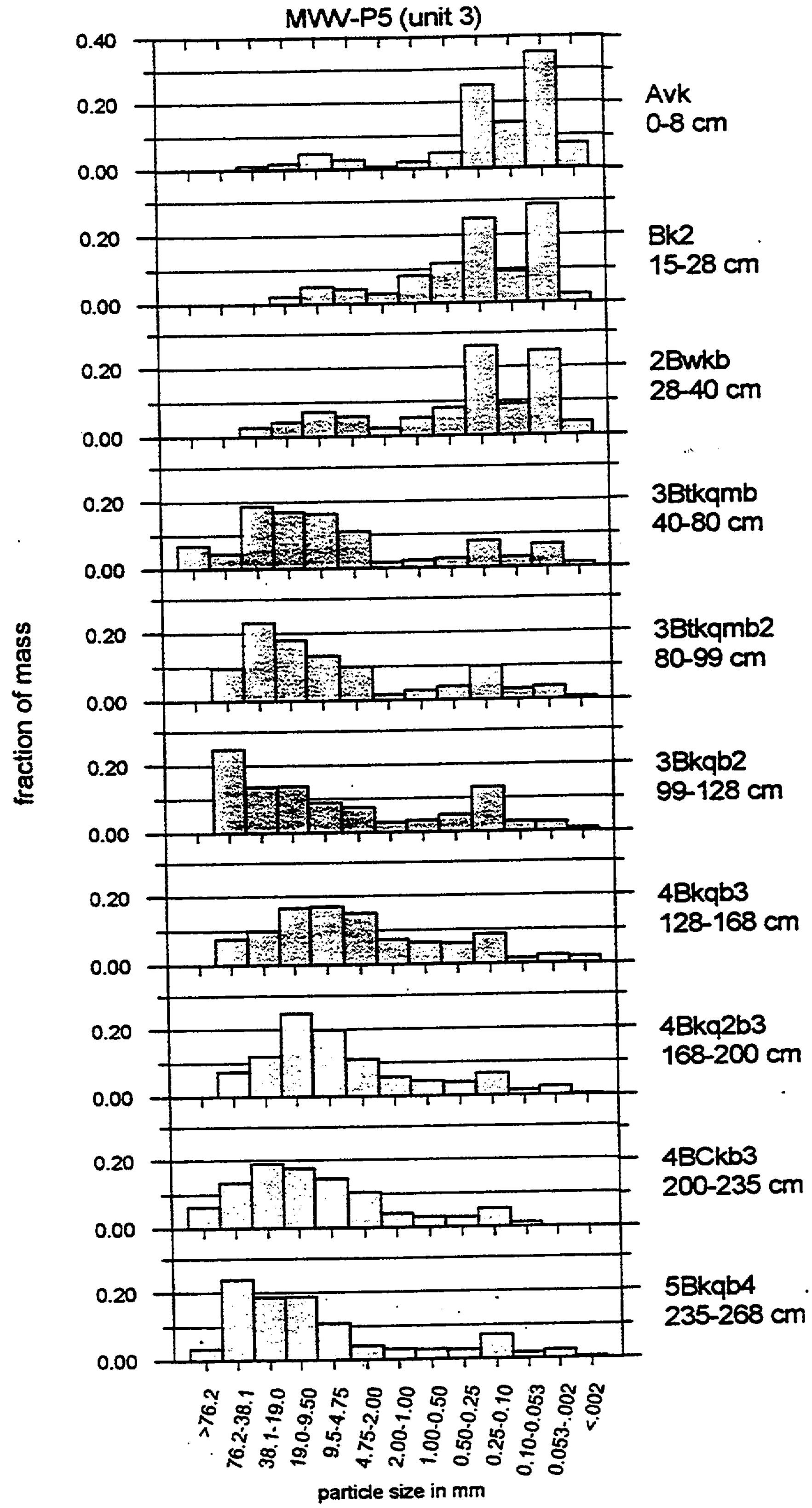

MWV-P5 (unit 3)
fraction of mass
0.40
0.20
0.00
Avk
0-8 cm
Bk2
15-28 cm
2Bwkb
28-40 cm
3Btkqmb
40-80 cm
3Btkqmb2
80-99 cm
3Bkqb2
99-128 cm
4Bkqb3
128-168 cm
4Bkq2b3
168-200 cm
4BCkb3
200-235 cm
5Bkqb4
235-268 cm
>76.2
76.2-38.1
38.1-19.0
19.0-9.50
9.5-4.75
4.75-2.00
2.00-1.00
1.00-0.50
0.50-0.25
0.25-0.10
0.10-0.053
0.053-.002
<.002
particle size in mm

10a

Fig 10

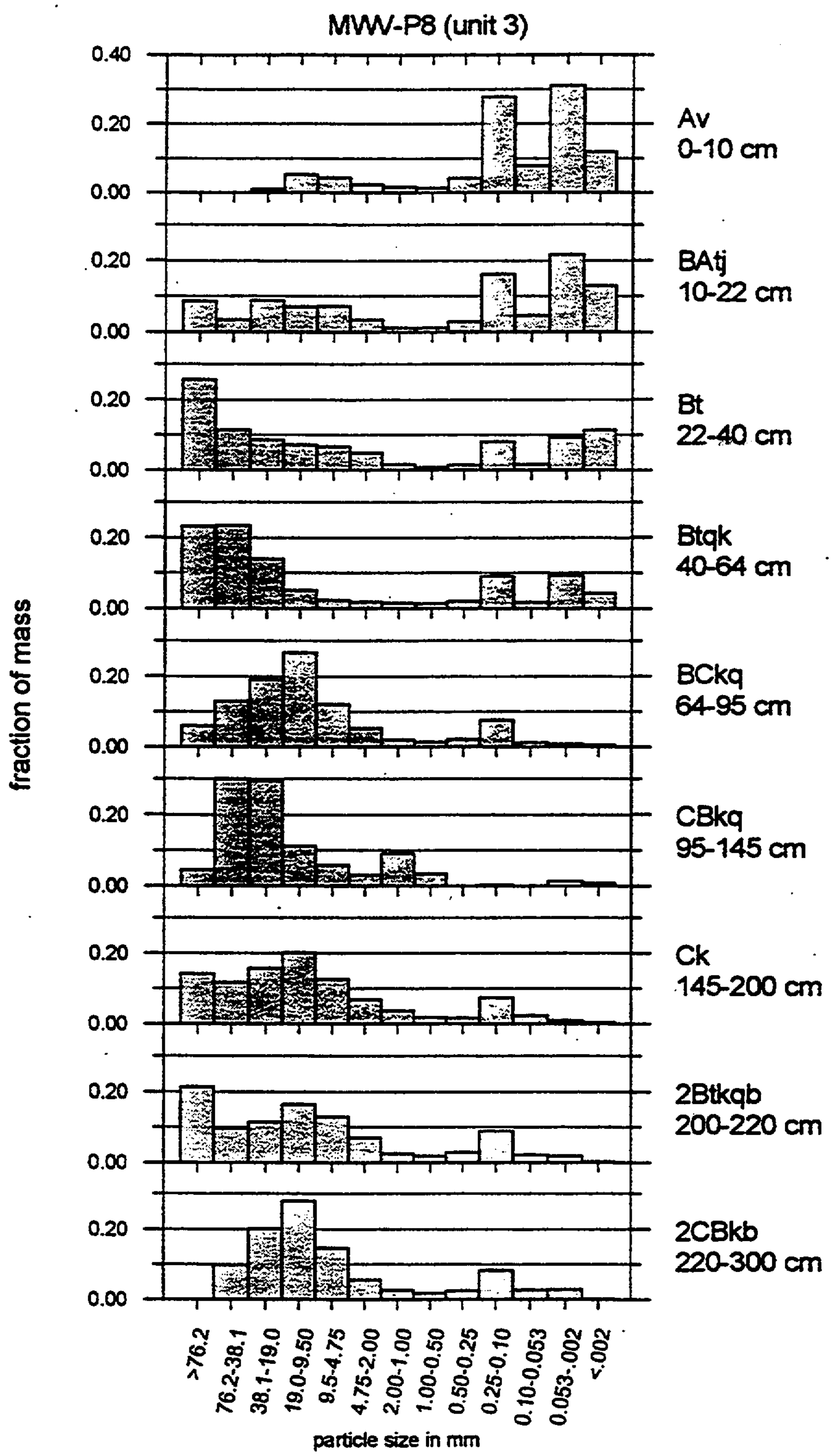

MWV-P8 (unit 3)
fraction of mass
0.40
0.20
0.00
Av
0-10 cm
BAtj
10-22 cm
Bt
22-40 cm
Btqk
40-64 cm
BCkq
64-95 cm
CBkq
95-145 cm
Ck
145-200 cm
2Btkqb
200-220 cm
2CBkb
220-300 cm
>76.2
76.2-38.1
38.1-19.0
19.0-9.50
9.5-4.75
4.75-2.00
2.00-1.00
1.00-0.50
0.50-0.25
0.25-0.10
0.10-0.053
0.053-.002
<.002
particle size in mm

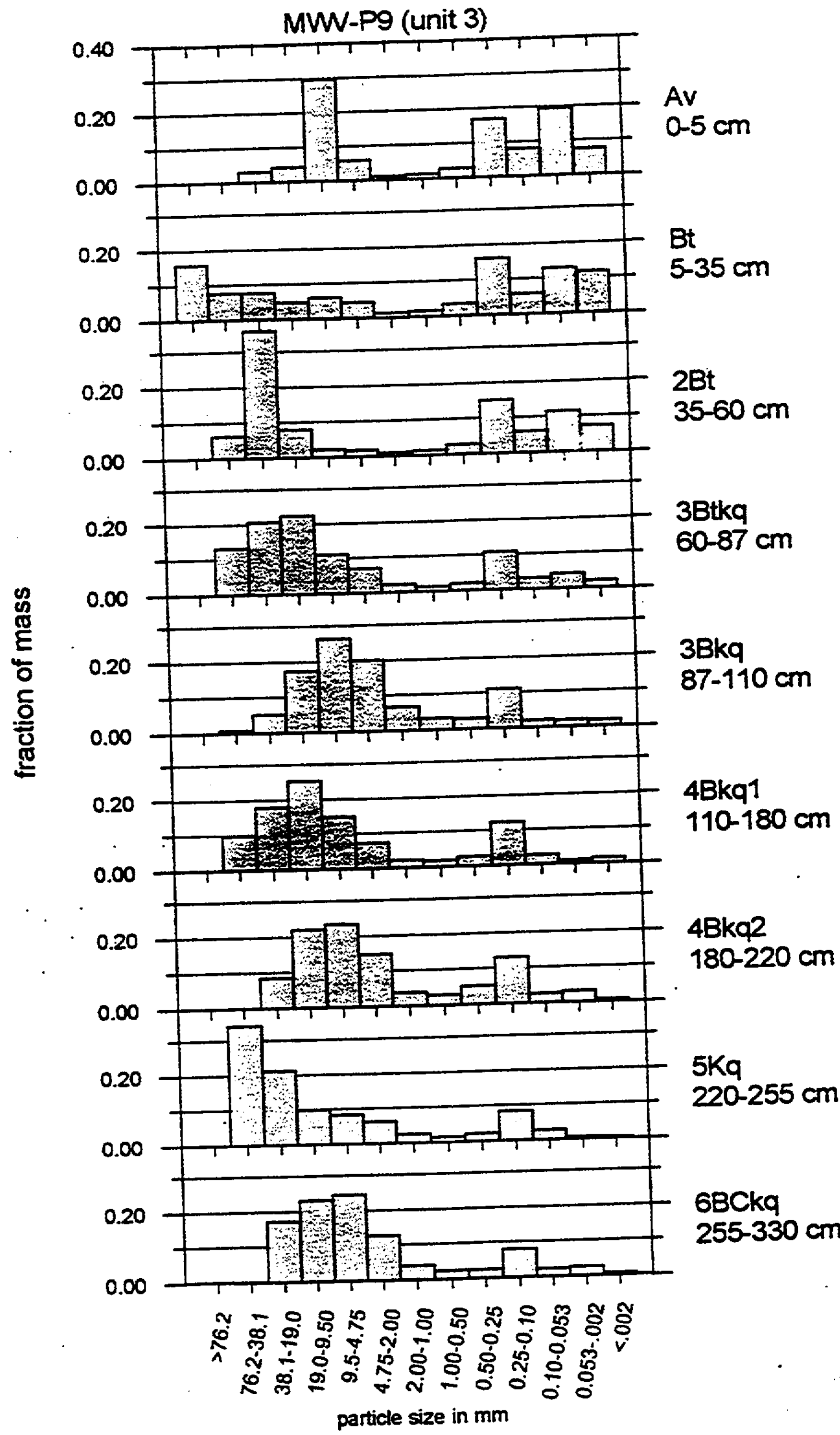
MWV-P9 (unit 3)
fraction of mass
0.40
0.20
0.00
Av
0-5 cm
Bt
5-35 cm
2Bt
35-60 cm
3Btkq
60-87 cm
3Bkq
87-110 cm
4Bkq1
110-180 cm
4Bkq2
180-220 cm
5Kq
220-255 cm
6BCkq
255-330 cm
>76.2
76.2-38.1
38.1-19.0
19.0-9.50
9.5-4.75
4.75-2.00
2.00-1.00
1.00-0.50
0.50-0.25
0.25-0.10
0.10-0.053
0.053-.002
<.002
particle size in mm

10c

Fi. 10

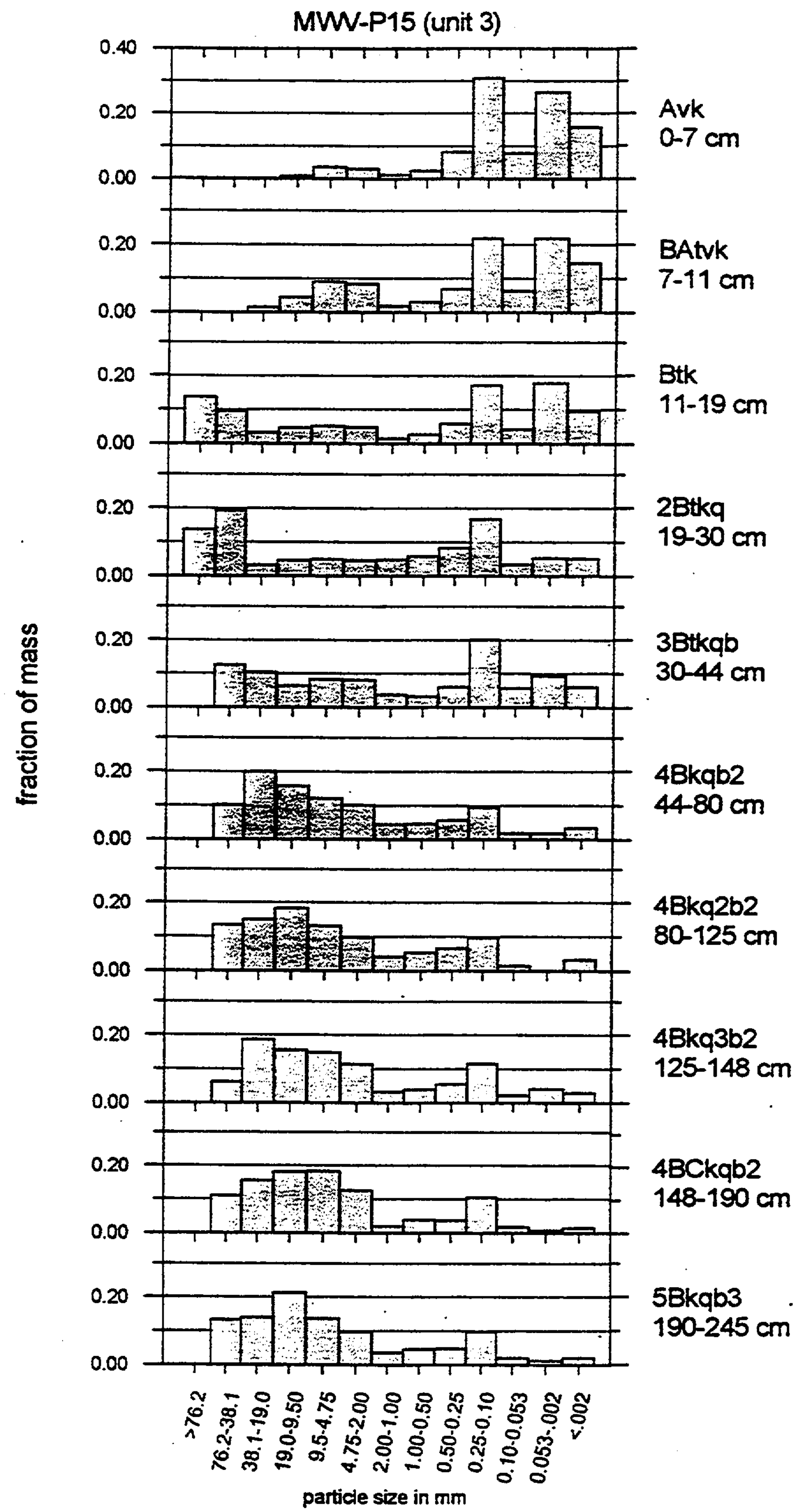
MWV-P15 (unit 3)
fraction of mass
0.40
0.20
0.00
Avk
0-7 cm
BAtvk
7-11 cm
Btk
11-19 cm
2Btkq
19-30 cm
3Btkqb
30-44 cm
4Bkqb2
44-80 cm
4Bkq2b2
80-125 cm
4Bkq3b2
125-148 cm
4BCkqb2
148-190 cm
5Bkqb3
190-245 cm
>76.2
76.2-38.1
38.1-19.0
19.0-9.50
9.5-4.75
4.75-2.00
2.00-1.00
1.00-0.50
0.50-0.25
0.25-0.10
0.10-0.053
0.053-.002
<.002
particle size in mm

10d

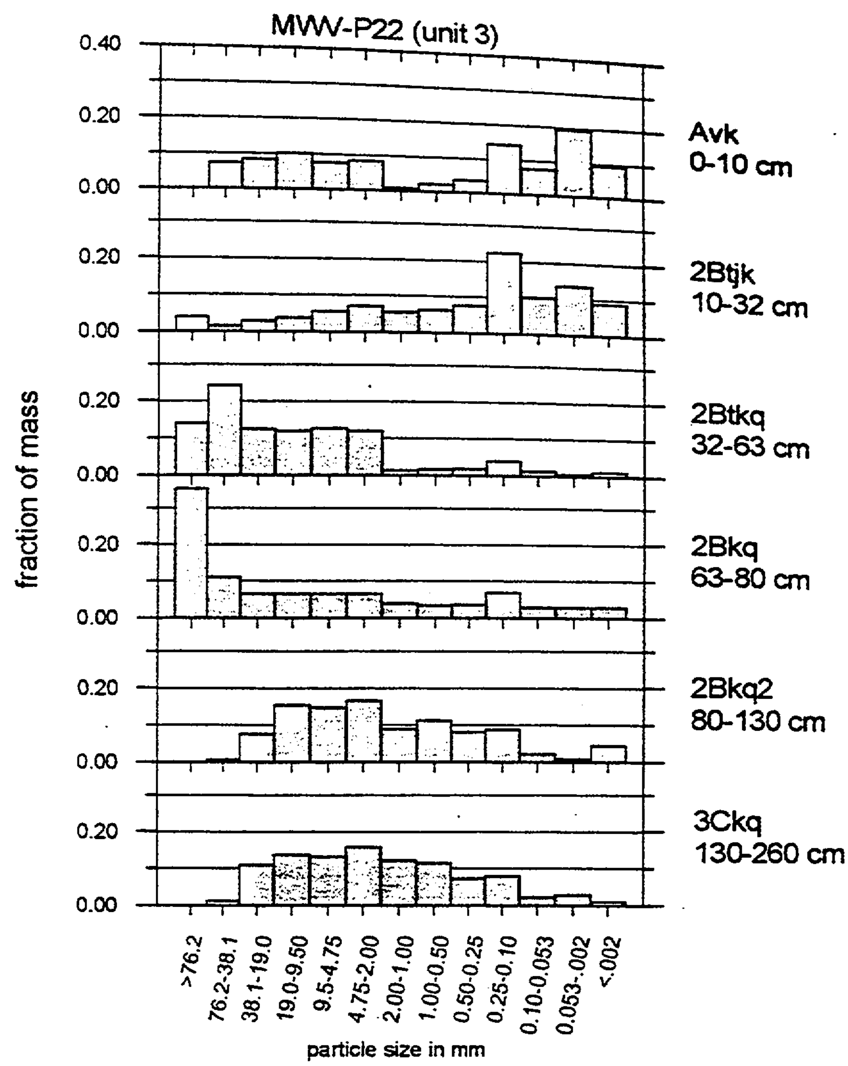
MWV-P22 (unit 3)
fraction of mass
0.40
0.20
0.00
Avk
0-10 cm
2Btjk
10-32 cm
2Btkq
32-63 cm
2Bkq
63-80 cm
2Bkq2
80-130 cm
3Ckq
130-260 cm
>76.2
76.2-38.1
38.1-19.0
19.0-9.50
9.5-4.75
4.75-2.00
2.00-1.00
1.00-0.50
0.50-0.25
0.25-0.10
0.10-0.053
0.053-.002
<.002
particle size in mm

10e

Fig 10e

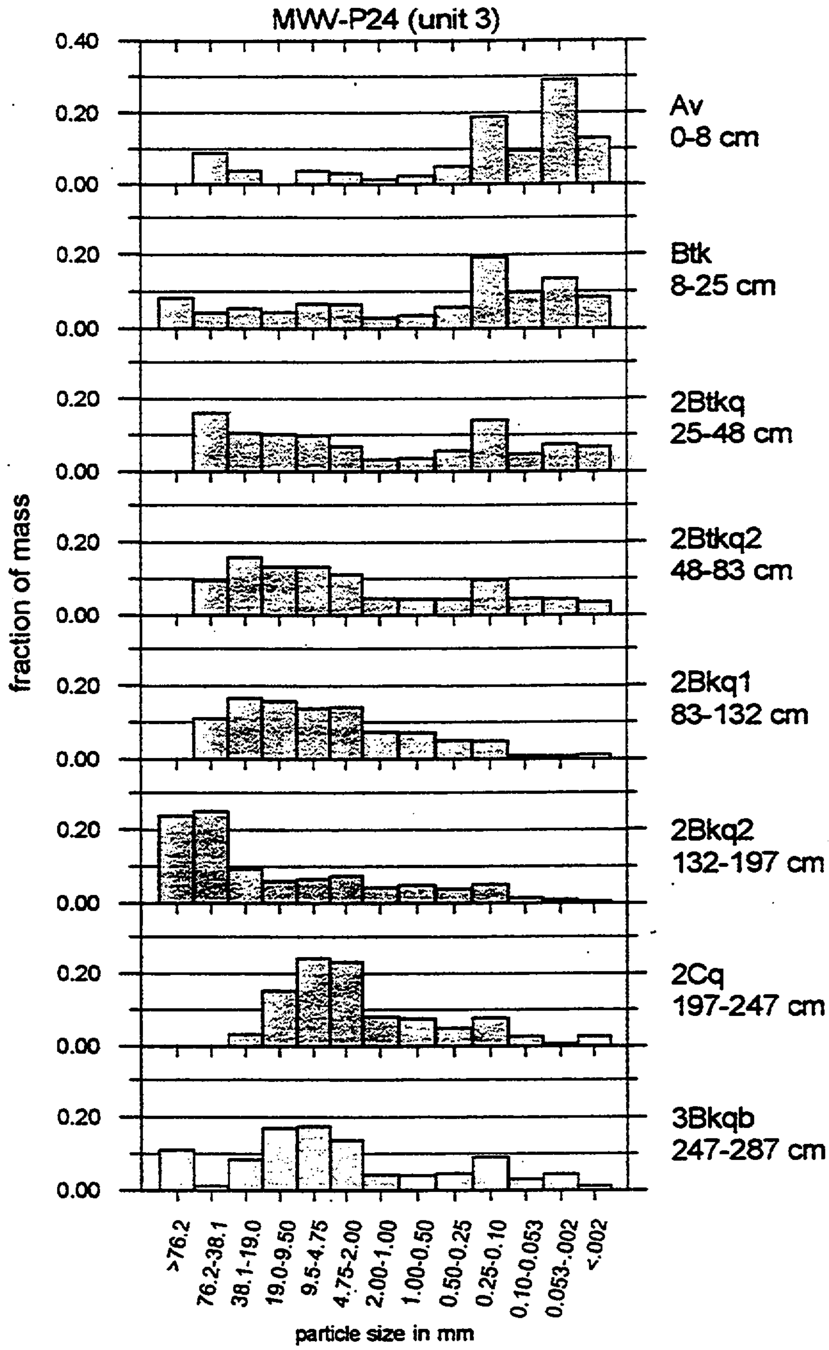

MWV-P24 (unit 3)
fraction of mass
0.40
0.20
0.00
Av
0-8 cm
Btk
8-25 cm
2Btkq
25-48 cm
2Btkq2
48-83 cm
2Bkq1
83-132 cm
2Bkq2
132-197 cm
2Cq
197-247 cm
3Bkqb
247-287 cm
>76.2
76.2-38.1
38.1-19.0
19.0-9.50
9.5-4.75
4.75-2.00
2.00-1.00
1.00-0.50
0.50-0.25
0.25-0.10
0.10-0.053
0.053-.002
<.002
particle size in mm

10F

F. 11

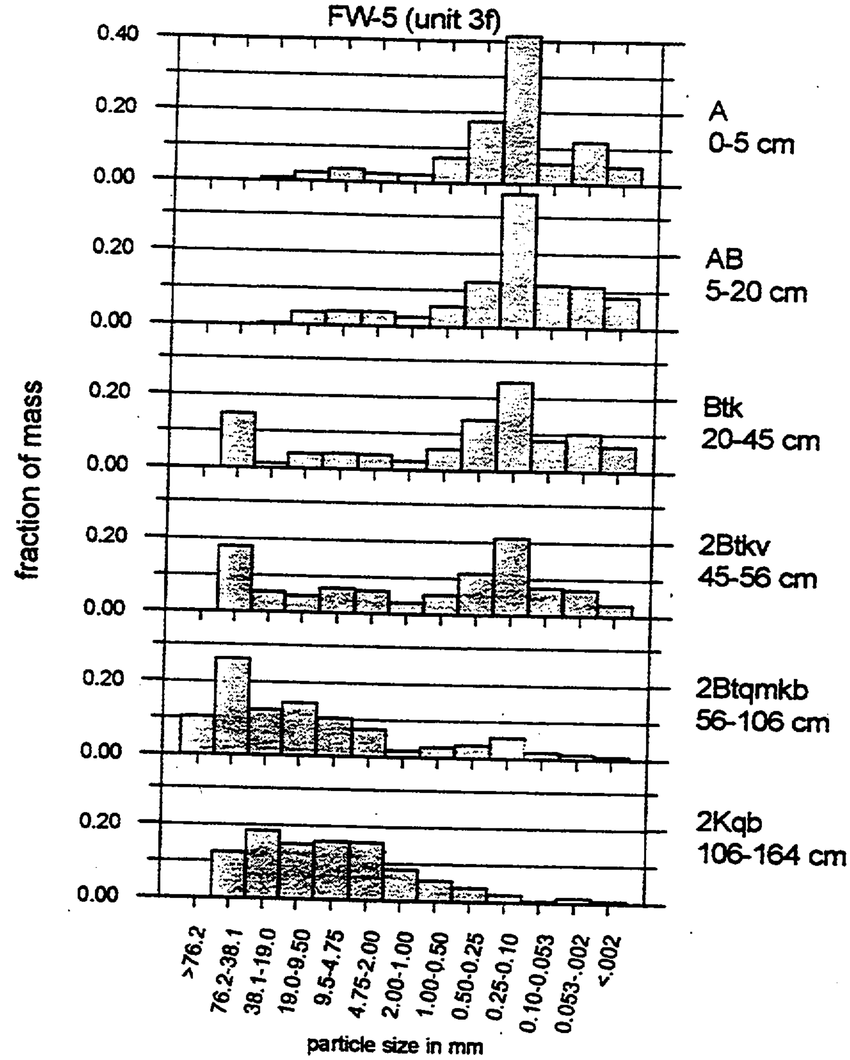
FW-5 (unit 3f)
fraction of mass
0.40
0.20
0.00
A
0-5 cm
AB
5-20 cm
Btk
20-45 cm
2Btkv
45-56 cm
2Btqmkb
56-106 cm
2Kqb
106-164 cm
>76.2
76.2-38.1
38.1-19.0
19.0-9.50
9.5-4.75
4.75-2.00
2.00-1.00
1.00-0.50
0.50-0.25
0.25-0.10
0.10-0.053
0.053-.002
<.002
particle size in mm

10g

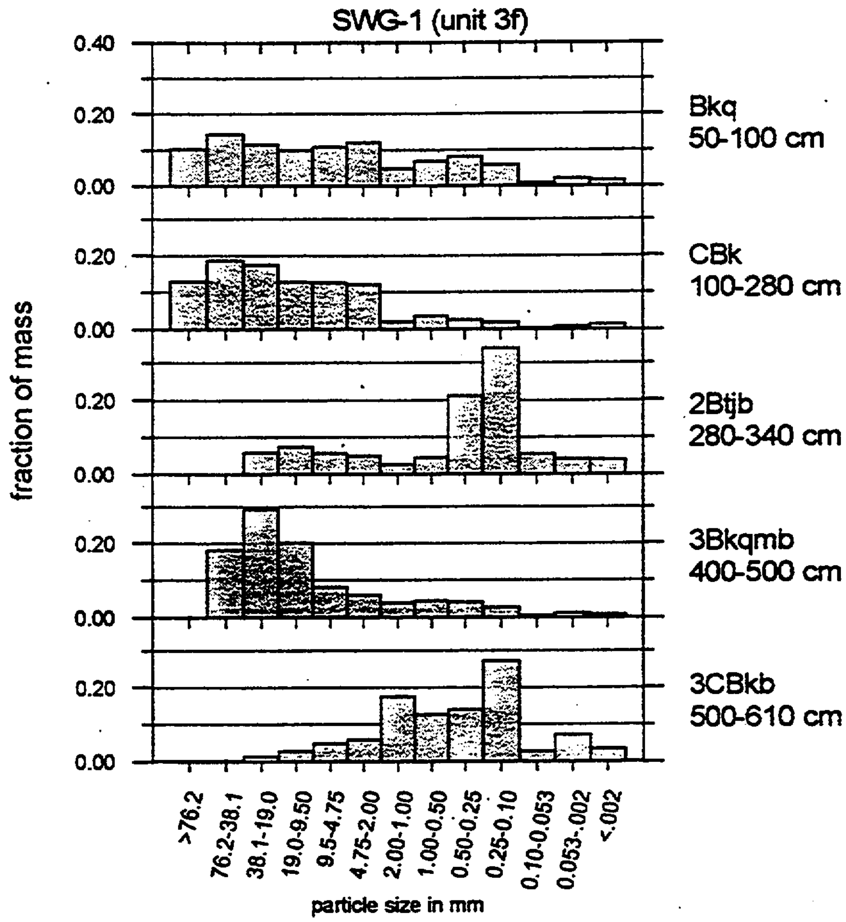
SWG-1 (unit 3f)
fraction of mass
0.40
0.20
0.00
Bkq
50-100 cm
CBk
100-280 cm
2Btjb
280-340 cm
3Bkqmb
400-500 cm
3CBkb
500-610 cm
>76.2
76.2-38.1
38.1-19.0
19.0-9.50
9.5-4.75
4.75-2.00
2.00-1.00
1.00-0.50
0.50-0.25
0.25-0.10
0.10-0.053
0.053-.002
<.002
particle size in mm

10h

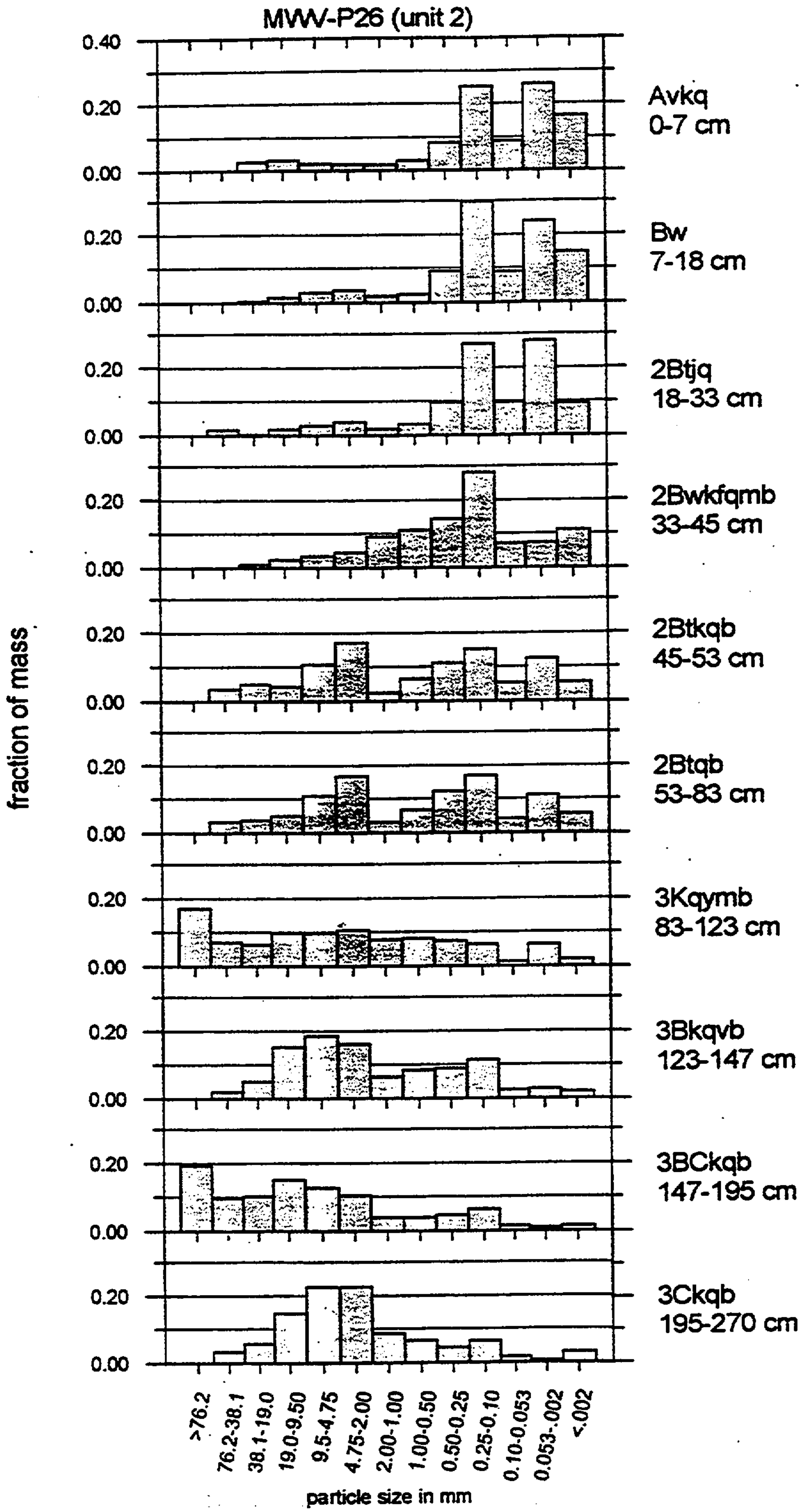
MWV-P26 (unit 2)
fraction of mass
0.40
0.20
0.00
Avkq
0-7 cm
Bw
7-18 cm
2Btjq
18-33 cm
2Bwkfqmb
33-45 cm
2Btkqb
45-53 cm
2Btqb
53-83 cm
3Kqymb
83-123 cm
3Bkqvb
123-147 cm
3BCkqb
147-195 cm
3Ckqb
195-270 cm
>76.2
76.2-38.1
38.1-19.0
19.0-9.50
9.5-4.75
4.75-2.00
2.00-1.00
1.00-0.50
0.50-0.25
0.25-0.10
0.10-0.053
0.053-.002
<.002
particle size in mm

11a

Fig 11a

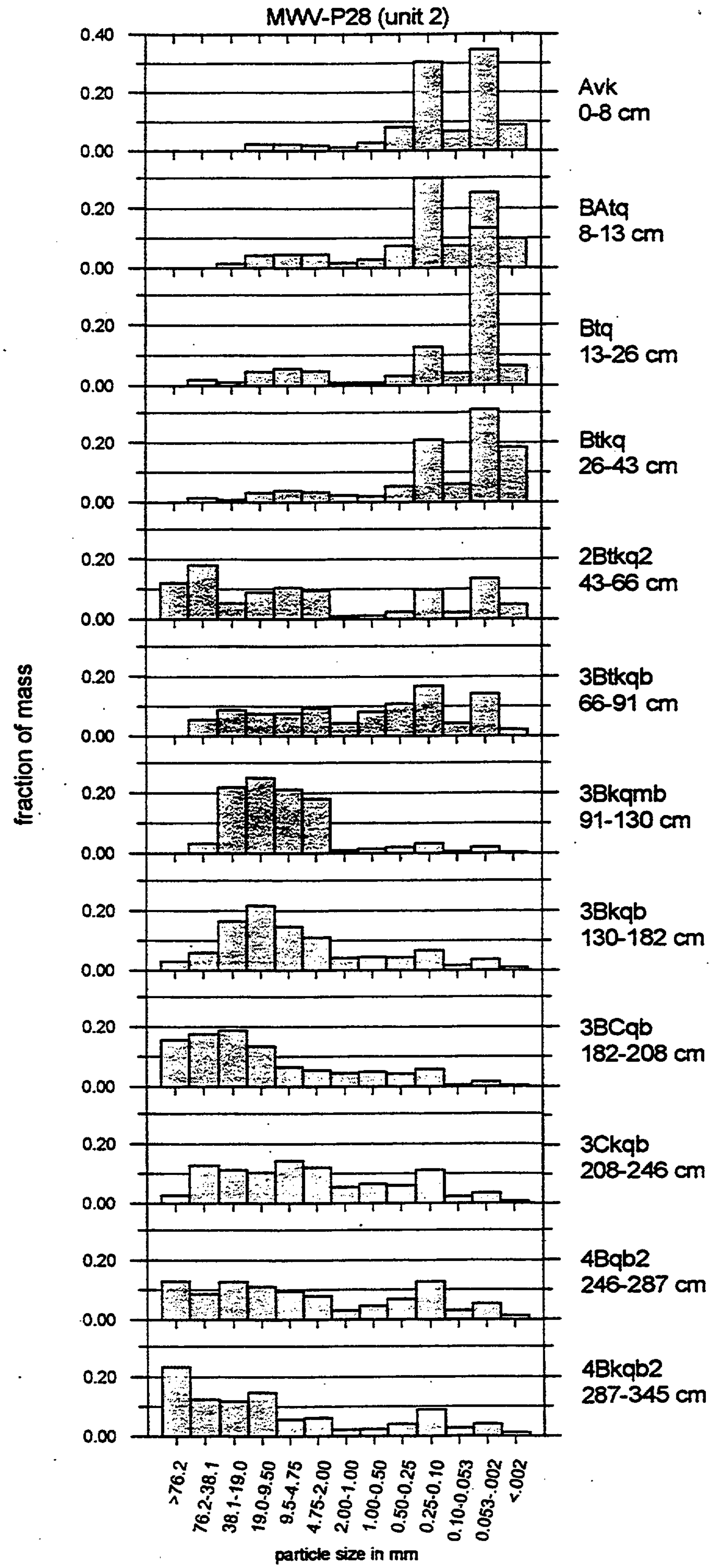
MWV-P28 (unit 2)
fraction of mass
0.40
0.20
0.00
Avk
0-8 cm
BAtq
8-13 cm
Btq
13-26 cm
Btkq
26-43 cm
2Btkq2
43-66 cm
3Btkqb
66-91 cm
3Bkqmb
91-130 cm
3Bkqb
130-182 cm
3BCqb
182-208 cm
3Ckqb
208-246 cm
4Bqb2
246-287 cm
4Bkqb2
287-345 cm
>76.2
76.2-38.1
38.1-19.0
19.0-9.50
9.5-4.75
4.75-2.00
2.00-1.00
1.00-0.50
0.50-0.25
0.25-0.10
0.10-0.053
0.053-.002
<.002
particle size in mm

116

F-116

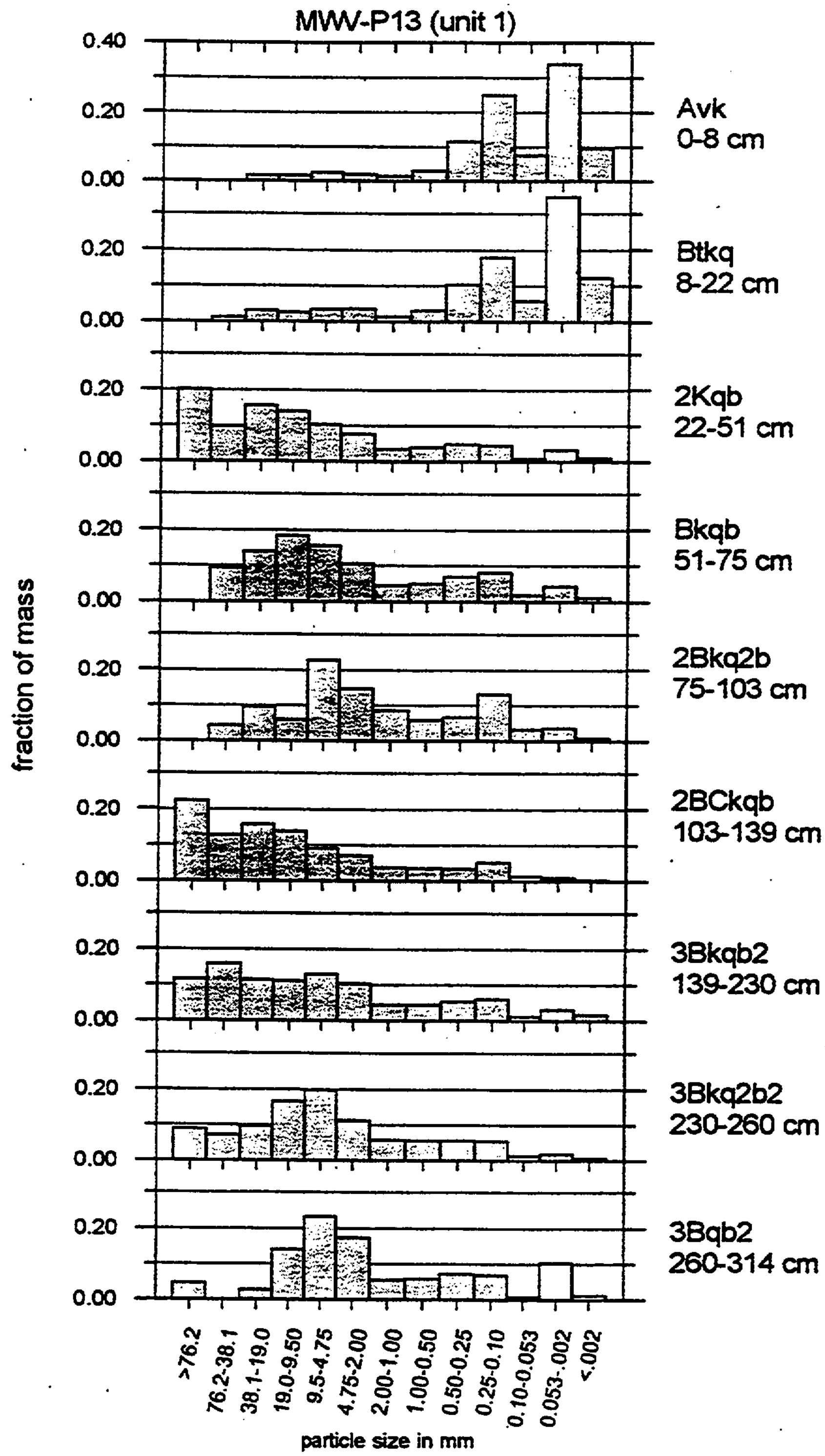
MWV-P13 (unit 1)
fraction of mass
0.40
0.20
0.00
Avk
0-8 cm
Btkq
8-22 cm
2Kqb
22-51 cm
Bkqb
51-75 cm
2Bkq2b
75-103 cm
2BCkqb
103-139 cm
3Bkqb2
139-230 cm
3Bkq2b2
230-260 cm
3Bqb2
260-314 cm
>76.2
76.2-38.1
38.1-19.0
19.0-9.50
9.5-4.75
4.75-2.00
2.00-1.00
1.00-0.50
0.50-0.25
0.25-0.10
0.10-0.053
0.053-.002
<.002
particle size in mm

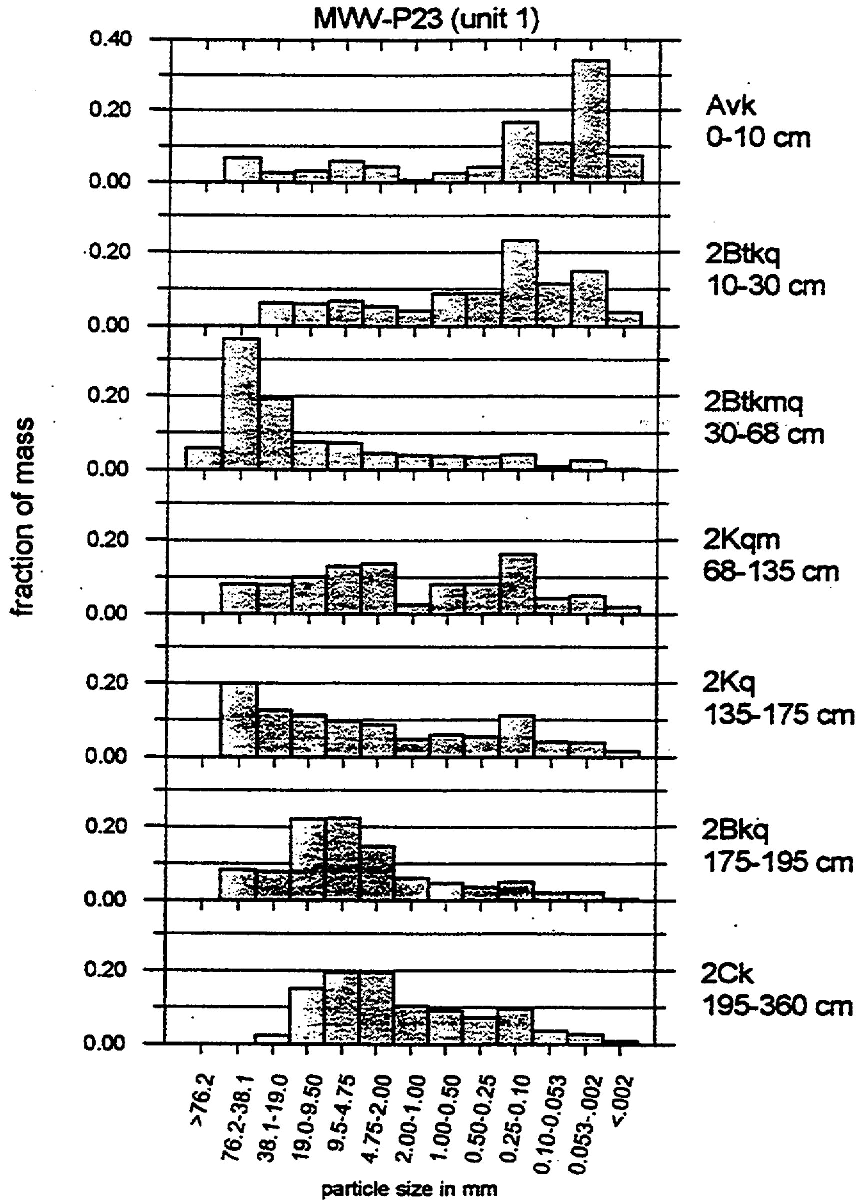
MWV-P23 (unit 1)
fraction of mass
0.40
0.20
0.00
Avk
0-10 cm
2Btkq
10-30 cm
2Btkmq
30-68 cm
2Kqm
68-135 cm
2Kq
135-175 cm
2Bkq
175-195 cm
2Ck
195-360 cm
>76.2
76.2-38.1
38.1-19.0
19.0-9.50
9.5-4.75
4.75-2.00
2.00-1.00
1.00-0.50
0.50-0.25
0.25-0.10
0.10-0.053
0.053-.002
<.002
particle size in mm

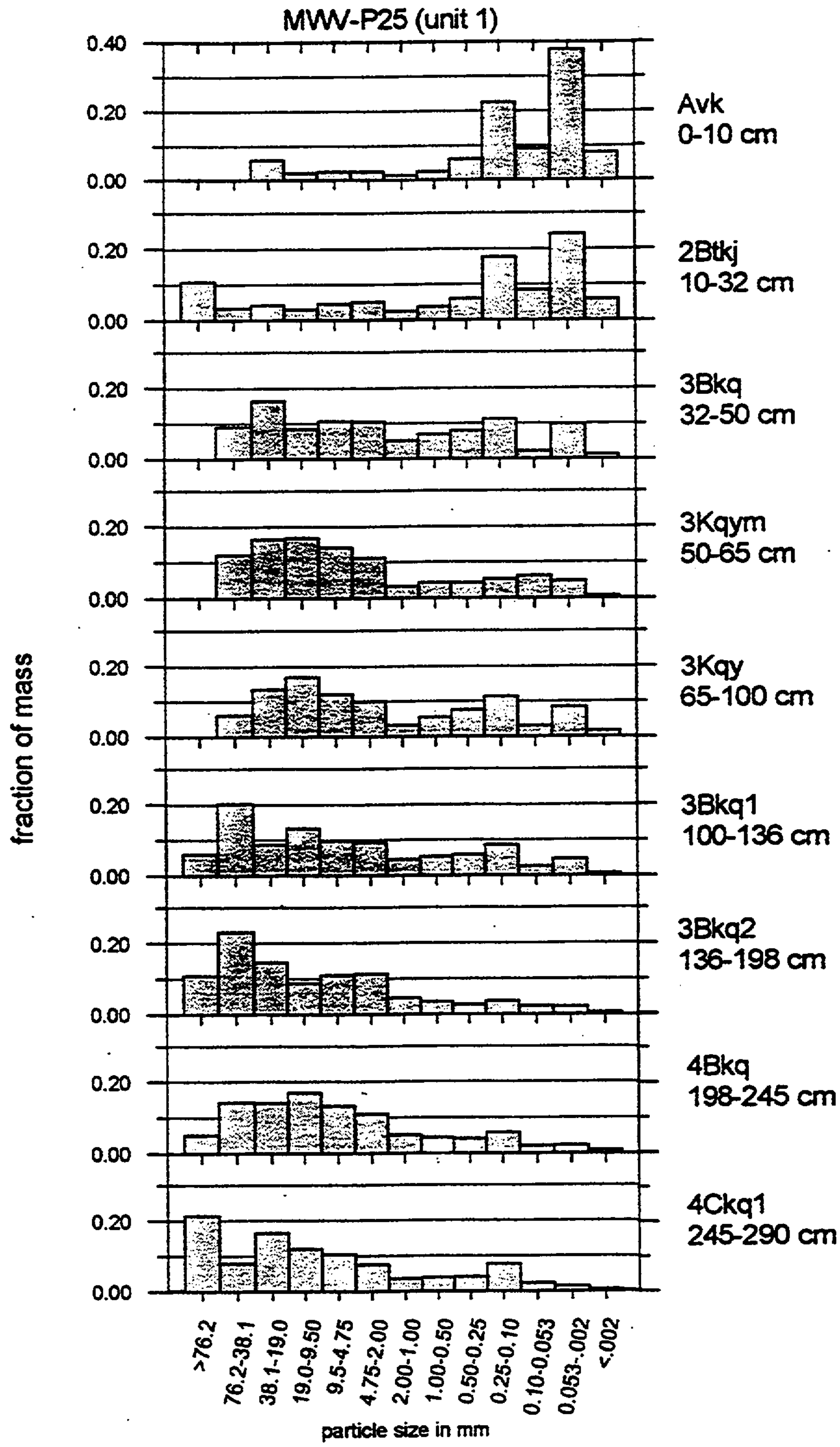

MWV-P25 (unit 1)
fraction of mass
0.40
0.20
0.00
Avk
0-10 cm
2Btkj
10-32 cm
3Bkq
32-50 cm
3Kqym
50-65 cm
3Kqy
65-100 cm
3Bkq1
100-136 cm
3Bkq2
136-198 cm
4Bkq
198-245 cm
4Ckq1
245-290 cm
>76.2
76.2-38.1
38.1-19.0
19.0-9.50
9.5-4.75
4.75-2.00
2.00-1.00
1.00-0.50
0.50-0.25
0.25-0.10
0.10-0.053
0.053-.002
<.002
particle size in mm

12c

CF1-SPI (unit 1)

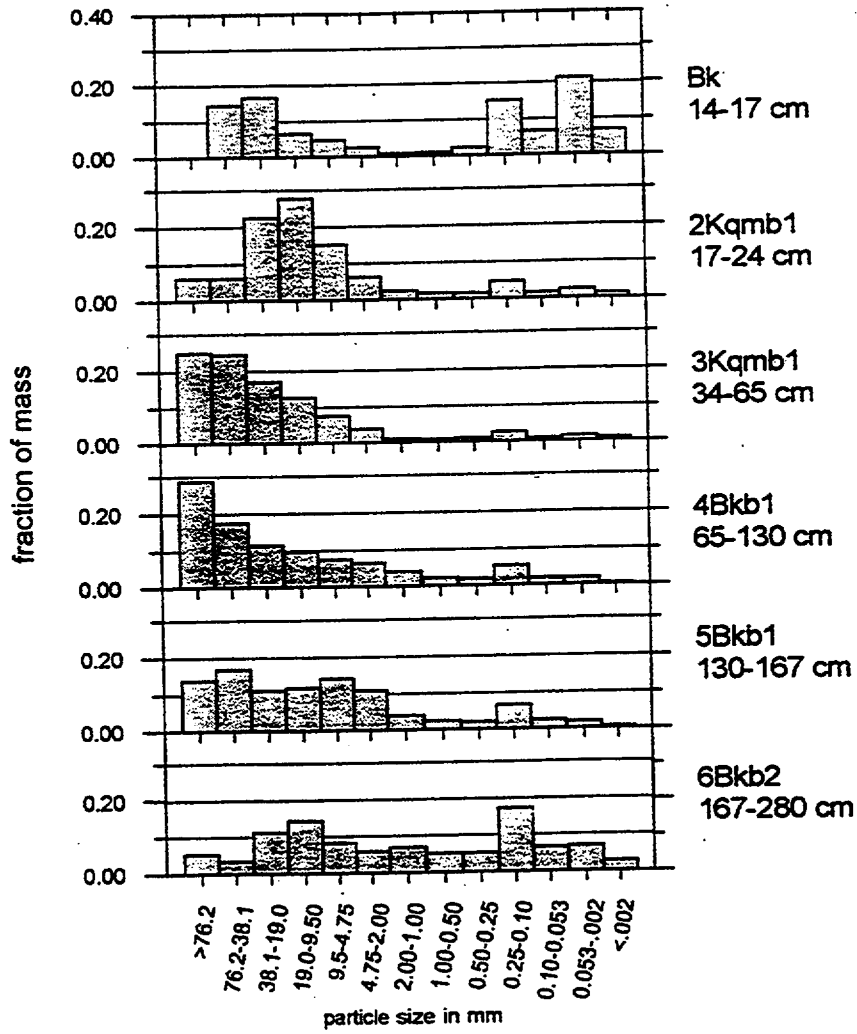

F. 17

CF1-SPII (unit 1)

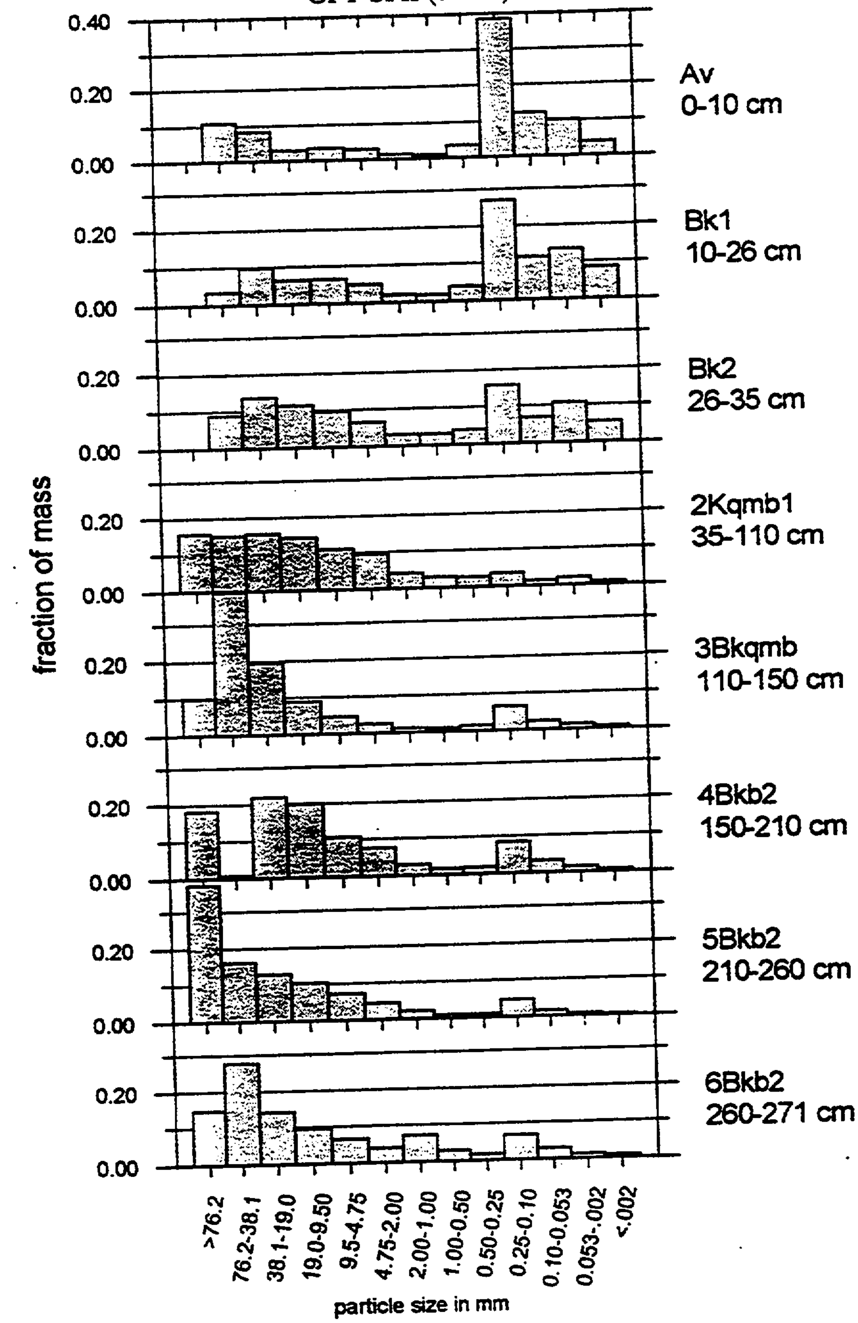

Fig 12e

Fig 12e

Figure 13

Alluvial Soil Evolution Model

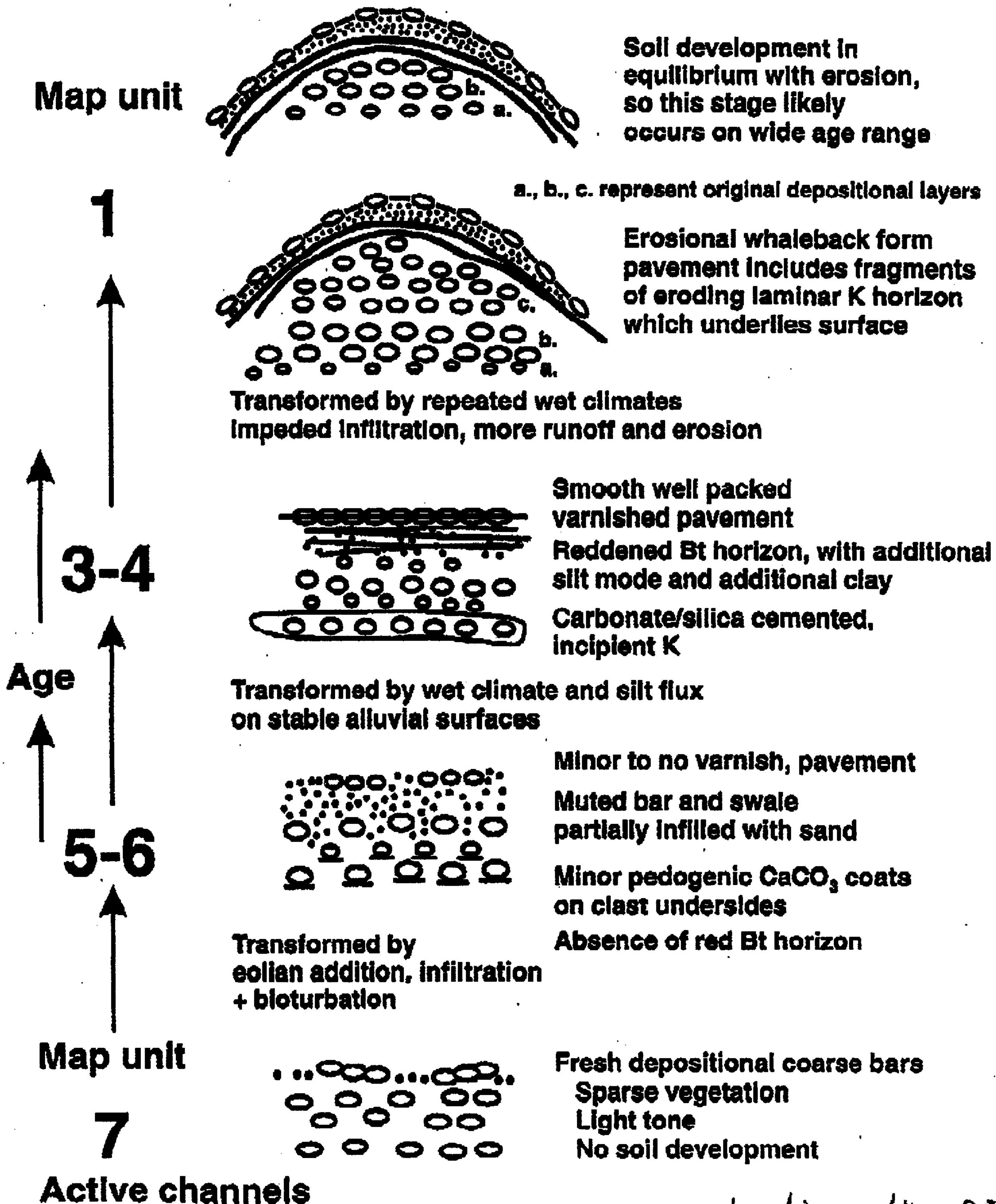

Lundstrom and others 95